SIGNAL PROCESSING MECHANISMS

IN THE

MAMMALIAN PERIPHERAL AUDITORY SYSTEM

JAMES L. WINSLOW

Ph.D. Thesis

March 1980

SIGNAL PROCESSING MECHANISMS IN THE MAMMALIAN PERIPHERAL AUDITORY SYSTEM

by

JAMES L. WINSLOW

A thesis submitted to the Faculty of Graduate Studies and Research
in partial fulfillment of the requirements for the degree of
Doctor of Philosophy

Department of Physiology
and
Biomedical Engineering Unit
McGill University
Montreal, Quebec, Canada
March 1980

ABSTRACT

Mechanisms of signal processing in the peripheral auditory system of mammals were investigated to develop an overall mathematical model. Each physiological signal processing block, the middle ear, basilar membrane, cilia, hair cell, synapse, and dendrites was analyzed separately. Dynamic formulations based on subsystem anatomy were used to incorporate nonlinearities.

Available steady state descriptions of the mechanical blocks based on frequency response experiments were rewritten in dynamic form. The hair cell model, based on its geometry and electrical environment, behaves linearly at low input amplitudes and nonlinearly at higher amplitudes.

Functions that yield input-output predictions for synapses were derived from experimental literature. Calculated transmitter quanta released per axon AP agrees with experimental values. The postsynaptic receptor mechanism was shown to have a saturating non-linearity and maximum conductance value in the order of 20 nanomhos, which causes millivolt depolarization in the dendrite.

Numerical simulations were made for the two types of afferent dendrites. The dendrite partial differential equation was shown to have nonlinear time varying synaptic boundary conditions. To preserve dendrite geometry, the discretized compartment version is a stiff differential equation system requiring a stabilized integration method with work space size of order N. Outer dendrites were shown to be most responsive to downsweeps in auditory input frequency, but, with reponse potential insufficient to generate APs. This is corroborated by the termination of outer afferent fibers in the spiral ganglion. The same compartment equations and constants, but different geometry, yielded simulations showing that the inner afferent dendrites have sufficiently large response potentials to generate APs.

RESUME

Les mécanismes ou traitement des signaux dans le système auditif périphérique chez les mammifères sont étudiés aux fins du développement du modèle mathématique. Chaque bloc physiologique du traitement des signaux, l'oreille moyenne, la membrane basillaire, les cils, les cellules ciliées, les synapses et dendrites, est analysés séparement. Par des formulations de la réponse dynamique basées sur l'anatomie des sous-systèmes les nonlinéarites ont pu être inclues dans le modèle.

Les descriptions existantes des éléments mécaniques exprimées sous forme de réponse en fréquence furent converties en équations différentielles dans le temps. Le modèle des cellules ciliées, basé sur la géometrie et les propriétes electriques du sous-système, démontre que la réponse des cellules est linéaire pour des amplitudes faibles et nonlinéaire pour des amplitudes plus grandes.

Les fonctions qui permettent des prédictions de l'entré-sortie des synapses furent dérivées de la litérature expérimentale. Les calculs des quantas libérés par potentiel d'action concordent avec les valeurs expérimentales connues. Le mecanisme récepteur post-synaptique démontre l'existence d'effets nonlinéaires de saturation avec conductance maximale de 20 nanomnos, ce qui produit une dépolarisation de l'ordre des millivolts dans les dendrites.

Des simulations numeriques ont été faites pour les deux types de dendrites afférents. On démontre que l'équation différentielle partielle des dendrites a des conditions limites aux synapses qui est nonlinéaire et fonction du temps. Afin de préserver la géometrie des dendrites, la version compartimentée discrète est un système d'équations

différentielles rigides (stiff) nécessitant une méthode d'intégration stabilisée et utilisant de l'espace de travail en mémoire proportionnel a l'ordre du système d'équations différentielles. On démontre aussi que les dendrites externes réagissent d'une facon plus grande a des balayages auditifs de fréquences décroissantes dans le temps; toutefois, le potentiel de la réponse est insuffisant pour générer des potentiels d'actions. Ceci est corroboré par les terminaisons des fibres afférentes externes du ganglion spirale. Les mêmes équations et constantes, employées avec une géometrie correspondant aux dendrites afférents internes, prédisent une réponse d'amplitude suffisante pour générer des potentiels d'action.

Chapter 1: INTRODUCTION

Chapter 2: LITERATURE REVIEW

CHAPTER 3: AUDITORY SYSTEM MECHANICS

Chapter 4: THE HAIR CELL

Chapter 5: HAIR CELL AFFERENT SYNAPSE

CHAPTER 6: COCHLEAR DENDRITES

Chapter 7: CONCLUSION

Chapter 8: ACKNOWLEDGEMENTS

CHAPTER 1: INTRODUCTION

1.1 Opening Remarks

1.2 Orientation

- 1.2.1 Anatomy and Physiology
- 1.2.2 Peripheral Auditory System

1.3 The Problem

- 1.3.1 Statement
- 1.3.2 Questions
- 1.3.3 Approach
- 1.3.4 Organization

CHAPTER 1

INTRODUCTION

1.1 OPENING REMARKS

The cochlea is the receptor organ of auditory input to mammals. It is notable that all mammals have almost identical cochleas, except for length of the cochlear partition which determines the range of response sound frequencies available to a particular species. This genetic parsimony of nature provides an aid in determining cochlea function, in that what is learned from one mammal can be applied in some form to another mammal. The cochlea as an input organ, encodes for the brain the immense variety of air borne vibration signals which have meaning to the organism. Consider the range of air borne sounds important to us humans and our fellow mammals, some to which we are in debt for our existence with respect to evolution. Loud or sudden noises often denote potential danger from the environment or predators. Communication signals for cooperative behavior such as food gathering, mating, and distress calls are encoded by this one organ. These important survival signals as well as the rich communication

utilized by humans using verbal language are transformed from a mechanical signal to the neural message transmitted to the brain. The brain then utilizes these signals for more uses than could be named in a day. What is the encoding process whereby the mechanical signal is transmitted to the brain and is it possible to describe this process in a quantitative computation model? This thesis is an analysis of the encoding performed by the cochlea with emphasis on the neural end of the process.

1.2 ORIENTATION

An overview of the cochlea is presented in this section. It is intended to provide an orientation to the structure and function which accomplish the sequence of processes in going from a mechanical to neural signal. The orientation is to bridge the gap from a standard medical school text book to this thesis. For detailed discussion and origin of scientific fact, the reader is refered to the literature review (Chapter 2) and chapters devoted to the individual processing structures (Chapters 3,4,5,6).

1.2.1 ANATOMY AND PHYSIOLOGY

The peripheral auditory structure is shown in figure:1.2.1.1. The external ear consists of the auricle (pinna) which receives air borne vibration signals of sound from the environment and the ear canal (external meatus)

which transmits the sound waves to the ear drum (tympanum) modified by a small amplification in pressure. The canal, by its length, serves to protect the ear drum from puncture, dirt and changes in humidity and temperature.

The middle ear consists of the ossicular chain (incus, malleus, and stapes) contained in the middle ear cavity, and the Eustachian tube which communicates with surrounding air via the nose and throat cavity. The middle ear cavity in higher mammals is enclosed by the temporal bone of the skull which in most laboratory animals is surrounded by the auditory bulla, a thin bony compartment attached to the skull.

Ear drum vibrations due to air borne sound pressure waves are conducted to the oval window of the fluid filled inner ear with an amplification in pressure. This amplification is done by a lever effect of the ossicles and more strongly by a reduction of area of ear drum to the stapes footplate. The middle ear also serves to match the impedance of the ear drum with that of the oval window. When sound waves pass from a low impedance substance to a high impedance substance such as air to liquid, less than 1/100 of the sound energy is absorbed by the liquid and the remainder is reflected. The middle ear also protects the cochlea from damaging sounds by contraction of the tensor tympani muscle and stapedius muscle to decrease the pressure transmission ratio of the middle ear. The static pressure

on both sides of the ear drum is equalized by the Eustachian tube which allows equilibration of middle air pressure with that of the atmosphere.

The inner ear is enclosed in a system of interconnecting cavities surrounded by the hard temporal bone or thickened wall of the bulla. These interconnecting cavities are called the bony labyrinth. Contained in the bony labyrinth is the membraneous labyrinth which contains the auditory cochlea and the vestibular receptor organs which respond to vector accelerations of the head. The outline of the labyrinth is shown in figure:1.2.1.2. The openings to the bony labyrinth are the oval and round windows, the cochlear aqueduct, the vestibular aqueduct, and the openings to the brain cavity through which enter the nerve and vascular supply of the labyrinth. Fluid exchange and regulation for the two labyrinthine fluids (perilymph and endolymph) occur through the two aqueducts, the cerebrospinal fluid space and endolymphatic sac. The snail shaped cochlea is the hydro-mechanical-neural system which converts mechanical vibrations to dendrite potentials which trigger axon action potentials that travel in the cochlear nerve. The cochlea is shown in uncoiled schematic form in figure:1.2.1.3. It is coiled around its bony central core, the modiolus, which contains the spiral ganglion from which emerges the cochlea nerve. A cross section view is shown in figure:1.2.1.4. A thin bony shelf protrudes from the

modiolus into the cochlear cavity. This bony shelf, known as the osseous spiral lamina, is connected to the opposite side of the cochlea by the basilar membrane and spiral ligament. This structure, the cochlear partition, runs from the large end (base) to the tip (apex) of the cochlea and divides the cochlea into two compartments. The superior compartment (scala vestibuli) communicates with the middle ear cavity via the oval window. The inferior compartment (scala tympani) communicates with the middle ear cavity via the round window. These two scalae communicate with each other via the helicotrema which is a space left by the cochlear partition not extending completely to the apex of the cochlea. The third compartment (scala media) is formed by Reissner's membrane which separates scala vestibuli from the basilar membrane. Scala media terminates prior to the termination of the cochlear canal at the apex, just before the helicotrema. The fluid in scala media is called endolymph. The fluid in scala vestibuli and scala tympani connected by the helicotrema is perilymph. The cross-sectional areas of the scalae and the osseous spiral lamina change in size along the length of the cochlea, becoming larger from apex to base. Opposite to these changes, the basilar membrane becomes narrower from apex to base. The basilar membrane changes in width by as much as 10 times.

When the window is pushed and pulled by the stapes foot

plate as is the normal response to sound wave vibrations of the ear drum, fluid pressure difference waves occur across the cochlear partition along its length. The mammalian cochlea has evolved in such a way that the basal end of the cochlear partition responds with largest amplitude of vibration to high frequencies, and the apical end to low sound frequencies, with a continuum in between.

Stria vascularis, a vascular layer of tissue, lines the cochlea along the outer wall of scala media. The stria vascularis secretes endolymph into scala media. Endolymph is similar in composition to intracellular fluid, i.e., high potassium and low sodium concentrations. Perilymph, the fluid in scala vestibuli and scala tympani, is similar to interstitial fluid with high sodium and low potassium concentrations. It is significant that these ion concentration gradients are the origin of electropotentials in the scalae fluids. Values are typically 100mV in endolymph of scala media, 7mV in the fluid surrounding the hair cells, and 5 to 7mV for perilymph.

Situated on the superior surface of the basilar membrane is the organ of Corti. It runs the entire length of the cochlear partition and is a complex multicellular structure and is the actual receptor organ of the auditory system. The cross-section view in figure:1.2.1.4 depicts Corti's organ with the structural arrangement of its components. The lower boundary is the basilar membrane on

which sits the relatively stiff stucture formed by the supporting cells and receptor cells. The supporting cells are the inner and outer pillar cells that form the triangular main support and the inner and outer phalangeal cells of Deiter which support the base of the hair cells. The cells of Deiter have rigid phalangeal processes that extend up to the apex of the sensory hair cells where they flatten out, and together with the apical extensions of the pillar cells, form the reticular lamina. The reticular lamina is a flat plate into which is fitted the top ends of the hair cells and pillar cells. Situated above the organ of Corti is the tectorial membrane which is attached to the spiral limbus along the length of the cochlea. It has the consistency and properties of a gel and does not have any sort of cell membrane.

The hair cells, embedded in the organ of Corti, are flask shaped with about 60 stereocilia projecting from their tops into the space between the reticular lamina and tectorial membrane. There are two sets of hair cells, the inner hair cells and the outer hair cells. The inner hair cells are found in a single row on the modiolar side of the tunnel of Corti formed by the triangular arch of pillar cells also known as rods of Corti. The outer hair cells are on the radial side of the tunnel of Corti away from the modiolus and are aligned in three rows. Since the only flexible part of the cochlear partition is the basilar

membrane, theory of mechanics predicts that the basilar membrane bends in an arch like a stressed beam and the organ of Corti rotates on it about the juncture of the basilar membrane and osseous spiral lamina. The modiolar side of the tectorial membrane is fixed to the limbus and the hair cell cilia are bent by contact with the tectorial membrane or fluid movement between the membrane and reticular lamina. The mechanical movement of the basilar membrane is converted into an electrical potential recordable from the hair cells.

From anatomical investigations it is seen that there are on each hair cell true synapses which transmit the receptor potential of the hair cell to dendrites of axons in the cochlear nerve. The dendrites enter the modiolus where they become myelinated, connect to somas in the spiral ganglion and thence continue as afferent axons in the cochlear nerve. There is a small percentage of the cochlea nerve axons which are efferent; their role is beyond the scope of this investigation. The response characteristics of these afferent axons are compatible with the frequency organization of the basilar membrane. That is, the optimal response frequency (characteristic frequency) of the afferent axons have a range corresponding to basilar membrane frequency response.

1.2.2 PERIPHERAL AUDITORY SYSTEM

The anatomy of the peripheral auditory system, cast in the form of an information flow diagram, is shown in figure:1.2.2. The location of the physiological processes or anatomical structures are indicated in the boxes. The variables or physical entities are shown as arrows from one box to the next. The outer ear receives sound pressure waves, P(t), which are conducted to the ear drum which responds by vibrating with displacement, D(t). The ear drum via the ossicles of the middle ear drives the oval window with volume displacement, VD(t). This oscillating volume displacement drives the intracochlear fluid pressure system which causes the oscillating basilar membrane displacement DBM(x,t) at distance x from the basal end. The organ of Corti transforms the displacement of the basilar membrane to a mechanical perturbation at the top of the hair cells which generate a receptor voltage RVHC(x,i,t) in the i-th hair cell at location x from the cochlear base. This receptor potential causes activation of the synapse onto the afferent dendrites effecting a voltage change,VSG(x,i,t) at the action potential generating site in a dendrite of type i, at location x, at time t. This dendrite voltage drives the spiral ganglion neurons whose axons constitute the afferent auditory portion of the eighth cranial nerve and carry action potentials with firing rate R(x,i,t) to the brain stem.

1.3 THE PROBLEM

1.3.1 STATEMENT

Although there is a plethora of literature on the peripheral auditory system, there is no way to predict action potential frequencies or post stimulus time histogram responses in the axons of the cochlear nerve for any auditory input to the mammalian ear. Until such predictions are possible, the system is still an open area of research. A phenomenon or process is just not understood until complete predictions are a reality. In examining the signal processing blocks of the peripheral auditory system, several questions arise for which predictive models are apropos and necessary to obtain answers.

1.3.2 QUESTIONS

There are two types of afferent dendrites in the cochlea (Spoendlin,1974). One type originates from the inner hair cells and another type from outer hair cells. what is the functional use of these two types of dendrites?

What are the response characteristics of the hair cells? With the advent of experimental recordings from hair cells (Mulroy et al,1974; Russell & Sellick,1977) is it possible to separate the hair cell response to basilar membrane displacements from the mechanical to conductance

change at the hair cell receptor surface? The first step is to find the input-output function of the hair cell using conductance at the receptor region as input and the cell's receptor potential as output.

In comparing the neural response of cochlear nerve axons with that of the basilar membrane, the neural tuning is sharper than the mechanical tuning curve (Evans & Wilson, 1973; Wilson, 1974; Inselberg,1978). What is the reason for this difference?

There are research attempts to electrically stimulate the cochleas of humans with nonfunctional ear drums, ossicles, or hair cells. There has been little effort to predict the proper induced signals for such auditory prostheses.

Can Rall's (1959,60,62a,62b) model and analysis of simple highly regular dendritic trees be extended to irregular branching patterns? This would allow investigation of naturally occurring dendrites. The outer dendrites of the cochlea are unsymmetric and irregular, but sufficiently uncomplicated to permit such an analysis as a test of the analysis and simulation.

Is it possible to analytically describe synapses so that they can be included in a model of neuron interaction? It is necessary to develop a proper input-output model for this transmission block.

In the simulation of irregular unsymmetric dendritic

trees, it is necessary to describe the dendrite with a partial differential equation that has differing constants along the dendrite. When this partial differential equation is put in discrete form for the space variable, a system of one hundred or more ordinary differential equations results. Is it possible to successfully simulate this system in a manner that is accurate enough and in a sufficiently short span of computational time, so as to not break the bank for computer charges?

1.3.3 APPROACH

The first step is to consider each of the processing blocks with respect to the completeness of the experimental literature for putting together a model for that block. Next, can a quantitative model be developed for those blocks which are incomplete in the cochlea ? One of the basic tenets of biology is that structure determines function. For the three neural components (hair cells, synapses, and dendrites) their structure is well known from cochlear anatomical literature, but direct experimental results are lacking for the peripheral auditory system. The approach is to utilize the structure of these components and the functional properties of the subcomponents such as passive neural membrane, transmitter release, synaptic receptor sites, and dendrite responses to produce a model of each processing block. Thus the dominant theme in constructing

the models is that structure determines function. It is also required that the overall computational model be able to predict the output for any input signal. This necessitates a dynamic model.

1.3.4 ORGANIZATION

To carry out the strategy, the thesis commences with this introductory chapter (1). The literature review (2) is an overall review because much of the literature is discussed within the analysis of the physiological blocks.

The existent models and available direct data from ear drum to hair cell cilia are analyzed and redeveloped in dynamic form in chapter 3. This is for perspective on the neural signal analysis and to satisfy the dynamic description requirement.

The hair cell chapter (4) analyzes the hair cell as a receptor organ and makes predictions as to its frequency response functions and changes due to its ionic environment.

The synapse chapter (5) analyzes the synapse presenting an input-output function for dendrite synaptic conductance as a function of pre-synaptic potential.

The dendrite chapter (6) develops a general model for predicting the response of a dendrite with irregular branching and unrestricted location of synapses. To numerically solve the dendrite system of equations, it was necessary to use the very recent innovations in computerized

numerical analysis for the solution of a system of stiff differential equations. The model and and method was then used to predict dendrite responses and distinguish between the two types of cochlear dendrites.

The conclusion chapter (7) contains some remarks on the peripheral auditory system as a large scale model. The model built on the premise that structure determines function, gives a certain perspective. Also some possible future experimental and theoretical work is indicated. Claims to originality are included in this chapter.

Acknowledgements are given in chapter 8.

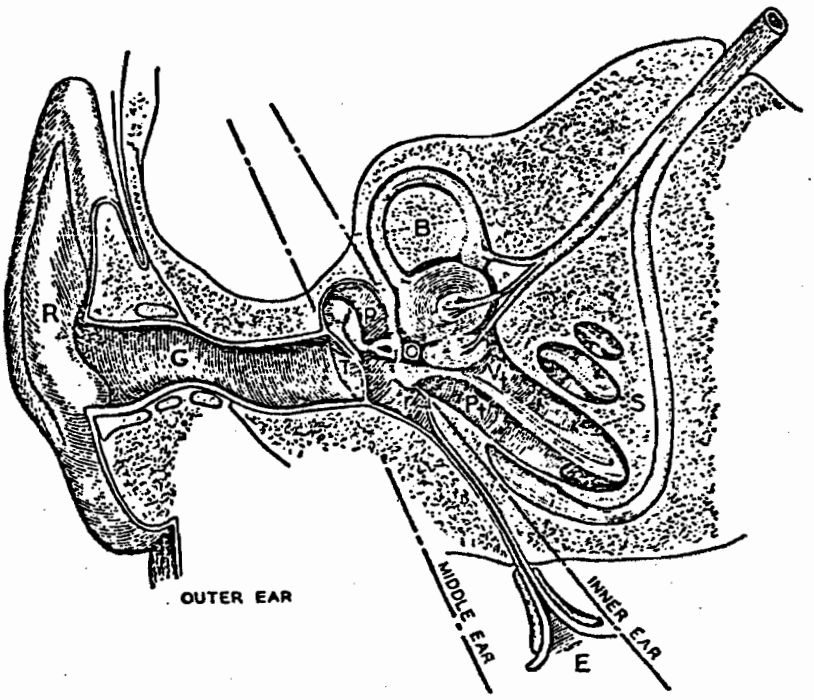

SEMIDIAGRAMMATIC SECTION THROUGH THE RIGHT EAR (CZERMAK): G, EXTERNAL AUDITORY MEATUS; T, MEMBRANA TYMPANI; P, TYMPANIC CAVITY; O, FENESTRA OVALIS; R, FENESTRA ROTUNDA; B, SEMICIRCULAR CANAL; S, COCHLEA; VT, SCALA VESTIBULI; PT, SCALA TYMPANI; E, EUSTACHIAN TUBE; R, PINNA.

Figure:1.2.1.1 Gross anatomy of the human ear. From Fletcher (1953, p75).

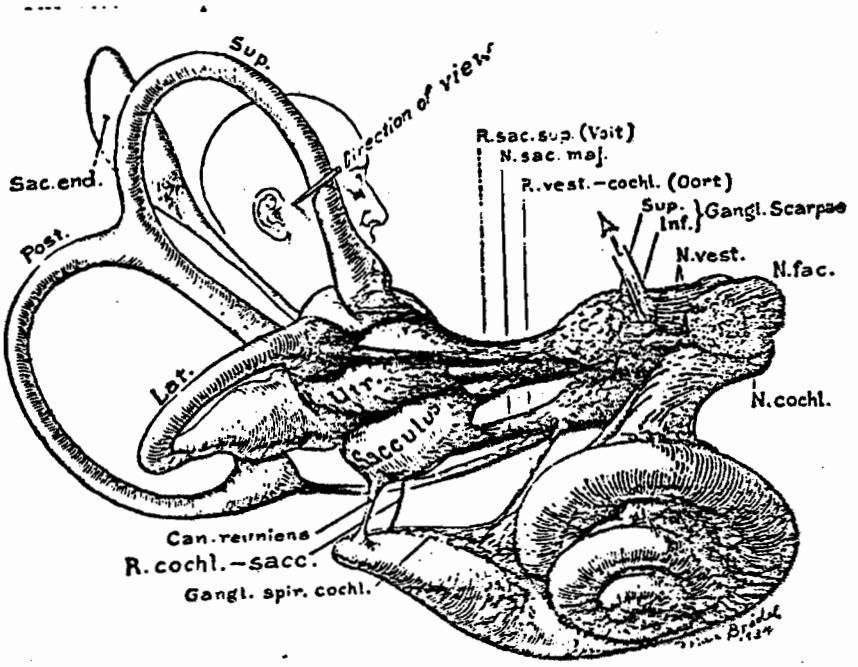

Figure:1.2.1.2 Brodal's detailed drawing of the membranous labyrinth and its innervation. From Hardy (1934, p 412, in Dallos, 1973,p8)

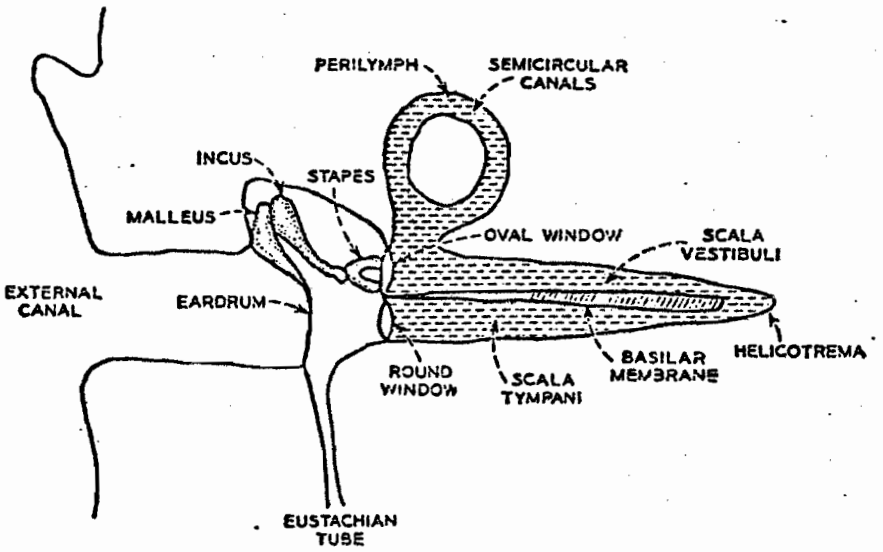

Figure:1.2.1.3 Schematic drawing of the cochlea and middle ear. From Flanagan (1960, fig. 1.)

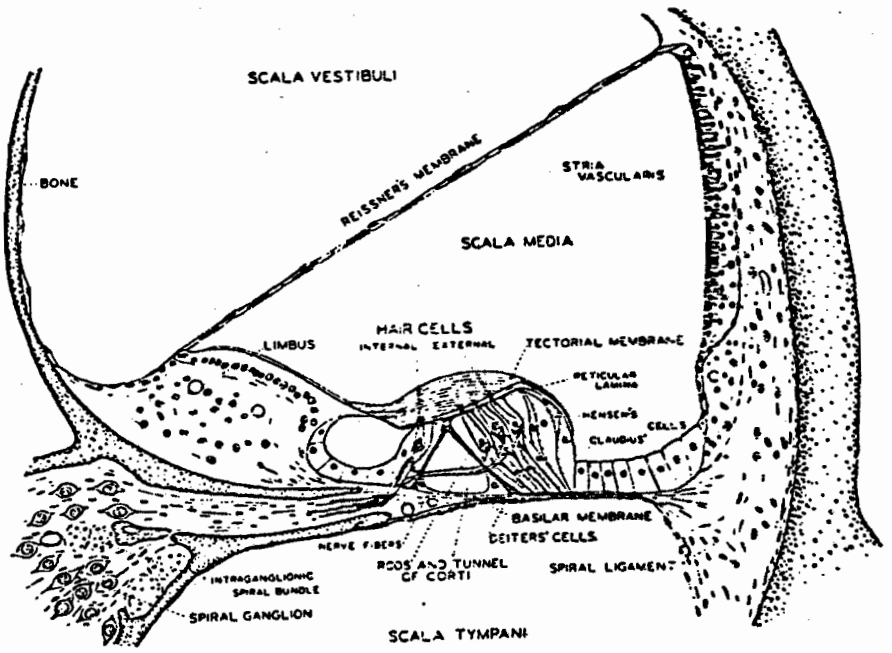

Figure: 1.2.1.4 Drawing of the cochlea in cross section. The drawing depicts the second turn. From Davis (1965).

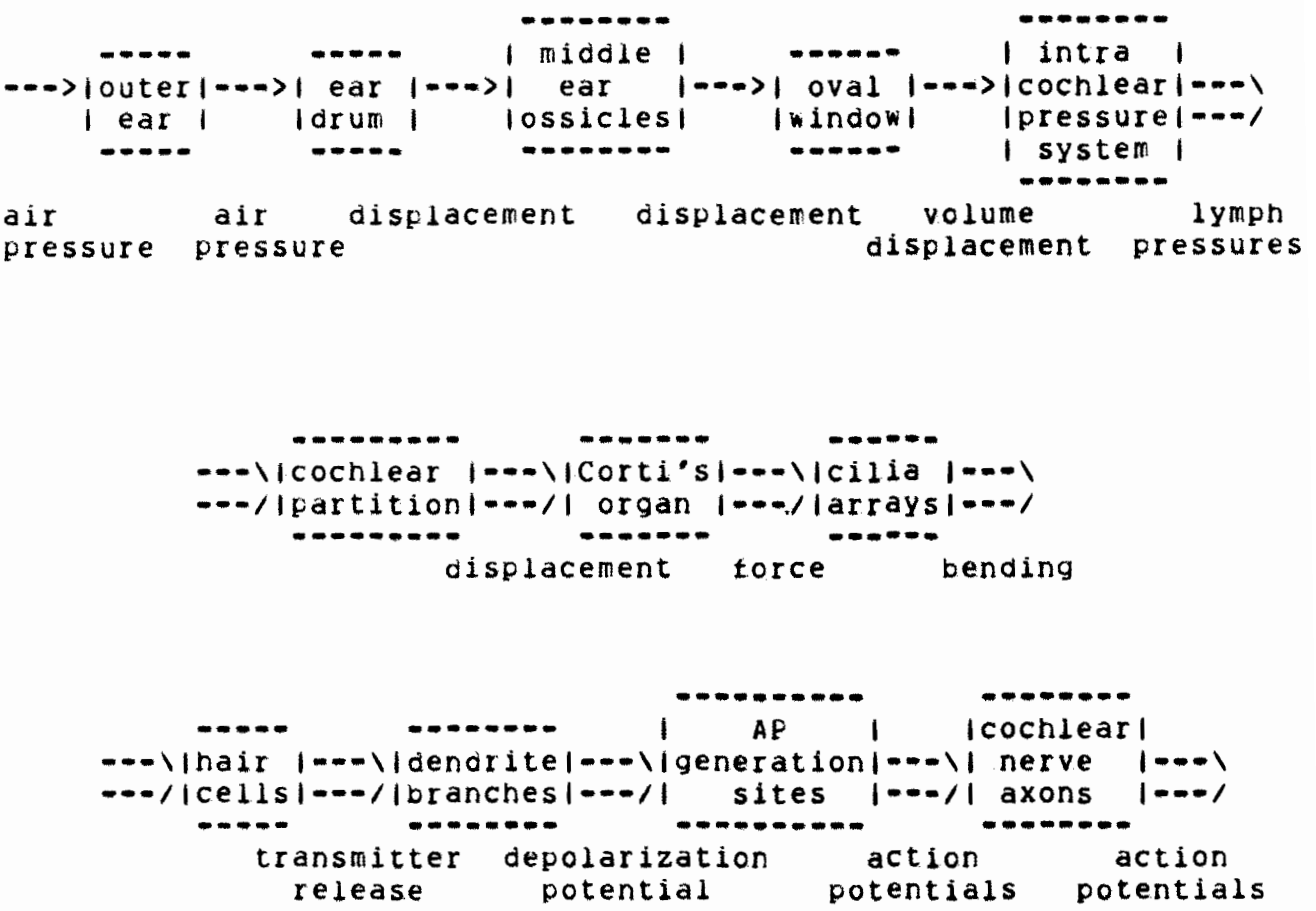

Figure:1.2.2 Information flow diagram for the auditory portion of the ear. The conversion of acoustic air pressure frequencies into action potentials on axons in the cochlear nerve. Double arrows denote parallel signals.

Brodal,M. (1946) Three unpublished drawings of the anatomy of the human ear. Saunders, Philadelphia, Penn.

Davis,H. (1965) A Model for transducer action in the cochlea. Cold Spring Harbor Sympos. Quant. Biol. 30:181-190.

Evans,E.F. & Wilson,J.P. (1973) The frequency selectivity of the cochlea. In: Basic Mechanisms in Hearing, A.R. Moller (ed.) Academic Press, N.Y. pp519-554.

Flanagan,J.L. (1960) Models for approximating basilar membrane displacement. Bell System Tech. J. 39:1163-1192.

Fletcher,H. (1953) Speech and Hearing in Communication. D. Van Nostrand, Inc., N.Y. 461P.

Hardy,M. (1934) Observations on the innervation of the macula sacculi in man. Anat.Rec. 59:403-418.

Inselberg,A. (1978) Cochlear dynamics: The evolution of a mathematical model. SIAM Rev. 20(2):301-351.

Mulroy,M.J., Altmann,D.W., Weiss,T.F., & Peake,W.T. (1974) Intracellular electric responses to sound in a vertebrate cochlea. Nature 249:482-485.

Rall,W. (1959) Branching dendritic trees and motorneuron membrane resistivity. Exp.Neurol. 1:491-527.

Rall,W. (1960) Membrane potential transient and membrane time constants of motor neurnons. Exp.Neurol. 2:503-532.

Rall,W. (1962a) Theory of physiological properties of dendrites. Ann.N.Y.Acad.Sci. 96:1071-1092.

Rall,W. (1962b) Electrophysiology of a dendritic neuron model. Biophys.J. 2:145-167.

Russell,I.J. & Sellick,P.M. (1977) Tuning properties of cochlear hair cells. Nature 267:858-860.

Spoendlin,H. (1974) Neuroanatomy of the cochlea. In: Facts and Models in Hearing, E.Zwicker & E.Terhardt (eds.) Springer-Verlag, N.Y. pp18-36.

Wilson,J.P. (1974) Basilar membrane vibration data and their relation to theories of frequency analysis. In: Facts and Models in Hearing, E.Zwicker & E.Terhardt (eds.) Springer-Verlag, N.Y. pp56-74.

CHAPTER 2: LITERATURE REVIEW

CHAPTER 2

LITERATURE REVIEW

2.0 INTRODUCTION

There is much literature on the peripheral auditory system. One of the most recent and up to date text books is Dallos (1973). It emphasizes cochlear mechanics and gross electrical potentials. As a conference proceedings, Moller (1973) presents a collection of papers on the auditory sytem from periphery to cortex with some psychoacoustics and specialized hearing in non-mammals. Along with these two contemporary books there is Jerger (1973) which is an audiology text book. Henderson, Hamernik, Dosanjh, and Mills (1976) is the proceedings of a conference on the effects of noise on hearing and appears to be the only collection of experimental studies of its kind in one source. Not so recent, but very contemporary in that it sets the style for modern peripheral auditory system research, is the book by Bekesy (1960) which is a collection of his work begun before World War II. On the psychoacoustic side of the ear drum is the text by Fletcher (1953) which characterizes the auditory signal between sound

source and recipient's ear drum, and is a must for understanding the nature of the signal entering the ear. Along with these books is the analysis of the effects of noise on man's auditory sytem, speech communications, and non-auditory system responses such as work performance, sleep, feelings of pain, vision, and blood circulation by Kryter (1970). A further source is two volume collection of lecture notes edited by Tobias (1970,72). A blend of anatomy and physiology on noise damage in the inner ear is given by Hirsh and coeditors (1976).

The collection of contemporary research papers on the peripheral auditory sytem comprises at least a six foot stack of reprints and xeroxed papers. With this collection of work it is impossible to completely predict a first order auditory neuron's response to sound signals of the complexity of speech and to distinguish the role of the two classes of afferent dendrites in the cochlea. The literature review is organized on the basis of technology, with only those reports that are relevant for this study.

Study of the peripheral auditory system began with a long gross anatomical period, devoid of signal measurement techniques. The modern era begins with the advent of five technologies: (1)microdissection and physical transducer techniques, (2)electrophysiological studies, (3)micro-anatomy by use of the transmission and scanning electron microscopes, (4)computer control and analysis for

experiments, and (5)mathematical analysis and simulation studies.

Bekesy (1960,66,71) beginning in 1928 developed dissection and measurement techniques to investigate the motion of the cochlear partition in response to sound. He verified Helmholtz's theory that the partition's mechanical response is best for high frequencies at the base and low ones at the apex.

Wever and Bray (1930) were the first to record an electrical signal from the ear, the gross cochlear microphonic. The first single neuron recordings in the peripheral auditory system were done by Galambos and Davis (1943,44,48) who recorded from higher-order neurons in the cochlear nucleus. The first undisputed demonstrations of responses from single first order neurons was by Tasaki (1954) and Tasaki and Davis (1955), according to Kiang et al (1965).

Although electron microscopes were utilized in science in the 1940's, they were not used on the ear until Engstrom (1958) and Smith and Sjostrand (1961) started the microanatomical investigations of the cochlea. Their reports described two separate types of nerve endings on hair cells. These two types of endings react differently to surgical lesions of the fibers of each type and were shown to be afferent and efferent in origin (Engstrom & Fernandez,1961; Iurato,1962; Kimura & Wersall,1962; Smith

& Rasmussen,1962; Spoendlin & Gacek,1963; Engstrom, Ades, & Andersonn (1966). The scanning electron microscope, first used on the cochlea by Bredberg et al (1972), has been instrumental in revealing the three dimensional structures of the cochlea.

The careful measurement of first order neuron responses to click and tone burst sound stimuli using a laboratory computer (DEC's LINC-8) for analysis was done by Kiang et al (1965).

The fifth technology necessary to accomplish the investigations of the modern era is that of mathematical analysis and simulation. It was Bekesy (1949,60) who started this approach in auditory research. He made mechanical models to simulate the motion of the basilar membrane and demonstrated that the major ingredient for a travelling wave and frequency place resonance is just a change in stiffness of the basilar membrane along its longitudinal axis. Since the conversion of mechanical to neural signals is a physical process, it is only natural that mathematical analysis and simulations have elucidated the process.

The evolution of a sixth technology was necessary as a substrate for all of the above five to occur. Electronics facilitates measurement, imaging, analysis, computer control, and simulation studies. In fact, it is not only the availability of electronic components but the cheapness

and miniaturization of electronics that make the other technologies possible, thus enabling the contemporary work in auditory neurophysiology research.

The literature on the peripheral auditory system divides naturally in two ways. One is by signal processing blocks. The second is into anatomy and signals. Since the the thesis is written in terms of of processing blocks, the anatomy-signals presentation is used here. The anatomical section is presented to portray the enormous understanding gained from careful consideration of structure in the cochlea where signal measurement is a recent phenomena. In contemporay understanding of cochlear function, the linkage of hair cell receptor conductance to membrane displacement as input remains almost solely dependent on anatomical facts and laws of physics without direct measurement of signals. Extensive citation of current cochlear investigations is deferred to the individual signal processing component section to avoid redundancy.

2.1 THE PERIPHERAL AUDITORY SYSTEM

2.1.1 GROSS ANATOMY

To provide roots to the past, a brief historical section is provided. An excellent, but now out of print, survey is given by Bast and Anson (1949) from the Greeks to the advent of the modern era and from which most of this

section is excerpted, except where indicated. Stein (1894) gives a detailed historical summary in German.

The earliest known statement about hearing is attributed to Diogenes (550-460 BC) who stated that perception of sound occurs via the shaking air contained in blood vessels. Hippocrates (460-377 BC) thought that it took place in the external ear passageway and the ear drum. It was Claudius Galen (131-201 AD) who observed the many curved passageways in the temporal bone which he said resembled a labyrinth.

Incrassia (1510-1580), in the Renaissance period, renewed the old Greek teachings about sound. There then followed a long period in which there were anatomical observations that gave rise to many theories, most of which did not survive much later experimental signal measurements in this century. In the interest of origin of fact, the highlights of these anatomical discoveries are presented.

Fallopius, in 1561, observed and labeled the cochlea in the labyrinth.

Coiter, in 1572, recognized the oval and round window.

Eustachio, in 1574, described the Eustachian tube.

Casserio, in 1600, made careful drawings of the ear and ear bones.

Willis, in 1674, destroyed the tympanic membranes of both ears of a dog and found that the dog could still hear.

Kircher, in 1673, described musical instruments of the

time as tubes which were used to increase the volume of sound and the sympathetic vibrations of string instruments. This influenced theories of auditory perception and led to cochlear resonance investigations many years later.

Perrault, in 1680, according to Shambaugh (1930), believed that a structure in the ear cavity vibrated in response to sound.

DuVerney in 1683 was the first to publish drawings of the cochlea with the spiralis ossea, semicanalis tensoris tympani, arteries and vessels of the outer ear, tympanic membrane, the middle ear bones with joint surfaces, and ligaments, and the semicircular canals and their ampullae. According to Shambaugh (1930), DuVerney believed that the lamina spiralis was the vibrating structure, and he located perception of low tones in the basal coil and high tones in the apex, because the bony plate is broader in the basal coil and becomes gradually narrower toward the apex.

Valsalva, in 1704, described the zona cochlea, now known as the cochlear partition.

Ruysch, in 1710, showed that there is no hole in the normal ear drum as was previously supposed.

James Winslow, in 1724, noted that the spiral lamina did not reach to the apex of the cochlea but that the two spaces communicated there.

Cassebohm, in 1735, used a magnifying glass for observing anatomical structures and referred to a fluid in

the ear.

Cotugno, in 1760, definitely proved the presence of a serous fluid in the labyrinth and was the first to associate it with the transmission of sound. He believed that sound waves move the stapes which moves the layrinthine fluid in which the nerves float in the cochlea or in a delicate membrane (zona cochleae). He thought that the two aqueducts drained off the fluid when the stapes is pressed inward.

Caldani, in 1773, cut the round window membane and when pressing on the stapes saw the fluid emerge from the round window.

Scarpa, in 1789, as described by Retzius (1881) and Bast and Anson (1949), used the magnifying glass in his dissections and visualized anatomical structures better by injection of an opaque fluid. He was the first to demonstrate the existence of two fluid filled sacs within the vestibule and canals within the semicircular canals. He did this by exposing the membranous sacs and canals by carefully dissecting away the bone and part of the first turn of the cochlea under a magnifying glass. He also noted that these membranous sacs are firmly anchored to the periosteum by means of fibrous strands of connective tissue.

2.1.2 MICROANATOMY

The old anatomical masters provided the general structure of the outer, middle, and inner ear. The

fine structure of the peripheral auditory system was revealed in the 1800's with the aid of the light microscope and the microanatomical structure in the middle of the 1900's with use of the transmission and scanning electron microscopes. Since structure determines function, structural information gives rise to function theories. Proof of the function theories awaited the signal measurement techniques of the middle 1900's. In accordance with this, only the anatomical facts which proved to be true and the first occurrence of a correct theory are given.

2.1.2.1 LIGHT MICROSCOPE FINDINGS

2.1.2.1.2 ANATOMY

Huscke (1824) observed in the cochlea the ridge of tall cells among which the nerves terminate and believed it to be a sensory papilla similar to that in the ampulla of a semicircular canal. Since he also observed the striae vascularis and the tall cells covering the limbus, he left us with Huschke's papilla, Huschke's teeth, and striae vascularis of Huschke (1835). He (1831) also noted that the inner ear started embryonic development as a pocket of skin.

At this time the concept of specific nerve energies appeared and influenced auditory theory. This is rather remarkable, considering the total lack of instrumentation for signal measurement at that time and is almost trivial

with the ubiquity of today's understanding of signal processing. According to Rutherford (1898), Newton in 1704, although a disbeliever in the wave theory of light, suggested that light induces vibrations in the retina which are transmitted to the brain and there originate the color sensations according to the length of the incoming vibrations. Johanes Muller in 1826 (in Rutherford, 1898) developed the theory of "specific energies" or "specific activities". It is similar to Newton's concept, but it was applied to all the senses. Herman (1878, in Rutherford, 1898) summed it up by saying "... there must, therefore, be at least as many sensory fibers as there are simple qualities of sensation."

Brescht (1836) introduced the terms perilymph and endolymph to describe Cotugno's fluid and Scarpa's fluid. He carefully described the relationship of the scala tympani, scala vestibuli, and vestibule and showed that the perilymph occupies all of the bony labyrinth that is not occupied by the semicircular canals, utricle and saccule. He thought that all of the cochlear space was filled with perilymph and missed the cochlear duct or scala media. He described perilymph as a thin, watery, saline fluid with albumin. He also observed the calcareous deposits and labeled them as otoliths and otoconia. It was suggested that they were dampers for prolonged vibrations.

Reissner (1851,1854) observed the membrane which bears

his name and thus discovered scala media.

Corti (1851) described in detail Huschke's papilla which is now known as the organ of Corti. He also left his name on the pillars of Corti, tunnel of Corti, hair cells (outer) of Corti, and membrane of Corti (tectorial membrane).

Deiters (1860) described the inner hair cells and their supporting cells. Now his name is associated only with the supporting cells.

Claudius (1858) described the cells lining the outer spiral sulcus, now known as the cells of Claudius. He showed also that the basilar membrane is a thin membrane where it spans the tunnel of Corti.

Helmholtz (1863) was stimulated by Corti's analysis of Huschke's papilla. Although the structure of the ear was still poorly understood, which led to certain misconceptions, and Helmholtz missed the scala media in his literature review, he contributed a great leap forward in his development of the resonance theory. He studied in detail the middle ear ossicles and described the ligaments of the malleus and incus. He deduced that the lever arrangement was such that movement of a small force but great amplitude at the ear drum was transformed to a movement of great force and small amplitude at the oval window, where he considered the vibrations to be conducted to the fluid in the labyrinth. He further reasoned that the

cochlear partition moves in response to this. In his own words:

"When the drumskin is driven inwards by increased pressure of air in the auditory passage, it also forces the auditory ossicles inward, as already explained, and as a consequence the foot of the stirrup penetrates deeper into the oval window. The fluid of the labyrinth, being surrounded in all other places by firm bony walls, has only one means of escape ... the round window with its yielding membrane. To reach it, the fluid of the labyrinth must either pass through the helicotrema, the narrow opening at the vertex of the cochlea, flowing over from the vestibular gallery into the drum gallery, or, as it would probably not have sufficient time to do this in the case of sonorous vibrations, press the membranous partition of the cochlea against the drum gallery. The converse action must take place when the air in the auditory passage is rarefied."

He supposed the cochlea to contain a large number of tiny resonators capable of responding to all the tones that can be heard. Each resonator was supposed to stimulate its own special nerve fiber and this, in turn, its own cell in the brain. The pillars of Corti were his candidates for the resonators, since at that time they were thought to be the nerve terminals (in Rutherford, 1898).

Hensen (1863) described the hair of the hair cells as rod like and showed the basilar membrane to be narrowest at the basal end, 41.25 microns, and widest at the apex, 495 microns, and accurately described scala media. In his words:

"When segments of the basilar membrane, depending on their width, are brought in movement by means of incoming tones, then necessarily the papilla (organ of Corti) must also move. The membrane of Corti (tectorial membrane) on the contrary cannot be influenced by such movement because it is attached only on those cells which are supported by the lamina ossea. Thus the "Stabchen" (stiff hairs) are more loosely or more firmly pressed (first those of the outer

cells)--against the mass of Corti's membrane. The question is how through this reduced or increased pressure on the hair a sensation can be elicited."

He was the first to use histological sections on the ear.

Hasse (1870) showned the lack of pillars of Corti in birds and amphibians and that birds can perceive tone. He noted that they have hair cells and a tectorial membrane.

Thus modern notions of hair cell stimulation emerge in the mid 1800's and even today are not completely resolved.

Helmholtz (1885), in the second English edition, acknowledges Hasse's and Hensens's work. He observed from these anatomists that the basilar membrane breaks easily in the radial direction, but the radial fibers have considerable tenacity. From this he suggested that the longitudinal tension is infinitesimal compared to the radial tension and claimed that the laws of their motion should be as if each radial basilar membrane fiber moved independently of all others.

"Consequently any exciting tone would set that part of the membrane into sympathetic vibration, for which the proper tone of one of its radial fibers that are stretched and loaded with the various appendages already described which corresponds most nearly with the exciting tone; and thence the vibrations will extend with rapidly diminishing strength on to the adjacent parts of the membrane."

Thus Helmholtz correctly anticipated Bekesy's experimental measurements over half a century later.

It is interesting that Helmholtz had disregarded the findings of Reissner (1854) and Kolliker (1861) that scala media separated scala tympani and scala vestibuli.

Retzius (1881) described the tectorial membrane as homogeneous and semi-gelatinous with the cilia projecting into or in contact with it.

Rutherford (1887) presented the telephone theory which simply stated that all the hair cells transform the sound vibrations into nerve vibrations and it is the "sensory cells" of the brain which produce the sensations of tone.

There now occurred a long period of little new anatomy until the electron microscopes were applied to the organ of Corti. Since signal measurements were still not available, there arose many theories and much discussion.

Using the light microscope for the initial lesion studies were Baginsky (1883) on dogs and Corradi (1891) on guinea pigs. They destroyed apical portions of the cochlea and observed that the animals responded to high but not to low tones.

Siebenmann (1897) made remarkably accurate camera lucida drawings of the organ of Corti which were verified when the scanning EM came along. He also showed the blood supply originating from the anterior interior cerebellar artery through the auditory nerve to the spiral ganglion and striae vascularis. A review and new results in microcirculation are given by Axelsson (1968).

Of the many theories of cochlea resonance, it was Fletcher (1930) who presented the space time pattern theory, the essence of which endured Bekesy's later investigations.

He suggested that the pitch of a tone is determined by both the position of its maximal stimulation of the basilar membrane and also by the time pattern sent to the brain with position more important for high notes and time for low notes.

Held (1926) and Lorente de No (1937) focused their attention on the innervation pattern of Corti's organ using the silver impregnation methods of Golgi and Cajal. Weston (1939) presented a relevant and still useful discussion of cochlea spiral ganglion comparative anatomy.

2.1.2.1.2 LESION STUDIES

Guild (1919) reported that ears of guinea pigs exposed to revolver shots at close range were found to have damage to hair cells and structural damage to the organ of Corti in the middle turn, fading off to the apical and basal turns.

Guild (1932) and Crowe, Guild, and Polvogt (1934) noted that in human ears with high frequency hearing loss there is marked degeneration of nerves and hair cell loss in the basal turn of the cochlea.

The lesion studies were refined by Schuknecht and Neff (1952) and Schuknecht (1953) who developed a scale in the cat for the maximal response frequency versus location along the basilar membrane.

2.1.2.2 ELECTRON MICROSCOPE FINDINGS

The light microscope investigations of the ear reached the limits of resolution and much detailed anatomy awaited the electron microscope. The first to use the transmission EM was Engstrom (1958) and then Smith and Sjostrand (1961), who analyzed the afferent and efferent nerve endings in guinea pigs. The number of papers starts increasing exponentially at this point, undoubtedly related to the fact that estimates of the percentage of scientists who ever worked, that are alive and working today, is in the order of 95%. Accordingly, only the highlights of the relevant literature are given here, since the analyses in later chapters contain many detailed references to EM findings.

Engstrom (1958) and Engstrom et al (1966) used the EM to investigate fine structure of the sensory papilla, particularly the pattern of hair cells, the surrounding supporting elements, the bundles of nerve fibers and nerve terminals. Also the mapping of cellular and neural elements in noise and drug damaged cochleas were described. This work, particularly the 1966 monograph, is useful in elucidating the afferent and efferent nerve terminals on the hair cells. These investigations were corroborated by Smith (1968) in the chinchilla.

Spoendlin (1963,66,69,70,71a,71b,72,73,79) used the EM to concentrate on the hair cells and innervation of Corti's organ in cat. He sorted out the afferent innervation

details by histological sections in various planes of the organ and counted fibers. These results are discussed in detail in the chapter on the dendrites (6).

An efferent nerve tract from the region of the superior olive in the brain stem was first described Rasmussen (1946). It was not until much later that terminals of these efferents were revealed, principally by the EM (Smith & Sjostrand, 1961; Smith, 1961,1968; Smith & Rasmussen, 1963; Smith, 1967; Kimura & Wersall, 1962; Iurato, 1962; Spoendlin & Gacek, 1963).

Bredberg, Ades, and Engstrom (1972) combined the results of a series of articles over many years using the scanning electron microscope. The scanning EM bridges the gap between the light microscope and transmission EM and is particularly useful in understanding the three dimensional structure of Corti's organ and the relationship between the components.

Bodian (1978) looked specifically for anatomical evidence of neuronal coupling of outer and inner dendrites and did not find any in Old World monkeys.

2.1.3 MECHANICS

The mechanical portion of the peripheral auditory system is divided into the external ear, the middle ear, the basilar membrane, and the organ of Corti.

2.1.3.1 EXTERNAL EAR AND EAR DRUM

The external ear is that portion of the ear on the distal side of the ear drum. Much work has been done in this area. Extensive discussions of the area are found in Jerger (1973) and Dallos (1973). The ear drum has been extensively measured and modelled. Recent work on the ear drum includes Khanna (1970) and Khanna and Tonndorf (1972) who obtained the displacement geometry. Funnell (1975) and Funnell and Laszlo (1978) used the finite element method to model the ear drum and found that a simple model of the ear drum as a plane membrane under tension is able to duplicate many of the measured characteristics qualitatively and proposed a thin isotropic curved shell as a new description of ear behavior. Shaw (1974) measured the frequency response of the sound pressure at the eardrum in humans as a function of free field sounds. In principle one could use his resulting transfer function to obtain sound pressure at the ear drum for a free field input. This would be the input to the model developed in this investigation.

2.1.3.2 MIDDLE EAR

The middle ear by its accessibility is an extensively researched area. Excellent discussions of it are given by Funnell (1972) and Dallos (1973). Borg (1973) investigated the middle ear muscle reflex. Further discussion is found in the detailed analysis of chapter 3.

2.1.3.3 COCHLEAR PARTITION

The cochlear partition experimental measurements come from different sources. Bekesy (1928,1960) started the mechanical measurements by using stroboscopic illumination techniques and verified the place resonance theory of Helmholtz (1896) and standing waves of Ewald (1903). Wilson and Johnstone (1972) measured displacements in guinea pigs using the capacitive probe technique. Johnstone and Boyle (1967) and Rhode (1971) used the Mossbauer effect in squirrel monkeys. Hefelstein (1973) using the Mossbauser technique in cats measured basilar membrane displacement at only the basal end of the cochlea, due to the hardness of the surrounding temporal bone. Rhode and Geissler (1974) showed a nonlinearity in BM displacement for large amplitude of sound.

An excellent mathematical and quite readable detailed treatment of the models for BM displacement is given by Inselberg (1978). It is beyond the scope of this report to review them here, particularly as a dynamic computational model is developed in chapter 3.

2.1.3.4 MECHANICAL TO NEURAL

From measurements of intracellular receptor potentials in hair cells of the lateral line organ (Harris & Flock,1967; Harris et al, 1970), alligator lizard auditory papilla (Weiss, Mulroy, & Altman, 1974; Mulroy, Altman,

weiss, & Peake, 1974) and guinea pig hair cells (Russell & Sellick, 1977), it appears that the hair cell has been unequivocally identified as the receptor cell in the peripheral auditory system. It is interesting that the concept of hair cells as receptor organs and movement of hair cell cilia as a transducer mechanism orginated independently from Hensen in 1863 and Helmholtz in 1863. Their conjecture was derived from purely anatomical observations and 19-th century theory of mechanics. In between came the anatomical verification that afferent cochlear nerve axons originate at hair cells (Lorente de No, 1937). Measurement of cochlear microphonic signals (Weaver & Bray, 1930) provided the first step beyond deductions based on anatomy. After section of the cochlear nerve, the microphonics remain. Recent models of basilar membrane movement depict the membrane in cochlear cross-section bending as an elastic beam (Inselberg, 1978; Allaire, 1972). Rhode and Geisler (1967) and Billone (1973) developed geometrical models for calculating amplitude of the opposing point radial shear displacement as a function of the midpoint basilar membrane displacement. Johnstone and Johnstone (1966) developed a model for hair cell body-to-cilia angle as a function of angular displacement in a variable resistance theory of cochlear potential generation. Laszlo (1968) used this in a lumped model for cochlear potential distribution along the cochlear

partition, which agreed with a large amount of microphonic data. Billone (1973) carefully analyzed the microanatomy and calculated the displacement of the hair cell superior surface with respect to basilar membrane midpoint displacement. He also analyzed the shear force on the hair cell cilia as a function of the relative displacements. This analysis was found to be in phenomenological agreement with differential cochlear microphonic data for low frequencies when the cochlear microphonic produced by a single hair cell is made proportional to forces on its cilia. Correlations of missing hair cells due to noise damage with hearing tests (Hawkins, 1976) and ototoxic drugs with cochlea microphonic response (Dallos, 1973) confirm hair cells as the receptor cells.

What is not unequivocally demonstrated is the means of conversion of basilar membrane movement into conductance at the receptor surface of the hair cell. The anatomy of the organ of Corti in which the hair cells are situated is well known. How the organ of Corti moves as a function of basilar membrane displacement cannot, as of now, be directly investigated. Optimally, one would want a motion picture of how it moves. Since this is not available, let us get an overview of the available theory. It is known that the hair cell receptor potentials are the result of rectification by the cilia (Bekesy, 1953; Flock & Wersall, 1952; Flock et al, 1962; Russel & Sellick, 1977; Mulroy et al, 1974).

Billone (1972,73) presented a rough model for area change of the cuticular free region at the cilia surface of the hair cell. The model requires currently unkown values for stiffness and damping for the cuticular plate attachment via the cuticular free region of the cell top. From investigations of mechanoreceptors, e.g., the muscle spindle (Shepherd, & Ottoson, 1965) and the Pacinian corpuscle (Gray & Sato, 1953), it is generally accepted that mechanoreceptors work by a membrane conductance change in response to a distortion of the membrane (Goldman, 1965). Thus, it seems reasonable that movement of the cilia somehow causes conductance changes in the structure at the top of hair cells. This is substantiated by Flock (1965) who demonstrated directional sensitivity of hair cells in lateral line organs. There is an anatomical basis for mechanical signal rectification (Wersall, Flock, & Lundquist, 1965). The auditory hair cell exhibits rectified receptor potential (Russell & Sellick, 1977). This function of cilia is confirmed by electron microscope pictures showing bent and disarranged hair cilia in guinea pig cochleas exposed to loud noises (Spoendlin,1976). The fact that the cells appear structurally undamaged and have damaged cilia arrays suggests that the cilia are the mechanical input to the hair cell receptor mechanism.

Thus it remains to obtain hair cell conductance as a function of cilia forces or bending angle and the receptor

response of hair cells as a function of conductance changes at the receptor surface.

2.1.4 ELECTROPHYSIOLOGY

2.1.4.1 GROSS POTENTIALS

The first recordings of cochlea signals were made by Wever and Bray (1930) using a gross electrode on the auditory nerve or various parts of the cochlea with a reference electrode in the animal tissue. This was the first recording of the cochlea microphonic signal. Adrian, Bronk, and Phillips (1931) thought that it was "nervous elements" in the cochlea. Guttman and Barrea (1937) showed that this electrical response remained when the nerve was cut. Howe and Guild (1937) found the microphonics in congenitally deaf albino cats, as was done with continued loud sounds by Davis et al (1934, 1935). Thus Stevens and Davis (1938) and Wever (1939) concluded that the microphonics originated from hair cells. Eyster, Bast and Krasno (1937) typified the objections that the microphonics remained when the organ of Corti also had structural damage. With the use of Kanamycin, a drug toxic to hair cells, it was shown that the microphonic disappears in those portions of guinea pig cochleas which have absent hair cells on histological examination (Dallos et al, 1972).

Since the cochlear microphonic is such an accessible

signal, many workers used it as an investigative tool for cochlear function. Much of the quantitative work was done by Dallos and his coworkers and is integrated in his text book (Dallos, 1973). Laszlo (1968,1970) and Kohlloffel (1971) provide mathematical descriptions of the cochlear microphonics along the cochlear partition.

The DC potentials in the cochlear compartments of the cat were measured by Sohmer et al (1971) and correspond with those of other mammals e.g. the guinea pig (Dallos,1973).

2.1.4.2 SINGLE UNIT POTENTIALS

Single neuron recordings in the peripheral auditory system are recordings of action potential occurrences in response to sound signal input typically just distal to the ear drum. These experiments yield overall system input-output responses. The aim of this thesis to develop predictive models for auditory mechanisms, so that they can be put together for an overall model. It is impossible to put all the components together because the relationship between hair cell conductance and cilia forces is missing. However, it is important to note the overall data that must eventually be satisfied. Thus the highlights of the overall input-output data are presented.

As was noted before, the first single auditory nerve axon recordings were by Tasaki (1954) and Tasaki and Davis (1955). Kiang, Watanabe, Thomas, and Clark (1962,1965)

provided the first compendium of auditory nerve recordings. Since then, many other workers have produced data that need to be satisfied by an overall model.

A survey of recent results is presented by Kiang (1968) and Kiang et al (1974). Evans and Wilson (1973) analyze their work and others for interpretation of the neural AP data. Rose et al (1967,71) investigated phase locking and stimulus intensity effects for cochlea axons in squirrel monkey. Work has been done by Sachs and Abbas (1974) in compiling a collection of AP rates versus SPL input levels at different frequencies in cat. All of these investigations indicate that saturating nonlinearities are present. A complete model of the peripheral auditory system must explain these findings.

2.2 EXISTENT OVERALL MODELS

There are two existent peripheral auditory system models. They were done by Weiss (1964) and Klatt (1964). Both reflect the state of knowledge available at that time.

Weiss used a linear mechanical system to represent the outer, middle, and mechanical parts of the inner ear, a nonlinear sigmoid curve for the transducer process, and a probabilistic threshold device with refractory properties for the action potential generation site. The data used to test the model were spontaneous activity, responses to sinusoidal stimuli, and responses to clicks obtained from

cochlear nerve axon recordings. His model demonstrated qualitatively similar results in the form of post-stimulus-time (PST) histogram responses to click input of sound. The predicted PST had a number of peaks with the time between the peaks equal to the reciprocal of characteristic frequency. The values of the intervals were insensitive to amplitude of input clicks, the occurrence times of peaks in response to clicks of opposite polarity were interleaved in time, and the occurrence times of peaks relative to the stimulus onset decreased when the intensity of stimulus was increased. He found that the intensity range required for the appearance of successive peaks in the PST histogram was larger for the model than for the axon data. He thought that the discrepancy was due to the lack of understanding of the actual nonlinear transducer function of the hair cells. The spontaneous rates were matched by calculating parameters in the model for each axon. The AP rate functions in response to sinusoidal input were not extensively matched.

Klatt used an electronic ladder analog to a linear system model for the Peterson-Bogert (1950) model of cochlear partition displacement. The neural part of the system was described by a threshold function with a refractory period corresponding to the neural refractory period. He also took weighted outputs from the primary first order neurons as inputs to second order neurons of the

cochlear nucleus. The second order neurons were also modeled as threshold devices with refractory period. He also included afferent inhibitory fibers from the cochlear nerve to the cochlear nucleus for assessing the degree of sharpening of tuning curves in the nucleus. The investigation concentrated on the output of the second order neurons and did not evaluate the primary neuron response, having utilized the work of Weiss.

Both of these overall models did not have the quantitative experimental measurements of the basilar membrane displacement using the capacitance probe or Mossbauer techniques. The recent understanding of cochlear innervation, hair cell intracellular recording, synaptic function and dendrite geometry, were not available when these models were developed. Thus, incorporation of basic mechanisms of neural devices in a cochlear model could not be expected at that time. These two models are interesting in that that they are able to exhibit as many properties as they do with such a simple structure. The neural elements were lumped into one probabilistic device. However, the neural elements are deterministic when decomposed into their component parts.

2.3 PERIPHERAL AUDITORY PROSTHESES

Medical or surgical treatment of human middle ear hearing loss is now quite common and fairly successful,

while treatment of losses originating in the cochlea or in the higher auditory pathways is almost never successful. There have been attempts to electrically stimulate the cochlea or cochlea nerve in the case of sensorineural hearing loss. One approach is to implant wires of some kind in scala tympani via the round window in an attempt to stimulate the hair cells, synapses, and or dendrites. A second approach is to stimulate the cochlear nerve directly by some kind of wrap-around electrode array, since the afferent part of the nerve rotates, as does the cochlea, to expose the axons such that all the frequencies are represented (Sando, 1965)

Volta (1800) applied about a 50 volt DC potential across two metal electrodes placed in his ears and reported auditory sensations. Subsequently, numerous experiments were attempted, continuing in today's technology. These attempts are reviewed by Simmons (1966,72), Sonn (1972), Michelson (1971,73) and Merzenick et al (1974). work is cited here. Simmons et al (1965) and Simmons (1966) made a well documented study of stimulating the cochlear portion of the eighth nerve with a complex of six stainless-steel electrodes permanently implanted in the modiolus region of a subject with total sensory neural hearing loss in the stimulated ear. He reported that stimulation was perceived as buzzing sounds from about 10 to 65 Hz and and as a steady sound up to about 300 Hz. Pitch discrimination was about 30

Hz in the 50 to 300 Hz range. Pitch discrimination could not be made above 300 Hz. The dynamic range from absolute threshold to discomfort was in the order of 20 dB. As a result, speech perception was impossible. Clark (1970) electrically stimulated cat cochlear nerve and reported that 300 Hz is the upper limit of frequency discrimination. He also reported that stimulation at the base of the cochlea could be recorded at the superior olive for high but not for low frequencies. This suggested that the electric field set up at the basal turn was insufficient to stimulate the apical (low frequency) region. He concluded that "if perceptive deafness is to be treated surgically, electrical stimulation in accordance with the place theory is more likely to be successful," and that "the greatest chance for success is obtained by electrical stimulation of the inner ear, with the electrodes placed close to the terminal fibers of the auditory nerve."

Michelson (1971) implanted bipolar electrodes in scala tympani in four patients with severe sensorineural hearing losses. He used a pair of gold wires inserted to mechanical contact with the tympanic side of the basilar membrane along the basal three-quarter turn. Sinusoidal electrical input to the electrodes produced noise-like sensations in two subjects, while the other reported sensations of pure tone. It is interesting to note that the latter two could distinguish between sine and square wave stimulation;

furthermore, intense amplitude speech signals yielded discrimination performance slightly above chance.

Sonn (1972) and Sonn, Jako and Feist (1971) developed a thin film multiple electrode array for long term scala tympani implantation. The electrode array consisted of 37 platinum conductors formed on both sides of a thin film plastic insulating substrate, produced by photolithographic techniques. The work had progressed through the electrode development, guinea pig tolerence, human subject workup and proposed surgery; but, fate intervened and Sonn died from complications in a gall bladder operation.

Thus, there have been attempts to develop electrical stimulation of the cochlea for sensorineural hearing loss. The results reflect the level of understanding of the neural mechanisms succeeding the mechanical parts. One of the purposes of this thesis is to analyze the neural components with the eventual aim of fitting them into a gross electrical stimulation model to predict the optimal artificial electrical input signal.

Adrian,E.D., Bronk,D.W., & Phillips.G. (1931) The nervous origin of the Wever and Bray effect. J. Physiol. Proc. 73:2P-3P.

Allíare,P.E. (1971) Two dimensional fluid waves and cochlear partition stiffness in the cochlea. Ph.D. Thesis, Northwestern Univ. 162P.

Allaire,P., S.Raynor, & Billone,M. (1974) Cochlear partition stiffness - a composite beam model. J. Acoust. Soc. Am. 55(6):1252-1258.

Axelsson,A. (1968) The vascular anatomy of the cochlea in the guinea pig and in man. Acta Oto-laryngol.Suppl. 243. 134P.

Baginsky,B. (1883) Zur Physiologie der Gehorschnecke. Sitzungsberichte d. Akad. d. Wissensch. 38:685.

Bast,T.H. and Anson,B.J. (1949) The Temporal Bone and the Ear. Charles C. Thomas, Pub. Springfield,Ill. 459P.

Bekesy,G.von (1928) Zur Theorie des Horens; die Schwingungsform der Basilarmembran. Phys.Z. 29:793-810.

Bekesy,G.von (1949) The vibration of the cochlea partition in anatomical preparation and in models of the inner ear. J. Acoust. Soc. Am. 21:233-245.

Bekesy,G.von (1953) Shearing microphonics produced by vibrations near the inner and outer hair cells. J. Acoust. Soc. Am. 25:786-790.

Bekesy,G.V. (1960) Experiments in Hearing. McGraw Hill, N.Y. 745P.

Bekesy,G.von (1966) Pressure and shearing forces as stimuli of labyrinthine epithelium. Arch.Otolaryngol. 84:122-130.

Billone,M. (1972) Mechanical stimulation of cochlear hair cells. Ph.D. Thesis. Northwestern Univ. 229P.

Billone,M. & Raynor,S. (1973) Transmission of radial shear forces to cochlear hair cells. J. Acoust. Soc. Am. 54:1143-1156.

Bodian,D. (1978) Synapses involving auditory nerve fibers in primate cochlea. Proc. Natl. Acad. Sci. USA 75(9):4582-4586.

Borg,E. (1973) On the neuron organization of the acoustic middle ear reflex. A physiological and anatomical study. Brain Res. 49:101-123.

Bredberg,G., Ades,H.W., & Engstrom,H. (1972) Scanning electron microscopy of the normal and pathologically altered organ of Corti. In: Inner Ear Studies, H.W. Ades & H. Engstrom (eds.) Acta Oto-laryng. Suppl. 301:3-48.

Clark,G.M. (1970) A neurophysiological assessment of the surgical treatment of perceptive deafness. Int. Audiol. 9:103-109.

Clark,G.M. (1975) A surgical approach for a cochlear implant; Anatomical study. J. Laryngol. Otol. 89(1):9-15.

Claudius,M. (1858) Ueber das Gehororgan der Cetecien. Kiel. (cited by Bast & Anson, 1949)

Corradi,C. (1891) Uber die Functionelle Wichtigkeit der Schnecke. Arch. f. Ohrenh. 32:1-14. (cited by Bast & Anson, 1949)

Corti,A. (1851) Recherches sur l'organe de l'ouie des Mammeferes. Ztschr. f. Wissenschft. Zool., vol. 3. (cited by Rutherford, 1887)

Crowe,S.J., Guild,S.R., & Polvogt,L.M. (1934) Observations on the pathology of high tone deafness. Bull. Johns Hopkins Hosp. 54:314-379.

Dallos,P. (1973) The Auditory Periphery. Academic Press. N.Y. 548P.

Dallos.P. (1973) Cochlea potentials and cochlea mechanics. In: Basic Mechanisms in Hearing. Moller,A. ed. Academic Press. N.Y. pp335-372.

Davis,H., Derbyshire,A.J., Lurie,M.H., & Saul,L.J. (1934) The electric response of the cochlea. Am. J. Physiol. 107:311-332.

Davis,H., Derbyshire,E.H., Kemp,M.H., & Upton,M. (1935) Functional and histological changes in the cochlea of the guinea pig resulting from prolonged stimulation. J. Gen. Psychol. 12:251-278.

Deiters, O. (1860) Untersuchungen uber die Schnecke der Vogel. Arch. f. Anat., Physiol. u. Wissenschft. Med. pp409-460. (cited by Bast & Anson, 1949)

Engstrom,H. & Wersall,J. (1958) The ultrastructural organization of the organ of Corti and of the vestibular epithelia. Exp. Cell Res. Suppl. 5:460.

Engstrom,H. & Fernandez,C. (1961) Discussion to Catherine A. Smith. Trans. Amer. Otol. Soc. 49:58.

Engstrom,H., Ades,H.W., and Andersonn,A. (1966) Structural Pattern of the Organ of Corti. Almquist & Wiksell, Stockholm. 172P.

Engstrom,H. (1967) The ultrastructure of the sensory cells of the cochlea. J. Laryng. Otol. 81:687-715.

Evans,E.F. & Wilson,J.P. (1973) The frequency selectivity of the cochlea. In: Basic Mechanisms of Hearing, A.R. Moller (ed.) Academic Press. N.Y. pp519-554.

Ewald,J.R. (1903) Zur Physiologie des Labyrinths. VII. Die Erzengung von Schallbildern in der Camer Acustica. Pfluger's Arch. 93:485-500.

Eyster,J.A.E., Bast,T.H., & Krasno,M.R. (1937) The orgin of cochlear potentials. Laryngoscope 47:461-479.

Flock,A. & Wersall,J. (1962) A study of the orientation of the sensory hair s of receptor cells in the lateral line organ of fish, with special reference to the function of the receptors. J. Cell Biol. 15:19.

Flock,A., Kimura,R., Lundquist,P., & Wersall,J. (1962) Morphological basis of directional sensitivity of the outer hair cells in the organ of Corti. J. Acoust. Soc. Am. 34(9):1351.

Flock,A. (1965) Transducing mechanisms in later line and canal organ receptors. Cold Spring Harbor Sympos. Quant. Biol. 30:133-146.

Fletcher,H. (1930) A space-time theory of hearing. J. Acoust. Soc. Am. 1:311-343.

Fletcher,H. (1953) Speech and Hearing in Communication. Van Nostran, Co. N.Y. 461P.

Funnell,W.R.J. (1972) The acoustical impedance of the guinea-pig middle ear and the effects of the middle ear muscles. M.Eng. Thesis, McGill Univ. Montreal. 93P.

Funnell,W.R.J. (1975) A theoretical study of ear drum vibrations using the finite element method. Ph.D. Thesis, McGill Univ., Montreal. 199P.

Funnell,W.R.J. & Laszlo,C.A. (1978) Modeling of the cat eardrum as a thin shell using the finite-element method. J. Acoust. Soc. Am. 63(5):1461-1467.

Galambos,R. & Davis,H. (1943) The response of single auditory-nerve fibers to acoustic stimulation. J. Neurophysiol. 6:39-57.

Galambos,R. & Davis,H. (1944) Inhibition of activity in single auditory nerve fibers by acoustic stimulation. J. Neurophysiol. 7:287-303.

Galambos,R. & Davis,H. (1948) Action potentials from single auditory-nerve fibers? Science 108:513.

Goldman,D.E. (1965) The transducer action of mechanoreceptor membranes. Cold Spring Harbor Sympos. Quant. Biol. 30:59-68.

Gray,J.A.B. & Sato,M. (1953) Properties of the receptor potential in Pacinian corpuscles. J.Physiol.122:610-636.

Guild,S.R. (1919) Deafness and its prevention. Report of the labyrinths of the animals used in testing of preventative measures. J. Lab. & Clin. Med. 4:153-180.

Guild,S.R. (1932) Correlations of histologic observations and the acuity of hearing. Acta Oto-Laryng. 17:207-248.

Guttman,J. & Barrera,S.E. (1937) The electrical potentials of the cochlea and auditory nerve in relation to hearing. Am. J. Physiol. 120:666-670.

Harris,G.G. & Flock,A. (1967) Spontaneous and evoked activity from the Zenopus Laevis lateral line. In: Lateral Line Detectors, P.H. Cahn (ed.) Bloomington,Ind. Indiana Univ. Press. pp135-161.

Harris,G.G., & Frishkopf,L.S., & Flock,A. (1970) Receptor potentials from hair cells of the lateral line. Science 167:76-79.

Hasse (1870) (cited by Bast & Anson, 1949)

Hawkins,J.E. (1976) Patterns of sensorineural degeneration in human ears exposed to noise. In: Effects of Noise on Hearing, Henderson,D., Hamernik,R.P., Dosanjh,D.S. & Mills,J.H. (eds.) Raven PRess. N.Y. pp91-110.

Hefelstein,W.M. (1973) Beitrag zur messung der akustisch bedingten bewegungen und identifikation des mechanischen teils des innenohrs der katze. Abhandlung zur Erlangun des Tiles eines Doktors der techneschen wissenschaften der Eidgenoessischen Technischen. Hochschule, Zuerich.

Helmholtz,H.L.F. (1863) Die Lehre von den Tonempfindungen alss Physiologische Grundlage fur die Theorie der Music. Braunschweig,F. Vieweg und Sohn.

Helmholtz,H.L.F. (1965) The Sensation of Tone, 2nd Ed. Translated by A. J. Ellis. Longmans Green and Co., London.

Henderson,D., Hamernik,R.P. Darshan,S., and Mills,J.H. eds. (1976) Effects of Noise on Hearing. Raven Press, N.Y. 565P.

Hensen,V. (1863) Zur Morphologie der Schnecke des Menschen und der Saugethiere. Ztschr. f. Wissensch. Zool. 13:481-512. (cited by Spoendlin, 1966)

Held,H. (1926) Die Cochlea der Sauger und der Vogel, ihre Entwicklung und ihr Bau. In: Handbook Norm. Pathol. Physiol. Springer, Berlin, Vol. II. pp467-534.

Hirsh,S.K., Eldredge,D.H., Hirsn,I.J., & Silverman,R.S. (eds.) (1976) Hearing and Davis Washington Univ. Press. St.Louis, Mo. 476P.

Howe,H.A. & Guild,S.R. (1933) Absence of the organ of Corti and its possible relation to the electrical auditory nerve responses. Anat. Rec. 55:20-21 (Suppl.)

Huschke,E. (1824) Beitr. zur Physiologie und Naturgechichte. Vol. 1. Ueber die Sinne. Weima, G.H.S. pr Landes-Industrie-Compoirs. (cited by Bast & Anson, 1949)

Huschke,E. (1831) Erste Bildungsgeschichte des Auges und Ohres. Versammlung Naturforscher u. Aerzte zu Hamburg. Isis von Oken, 950P. (cited by Bast & Anson, 1949)

Huschke,E. (1835) Ueber die Gehorzahne, einen eigenthumlichen Apparat in der Schnecke dese Vogelohrs. Arch. f. Anat., Physiol. u. Wissensch. Med. pp335-346. (cited by Bast & Anson, 1949)

Inselberg,A. (1978) Cochlear dynamics: The evolution of a mathematical model. SIAM Rev. 20(2):301-351.

Iurato,S. (1962) Functional implications of the nature and submicroscopic structure of the tectorial and basilar membranes. J. Acoust. Soc. Am. 34(7):1386.

Jako,G.J. (1978) Electrical stimulation of the human cochlea and the flexible multichannel intracochlear electrode. Sympos. Sensorineural Deafness. Otolaryng. Clin. North Am. 11(1):235-240.

Jerger,J. ed. (1973) Modern Developments in Audiology. Academic Press. N.Y. 521P.

Johnstone,J.R. & Johnstone,B.M. (1966) Origin of the summating potential. J. Acoust. Soc.Am. 40:1405-1413.

Johnstone,B.M. & Boyle,A.J. (1967) Basilar membrane vibration examined with the Mossbauer technique. Science 158:390-391.

Johnstone,B.M. & Yates,G.K. (1974) Basilar membrane tuning curves in the guinea pig. J. Acoust. Soc. Am. 55:584-587. Kiang,N.Y.S., Watanabe,T., Thomas,E.C., & Clark,L.F. (1962) Stimulus coding in the cat's auditory nerve. Ann. Otol. Rhino. Laryngol. 71:1009-1027.

Kiang,N.Y.S., Watanabe,T., Thomas,E.C., & Clark,L.F. (1965) Discharge patterns of single fibers in the cats auditory nerve. M.I.T. Press, Cambridge, Mass. 151P.

Kiang,N.Y.S. (1968) A survey of recent developments in the study of auditory physiology. Ann. Oto. Rhino. Laryngol. 77(4):656-686.

Kiang,N.Y.S., (1974) Tails of tuning curves of auditory-nerve fibers. J. Acoust. Soc. Am. 55(3):620-630.

Khanna,S.M. (1970) A holographic study of tympanic membrane vibration in cats. Ph.D. Thesis, City University of N.Y. 214P.

Khanna,S.M. & Tonndorf,J. (1972) Tympanic membrane vibrations in cats studied by time averaged holography. J. Acoust. Soc. Am. 51(6):1904-1920.

Kimura,R. & Wersall,J. (1962) Termination of the olivo-cochlear bundle in relation to the outer hair cells of the organ of Corti in guinea pig. Acta Oto-Larngol. 55:11.

Kohlloffel,L.U.E. (1971) Studies of the distribution of cochlear potentials along the basilar membrane. Acta. Oto-Laryngol. Suppl.No. 288 pp1-66.

Kohlloffel,L.U.E. (1972a) A study of basilar membrane vibrations 1. Fuzziness-detection: A new method for the analysis of microvibrations with laser light. Acustica. 27:49-65.

Kohlloffel,L.U.E. (1972b) A study of basilar membrane vibrations II. The vibratory amplitude and phase pattern along the basilar membrane (post-mortem). Acustica. 27:66-81.

Kohlloffel,L.U.E. (1972c) A study of basilar membrane vibrations III. The basilar membrane frequency response curve in the living guinea pig. Acustica. 27:82-89.

Kolliker,R.A. (1861) Entwicklungschlichte des Menschen under der Hoheren Tiere. Leipzig, W. Engelmann. (cited by Bast & Anson, 1949)

Klatt,D. (1964) Theories of aural physiology. Ph.D. Thesis. Univ. of Michigan. 149P.

Kryter,K.D. (1970) The Effects of Noise on Man. Academic Press. N.Y. 633P.

Laszlo,C.A. (1968) Measurement, modelling and simulation of the cohlear potentials. Ph.D. Thesis. McGill University, Montreal, Canada. 265P.

Laszlo,C.A., Gannon,R. & Milsum,J.H. (1970) Measurement of the cochlear potentials of the guinea pig at constant sound pressure level at the eardrum. I. cochlear-microphonic amplitude and phase. J. Acoust. Soc. Am. 47(4):1063-1070.

Lawrence,M. (1970) Circulation in the capillaries of the basilar membrane. Laryngoscope 80(9):1364-1375.

Lorente de No,R. (1937) The sensory endings in the cochlea. Laryngoscope 47:373-377.

Merzenick,M.M., Schindler,D.N., White,M.W. (1974) Feasibility of multichannel scala tympani stimulation. Laryngoscope 84(11):1887-1893.

Michelson,R.P. (1971) Electrical stimulation of the human cochlea. A preliminary report. Arch. Otolaryngol. 93(3):317-323.

Michelson,R.P., Mezenick,M.M., Pettit,C.R., & Schindler,R.A. (1973) A cochlear prothesis: Further clinical observations; preliminary results of physiological studies. Laryngoscope. 83:1116-1122.

Moller,A.R. ed. (1973) Basic Mechanisms in Hearing. Academic Press. N.Y. 941P.

Mulroy,M.J., Altman,D.W., Weiss,T.F. & Peake,W.T. (1974) Intracellular electric responses to sound in a vertebrate cochlea. Nature 249(5456):482-485.

Peterson,L.G. & Bogert,B.P. (1950) A dynamical theory of the cochlea. J. Acoust. Soc. Am. 22(3):369.

Reissner,E. (1851) De auris internae formatione. Diss Dorpati Livonorum. (cited by Bast & Anson, 1949)

Reissner,E. (1854) Zur Kenntniss der Schnecke im Gehororgan der Saugethiere und des Menschen. Arch. f. Anat., Physiol. u. wissensch. Med. pp420-427. (cited by Bast & Anson, 1949)

Retzius,M.G. (1881) Das Gehorogan der Wirbeltiere. Biologische Untersuchungen, vol. 1; Stockholm, Samson & Wallin, Vol. 2, 1884. (cited by Bast & Anson, 1949)

Rhode,W.S. & Geisler (1967) Model of the displacement between opposing points on the tectorial membrane and reticular lamina. J. Acoust. Soc. Am. 42:185-190.

Rhode,W.S. (1971) Observations of the vibration of the basilar membrane in squirrel monkeys using the Mossbauer technique. J. Acoust. Soc. Am. 49(2):1218-1231.

Rhode,W.S. & Robles,L. (1974) Evidence from Mossbauer experiments for nonlinear vibration in the cochlea. J. Acoust. Soc. Am. 55:588-596.

Rose,J.E., Brugge,J.F., Anderson,D.J., & Hind,J.E. (1967) Phase-locked response to low frequency tones in single auditory nerve fibers of the squirrel monkey. J. Neurophysiol. 30:769-793.

Rose,J.E., Hind,J.E., Anderson,D.J., &Brugge,J.F. (1971) Some effects of stimulus intensity on response of auditory nerve fibers in squirrel monkey. J. Neurophysiol. 34:685-699.

Russell,I.J. & Sellick,P.M. (1977) Tuning properties of cochlear hair cells. Nature 267:858-860.

Rutherford,W. (1887) A new theory of hearing. J. Anat. & Physiol. 21:166-168.

Rutherford,W. (1898) Tone sensation with reference to the function of the cochlea. Lancet, 2:389-394 (New Series).

Sachs,M.B. & Abbas,P.J. (1974) Rate versus level functions for auditory-nerve fibers in cats: tone burst stimuli. J. Acoust. Soc. Am. 56(6):1835-1847.

Sando,I. (1965) The anatomical interrelationships of the cochlear nerve fibers. Acata Oto-Laryngol. 59(5):417-436.

Scarpa,A. (1789) Anatomical disquisitiones de auditu et olfactu. Iicini. (cited by Bast & Anson, 1949)

Schuknecht,H.F. & Neff,W.D. (1952) Hearing losses after apical lesions in the cochlea. Acta Otolaryngol. Stockholm) 42:263-274.

Schuknecht,H.F. (1953) Techniques for study of cochlear function and pathology in experimental animals. Development of the anatomical frequency scale for the cat. A.M.A. Arch. Otolaryngol. 58:377-397.

Shaw,E.A.G. (1974) Transformation of sound pressure level from the free field to the ear drum in the horizontal plane. J. Acoust. Soc. Am. 56(6):1848-1861.

Shepherd,G.M. & Ottoson,D. (1965) Response of the isolated muscle spindle to different rates of stretching. Cold Spring Harbor Sympos. Quant. Biol. 30:95-104.

Siebenmann,F. (1897) Mittelohr und Labyrinth. Bardeleben's Handbuch d. Anat. d. Menschen. No. 5, 1-11, Jena.

Simmons,F.B., Epley,J.M., Lummis,R.C., Guttman,N., Frishkopf,L.D., Harmon,L.D., & Zwicker,E. (1965) Auditory nerve: Electrical stimulation in man. Science 148(3666):104-106.

Simmons,F.B. (1966) Electrical stimulation of the auditory nerve in man. Arch. Otolaryngol. 84:2-54.

Simmons,F.B. (1969) Cochlear implants. Arch. Otolaryngol. 89:87-95.

Simmons,F.B. & Glattke,J.J. (1972) Comparison of electrical and acoustical stimulation of the cat ear. Ann. Otol. Rhino. Laryngol. 81(5):731-738.

Smith,C.A. (1961) Innervation pattern of the cochlea. The internal hair cell. Ann. Otol. Rhinol. Laryngol. 70:504.

Smith,C.A. & Sjostrand,F.S. (1961) Structure of the nerve endings on the external hair cells of the guinea pig cochlea as studied by serial sections. J. Ultrastructure Res. 5:523-556.

Smith,C.A. & Rasmussen,B. (1962) Recent observations on the olivo-cochlear bundle. Ann. Otol. Rhino. Laryngol. 72:489.

Smith,C.A. (1967) Innervation of the organ of Corti. In: Submicroscopic Structure of the Inner Ear, Iurato,S. (ed.) Oxford: Pergamon Press.

Smith,C.A. (1968) Ultrastructure of the organ of Corti. Advan. Science. (june):419-433.

Sohmer,H.S., Peake,W.T., & Weiss,T.F. (1971) Intracochlear potential recorded with micropipets. I. Correlations with micropipet location. J. Acoust. Soc. Am. 50:572-586.

Sonn,M. (1972) An artificial cochlea for the sensory deaf: presurgical developement. Raytheon Co., Portsmouth, R.I. 146P.

Sonn,M. (1974) An artificial cochlea for the sensory deaf: presurgical development. J. Aud. Res. 14:89-108.

Sonn,M.,Jako,G.J.& Feist,W.M. (1971) Deposition of platinum on Teflon and parylene by sputtering. Rev. Sci. Instr. 42:1076-1077.

Sonn,M. & Feist,W.M. (1974) A prototype flexible microelectrode array for implant-prosthesis applications. Med. Biol. Eng. 778-791.

Spoendlin,H.H. & Gacek,R.R. (1963) Electronmicroscopic study of the efferent and afferent innervation of the organ of Corti in the cat. Ann. Otol. Rhin. Laryng. 72(3):660-687.

Spoendlin,H.H. (1962) Ultrastructural features of the organ of Corti in normal and Acoustically stimulated animals. Ann. Otol. 71:657-677.

Spoendlin,H.H. (1966) The organization of the cochlear receptor. Adv. Oto-Rhinolaryng. (Fortschitte der Hals-Nasen-Ohrenheilkunde) Vol. 13 227P.

Spoendlin,H.H. (1969) Innervation patterns in the organ of Corti of the cat. Acta Otolaryngol. 67:239-254.

Spoendlin,H.H. (1970) Structural basis of peripheral frequency analysis. In: Frequency Analysis and Periodicity Dectection in Hearing. Plomp,R, Smoorenburg,G.F., & Soesterberg,J. (ed.) Sijthoff, Leiden. pp1-40.

Spoendlin,H.H. (1971a) Degeneration behavior of the cochlear nerve. Arch. klin. exp. Ohr., Nas. u. Kelilk. Heilk. 200:275-291.

Spoendlin,H.H. (1971b) Primary structural changes in the organ of Corti after acoustic overstimulation. Acta Otolaryngol. (Stockh.) 71:166-186.

Spoendlin,H.H. (1972) Innervation densities of the cochlea. Acta Otolaryngol. 73:235-248.

Spoendlin,H.H. (1973) The innervation of the cochlear receptor. In: Basic Mechanisms in Hearing, Moller,A. (ed.) Academic Press. N.Y. pp185-234.

Spoendlin,H.H. (1974) Neuroanatomy of the cochlea. In: Facts and Models in Hearing. Zwicker,E. & Terhardt,E. (eds.) Springer-Verlag. N.Y. pp18-36.

Spoendlin,H. (1976) Anatomical Changes following various noise exposures. In: Effects of Noise on Hearing. Henderson,D., Hamernik,R.P., Dosanjh,D. & Mills,J. (eds.) Raven Press, N.Y. pp69-90.

Spoendlin,H.H. (1979) Neural connections of the outer haircell system. Acta Otolaryngol. 87:381-387.

Stein, Stanislaus von (1894) Funktionen der Einzelen Theile des Ohrlabyrinth. (Original in Russian, 1892) Translated into German in 1894 by Dr. C. von Krzywicki. Jena, Gustav Fischer.

Stern,L.W. (1895) Die Literature uber die nicht-Akustische, Function des Inneren Ohres. Arch.F.Ohern Heilk. 13(14). (cited by Bast & Anson, 1949)

Stevens,S.S. & Davis,H. (1938) Hearing. Its Psychology and Physiology. Wiley & Sons, Inc. N.Y.

Tasaki,I. (1954) Nerve impulses in individual auditory nerve fibers of guinea pig. J. Neurophysiol. 17:97-122.

Tasaki,I. & Davis,H.,H. (1955) Electric responses of individual nerve elements in cochlea nucleus to sound stimulation (guinea pig). J. Neurophysiol. 1 8:151-158.

Tobias,J.V. (1970) Foundations of Modern Auditory Theory, Vol. 1. Academic Press. N.Y. 462P.

Tobias,J.V. (1972) Foundations of Modern Auditory Theory, Vol. 2. Academic Press. N.Y. 550P.

Volta,A. (1800) On the electricity excited by the mere contact of conducting substances of different kinds. Trans. Roy. Soc. Phil. 1(90):403-431.

weston,J.K. (1937) Observations on the distribution of ganglion cells and fibers related to the saccule and the basal coil of the cochlea. Acta Neerlandica Morphol. Normalis Pathologicae. 1:136-150.

weston,J.K. (1939) Notes on the comparative anatomy of the ganglion cells associated with the vertebrate inner ear sensory areas. J. Anat. 73:263-238.

weiss,T.F. (1964) A model for firing patterns of auditory nerve fibers. Tech. Rep. No. 418. Res. Lab. Electronics. PH.D. Thesis, M.I.T. Cambridge, Mass.

weiss,T.F. (1966) A model of the peripheral auditory system. Kybernetik 3 Bd., Heft 4:153-175.

weiss,T.F., Mulroy,M.J., & Altman,D.W. (1974) Intracellular responses to acoustic clicks in the inner ear of the alligator lizard. J. Acoust. Soc. Am. 55(3):606-619.

wersall,J., Flock,A., & Lundquist,P.G. (1965) Structural basis for directional sensitivity in cochlear and vestibular sensory receptors. Cold Spring Harbor Sympos. Quant. Biol. 30:115-132.

wever,E.G. (1939) The elecrical responses of the ear. Psychol. Bull. 36:143-187.

wever,E.G. & Bray,C.w. (1930) Auditory nerve impulses. Science 71:215.

Wilson,J.P. & Johnstone,J.R.(1975) Capacitive prove measures of basilar membrane vibration. In: Symposium on Hearing. IPO, Einthoven, The Netherlands. pp172-181.

CHAPTER 3: AUDITORY SYSTEM MECHANICS

CHAPTER 3
AUDITORY SYSTEM MECHANICS

3.0 INTRODUCTION

The aim of this chapter is to describe the chain of signal processing from the ear drum through the (1)middle ear, (2)basilar membrane, and (3)mechanical part of Corti's organ. The available experimental data and analytic descriptions are described and evaluated to find the best set of equations for an overall model. The precepts in choosing these descriptions are (1)they fit the experimental data and (2) they are computationally tractable. It is necessary that the steady state descriptions in the literature be redeveloped in dynamic form. The emphasis on the conditions from which the the equations arise is not to be underestimated as the equations can be considered accurate only under these controlled experimental circumstances. Consequently, the obsession with experimental conditions is warranted. The availability of the mechanical analyses is a prerequisite for the investigation of the neural signal processing mechanisms.

3.1 MIDDLE EAR

3.1.0 INTRODUCTION

The starting point in an overall computational model is the air pressure signal in time that reaches the ear drum. This point is chosen because the signal is delivered here by the commonly used acoustical ear bar with probe tube microphone utilized in animal experiments. Sound characteristics are as conventionally measured just distal to the ear drum in animal experiments.

The detailed block diagram of figure:3.1.0 shows the pertinent variables for the middle ear. The time varying air pressure signal, P(t), strikes the ear drum causing a volume displacement velocity of the ear drum, VVED(t), from which the displacement of the manubrium, DM(t), initiates movement in the ossicular chain, then displacement of the stapes, DS(t).

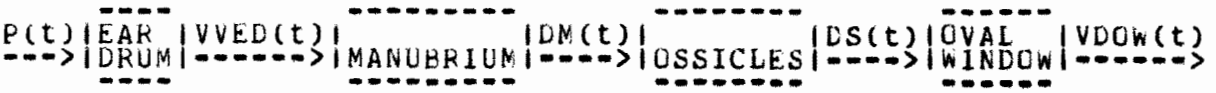

Figure:3.1.0 Detailed block diagram of the middle ear.

3.1.1 EXPERIMENTAL DATA

If one takes sound pressure at the ear drum, P(t), as input and displacement of the stapes, DS(t), as output, then a functional characterization of the middle ear is possible. If the ratio of maximum stapes displacement to maximum sound pressure amplitude and the phase angle, θ, between these two variables are measured, then a complete description of the transfer properties of the middle ear is achieved, in so far as the middle ear acts as a linear system. Guinan and Peake (1967) made these measurements in cat and demonstrated that it is a linear system. They used barbiturate anesthesia (DIAL) which eliminates middle ear muscle contractions (Simmons,1959; Carmel & Starr, 1963; Baust & Berlucchi, 1964). Thus their measurements apply only to conditions in which the middle ear muscles are in a relaxed state. The method was to present a sinusoidal signal of frequency f, via an ear bar at the tympanic ring with the pinna and external auditory canal amputated. The sound pressure was monitored by a condenser microphone attached to a probe tube that was a few millimeters from the tympanic membrane. The bulla was opened, using a ventral approach, and the stapes sprayed with small (<2mu) particles of silver. Stapes displacement was measured by using stroboscopic illumination and observing the location of the lighted silver particles through a light microscope. They

found the displacements of the stapes to be pistonlike, that is, in and out along its long axis.

Their measurements indicate that stapes displacement is an approximately linear function of sound pressure up to 130 dB SPL for frequencies below 2000 Hz and to higher SPL for frequencies above 2000 Hz. For amplitudes above these levels, the increase of stapes displacement with increasing sound pressure became increasingly nonlinear.

The output variable, stapes displacement, DS(t), pushes the oval window in and out, as a "drum head". The oval window then increases and decreases the pressure in the scala vestibuli of the cochlea. Since the oval window generates compression and rarefaction waves in the perilymph, the fluid of the scala vestibuli, it is a hydraulic system where the appropriate variable is volume displacement of the oval window, VDOW(t) (Dallos, 1973, p98). Now the volume displacement of the oval window is A*DS(t), where A is the area of the stapes footplate. The input to the model for basilar membrane displacement is volume displacement of the oval window rather than stapes displacement. Guinan and Peake determine an average wet stapes footplate area of 1.26 mm^2 from four cat stapes. This agreed with Wever, Lawrence, and Smith (1948).

Since the middle ear input-output variables are linearly

related for normal physiological input range (less than 90 dB SPL), it is possible to use the transfer function method. The transform method for this model has the useful property that given the amplitude and phase frequency response curves for a linear system, it is possible to derive the differential equation that describes the system (Wiley, 1960, Ch 8). The differential equation is then available to predict the dynamic response of the system to an input which is not a sine wave.

Let the variables be defined as follows:

t = time

P(t) = air pressure just distal to the ear drum (< 3mm.)

VDED(t) = volume displacement velocity of the ear drum

$= D_t VVED(t)$

where D_t denotes the derivative with respect to time

DU(t) = displacement of the umbo

DS(t) = displacement of the stapes footplate for piston motion

A = area of stapes footplate

VDOW(t) = volume displacement of the oval window

For a bounded piecewise continuous function, x(t), with x(t)=0 for t<0, let the Laplace transform of x(t) be denoted as

$$L(x(t)) = \int_0^{\infty} x(t)*e^{-s*t}\,dt$$

The block diagram of the middle ear can be condensed to conform with the experimental curves of Guinan and Peake. It now takes the following form.

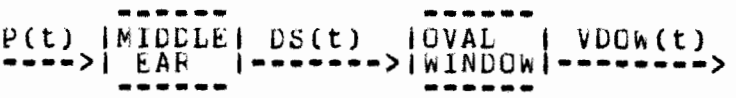

In Laplace transform notation, the block diagram becomes:

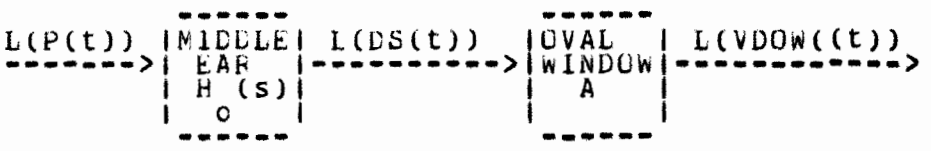

$H_o(s)$ = transfer function of the ear drum and ossicles.

$$= \frac{L(DS(t))}{L(P(t))}$$

$$L(VDOW(t)) = L(A*DS(t))$$

$$= A*H_o(s)*L(P(t))$$

and the overall transfer function of the middle ear

$$H_{me}(s) = A*H_o(s)$$

The response curves of the middle ear given by Guinan and Peake (1967) are in the form

$$\log_{10}\left|\frac{DS_{pp}}{P_{rms}}\right| \text{ versus f and } \log_{10}\left|\frac{VDOW_{pp}}{P_{rms}}\right| \text{ versus f}$$

It is required that these experimental curves be related to the amplitude response curves of the Laplace transform. That is, one needs to evaluate

$$\log_{10}\left|\left| H_{me}(s) \right|\right| \quad \text{versus } t$$

and

$$\theta = \text{Arctan}\left[\frac{\text{Im}(H_{me}(s))}{\text{Re}(H_{me}(s))}\right] \quad \text{versus } f$$

where $s = i*2*pi*f$ and $||x||$ denotes the magnitude of a complex number. Observe that $H_{me}(s) = ||H_{me}(s)||*\exp(i*\theta)$. Using the properties of complex variables and the complex norm, it can be shown that

$$||H_{me}(s)|| = \frac{VDOW_{max}}{P_{max}} \Big|_{f}$$

$$= \frac{1}{2\sqrt{2}} * \frac{VDOW_{pp}}{P_{rms}} \Big|_{f}$$

$$= \frac{1}{A*2\sqrt{2}} * \frac{DS_{pp}}{P_{rms}} \Big|_{f}$$

The peak to peak (pp) measurements were the ones plotted and P(t) is usually measured as sound pressure level, SPL, which by definition means the rms value. Figure:3.1.1.1 shows $\log_{10}(DS_{pp})$ versus $\log_{10} f$, at P_{rms}=120 dB SPL and θ versus $\log_{10} f$, for the bulla and septum open (bso). The bulla and septum were open because it was necessary to remove them to see the ossicles.

It has been well demonstrated (Møller,1963; Onchi,1961; Mundie,1963; webster,1962; Møller,1965; Tonndorf et al,1966; Benson & Eldridge,1955) in several species that altering middle ear cavities can have appreciable effects on the transmission of the middle ear. As a result of this, Guinan and Peake, in the previously cited study, studied the effects of opening the bulla and removing the bony septum in the cat.

Their procedure was to record a cochlear microphonic electric response with a gross electrode on the round window and reference electrode in neck muscle. They obtained an average round window response at a given sound pressure and a number of frequencies with the bulla and/or septum closed shown in figure 3.1.1.2a. After opening the bulla (or septum), the sound pressure level was adjusted at each frequency until the averaged electric response was the same amplitude that it had been before opening shown in figure 3.1.1.2b. The averaged round window responses and sound pressure signals were then recorded for the new condition. The effect of the opening was obtained from the ratios of the sound pressure amplitudes and from the the phase shifts in the two signals. The round window is usually approached by opening the bulla. So to measure the effect of opening the bulla, they recorded the electric response with a wire placed

outside the bulla (Rosenblith & Rosenzswig, 1951) or by closing the bulla after placing the wire near the round window. The results from both techniques agreed. The curves obtained for stapes motion with the bulla and bony septum open were combined with the curves for the effect of opening the bulla and bony septum, using the method of "constant response" (op.cit.p1250). It can be shown using the rules of complex variables that (bso = bulla & septum open, c = bulla & septum closed)

$$H_{bso}(s) = H_{c}(s) * \frac{L[P(t)_{c}]|_{s}}{L[P(t)_{bso}]|_{s}}$$

Taking magnitudes and $\log_{10}$ of both sides, with rearrangement gives

$$\log_{10}||H_{c}(s)|| = \log_{10}||H_{bso}(s)|| - \log_{10}\frac{|P_{max}|_{c}|_{s}}{|P_{max}|_{bso}|_{s}} \qquad (1)$$

using Arctan instead of log and magnitude gives

$$\text{Arctan}[H_{c}(s)] = \text{Arctan}[H_{bso}(s)] - \text{Arctan}\frac{|P_{max}|_{c}|_{s}}{|P_{max}|_{bso}|_{s}} \qquad (2)$$

where Arctan[z] = arctan(Im(z)/Re(z)).

Now equation (1) is just the magnitude curve (right hand scale) figure:3.1.1.1 minus the curve of figure:3.1.1.2b. Similarly, for the phase angle of equation (2), the phase angle is just the phase angle of figure:3.1.1.1 minus that of

figure 3.1.1.2b. The result is shown in figure:3.1.1.3. Similarly, the magnitude and phase plots for $H_{bo}(s)$, the middle ear transfer function with only the bulla open, can be deduced.

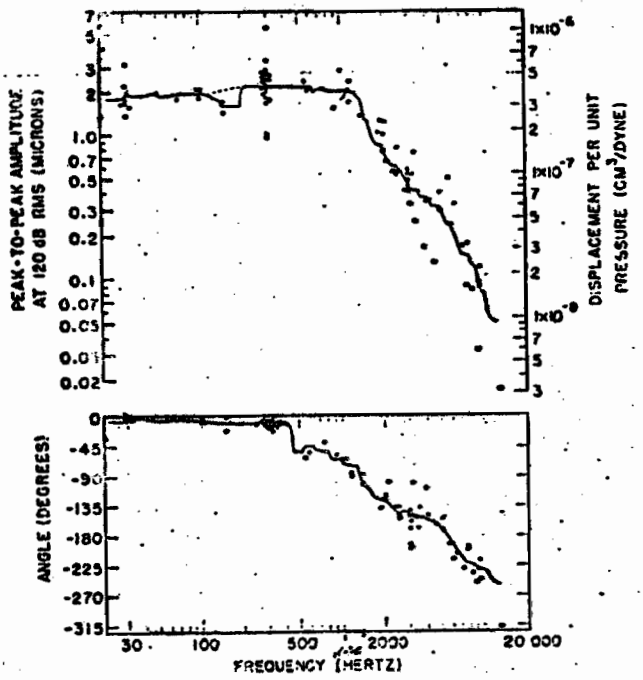

Figure:3.1.1.1 $\log_{10}(DS_{pp})$ versus $\log_{10} t$ at P_{rms} dB SPL and θ verus $\log_{10} t$ for bulla and septum open. From Guinan & Peake (1967).

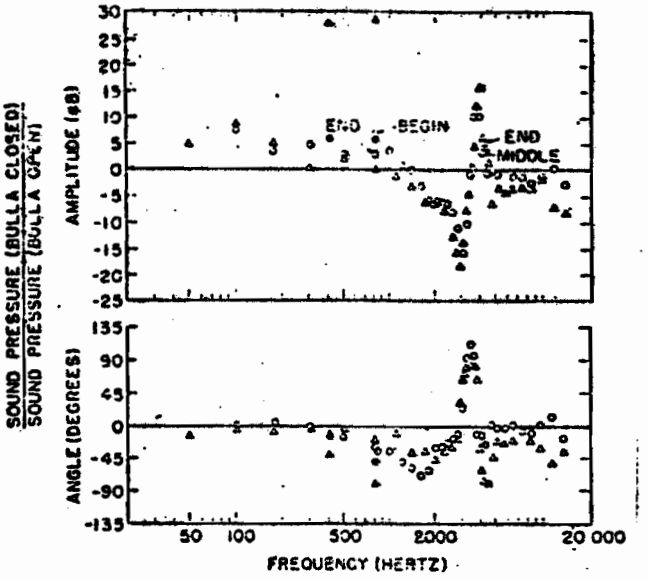

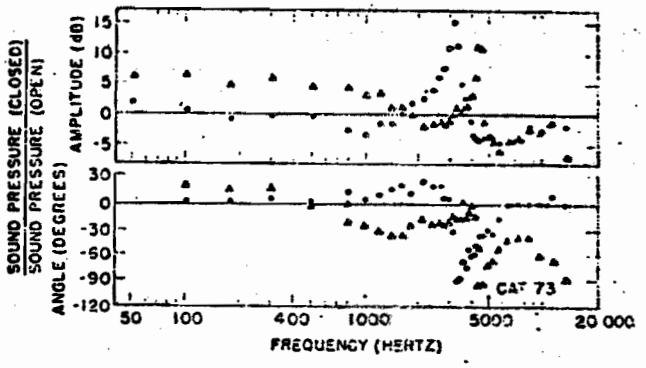

Figure:3.1.1.2 Round winddw electric response. $\text{Log}_{10}(V_{pp})$ versus $\text{log}_{10} f$ and θ verses $\text{log}_{10} f$. (a)Bulla and septum closed. (b)Bulla and septum open. From Guinan & Peake (1967).

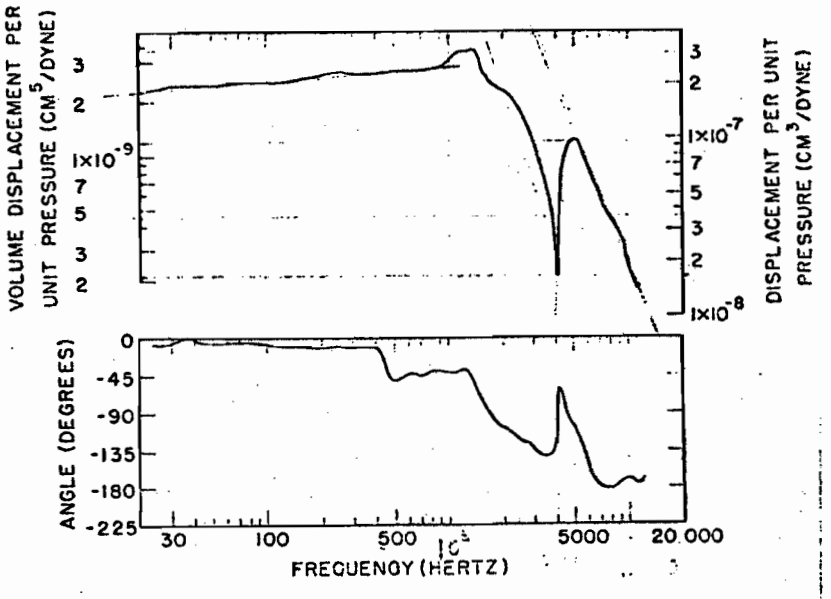

Figure:3.1.1.3 Overall frequency response curves for middle ear with bulla and septum closed. From Guinan & Peake (1967).

3.1.2 DYNAMIC DESCRIPTION

The experimental data presented in the previous section is for a steady state situation with sine waves as driving functions. It was also shown that the system is linear. That is, the ratio of oval window volume displacement to ear drum sound pressure is a constant number, for each one input frequency in the the cat's audible range. Using the frequency response curve and phase plot, one can fit these curves by a transfer function that is the ratio of two polynomials (Kuo,1967,chpt 2). Then by taking the inverse transform of this curve fitted transfer function, the corresponding linear differential equation describing the system is obtained. A variation of this approach is to consider the physical blocks of the system with their impedances, then derive the transfer function. Magnitude of the transfer function can be fitted to the amplitude response curve by suitable calculation of the constants to fit the curves. This approach was utilized by Peake and Guinan (1967). This approach is followed here in modified form.

Recall the acoustical-mechanical-electrical analog correspondences (Wiley,1960).

sound pressure <=> force <=> voltage

volume velocity <=> displacement velocity <=> current

Here a modified (Funnell,1972) form of Peake and Guinan's

block diagram of the middle ear is utilized and is shown in figure:3.1.2.1. The first block stands for the volume of the external ear that is between the sound source and the ear drum. The volume velocity leaving this block passes through the eardrum into the middle-ear cavities. Some of the volume velocity enters the malleo-incudal complex; then through the incudostapedial joint, then to the stapes and the cochlea.

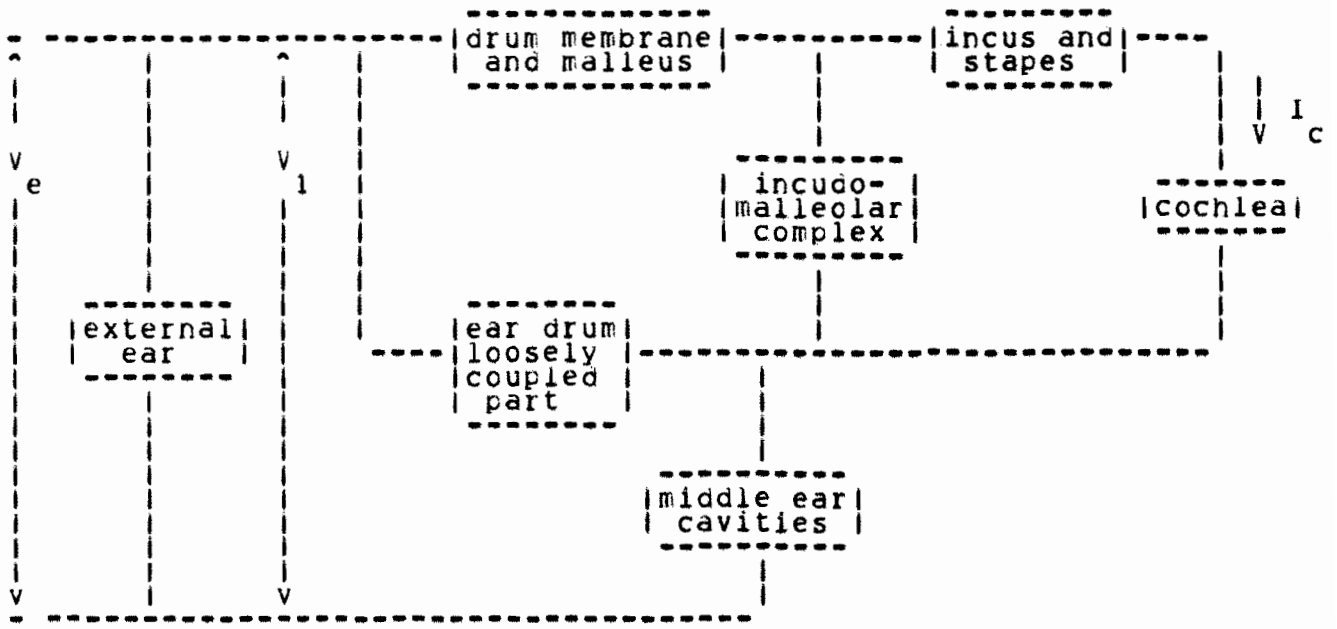

Figure:3.1.2.1 The overall block diagram of the middle ear modified after Funnell (1972) from Peake and Guinan (1967). V_e is sound pressure level at the external ear, V_1 is sound pressure at the ear drum, and 1_c is volume velocity of the oval window.

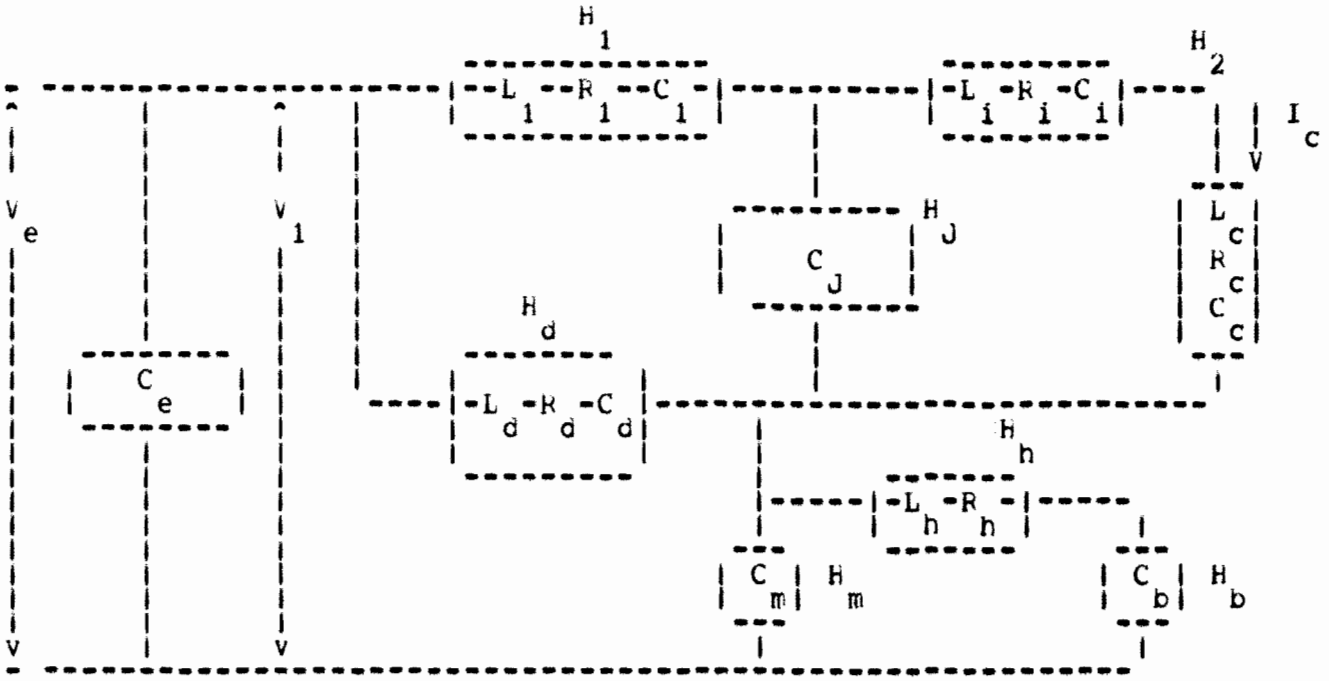

Figure:3.1.2.2 Acoustical circuit model of middle ear. H_1 is the impedance of the ear drum and malleus, H_d is the impedance of the ear drum (loosely coupled part), H_2 is the lumped impedance of the incus and stapes complex and the cochlea, H_h is the impedance of the hole connecting the middle ear cavity and H_b is the impedance of the bulla cavity. V_1 is the sound pressure level at the ear drum and I_c is the volume velocity of the oval window.

The modelling of the cavities is done by identifying distinct chambers as capacitors and the passages between the chambers as an inductor and resistor in series. The incudo-malleolar joint is taken to be predominantly compliant (Peake & Guinan,1967) and the other blocks taken as acoustical RLC branches. The resultant acoustical circuit model is shown in figure:3.1.2.1&2. The definition of the variables is given below:

I_c = volume velocity of oval window

V_1 = input sound pressure at ear drum

L_1 = inertia of ear drum and malleus

R_1 = resistance "

C_1 = compliance "

L_i = inertia of incus and stapes

R_i = resistance "

C_i = compliance "

L_c = inertia of cochlea

R_c = resistance "

C_c = compliance "

$L_2 = L_i + L_c$

$R_2 = R_i + R_c$

$(C_2)^{-1} = (C_i)^{-1} + (C_c)^{-1}$

L_h = acoustic mass of hole connecting ectotympanum to bulla cavity

R_h = acoustic resistance of hole connecting ectotympanum to bulla cavity

C_b = compliance of air in bulla cavity (entotympanum)

C_m = compliance of air in middle ear cavity (ectotympanum)

C_J = compliance of incudo-malleolar joint

H_h = lumped impedance of the hole connecting bulla and middle cavities

H_m = impedance of the middle ear cavity

H_b = impedance of the bulla cavity

The relationship of interest is volume velocity of the oval window versus sound pressure at the ear drum. That is,

$$\frac{I_c}{V_1} = \frac{L[VDOW(t)]}{L[P(t)]}$$

By consideration of figure:3.1.2, note that opening the bulla makes $H_b=0$ or equivalently $C_b=\infty$, which gives us $H_{me}(s)=H_{bo}(s)$. Opening both the bulla and septum gives $H_m=0$, thus $H_{me}(s)=H_{bso}(s)$. with the bulla and septum intact, $H_{me}(s)=H_c(s)$, by notation of the previous section.

Since in Laplace transform theory, impedances add algebraically, the impedance with the bulla and septum intact is

$$H_c(s) = \frac{(H_m + H_h + H_b)(H_J)}{(H_J)^2 (H_m + H_h + H_b) - [(H_1 + H_J)(H_m + H_h + H_b) + H_m (H_m + H_h + H_b)](H_J + H_2)}$$

$$= \frac{A_2 s^2 + A_1 s + A_0}{B_4 s^4 + B_3 s^3 + B_2 s^2 + B_1 s + B_0} = \frac{L[VDOW(t)]}{L[P(t)]}$$

where

$A_2 = L_h / C_J$

$A_1 = R_h / C_J$

$A_0 = (C_m^{-1} + C_b^{-1}) / C_J$

$B_4 = -L_1 L_h$

$B_3 = -(R_1 L_h + L_1 R_h)$

$B_2 = (C_J^{-1} L_h) - [L_1 (C_m^{-1} + C_b^{-1}) + R_1 R_h + (C_1^{-1} + C_J^{-1} + C_m^{-1}) L_h]$

$B_1 = (C_J^{-1} R_h) - [R_1 (C_m^{-1} + C_b^{-a}) + C_J^{-1} R_h + (C_1^{-1} + C_J^{-1} + C_m^{-1}) R_h]$

$B_0 = C_J^{-1} (C_m^{-1} + C_b^{-1}) - (C_1^{-1} + C_J^{-1} + C_m^{-1})(C_m^{-1} + C_b^{-1}) + (C_b^{-1})$

The Bode plots for $H_c(s)$ are shown in figure:3.1.1.3. The inverse Laplace transform of

$$\sum_{n=0}^{4} B_n s^n \, L[VDOW(t)] = \sum_{n=0}^{2} A_n s^n \, L[P(t)]$$

yields the differential equation for this system.

$$\sum_{n=0}^{4} B_n D_t^{(n)} VDCW = \sum_{n=0}^{2} A_n D_t^{(n)} P$$

For the bulla open and septum closed, the impedance is that for H_{me} with $H_b=0$, and the differential equation follows, mutas mutandi. Likewise, for bulla and septum open, $H_m=0$ and $H_m=0$.

I did the algebra to derive the constants from the steady state model and calculated them finding that they agree with those values published (Peake & Guinan,1967).

$C_1 = 7.6*10^{-1}$ Farads

$C_2 = C_1$

$R_1 = 0.0$ Ohms

$R_2 = 390$ Ohms

$L_2 = 0.72*10^{-2}$ Henries

$L_1 = 2.24*10^{-2}$ Henries

$C_J = 0.45*10^{-2}$ Farads

$L_h = 1.4 *10^{-2}$ Henries

$R_h = 22$ Ohms

$C_b = 3.0 *10^{-7}$ Farads

$C_m = 1.9 *10^{-7}$ Farads

3.2 BASILAR MEMBRANE

3.2.1 STRATEGY OF THE BM MOTION MODEL IN CAT

The input to the hydromechanical system driving the basilar membrane model (BMM) is volume velocity of the oval window, VVOW(t). The output is D(x,t) displacement of the basilar membrane at location x, measured from the oval window, at time t. The only available cat data (Hefelstein,1974) is at one location on the partition near the basal end, due to the hardness of cat temporal bone. This is resolved by adapting experimental and modeling results from species with structurally identical organ of Corti, except for length differences. To effect this strategy, the "maximum response frequency map" of the cat basilar membrane is utilized. This mapping is given by the function MRF(x) which gives the frequency that produces the maximum BM displacement at location x, for a sinusoidal input signal. For the cat, this function is available from lesion studies (Schuknecht & Neff, 1952; Schuknecht, 1953).

There are several experimental and theoretical studies available for BM displacement. This model utilizes the Mössbauer measurements (Rhode,1971; Rhode & Robles,1974). These measurements show nonlinearities in displacement of the BM with respect to displacement of the stapes. These nonlinearities have been fitted by Kim (1972) and Kim et al

(1973) using normalized displacement in a system of nonlinear differential equations. This approach is used here, but with the addition of proper displacement based on the analysis of Wilson (1974) which revealed that the ratio of BM displacement to stapes displacement versus frequency is very close for all mammals on which measurements are available. Thus it is possible to produce a function D(x,t) versus VVOW(t) that is accurate and computationally efficient enough to be suitable for simulation.

3.2.2 THE MRF FUNCTION

The basilar membrane has been shown to be constructed such that each location x measured from the oval window has a frequency associated with it that produces the greatest displacement when compared to all other frequencies with the same input amplitude. This was first discovered by Bekesy (1947) using direct optical measurement of displacement and all subsequent measurements of BM displacement in mammals have only resulted in an improvement in accuracy. Schuknecht and Neff (1952) and Schuknecht (1953) in cat organ of Corti using restricted surgical lesions with conditioned response measurements of audiograms, followed by histological localization of the lesions, produced a functional relationship between frequency and position along the basilar

membrane in cat. The direct measurement of displacement versus location in the cat is, as of now, unmeasured.

The version of the function which this analysis uses is

$$f = MBF(x)$$
$$= (52.0*10^{3})(0.00357)^{(x/L)}$$

were x is distance from the basal end of the cochlea in mm. and L is length of the basilar membrane in mm. The value used is 23.0mm. This function is from Kiang, Moxon and Levine (1970,p245) and is based on Schuknecht's curve B (Schuknecht,1953).

3.2.3 KIM'S NONLINEAR BM MODEL

A dynamic model for the displacement of the basilar membrane in time, at a fixed distance from the oval window, is developed here. The model is based on the nonlinear model of Kim (1975); however, the output is in real displacement units and attention is paid to detail in quantifying the nonlinear characteristics of displacement. This is done for locations whose maximum response frequency (MRF) is greater than 500 Hz.

When the displacement of the BM at a point is examined, it is found that normalized frequency response curves are remarkably similar in shape. Representation of the frequency response of different points on the BM is possible by normalizing the stimulus frequency relative to the maximum response frequency (MRF) of the point, with the parameters of the model held constant. Flanagan (1964) used this approach to develop a linear model for BM displacement. This approach is used here.

The frequency response curves of Rhode (1971), as shown in figure:3.2.3.1, are used as representative curves because the stimulus amplitudes are within the normal dynamic range of the auditory system (< 90 dB SPL). Furthermore, when the phase response of the points on the BM are considered, and the $\log_{10}(f)$ axis is normalized with respect to MRF, the curves have the same shape.

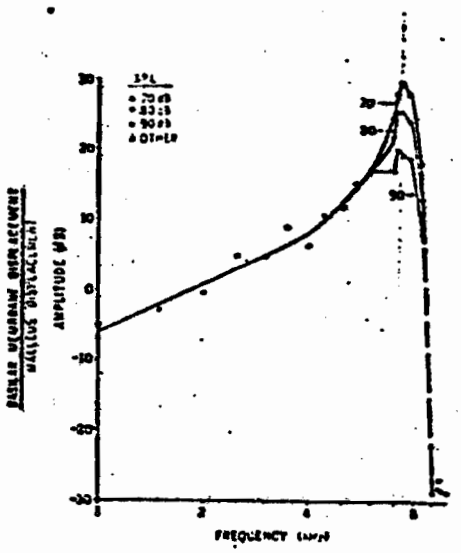

Rhode (1971)

Figure:3.2.3.1 Basilar membrane frequency response curves. From Rhode (1971).

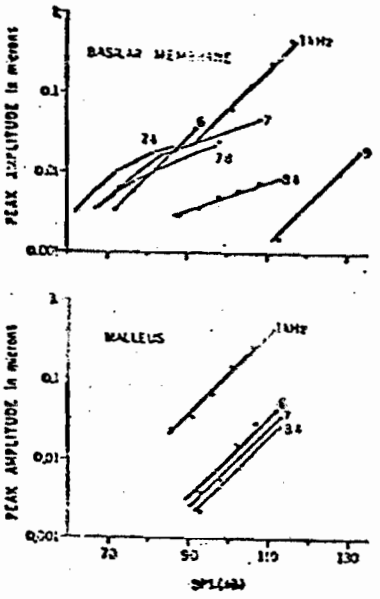

Figure: 3.2.3.2 Nonlinearity of the basilar membrane demonstrated by frequency responses shown at different input amplitude levels. From Rhode (1971).

Since the experimental measurements of BM displacement are with respect to stapes displacement and DS=VVCW/A, DS is used in the following computational model. Output is displacement of the BM at distance X_b from the base at time t, $DBM(X_b,T)$. In developing the model, the time scale is normalized with respect to the period of the MRF for the BM point under consideration. This dimensionless time is denoted by $\underline{t}$. Also the amplitude scale of the input and output are normalized. The variables are listed below.

t = time (millisec.)

MRF = maximum response frequency at location x_B (Hz)

x_b = distance on basilar membrane from base (mm.)

x_a = distance on basilar membrane from apex (mm.)

= LBM - x_b

LBM = length of basilar membrane

= 23.0 mm.

TMRF = period of MRF at location x_b (sec.)

= 1/MRF

$\underline{t}$ = time normalized with respect to TMRF (dimensionless)

= t/TMRF = t*MRF

DS = displacement of stapes

$\underline{DS}$ = displacement of stapes with respect to DS0

= DS/DS0 (dimensionless)

$DBM(x_b,t)$ = displacement of BM at location x_b, time t

$DBM(x_b,\underline{t})$ = displacement of BM at location x_b, time $\underline{t}$

$f(\underline{t})$ = displacement of BM at location x, time $\underline{t}$, normalized with respect to DBM0

= $DBM(x_b,\underline{t})/DBM0$ (dimensionless)

$DBM0(x_b)$ = reference displacement of BM at location x_b

DS0 = reference displacement of stapes

As regards the nonlinear behavior of the BM as seen in the frequency response curves at a point on the cochlear partition, as shown in figure:3.2.3.2, it is assumed that as the input stapes displacement goes to zero, output becomes linear. The procedure for the model is to obtain a manageable form of the transfer function to fit the empirical data, e.g., Bekesy (1960) and Rhode (1971). Afterwards, convert this transfer function into a nonlinear differential equation which takes into account the nonlinear phenomena.

The normalized transfer function for a second order system is may be written

$$\bar{H}(\bar{w}) = \frac{1}{1 - (\bar{w})^2 + 2*i*a*\bar{w}}$$

where

$$\bar{w} = \frac{w}{w_{0N}}$$

where a and w_{0N} are constants. The BM motion and the second-order system $\bar{H}(\bar{w})$ show asymmetrical amplitude curves with respect to the peak frequencies. Also the qualitative shapes of the phase curves are very close to those of the BM. However, note that the BM motion amplitude plot has slopes much steeper than that of the transfer function $\bar{H}(\bar{w})$. This is taken care of by noting that the transfer function for N cascaded second order systems is

$$\tilde{H}(w/w_{0N}) = \prod_{k=1}^{N} \frac{1}{1 - (w/w_{0k})^2 + 2*i*a*(w/w_{0k})}$$

To improve the possibility of relating each of the second-order subsystems to a portion of the basilar membrane, each element is made slightly different. Accordingly, the transfer function $\tilde{H}(w)$ is modified using

$$w_{0K} = K^{(N-k)} * w_{0N}$$

Kim (1972,sec 4.3), in discussing how to relate the unilateraly coupled structure of the second-order subsystems to the unilateral (base to apex) propagation of the travelling wave of BM displacement, remarks that each of the second order subsystems would correspond to a portion of the BM. This correspondence would make the resonant frequency of each of the ten elements different. To mimic the distribution of characteristic frequencies along the BM, the parameter a is constant for all elements of the model. With this in mind, let

$$K = \frac{w_{0,k-1}}{w_{0,k}} \geq 1 \qquad \text{for } k=2,3,\ldots,N.$$

Substituting this into the equation for $\tilde{H}(w)$ yields

$$\tilde{H}(w) = \prod_{k=1}^{N} \frac{K^{2*(N-k)}}{K^{2*(N-k)} + (w)^2 + 2*i*w*a*K^{(N-k)}}$$

Note that all the parameters in the last equation defining $\tilde{H}(\bar{w})$ are dimensionless. When the values of a and N are simultaneously adjusted to produce appropriate sharpness of the amplitude vs $\log_{10}(f)$ curve, figure:3.2.3.1, the values are N=10 and a=0.25. The value of N is consistent with proper phase shifts in the original data, which shows 7*pi to 10*pi radians of cummulative phase shifts over the response frequency range. A second order system has a maximum phase shift of pi radians and so a cascade of ten second order systems has a maximum phase shift of 10*pi radians.

The only parameters left to evaluate are K, and w_{ON}. The value of K should be close to 1.0 and from the previous discussion it is required that $K>1$; so Kim arbitrarily chose K=1.03. The maximum response frequency, MRF, determines w_{ON}. Kim found from his simulation studies that the amplitude of the output for sine wave inputs of constant amplitude is seen to be maximum at $\bar{w}=1.06$. Now since $\bar{w}=w/w_{ON}$,

$$w_{max} = \bar{w}_{max} * w_{ON}$$

thus

$$w_{ON} = 2*pi*MRF/1.06$$

The output of the linear model is shown in figure:3.2.3.3.

To continue the plan, it is required to convert the transfer function $\tilde{H}(\bar{w})$ into a system of linear differential equations. It is the transfer function of N cascaded blocks, each with transfer function

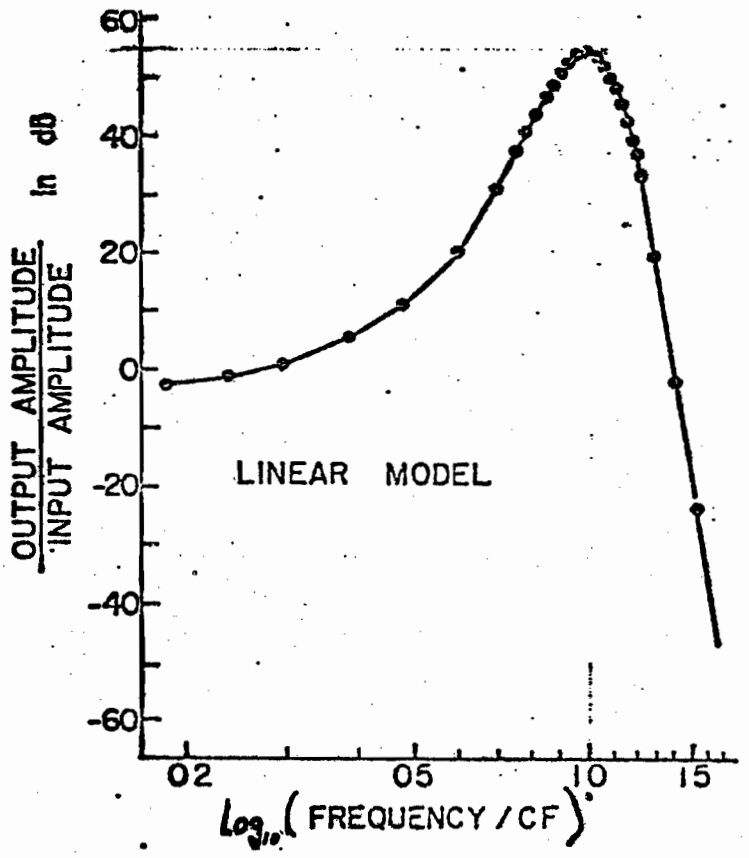

Figure:3.2.3.3 Ratio of output to input amplitude versus $\log_{10}(f/MRF)=\log_{10}(W/1.06)$ for the linear model.

$$H_k(\bar{w}) = \frac{(\bar{w}_k)^2}{(\bar{w}_k)^2 - (\bar{w})^2 + 2*i*\bar{w}*\bar{w}_k}$$

Let $x_{k-1}(t)$ be the input of the k-th element and $x_k(t)$ be the output. The differential equation of the k-th element is

$$D_t^2 x_k(\bar{t}) + 2*a*\bar{w}_k*D_t x_k(\bar{t}) + (\bar{w}_k)^2*x_k(\bar{t}) = (\bar{w}_k)^2*x_{k-1}(\bar{t})$$

where $\bar{t} = w_N*t$ is dimensionless time.

The transfer function $\tilde{H}(\bar{w})$ now may be replaced by N simultaneous second order linear differential equations.

$$D_t^2 x_1(\bar{t}) + 2*a*\bar{w}_1*D_t x_1(\bar{t}) + (\bar{w}_1)^2*x_1(\bar{t}) = (\bar{w}_1)^2*\underline{\underline{DS}}(\bar{t})$$

$$D_t^2 x_2(\bar{t}) + 2*a*\bar{w}_2*D_t x_2(\bar{t}) + (\bar{w}_2)^2*x_2(\bar{t}) = (\bar{w}_2)^2*x_1(\bar{t})$$

$$\vdots$$

$$D_t^2 x_N(\bar{t}) + 2*a*\bar{w}_N*D_t x_N(\bar{t}) + (\bar{w}_N)^2*x_N(\bar{t}) = (\bar{w}_N)^2*x_{N-1}(\bar{t})$$

$$\underline{\underline{\underline{DBM}}}(\bar{t}) = x_N(\bar{t})$$

This set of equations yields the output $\underline{\underline{\underline{DBM}}}(\bar{t})$, the normalized displacment of the basilar membrane at time $\bar{t}=t*w_N$, for the point on the basilar membrane with maximum response frequency MRF.

To finish the plan, these second order differential equations are altered to fit the nonlinear phenomena in the experimental data. The nonlinearization is done principally to match the nonlinear frequency response curves from Mossbauer measurements of Rhode (1971), figure:3.2.3.1. In this plot of peak membrane, displacement saturates with increasing sound pressure level. It has been shown (Guinan & Peake,1967; Rhode,1971) that displacements of the malleus and stapes are linear functions of sound pressure level, SPL dB. Thus saturation of BM displacement with respect to increasing sound pressure level is due to increasing stapes displacement. Saturation is most pronounced for sine input frequencies close to the MRF of the recording site on the BM, as seen in figure:3.2.3.1. Also the MRF decreases as the sound pressure level increases. Since the middle ear is linear, the MRF at a given stapes displacement amplitude decreases as the displacement of the stapes increases.

If $MRF(x_b,DS)$ is the MRF for the BM location and input stapes peak displacement DS, then

$$MRF(x_b,DS2) < MRF(x_b,DS1), \quad \text{when } DS2 < DS1$$

There is a second example of the BM's nonlinearity which is deduced from the the analysis of the response of the cochlear nerve axons to two closely spaced in time clicks of opposite polarity reported by Goblick and Peiffer (1969). They deduced that nonlinearity is due to the basilar membrane.

Of the terms for $D_{tt}x$, $D_t x$, and x in the system of simultaneous second-order linear differential equations, consider the $D_t x_k$ and x_k terms for nonlinearization. Notice that in the simple transfer function

$$H_k(\bar{w}) = \frac{(\bar{w}_k)^2}{(\bar{w}_k)^2 - (\bar{w})^2 + 2*i*\bar{w}*\bar{D}_k}$$

where

$$\bar{D}_k = a*\bar{w}_k$$

when $\bar{w}$ is near $\bar{w}_k$, the denominator is dominated by the $2*i*\bar{w}*\bar{D}_k$ term. This is important because the nonlinearity is for input frequencies near the maximum response frequency. The $2*i*\bar{w}*\bar{D}_k$ term corresponds to $D_t x$. If the parameter $\bar{D}$ changes as a function of input amplitude, variations of $\bar{D}$ are induced in the overall transfer function for $\bar{w}$ near $\bar{w}_{0k}$. For $\bar{w}$ far away from $\bar{w}_k$, $((\bar{w}_k)^2 - \bar{w}^2) >> 2*\bar{w}*D_k$, and the variations of $\bar{D}_k$ do not significantly affect the transfer function for this range of w. The change of $\bar{D}_k$ should be such that $\bar{D}_k$ increases as the input amplitude increases since the saturation of the output amplitude corresponds to the decrease of the amplitude of the transfer function.

From the shape of the frequency response data curve, note that localization of the saturation for input frequencies near the MRF causes a decrease of Q, a measure of tuning sharpness. Decreasing Q for increasing input amplitude is consistent with the assumption that $\bar{D}_k$ increases with the increasing input amplitude. The Q of each element of the model is proportional to $\bar{w}_k/\bar{D}_k$ and hence the increase of $\bar{D}_k$ corresponds to the decrease of Q. The decrease of Q for each element of the model leads to the decrease of Q for the overall system. The assumption of the increasing $\bar{D}_k$ for increasing input amplitude can also account for the nonlinearity in which an increase of the input amplitude causes a decrease of the MRF. The MRF of the k-th element is given by

$$MRF_k = (2*pi)^{-1} * \bar{w}_k * \left| 1 - 2*(\bar{D}_k/\bar{w}_k) \right|^{1/2}$$

$$= (2*pi)^{-1} * \bar{w}_k * \left| 1 - 2*a^2 \right|^{1/2}, \quad \text{if } a \leq 2^{-1/2}$$

$$= 0, \text{ if } a > 2^{-1/2}$$

Now if $\bar{D}_k$ increases, then the maximum response frequency of each element decreases and the MRF of the overall system also decreases as the input amplitude increases. Changing the coefficient of the x_k term in each of the second-order equations leads to conflicts with the direction changes of the

non linearities. Of the two possible terms to change coefficients, the $D_t x_k$ term is chosen. Consideration of the Duffing equation (Stern,1965,p480)

$$D_t^2 x + 2*D*D_t x + (w_0)^2*(1 + u*x^2)*x = A*\sin(w*t), \quad w>0$$

reveals that increasing the input amplitude causes an increase in maximum response frequency and an increase in Q. Based on the preceding observations, the D_t term is nonlinearized by using the following equation on each k-th block.

$$D_t^2 x_k + 2*\bar{D}_k(1 + u*(D_t x_k)^2)D_t x_k + (\bar{w}_k)^2 * x_k = (\bar{w}_k)^2 * \bar{x}_{k-1}(t)$$

Only the parameter u is left to adjust for the nonlinear model. The absolute value of u is unimportant since the quantity $u*(D_t x_k)^2$ determines the degree of nonlinearity, and thus, has function importance only with a given input amplitude. The constant u is set at 256, and the input amplitude and C are adjusted simultaneously to reproduce the empirical data. To reproduce the previously mentioned two-click data (Goblick & Pfeiffer,1971) it is required that $C=1.25*(w_{0N})^2$.

In summary x_b is distance from oval window with MRF, and

$w_{0n} = 2*pi*MRF/1.06$

$w_{0k} = w_{0k}*K^{N-K}$

$D_k = a*w_{0k}$

$N = 10$

$C = 1.25*(w_{0N})^2$

$a = 0.25$

$u = 256.0$

3.2.4 SCALE CONSTANTS

It is necessary to scale Kim's model to match up with the input stapes displacement in real displacement units, the output BM displacement in real units (Kim's model was for output/input in dB only). Furthermore, it is required to adjust the maximum displacement for each location x along the BM when f=MRF(x).

From Guinan and Peake (1967), note that the ratio of output/input for the middle ear as f-->0 is

$$\left|\left|H_{me}(s)\right|_{s=i*2*pi*f}\right|_{f->0} = \left|\frac{DS}{P}\right|_{f->0} = 3.8*10^{-7} \text{ (cm}^3\text{/dyne)}$$

$$= 3.8*10^{-8} \text{ (M}^3\text{/N)}$$

where 1 dyne is 10^{-5} Newtons. When the input is zero dB SPL, the stapes displacement is

$$DS0 = DS|_{f->0} = (3.8*10^{-8}\ M^3/N)*(20*10^{-6}\ N/M^2) = 7.6*10^{-13}\ M$$

The input DSK to Kim's model is in dB referenced to 2^{-19} zero to peak; thus

$$DSK = \frac{2^{-19}}{7.6*10^{-13}\ M} * DSM = \frac{2^{-19}}{0.76} * DS$$

where DSM is in meters and DS, which is used in the simulation, is in 10^{-12} meters. The output, DBMK, of Kim's model is in dB re 2^{-19} zero to peak. Wilson (1974) gathered all the experimental data on the BM displacment for input

frequency f=MRF(x_b) versus MRF. A function was fitted to this curve and shown in figure:3.2.4. The function is

$$RMDBM(f)=-10+10*\log_{10}(f)+10*\log_{10}[1+(f/f_1)^2]-20*\log_{10}[1+(f/f_2)^2]^{1/2}$$

where f=MRF(x_b), $f_1=10^3$ Hz, and $f_2 = 7.37*10^3$ Hz. Now the actual displacement of the BM is given by

$$DBM(x_b,t) = RMDBM(x_b)*(DS|_{SPL=0})*DBMK/2^{-19}$$

$$= RMDBM(x_b)*7.6*10^{-13}*DBMK/2^{-19}$$

Having properly adjusted the constants for the model, the finished model for the BM becomes (units for DS and DBM are pico meters):

$$DSK = \frac{2^{-19}}{0.76}*DS$$

$$D_t^2 x_1(t) + 2*D_1*[1 + u*(D_t x_1)^2]*D_t x_1(t) + (w_{01})^2*x_1(t) = C*DSK$$

$$D_t^2 x_2(t) + 2*D_2*[1 + u*(D_t x_2)^2]*D_t x_2(t) + (w_{02})^2*x_2(t) = C*x_1(t)$$

$$\vdots$$

$$D_t^2 x_N(t) + 2*D_N*[1 + u*(D_t x_N)^2]*D_t x_N(t) + (w_{0N})^2*x_N(t) = C*x_{N-1}(t)$$

$$DBMK(x_b,t) = x_N(t)$$

$$DBM(x_b,t) = RMDBM(x_b)*DS0*DBMK/2^{-19}$$

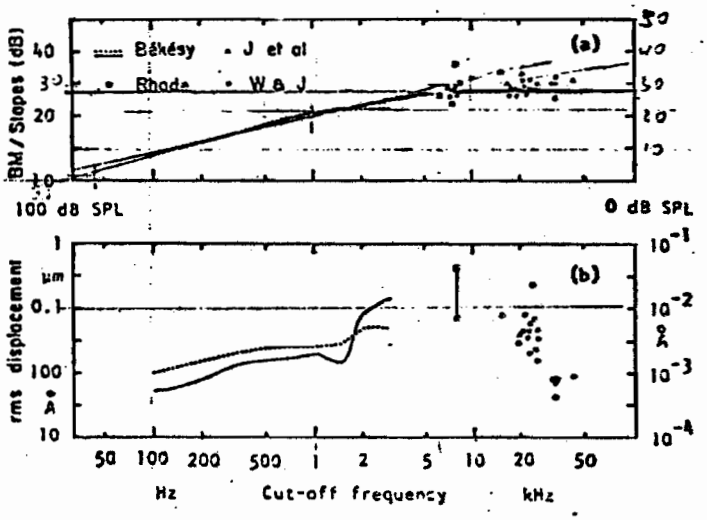

Wilson (1974)

Figure:3.2.4 Plot of maximum displacement of the BM at the frequency equal to that of the MRF for the recording site.

3.2.5 BASILAR MEMBRANE IN SIMULATED FORM

The last set of equations are more easily simulated by a digital computer if they are rewritten as simultaneous first order differential equations. Consider the k-th equation.

$$D_t^2 x_k(t) + 2*D_k*[1 + u*(D_t x_k)^2]*D_t x_k(t) + (w_{0k})^2*x_k(t) = C*x_{k-1}(t)$$

now let

$$y_k(t) = D_t x_k(t)$$

hence

$$D_t y_k(t) = D_t^2 x_k(t)$$

$$= -[\,2*D_k(1 + D_t x_k)*D_t x_k + (w_{0k})^2*x_k\,] + C*x_{k-1}(t)$$

The system of nonlinear differential equations becomes

$$x_0(t) = DSK(t)$$

$$D_t x_1(t) = y_1(t)$$

$$D_t y_1(t) = -[\,2*D_1(1 + D_t x_1)*D_t x_1 + (w_{01})^2*x_1\,] + C*x_0(t)$$

$$D_t x_2(t) = y_2(t)$$

$$D_t y_2(t) = -[\,2*D_2(1 + D_t x_2)*D_t x_2 + (w_{02})^2*x_2\,] + C*x_1(t)$$

$$\vdots$$

$$D_t x_k(t) = y_k(t)$$

$$D_t y_k(t) = -[\,2*D_k(1 + D_t x_k)*D_t x_k + (w_{0k})^2*x_k\,] + C*x_{k-1}(t)$$

$$\vdots$$

$$D_t x_N(t) = y_N(t)$$

$$D_t y_N(t) = -[\,2*D_N(1 + D_t x_N)*D_t x_N + (w_{0N})^2*x_N\,] + C*x_{N-1}(t)$$

$$DBMK(x_0, t) = x_N(t)$$

In matrix form

$$D_t[\underline{Z}(t)] = \underline{B}(t)*\underline{Z}(t) + \underline{A}(t)$$

where

$$\underline{Z}(t) = \begin{vmatrix} z_1(t) \\ z_2(t) \\ z_3(t) \\ z_4(t) \\ \vdots \\ z_{2N-1}(t) \\ z_{2N}(t) \end{vmatrix} = \begin{vmatrix} x_1(t) \\ y_1(t) \\ x_2(t) \\ y_2(t) \\ \vdots \\ x_N(t) \\ y_N(t) \end{vmatrix} = \begin{vmatrix} x_1(t) \\ \dot{x}_1(t) \\ x_2(t) \\ \dot{x}_2(t) \\ \vdots \\ x_N(t) \\ \dot{x}_N(t) \end{vmatrix} \qquad A(t) = \begin{vmatrix} 0 \\ C*DSK(t) \\ 0 \\ 0 \\ \vdots \\ 0 \\ 0 \end{vmatrix}$$

$$\underline{B}(t) = \begin{vmatrix} 0 & 1 & 0 & 0 & \cdots & 0 & 0 \\ -(w_{0k})^2 & B_{2,2} & 0 & 0 & \cdots & 0 & 0 \\ 0 & 0 & 0 & 1 & \cdots & 0 & 0 \\ 0 & 0 & -(w_{0k})^2 & B_{4,4} & \cdots & 0 & 0 \\ \vdots & \vdots & \vdots & \vdots & & \vdots & \vdots \\ 0 & 0 & 0 & 0 & \cdots & 0 & 1 \\ 0 & 0 & 0 & 1 & \cdots & -(w_{0k})^2 & B_{2N,2N} \end{vmatrix}$$

where

$$B_{2i,2i} = -2*D_i[1 + u(y_i(t))^2]$$

Now

$$\underline{Z}(t+h) = \int_t^{t+h} \dot{\underline{Z}}(t)dt$$

The result of a simulation using this model is shown in figure:3.2.5.

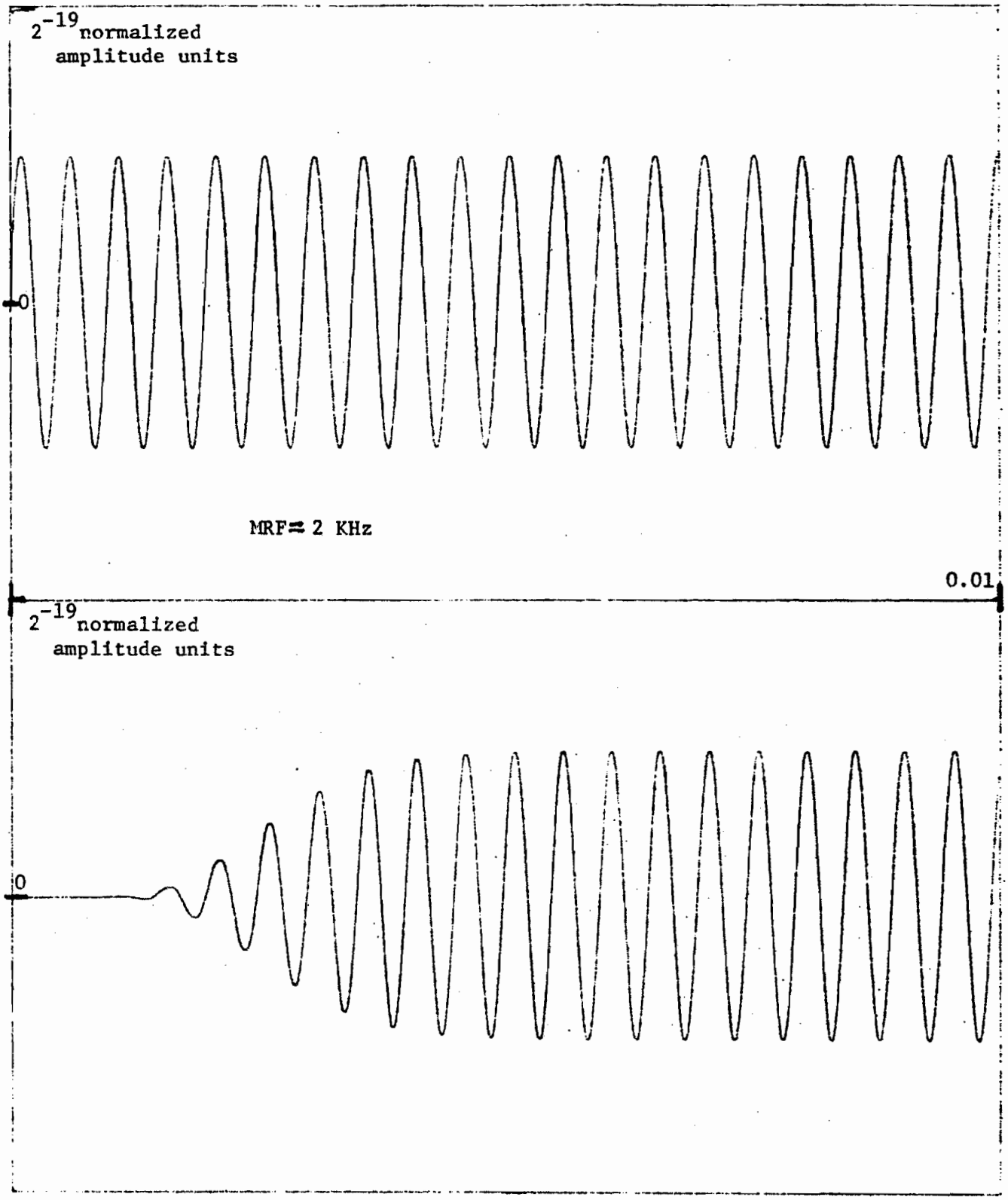

Figure: 3.2.5 Response of nonlinear basilar membrane model for sine wave input. Input frequency f=MRF, DSK=2^{-19}. Top is input and bottom is output.

3.2.6 REMARKS

Thus a suitable description for basilar membrane displacement, at a distance from the oval window, was found as a function of oval window displacement. The available experimental results show a nonlinearity for this signal processing block. Kim's model was used with his suggested nonlinear elements. The displacement at a specific cochlear partition position is then available using Wilson's plots for maximum displacement versus position. The analysis utilized here has a distinct advantage in being computable in a reasonable time span. This is of course important when the mechanical blocks are combined with the neural signal processing blocks.

3.3 BM TO HAIR CELL CILIA

3.3.0 INTRODUCTION

The next block in the physiological processing of sound is the conversion of displacement of the basilar membrane into a force acting on the inner and outer hair cells. In this section the radial shear force acting on the cuticular plate of the hair cells is obtained as a function of the BM displacement. The extraordinarily perspicacious work of Billone (1972) and Billone and Raynor (1973) provide the analysis for these function. Their model is based on the fine anatomy of the hair cells and movement with respect to the tectorial membrane in the organ of Corti. This analysis, based on structure and laws of physics, is necessitated by the technical impossibility of measuring actual displacements and forces in Corti's organ. This technical barrier means that this kind of analysis is the only solution available at this time.

3.3.1 ANATOMICAL BASIS FOR THE MODEL

Much anatomical work has been done on the structure of the organ of Corti, for example, Engstrom et al (1962), Engstrom (1970), Fernandez (1952), Kimura (1965, 1966), Spoendlin (1966), Lindeman, Ades, Bredberg, & Engstrom (1971)

and Lim (1972). Figure:3.3.1.1 depicts a cross section view of the cochlea. Figure 3.3.1.2 shows the fine structure of the organ of Corti. This figure shows Hensen's stripe and Hardesty's membrane which are attached to the tectorial membrane and are immediately superior to the cilia.

Bekesy (1951, 1953a,b) suggested that both radial and longitudinal shear forces may be important mechanical stimuli to the hair cells. Billone (1973) made calculations which indicate that the radial displacements are much larger than the longitudinal displacements. Wersall and Flock (1967) did a morphological study of the directional sensitivity of hair cells and agree that the radial displacements are the greater influence. Davis (1965) hypothesized that shear forces act on the receptor pole of the hair cell and cause a change in the ion conductance of some sensitive region on the cell surface. Engstrom et al (1962) speculated that the "essentially excitable structure" is the cuticular free region on the top of the hair cell. The shear force on the dense cuticular plate can be assumed to move the plate against the softer cuticular free region. It is therefore necessary to calculate the shear forces transmitted to the cuticular plate.

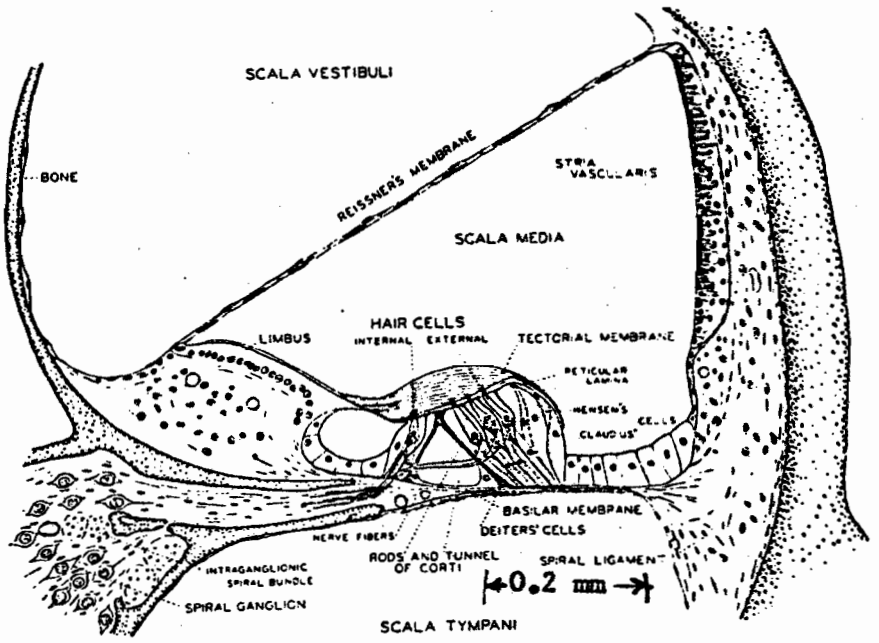

Figure:3.3.1.1 The cross section of one turn of the cochlea at midmodiolar region. From Davis (1965).

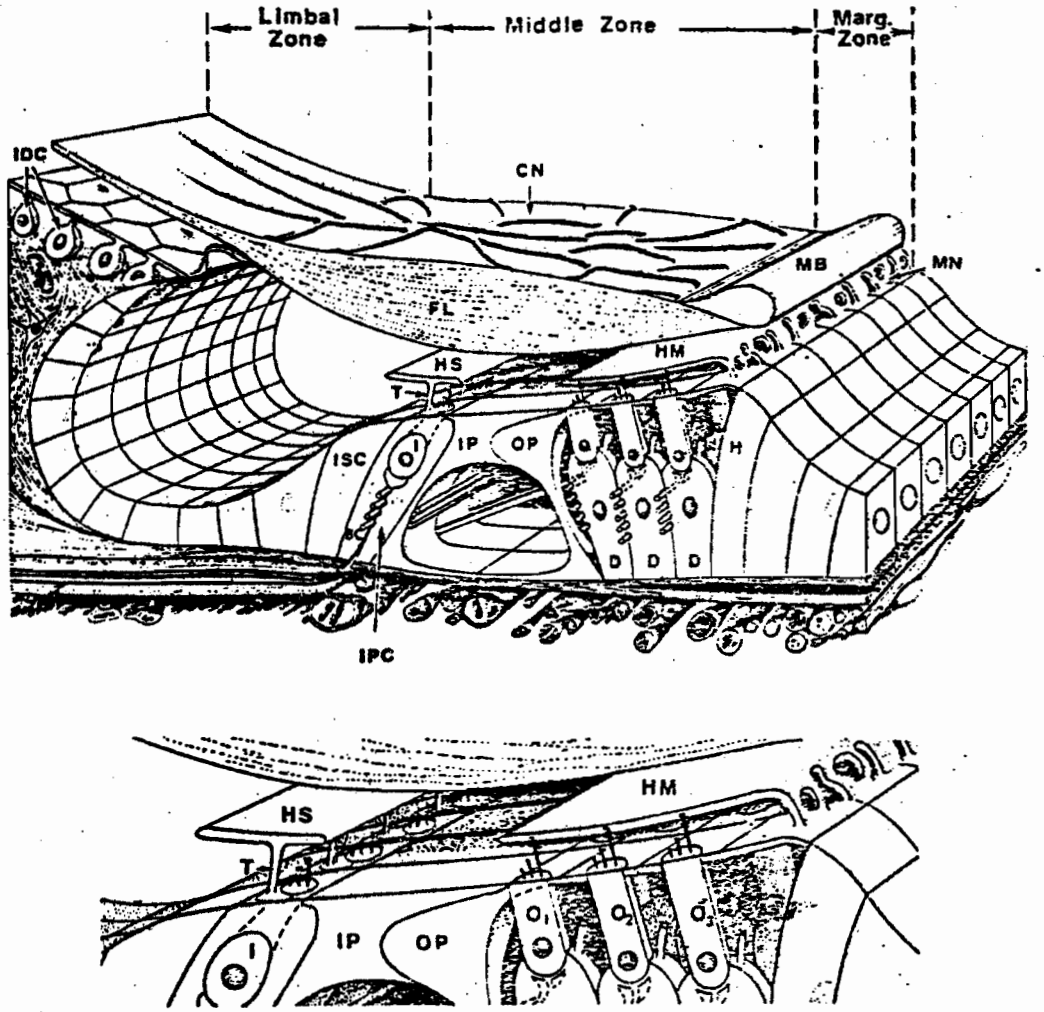

Figure:3.3.1.2.A Substructures of the tectorial membrane and its relation to the organ of Corti. The top is anchored by the trabeculae (T) of Hensen's stripe (HS) and the marginal net (MN). Hardesty's membrane (HM) is above the outer hair cells. The marginal band (MB), fibrous layer (FL), interdental cell (IDC), inner sulcus cell (ISC), inner border cell (BC), inner phalangeal cell (IPC), inner pillar cell (IP), outer pillar cell (OP), Deiter's cell (D), and Hensen' cell (H) are shown.

Figure:3.3.1.2.B An enlarged view of the sensory hair-tectorial membrane junction. The first, second, and third outer hair cells are marked by O_1, O_2, O_3.(Lim,1972)

3.3.2 RADIAL SHEAR DISPLACEMENT

This physiological block takes as input the displacement $D=DBM(x_b,t)$ of the BM at a distance x_b from the oval window and produces as output, the shear force S_j on the hair cells where j=1 denotes the inner hair cells and j=2,3,4 denote the outer hair cells at x_b.

Rhode and Geisler (1967) and Billone (1973) have developed geometrical models for calculating the amplitude of radial shear displacement S of a hair cell opposite a point on the tectorial membrane, as a function of the midpoint basilar membrane displacement. Both models assume rigid bodies for the organ of Corti and the tectorial membrane. The Billone model has the advantage of assuming a separation of the tectorial membrane (TM) and the reticular membrane (RM) except at the outer tip of the TM where sliding contact is maintained, whereas the Rhode and Geisler model assumes that all opposing points on the two membranes are in contact for the rest position. It seems that the Billone model much more accurately depicts the actual movements of the organ of Corti and the tectorial membrane. In these models, the shear displacement decreases monotonically along the cochlea from base to apex (3 to 0.5 in the Rhode and Geisler model and 2 to 0.75 in the Billone model). Both models predict that the relationship between S and D is linear and frequency

independent within the normal auditory range. The shear displacement above an inner hair cell is approximately the same as that above an outer hair cell (less than 40% difference for the Rhode and Geisler model and less than 1% difference for the Billone model).

Following Billone (1973), the model shown in figure:3.3.2 is used. It is used, according to Billone and Raynor (1973), because

> "1. It allows for a separation between the tectorial and reticular membranes above the hair cells. This is consistent with anatomical observations, and it is a critical factor in the shear force analysis.
> 2. It incorporates a beam model for basilar membrane deflection which is based on both the structure and the performance of the basilar membrane."

The essential features of this model include: (1) The BM moves a beam (an arc in cross-section of the cochlea); (2) The configuration consisting of inner and outer pillar cells, with the hair cells and reticular membrane rotating as a rigid body about a hinge at the spiral lamina (BSL) where the BM joins the inner wall of the cochlea; (3) The tectorial membrane remains rigid with a hinge at the spiral limbus and a sliding bearing where it rests on the reticular membrane by means of Hardesty's membrane.

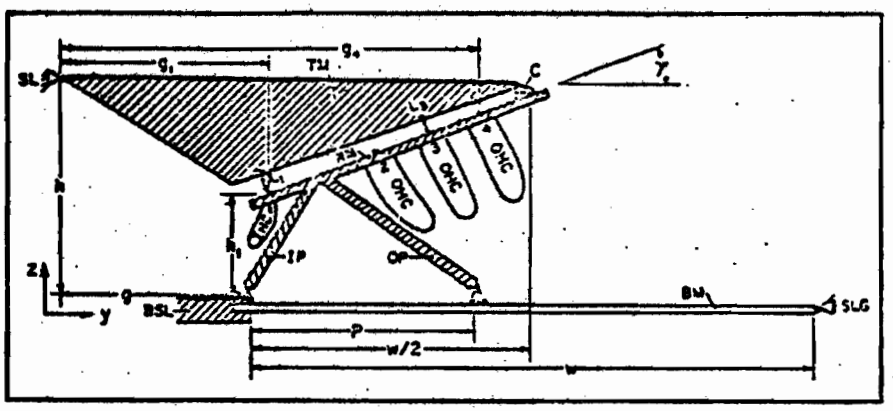

Figure:3.3.2.A Radial shear displacement model. The tectorial membrane (TM), reticular membrane (RM), pillars of Corti (IP,OP), bony spiral lamina (BSL), spiral limbus (SL), and the spiral ligament (SLG) are treated as rigid bodies. The basilar membrane (BM) is treated as a flexible beam.

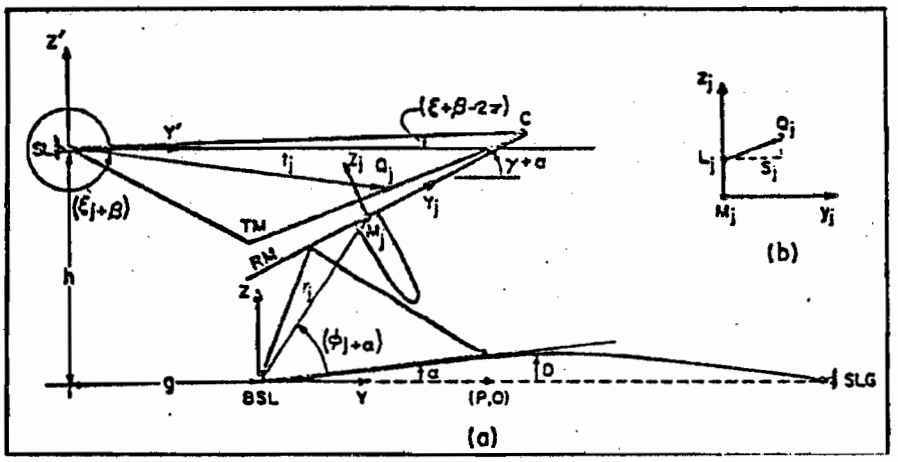

Figure:3.3.2.B Response of the radial shear displacement model to a positive BM displacement (D). The organ of Corti rotates through an angle alpha about BSL. The TM rotates through an angle beta about SL. The opposing point Q_j on the TM moves a distance S_j in the shear direction relative to the reticular membrane point M_j. (Billone,1973).

For BM displacements (D) which are small compared to membrane width (w), the relationship between S_j, the shear force on the j-th hair cell, as a function of D is derived by Billone (1973) and found to be:

$$S_j = G_j(x) D, \quad j = 1, 2, 3, 4, \tag{A1}$$

$$G_j(x) = (\tfrac{4}{3} C_{4j}/w)[2(P/w)^3 - 3(P/w)^2 + 1], \tag{A2}$$

$$C_{4j} = 2\csc(2\gamma)\{(1-C_2)[L_j + r_j \sin(\varphi_j - \gamma)] + C_3(g\sin\gamma + h\cos\gamma)\}/(\tan\gamma + \operatorname{ctn}\gamma), \tag{A3}$$

$$C_3 = (C_2 - C_1\tan\xi)\cos^2\xi/(y_{co}+g), \tag{A4}$$

$$C_2 = y_{co}\sec^2\gamma + (C_1 + r_1\sin\varphi_1 - r_1\cos\varphi_1\tan\gamma)\tan\gamma, \tag{A5}$$

$$C_1 = \frac{(h - z_{co}\sec^2\gamma)y_{co} + (h - r_1\sin\varphi_1 + r_1\cos\varphi_1\tan\gamma)z_{co}\tan\gamma}{g + y_{co}\sec^2\gamma - (h - r_1\sin\varphi_1 + r_1\cos\varphi_1\tan\gamma)\tan\gamma}, \tag{A6}$$

$$y_{co} = \tfrac{1}{2}w, \tag{A7}$$

$$z_{co} = h_1 + (\tfrac{1}{2}w - g_1 + g)\tan\gamma, \tag{A8}$$

$$l' = [(y_{co}+g)^2 + (z_{co}-h)^2]^{\frac{1}{2}}, \tag{A9}$$

$$\xi = \arctan[(z_{co}-h)/(y_{co}+g)], \tag{A10}$$

$$r_1 = [(g_1-g)^2 + h_1^2]^{\frac{1}{2}}, \tag{A11}$$

$$\varphi_1 = \arctan[h_1/(g_1-g)] \tag{A12}$$

$$r_j = \tfrac{1}{4}\{[(4-j)g_1 + jg_4 - 4g]^2 + [4h_1 + j(g_4-g_1)\tan\gamma]^2\}^{\frac{1}{2}}, \quad j \neq 1, \tag{A13}$$

$$\varphi_j = \arctan\{[4h_1 + j(g_4-g_1)\tan\gamma]/[(4-j)g + jg_4 - 4g]\}, \quad j \neq 1, \tag{A14}$$

$$l_j = [(g + r_j\sin\varphi_j - L_j\sin\gamma)^2 + (h - r_j\sin\varphi_j - L_j\cos\gamma)^2]^{\frac{1}{2}}, \tag{A15}$$

$$\xi_j = -\arctan[(h - r_j\sin\varphi_j - L_j\cos\gamma)/(g + r_j\sin\varphi_j - L_j\sin\gamma)], \tag{A16}$$

$$L_j = \{[(z_{co} - r_j\sin\varphi_j)^2 + (y_{co} - r_j\cos\varphi_j)^2]/[(z_{co} - r_3\sin\varphi_3)^2 + (y_{co} - r_3\cos\varphi_3)^2]\}^{\frac{1}{2}}. \tag{A17}$$

The nine parameters w, h, h_1, g, g_1, g_4, gamma, L_3, P are found from the literature and vary as a function of x_b, the distance along the BM from the oval window. Let

X_{bn} = normalized length from the oval window

= x_b/BMLEN

where BMLEN = length of BM. Fernandez (1952) gives the width of the guinea pig BM as

$$w = (1.99*X_{bn} + 1.33*10^{-2}\ \text{cm.})$$

Since X_{bn} is normalized, it will be used here for the cat, with BMLEN=23.0 (Schuknecht,1953).

Rhode and Geisler (1967) provide the next six parameters which were measured in cat.

$$h = (10.359*X_{bn} + 1.07)*10^{-4} \quad \text{meters}$$

$$h_1 = (0.0033*X_{bn} + 0.459)*10^{-4} \quad \text{meters}$$

$$g = (1.01*X_{bn} + 0.242)*10^{-4} \quad \text{meters}$$

$$g_1 = (1.04*X_{bn} + 0.324)*10^{-4} \quad \text{meters}$$

$$g_4 = (1.34*X_{bn} + 0.755)*10^{-4} \quad \text{meters}$$

$$\text{gamma} = (0.103*X_{bn} + 0.265)*10^{-4} \quad \text{radians}$$

Kimura's (1965) work on the squirrel monkey provides a source for the parameter L_3. The spacing between the tectorial membrane and reticular membrane at the hair cell j=3.

$$L_3 = (0.04*X_{bn} + 0.016)*10^{-4}\ M$$

Billone measured the ratio (P/w) in cat and found P to be:

$$P = (0.796*X_{bn} + 0.532)*10^{-4}\ M$$

3.3.3 SHEAR FORCES ACTING ON THE CUTICULAR PLATES

3.3.3.1 DESCRIPTION OF THE SHEAR FORCE MODEL

Now that $S_j = G_j(x_b) * DBM(x_b,t)$, the radial shear displacement of opposing points on the tectorial and reticular membranes is known for the j=1,2,3,4 hair cells, it is necessary to obtain the shear force acting on the cuticular plate of the j=1,2,3,4 hair cells at location x_b. The basic features of the model for shear force SF_j acting on the cuticular plate of the j-th hair cell is shown in Figure:3.3.3.1.

The cuticular plate in which the cilia are embedded at the superior surfaces of the hair cell is treated as a rigid body that is tightly held in place by its stiff attachment to the reticular membrane (Spoendlin, 1966). This assumption implies that the motion of the cuticular plate relative to the reticular membrane is small compared to S_j. The cilia are treated as cylindrical cantilevered beams of uniform cross section and modulus of elasticity. The cilia emerge from their built-in support at the cuticular plate into the viscous endolymph fluid that fills the space between the tectorial and reticular membrane.

None of the inner hair cell (IHC) cilia make contact with the tectorial membrane (Lim 1972). These cilia experience a viscous drag induced by the movement of the

endolymph fluid. The outer hair cell cilia are embedded in shallow grooves in the tectorial membrane (Engstrom et al, 1962; Kimura, 1966; Lim, 1972). This TM contact is suitable for transmitting the radial shear forces to the tall cilia without exerting any axial forces or moments. The remaining rows of OHC cilia are not connected to the tectorial membrane.

The IHC cilia are arranged in three long parallel rows with 10 to 20 cilia in each row. All the cilia are assumed to have the same diameter and the height of each row increases progressively as the position of the row approaches the cuticular free region (CFR). The center to center distance between cilia in a row is approximately three radii, which is also used for the center to center distance between rows of cilia. The average height of cilia per cell increases with the cell position along the cochlea from base to apex.

The OHC cilia model is similar to that of the IHC cilia; except (a) the number of rows per cell increases from three to six with twenty to forty cilia per row, depending upon the species and location along the cochlea; (b) the number of cilia per cell decreases from stapes to helicotrema; and (c) the center to center spacing is less than three cilium radii.

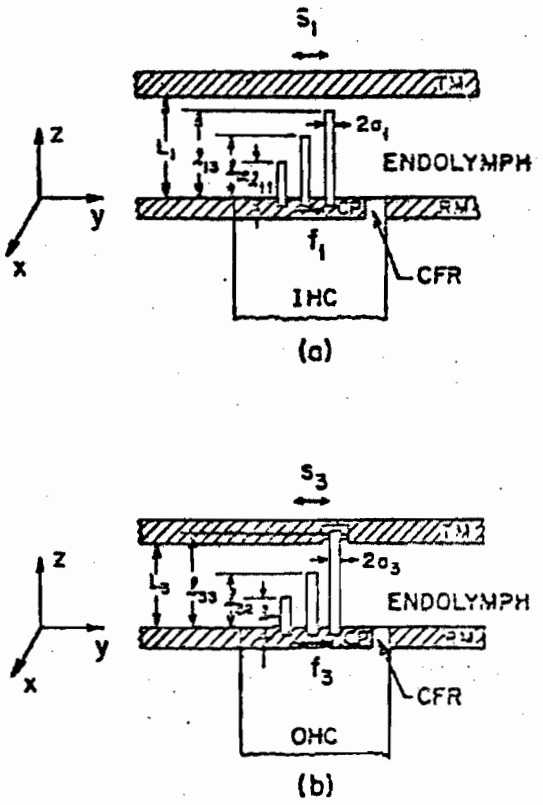

Figure:3.3.3.1 Radial view of shear force model for inner (a) and outer (b) hair cells. Vibration of the tectorial membrane shears the embedded OHC cilia directly and the free OHC and IHC cilia through the medium of the viscous endolymph. The cilia transmit these forces to the cuticular plate (CP). (Billone,1973).

The cilia are analyzed as beams with constant geometrical and material properties; however, the cilia taper down to about half of their maximum diameters, and become more dense as they approach the cuticular plate. The stiff rootlet which anchors a cilium to the cuticular plate continues up the center of the cilium a short distance adding to both the density and stiffness of the neck. The stiffness per unit length of a beam in bending is proportional to the product of the fourth power of the radius (a^4) and the modulus of elasticity (E). Although the decreasing radius tends to weaken the cilium neck, the increasing modulus of elasticity tends to strengthen the neck region. To a first approximation, the product of these two parameters ($E*a^4$) is assumed to be constant along the axis of the cilium. It is well known that the cilia are arranged in "W" patterns. The shape of the row may affect the transmission of viscous forces; however, it has no effect on the shear forces acting on the embedded tips of the tall OHC cilia. Consequently, it is assumed that the OHC cilia are arranged in straight rows, for the shear force analysis.

The radial shear displacement of the top of the hair cells at the reticular membrane with respect to the tectorial membrane induces motion in both the endolymph

fluid and the ends of the tall OHC cilia which are in direct contact with the TM. A free cilium is subjected to a viscous drag per unit length which is proportional to the product of the viscosity (mu) and the velocity difference between itself and the fluid. An embedded cilium is driven primarily by the shear force acting on its TM contact location. For each case, the cilium transmits the shear force to the cuticular plate in which it is rooted.

3.3.3.2 SHEAR FORCE TRANSMITTED BY IHC FREE CILIA

3.3.3.2.0 STRATEGY

The analysis of the viscous drag transmitted to the cuticular plate by a free cilium is divided into three parts: (a)The calculation of the fluid velocity profile V between the tectorial and reticular membranes far away from the cilia. (b)The computation of the drag per unit length on a rigid cilium which is a member of an array of cilia and is exposed to a free stream velocity V. (c)The evaluation of the shear force transmitted to the cuticular plate by a flexible cilium beam which is in a viscous flow field. The flow is assumed to be incompressible and laminar. Furthermore, since the cilia are long compared to their diameters and the relative vertical displacement between the membranes is small, the fluid velocity in the vertical direction z is neglected.

3.3.3.2.1 FLUID FLOW BETWEEN TM AND RM

Away from the cilia, the fluid flow between tectorial and recticular membranes is assumed to be an oscillating Couette flow as in figure:3.3.3.2.2. The equation and boundary conditions for this flow field are:

$$\rho D_t V = \mu D_z^2 V$$

$$V(0,t) = 0$$

$$V(L,t) = D_t S_j$$

where rho is the density of endolymph. The solution given by Lamb(1945) via Billone (1973) is

$$V = (z/L) D_t S_j$$

For this problem, $\rho \approx 1$ g/cm^3, $\mu \approx 10^{-2}$ dyne*sec/cm^2, and L varies from $6*10^{-4}$ to $2*10^{-4}$ cm as w varies from 10^2 to 10^5 rad/sec. So $\rho w L/\mu < 0.4$, and the slow viscous flow ($\rho w L^2/\mu \ll 1$) solution is a reasonably good approximation for the flow between TM and RM even at high auditory frequencies.

3.3.3.2.2 DRAG FORCE ON A RIGID CILIUM IN AN ARRAY

In any XY plan far away from the cilia, the oscillating flow is uniform as shown in figure:3.3.3.2.2. The flow in the neighborhood of the cilia has both x and y components (u,v). As the cilia are treated as infinitely long in this analysis, no motion in the z direction is induced. The number of cilia in a row is considered to be infinite. The drag analysis simplifies in this case because the fluid streamlines are symmetric about the y axis of each cilium and the drag is the same on all of the cilia in a row, which is particulary reasonable for IHC cilia. Each cell carries about 20 cilia per row; however, the hair cells are so close together that a row is effectively as long as the cochlea and includes thousands of cilia.

The continuity equation for an incompressible flow with no motion in the z direction is

$$D_x u + D_y u = 0$$

Stokes equations for slow viscous flow are a good approximation to the momentum equations for flow through a row of cilia (Billone&Raynor,1973).

$$mu*(D_{xx} u + D_{yy} u) = D_x P$$

$$mu*(D_{xx} v + D_{yy} v) = D_y P$$

where P is the pressure. The boundary conditions in the XY plane for this problem are :

u = v = 0, on all cylinder surfaces

v --> 0, as |y|-->oo

v --> V

Miyagi (1958) via Billone and Raynor (1973) gives the solution for the velocity field through a single row of infinitely long circular cylinders. The drag per unit length on a cylinder in a single row is

$$D_v = 8*pi*c*mu*V$$

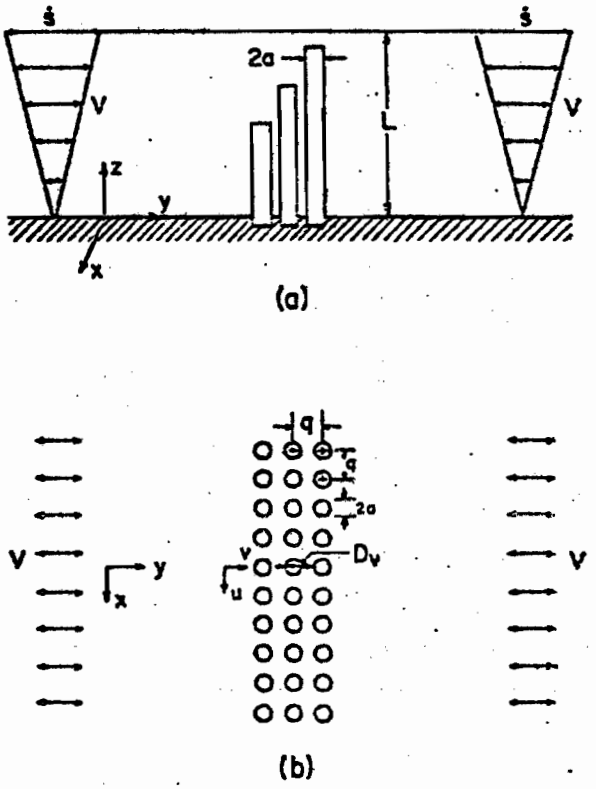

Figure:3.3.3.2.2 Fluid flow between tectorial and reticular membranes. From Billone (1973).

For cases in which the cylinders are very close ($0.35<(a/q)<0.5$), Miyagi suggests the following form for the drag coefficient

$$c = 0.63*(1 - 2a/q)^{-2}$$

For IHC cilia $a/q \cong 0.3$ and $D_v = 8*pi*c*mu*V$ can be used to calculate $c \cong 4$. So the drag per unit length on an IHC cilum is

$$D_v = 100*mu*V$$

The total force f_v transmitted by a rigid free cilium is found by integrating the drag per unit length along the length l of the cilium

$$f_v = \int_0^l D_v\,dz = \int_0^l 8*pi*c*mu*(z/L)*D_t S_j\,dz = 4*pi*c*mu*(l/L)^2*D_t S_j$$

3.3.3.2.3 SHEAR FORCE TRANSMITTED BY FREE CILIUM

The drag formula calculated in the previous section can be modified to include the possible motion of a free cilium. A cilium beam deflects a distance n(z,t) in the y direction in response to an applied load as in figure:3.3.3.2.3. Since viscous drag loading the cilium is proportional to the velocity difference between the free stream flow and the cilium, the drag equation $D_v = 8*pi*c*mu*V$ is modified to

$$D_V = 8*Pi*c*mu*(V - D_t n)$$

The fundamental frequency of a cilium in bending is in the ultrasonic range (Billone&Raynor,1973), which implies that, for acoustic frequencies, the inertia term in the dynamic beam equation is much smaller than the elastic restoring force. Neglecting the inertia term and assuming deflections which are small compared to the length of the cilium, the displacement equation is

$$E*I*D_z^4 n = D_v$$

where $I=0.75*pi*a^4$ is the area moment of the cross section and E is Young's modulus. Combining the equations for V and these last two equations gives

$$D_z^4 N + e*D_t N = (e/L)*z*D_t \dot{S}$$

where

$$e = \frac{8*pi*c*mu}{E*I} \quad \text{and} \quad \dot{s} = D_t S_j$$

where j is for the j-th outer hair cell.

The boundary conditions are determined from noting that at the cuticular plate end of the cilium, the deflection and slope are zero while the moment and shear area are zero at the free end. Accordingly, these conditions are:

$$n(0,t) = 0$$

$$D_z n(0,t) = 0$$

$$E*I*D_z n(l,t) = 0$$

$$-E*I*D_z n(l,t) = 0$$

where l is the length of the cilium.

Figure:3.3.3.2.3 Free body diagrams for a free cilium(a) and embedded cilium(b). n is the displacement of the neutral axis in response to drag (D_v) and elastic shears ($-f_v$,$-f_e$,f_{TM}). f_{TM} is the shear which the tectorial membrane exerts on the tip of an embeoded cilium. (Dallone,1973).

The block diagram for the shear force transmitted to the cuticular plate by one flexible free cilium is summarized in block form below.

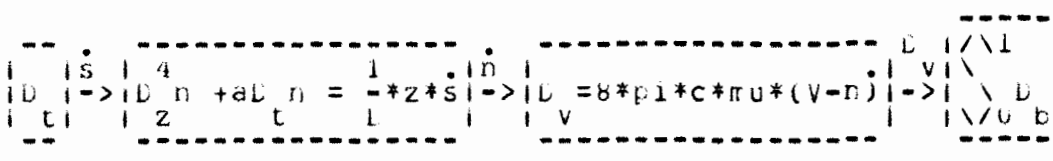

where S_j is the radial shear force acting on the cilia of the j-th hair cell at distance x_b from the oval window. The drag per unit length D_v is a function of both z and t.

To simulate these equations for the shear force transmitted to the cuticular plate by one flexible free cilium, it is necessary to solve the partial differential equation for n(x,t).

3.3.3.3 SHEAR FORCE TRANSMITTED BY AN EMBEDDED CILIUM

The equation of motion for a cilium which makes contact with the tectorial membrane is the same as that for a free cilium. The difference between the two classes of cilia appears in one of the boundary conditions at the TM end of the cilia, z=l. While the free cilium experiences no shear at its TM end, the embedded cilium is sheared by the motion of the tectorial membrane. Consequently, the boundary condition

$$-E*I*D_z^3 n(l,t) = 0$$

is replaced by the condition that the displacement of the TM

end of an embedded cilium is equal to the TM displacement of S_j.

$$N(l,t) = S_j$$

The force f_e transmitted by an embedded cilium to the cuticular plate is found by calculating the shear which the cilium exerts on the cuticular plate. According to elementary beam theory, the shear force acting on the support of a deflected cantilevered beam is

$$f_e = -E*I*D_z^3 n(0,t)$$

Billone and Raynor (1973) state that for $k<1$, where $k=(8*pi*c*mu/(E*I))^{1/4}$, the viscous effects are negligible and the solution becomes that for the shear transmitted by a cantilevered beam subjected to an end displacement s.

$$f_e = \frac{3*E*I}{l^3}*s$$

3.3.3.4 TOTAL SHEAR FORCE TRANSMITTED TO CUTICULAR PLATE

3.3.3.4.1 INNER HAIR CELLS

The shear force F_l transmitted by cilia to the cuticular plate of an inner hair cell is calculated by adding up the force contribution of each cilium for that hair cell. All the IHC cilia are free, so the force

transmitted by each IHC cilium is given by f_v with l being the length of that cilum. Let

n = the n-th row of cilia; n=1 for shortest, n=3 for longest

l_{1n} = length of cilia in the n-th row

T_1 = number of cilia per IHC

So the force exerted by a cilium in the n-th row is given by

$$f_{1n} = f_v \Big|_{l=l_{1n}}$$

Recall that the inner hair cells are denoted by j=1. The total force acting on an IHC cuticular plate is given by

$$F_1 = \frac{T_1}{3} \sum_{n=1}^{3} f_{1n}$$

3.3.3.4.2 OUTER HAIR CELLS

The total shear force F_3 acting on an OHC cuticular plate consists of forces transmitted by both free and embedded cilia. Let

N_3 = total number of rows of cilia per OHC

J_3 = number of free rows of cilia per OHC

l_3 = effective length of an embedded cilia

= (total length - embedded part)

l_{3n} = length of an OHC cilium in the n-th row of cilia where the shortest row is labeled n=1

T_3 = total number of cilia per OHC

F_{f3} = total force transmitted by free OHC cilia to the cuticular plate

F_{e3} = total force transmitted by embedded OHC cilia to the cuticular plate

The total force exerted by all the free cilia on the OHC cuticular plate is

$$F_{f3} = \sum_{n=1}^{J_3} N_{f3n} * f_{f3n}$$

where N_{f3n} is the number of free cilia per row per OHC and F_{f3n} is the force exerted by one free cilium on an OHC cuticular plate, in row n of the OHC cilia.

$$F_{f3} = \frac{T_3}{N_3} \sum_{j=1}^{J_3} f_{f3n}\Big|_{l=1}^{l_{3n}} = \frac{T_3}{N_3} * J_3 * f_{3v}\Big|_{l=1}^{l_3}$$

The force exerted by all the embedded cilia (the tallest row) on the OHC cuticular plate is given by

$$F_{e3} = N_{e3} * f_{e3}$$

where N_{e3} is the number of embedded cilia in the single row of embedded cilia per OHC and F_{e3} is the force exerted by one embedded cilium on an OHC cuticular plate. So

$$F_{e3} = T_3 * \frac{N_3 - J_3}{N_3} * f_{3v}\Big|_{l=1}^{l_3}$$

Now the total force on the OHC cuticular plate is the sum of the forces exerted by the free and embedded cilia.

$$F_3 = F_{E3} + F_{F3}$$

3.3.3.5 PARAMETERS IN CUTICULAR PLATE SHEAR FORCES

The values for most of the parameters are given in table:3.3.3.5 from Billone and Raynor (1973,table I). After careful checking of the sources from which the parameter values originated, it seems that values in the table and those presented are quite accurate and very impressive as biological data.

Parameter	IHC (1)	OHC (3)	Source
Shear displacement (S)	See Figs. 4 and 5	See Figs. 4 and 5	...
Endolymph viscosity (μ)	0.01 dyn-sec/cm^2	0.01 dyn-sec/cm^2	Rossi and Vilstrup *et al.*, for Shark
Young's modulus (E)	$10^3 < E < 10^{11}$ dyn/cm^2	$10^3 < E < 10^{11}$ dyn/cm^2	To be chosen to match CM data
Number of cilia per cell (T)	~~40~~ [illegible]	120–60 x_p	Engstrom *et al.*, Kimura, and Spoendlin
Number of rows of cilia (N)	3	3	Engstrom *et al.*, Spoendlin
Number of free rows (J)	3	2	Estimated
Cilium radius (a)	0.15×10^{-4} cm	0.12×10^{-4} cm	Kimura's micrographs of guinea pig cilia
Center-to-center cilia spacing (q)	0.5×10^{-4} cm	0.3×10^{-4} cm	Kimura's micrographs of guinea pig cilia
TM–RM spacing (L)	See Appendix A	$(4x_p+1.6)\times10^{-4}$ cm	Kimura's squirrel monkey data
Cilium lengths (l)	$l_{11}=0.5l_{13}$ $l_{12}=0.75l_{13}$ $l_{13}=(4x_p+2)\times10^{-4}$ cm	$l_{31}=0.5l_{33}$ $l_{32}=0.75l_{33}$ $l_{33}=(4x_p+2)\times10^{-4}$ cm	Kimura's squirrel monkey data and Spoendlin's cat data

Table:3.3.3.5 Parameter values used for the shear force calculations. The notation using subscripts depicts a variable X_{ij} where i denotes the i-th hair cell (i=1 for IHCs; i=2,3,4 for OCHs moving radially) and j denotes the j-th row of cilia on a hair cell (j=1 for shortest, j=2 for middle row, and $j=N_i$ for the tallest row). (Billone & Raynor,1973).

Some parameters remain to be evaluated. Young's modulus, E, was determined from consideration of the cochlear microphonics. Microphonic output H from a cell is related to shear force by a constant, then calculated using the formulae

$$CM_1 = H*F_1 \quad \text{for IHC}$$

$$CM_3 = H*F_3 \quad \text{for OHC}$$

Since there are approximately four OHC to each one IHC, the CM (as is usually recorded differentially, scala tympani minus scala vestibuli) would be

$$CM = H*(4*F_3 + F_1)$$

and the ratio of the CM due to inner hair cells alone to the normal total CM is

$$\frac{|CM_1|}{|CM|} = \frac{|F_1|}{|4*F_3 + F_1|}$$

which was compared to measurements made from Kanamycin studies by Dallos et al (1972). Billone (1973) found E = $3*10^9$ dynes/cm^2 to cause the best fit.

3.4 CONCLUSION

In this chapter it has been shown that there exist sufficent experimental results in the literature to develop a computational model for the middle ear, basilar membrane and forces on the hair cell cilia. It was seen that the steady state descriptions can be written as differential equations to produce a dynamic formulation.

The middle ear is described by transfer function fitted to the data obtained by Guinan and Peake (1967), then rewritten in differential equation form for dynamic simulation rather than the steady state view point. The basilar membrane was able to be described in a dynamic form using modified version of Kim's (1972) nonlinear normalized analysis. The actual peak displacements were shown to be available from Wilson's (1974) analysis. The equations obtained here have the distinct advantage that they are computable in a reasonable time limit. Thus we are ready for the analysis of the neural portion of the cochlea.

Baust,W. & Berlucchi,G. (1964) Reflex response to clicks of cat's tensor tympani during sleep and wakefulness and the influence theoreon of the auditory cortex. Arch. Ital. Biol. 102:686-712.

Bekesy,G.von (1947) The variation of phase along the basilar membrane with sinusoidal vibrations. J. Acoust. Soc. Am. 19:452-460.

Bekesy,G.von (1951) Microphonics produced by touching the cochlear partition with a vibrating electrode. J. Acoust. Soc. Am. 23:29-35.

Bekesy,G.von (1953a) Description of some mechanical properties of the organ of Corti. J. Acoust. Soc. Am. 25:770-785.

Bekesy,G.von (1953b) Shearing microphonics produced by vibrations near the inner and outer hair cells. J. Acoust. Soc. Am. 25:786-790.

Benson,R.W.& Eldridge,D.H. (1955) Variations in sound pressure produced in guinea-pig ears due to normal and abnormal eardrums. J. Acoust. Soc. Am. 27:373-375.

Billone,M. (1972) Mechanical stimulation of cochlear hair cells. Ph.D. Thesis. Northwestern Univ. 229P.

Billone,M. & Raynor,S. (1973) Transmission of radial shear forces to cochlear hair cells. J. Acoust. Soc. Am. 54:1143-1156.

Carmel,P.W. & Starr,A. (1963) Acoustic and nonacoustic factors modifying middle-ear muscles in waking cats. J. Neurophysiol. 26:598-616.

Dallos,P.M. (1973) The Auditory Periphery. Academic Press. N.Y. 548P.

Dallos,P.M., Billone,M.C., Durrant,J.D., Wang,C.Y., & Raynor,S. (1972) Cochlear inner and outer hair cells: Functional differences. Science 177:356-358.

Davis,H. (1965) A model for transduction action in the cochlea. In: Cold Spring Harbor Symp. Quant. Biol., Frisch,L. (ed.) 30:181-190.

Engstrom,H. Ades,H.W. & Hawkins,J.E. (1962) Structure and functions of the sensory hairs of the inner ear. J. Acoust. Soc. Am. 34:1356-1363.

Engstrom,H., Ades,H.W. & Bredberg,G. (1970) Normal structure of the organ of Corti and the effect of noise-induced cochlear damage. In: Sensorineural Hearing Loss. Wolstenholme,G.E.W. & Knight,J. (eds.) (J. & A. Churchill, London. pp127-156.

Fernandez,C. (1952) Dimensions of the cochlea (guinea pig). J. Acoust. Soc. Am. 24:519-523.

Fernandez,C., Butler,R., Konishi,T., Honrubia,V. & Tasaki,I. (1962) Cochlear potentials in the rhesus and squirrel monkey. J. Acoust. Soc. Am. 34:1411-1117.

Flanagan,J.L. (1962) Computational models for basilar membrane displacement. J. Acoust. Soc. Am. 34:1370-1376.

Funnell,W.R.J. (1972) The acoustical impedance of the guinea-pig middle ear and the effects of the middle ear muscles. M.Eng. Thesis, McGill Univ. Montreal. 93P.

Goblick,T.J.Jr., & Peiffer,R.R. (1969) Time-domain measurements of cochlear nonlinearities using combination click stimuli. J. Acoust. Soc. Am. 46:924-938.

Guinan,J.J.,Jr. & Peake,W.T. (1967) Middle-ear characteristics of anesthetized cats. J. Acoust. Soc. Am. 41:1237-1261.

Hefelstein,W.M. (1973) Beitrag zur messung der akustisch bedingten bewegungen und identifikation des mechanischen teils des innenohrs der katze. Abhandlung zur Erlangun des Tiles eines Doktors der techneschen wissenschaften der Eidgenoessischen Technischen. Hochschule, Zuerich.

Kiang,N.Y.S., Moxon,E.C., & Levine,R.A. (1970) Auditory-nerve activity in cats with normal and abnormal cochleas. In: Sensorineural Hearing Loss. Wolstenholme,G.E.W. & Knight,J. (eds.) A Ciba Foundation Symp. J. & A. Churchill, London. pp241-273.

Kim,D.O. (1972) A nonlinear model for basilar membrane motion and related phenomena of single cochlear nerve fibers. Sc.D. Thesis. Washington Univ. St. Louis, Mo.

Kim,D.O., Molnar,C.E., & Pfeiffer,R.R. (1973) A system of nonlinear differential equations modeling basilar-membrane motion. J. Acoust. Soc. Am. 54:1517-1529.

Kimura,R.S. (1965) Hairs of the cochlear sensory cells and their attachment to the tectorial membrane. Acta Oto-laryngol. 61:55-72.

Kuo,B.C. (1967) Automatic Control Systems, 2nd Ed. Prentice Hall, Inc. Englewood Cliffs, N.J. 523P.

Lamb,H. (1945) Hydrodynamics. 6th ed. Dover, N.Y.

Lim,D.J. (1972) Fine morphology of the tectorial membrane. Its relationship to the organ of Corti. Archives Otolaryngol. 96:199-215.

Lindeman,H.H., Ades,H.W., Bredberg,C., & Engstrom,H. (1971) The sensory hairs and the tectorial membrane in the development of the cat's organ of Corti. A scanning electron microscope study. Acta Otolaryngol. (Stockh.) 72:229-242.

Miyagi,T. (1958) Viscous flow at low Reynolds numbers past an infinite row of equal circular cylinders. J. Physical Soc. Japan 13:493-496.

Moller,A.R. (1965) Network model of the middle ear. J. Acoust. Soc. Am. 33:168-176.

Mundie,J.R. (1963) The impedance of the ear--A variable quantity. Proc. Middle Ear Function Sem. Rept. No. 576. U.S. Army Med. Res. Lab., Ft. Knox, Ky.

Onchi,Y. (1961) Mechanism of the middle ear. J. Acoust. Soc. Am. 33:794-805.

Peake,W.T. & Guinan,J.J.,Jr. (1967) Circuit Model for the cat's middle ear. Mass. Inst. Technol., Res. Lab. Electronics. Quart. Progr. Rept. 84:320-326.

Rhode,W.S. & Geisler,C.D. (1967) Model of the displacement between opposing points on the tectorial membrane and reticular lamina. J. Acoust. Soc. Am. 42:185-190.

Rhode,W.S. (1971) Observations of the vibration of the basilar membrane in squirrel monkeys using the Mossbauer technique. J. Acoust. Soc. Am. 49:1218-1231.

Rhode,W.S. & Robles,L. (1974) Evidence from Mossbauer experiments for nonlinear vibration in the cochlea. J. Acoust. Soc. Am. 55:588-596.

Rosenblith,W.A. & Rosenzswig,M. (1951) Electrical responses to acoustic clicks: Influence of electrode location in cats. J. Acoust. Soc. Am. 23:583-588.

Schuknecht,H.F. & Neff,W.D. (1952) Hearing losses after apical lesions in the cochlea. Acta Otolaryngol. (Stockholm) 42:263-274.

Schuknecht,H.F. (1953) Techniques for study of cochlear function and pathology in experimental animals. Development of the anatomical frequency scale for the cat. A.M.A. Arch. Otolaryngol. 58:377-397.

Simmons,F.B. (1959) Middle ear muscle activity at moderate sound levels. Ann. Otol. Rhinol. Laryngol. 68:1126-1143.

Spoendlin,H.H. (1966) The organization of the cochlear receptor. Adv. Oto-Rhinolaryngol. (Fortschritte der Hals-NasenOhrenheilunde) Vol. 13. 227P.

Stern,T.E. (1965) Theory of Nonlinear Networks and Systems. Addison Wesley, Reading, Mass.

Tonndorf,J. & Khanna,S.M. (1966) Some properties of sound transmission in the middle and outer ears of cats. J. Acoust. Soc. Am. 41:513-521.

Webster,D.B. (1962) The function of the enlarged middle ear cavities of the kangaroo rat. Dipodomys. Physiol. Zool. 35:248-255.

Wersall,J., Flock,A. & Lundquist,Per-G. (1965) Structural basis for directional sensitivity in cochlear and vestibular sensory receptors. Cold Spring Harbor Symp. Quant. Biol. 30:115-131.

Wersall,J. & Flock,A. (1967) Morphological aspects of cochlear hair cell physiology. In: Sensorineural Hearing Procesess and Disorders. Graham,A.B. (ed.) Little, Brown & Co., Boston.

Wever,E.G., Lawrence,M. & Smith,K.R.(1948) The middle ear in sound conduction. Arch Oto-Laryngol. 48:19-35.

Wiley,C.R. (1960) Advanced Engineering Mathematics. McGraw-Hill. N.Y. 696P.

Wilson,J.P. (1974) Basilar membrane data and their relation to theories of frequency analysis. In: Facts and Models in Hearing, E.Zwicker and E.Terhardt, Eds. Springer-Verlag, Berlin. pp55-63.

CHAPTER 4: THE HAIR CELL

CHAPTER 4
THE HAIR CELL

4.0 INTRODUCTION

The role of the hair cells is to convert the sound induced mechanical motion of Corti's organ into a receptor potential change which then affects the synapses, thus transmitting the signal to the afferent neurons of the cochlear nerve. Is it possible to develop a quantitative description of a receptor cell, in this case a hair cell, as a function of conductance change at the receptor surface? The development of such a model is important for several reasons. There is a paucity of proper quantitative input-output descriptions for receptor cells in the literature. Given a model for hair cell function, it can be decided whether or not the normally occurring gross potential changes in the scalae have any effect on hair cell response. The hair cells are the first opportunity to electrically influence the auditory signal on its path to the brain. An analysis of hair cell function is necessary to ascertain the affect of an implanted cochlear prosthesis. In the development of an overall model for cochlear signal

processing, the hair cell model is an essential submodel. Davis (1961) proposed a phenomenological model of the cochlear hair cells as receptors. It has the cell facing scala media and imbedded in the organ of Corti. This conceptual structure is used for the quantitative model. Thus the aim of this chapter is to develop and analyze a model for the hair cell and make some predictions.

4.1 STRUCTURE

4.1.1 ANATOMY

Inner and outer hair cells are depicted in figure:4.1. At the top of the cell there are cilia embedded in a dense cuticular plate region (CP) surrounded by what is called the cuticular plate free region (CPF). The kinocilium typically found on vestibular hair cells drops off during fetal development of the cochlea (wersall et all, 1965), leaving behind its basal body or centriole. The popular conjecture as to mode of action for the cilia is that their movement causes a conductance change at the top of the cell. From studies on lateral line organ hair cells (Harris et al, 1970; Flock, 1975) and the studies on the auditory papilla of the alligator lizard (Mulroy et al, 1975) it has been shown qualitatively that the cilia are moved as a result of the shear forces acting on the cilia. This idea was first advanced by Bekesey (1960), who used a vibrating needle

perpendicular to the tectorial membrane with vibrations of the point in the same plane as the tectorial membrane and measured the cochlear microphonic. He concluded that radial movements are more effective at stimulating the hair cells than longitudinal movements. What remains unresolved is the actual form of the mechanical distortion of the top surface of the hair cell when there is a mechanical shear force acting on the cilia. Malcolm (1975) suggested that the cilia open up spaces between them at their insertion in the cuticular plate. It seems more reasonable to accept the conjecture of Engstrom et al (1962) and Billone (1972) that the cuticular plate remains as a stiff plate and deforms the cuticular free region around it. Lim (1972), from scanning electron microscope studies of guinea pig organ of Corti reports a "dense amorphous material" between the sensory hairs. When the tall sensory hairs are bent, this amorphous substance holds the hairs together." When the decapsulated Pacinian corpuscle is mechanically deformed, the generator potential increases and the controlling variable is a percentage increase in membrane area (Loewenstein, 1961, 1965). On this basis it is assumed that the cilia and cuticular plate move as a unit, deforming the cuticular plate free region at the top of the cell, inducing a change in the permeabilities of sodium, potassium and chloride. 1

make the assumption that all three permeabilities are changed because the deformation of the cuticular plate free region is mechanical, which would suggest a non-specific effect. The conceptual idea is that the receptor membrane is like a rubber sheet with holes in it. When the sheet is stretched, the holes are enlarged. The nonspecific ion conductance changes for mechanoreceptor membrane appears in the literature as a postulate (Goldman, 1965).

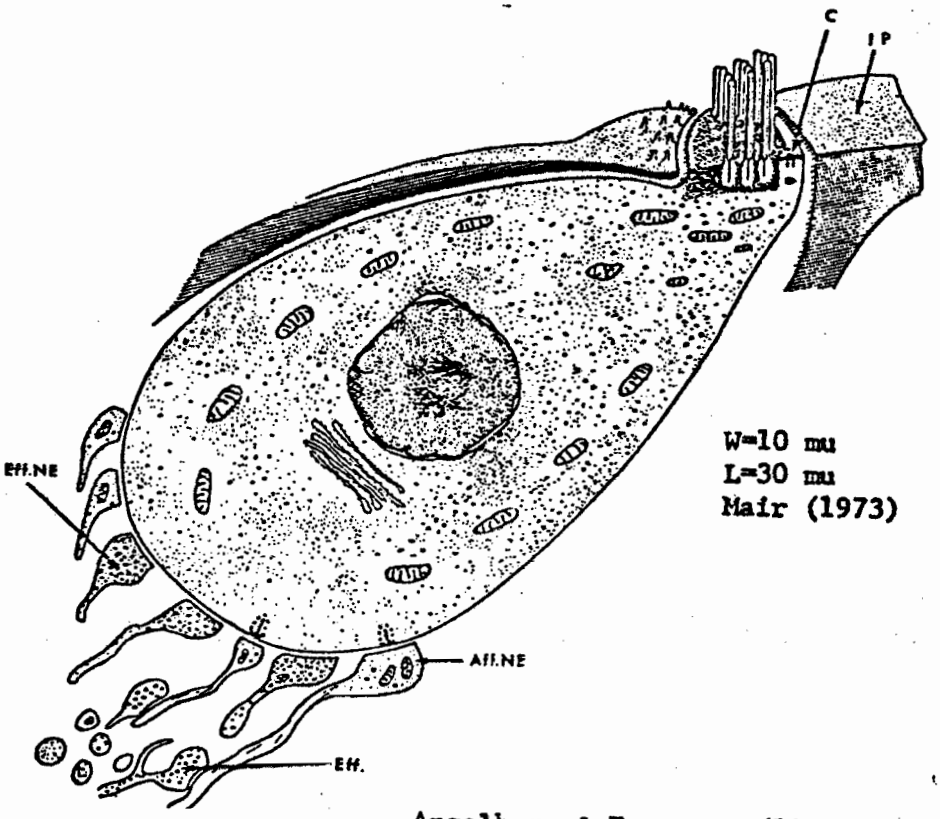

Figure 4.1a A typical mammalian inner hair cell in the organ of Corti. From Angelborg & Engstrom (1973).

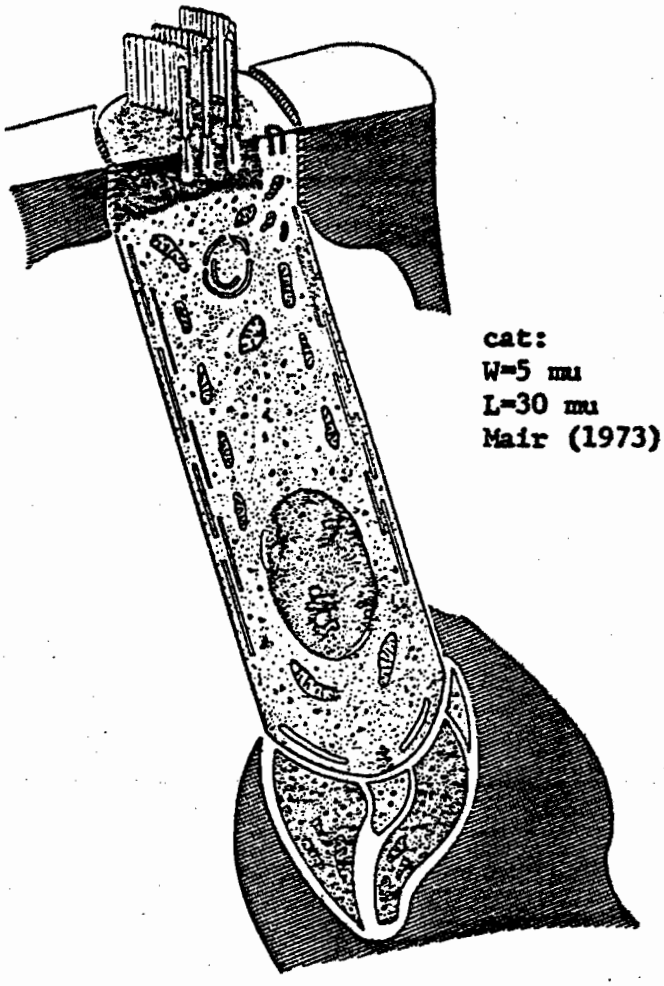

Figure:4.1b A typical mammalian outer hair cell in the organ of Corti. From Angelborg & Engstrom (1973).

4.1.2 ENVIRONMENT

Due to their position in Corti's organ, hair cells have surfaces that are exposed to two different electrical and ionic media. From figures: 4.1.2.1 and 4.1.2.2 note that the tops of the hair cells are exposed to the fluid in scala media, where as the sides and bottoms of the cells are exposed to the fluid in the spaces of Nuel around the cells between the reticular lamina and the basilar membrane.

The stria vascularis on the outer surface of scala media along the cochlea is responsible for producing the fluid in scala media, endolymph. Figure:4.1.2.1 shows the stria vascularis in the cochlea. Figure:4.1.2.2 depicts the mechanism for the production of endolymph, the main points of which are a typical sodium-potassium pump on the cell wall bordering on the extracellular fluid compartment surrounding the capillaries of the stria vascularis. The surface of these cells bordering on scala media is highly permeable to sodium and potassium (Johnston & Sellick, 1972). The result of the stria vascularis border cells structure is an endolymph containing high potassium and chloride with low sodium concentrations.

Flock (1973), using excised freeze dried guinea pig cochleas with X-ray spectroscopy, reports "emission from Cl and K in scala media, from these ions in the same relative

proportions in the tectorial membrane and inner sulcus, but from Cl only in scala tympani. It is concluded that the tectorial membrane and subtectorial space belong to the endolymphatic compartment." Due to the ionic concentration gradients across the border cells of the stria vascularis, there exists a potential of 103 mV average in cat scala media (Sohmer, Weiss, & Peake, 1971).

The fluid surrounding the bodies of the hair cells was originally thought to be distinct from endolymph of scala media and distinct from perilymph of scala tympani. Since endolymph has high potassium and low sodium concentrations, many authors (Smith et al., 1954; Tasaki et al., 1954; Citron et al., 1965; Davis, 1957) have postulated that the tunnel of Corti could not contain endolymph because the non-myelinated dendrites of the cochlear nerve neurons originating at the hair cells could not function in a high potassium environment; consequently it is more like perilymph.

The potential in the fluid around the bodies of the hair cells is taken as +7 mV with respect to the blood compartment referenced to ground from measurement of cat scala vestibuli (Sohmer, Weiss, & Peake, 1971). The ionic concentrations and voltages for the various compartments are summarized in table:4.1.2 and figure:4.1.2.3.

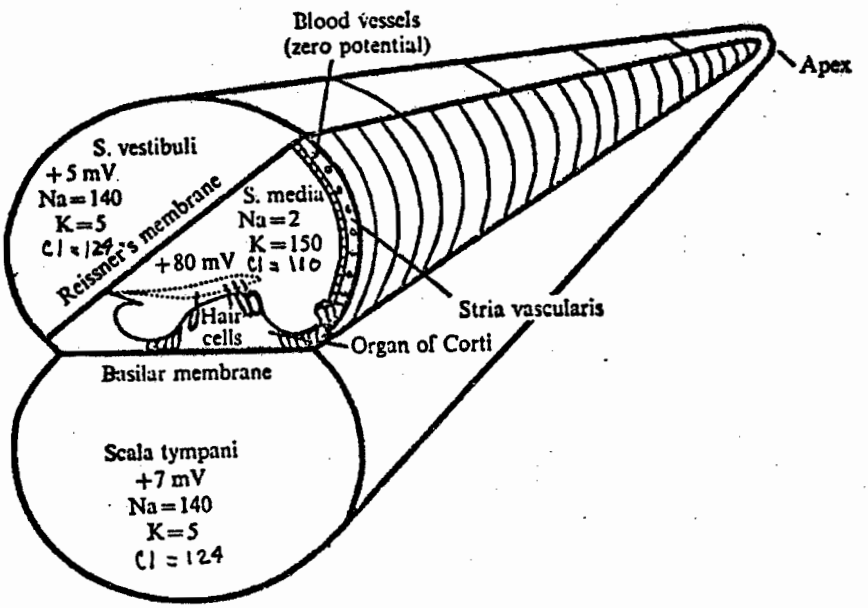

Figure:4.1.2.1 The cochlea in schematic form. The mammalian cochlea is coiled, ranging from a quarter turn in echidna (monotreme) to four turns in the guinea pig. For guinea pigs, the surrounding bone is soft and thin, but in man and cats it is the hard temporal bone. The scala vestibuli and scala tympani are connected at the apex by a small canal (helicotrema). Ionic concentrations are millimoles/liter and the voltages are with respect to plasma, which is the usual reference in neurophysiology work. From Johnston and Sellick (1972).

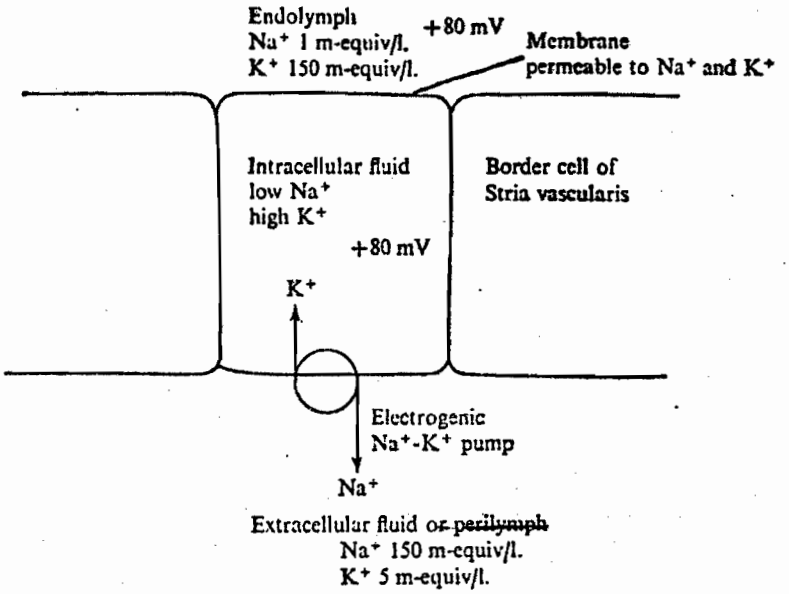

From Johnstone & Sellick (1972)

Figure:4.1.2.2 The transport system of the stria vascularis border cells. The electrogenic Na-K pump is located on the plasma side of the border cell.

TABLE 4.1.2 Guinea pig cochlear fluid composition (milliM.)

PERILYMPH	ENDOLYMPH	CSF	SERUM	SOURCE
---------- sodium				
150.3 +- 2.1	15.8 +- 1.6	152.0 +- 1.8	138.6 +- 1.9	2
148	26	150	140	3
137 +- 2.7	1.8 +- 0.1	-	-	7
135	-	-	-	8
150	79	-	-	10
143	54	-	-	1
---------- potassium				
4.8 +- 0.4	144.4 +- 4.0	4.2 +- 0.5	-	2
5.0	142.0	4.0	4.5	3
-	138	-	-	6
3.6 +- 0.4	151 +- 3.8	-	-	7
3.7	-	-	-	8
10	130 +- 12	-	-	10
1.7	13	-	-	1
---------- calcium				
3.0 +- 0.2	3.0 +- 0.2	3.0 +- 0.2	-	4
2.08+- 0.19	-	2.42+-0.22	4.50+-0.40	9
---------- magnesium				
2.0 +- 0.2	0.9 +- 0.2	2.0 +- 0.2	-	4
---------- chloride				
121.5 +- 1.2	107.1+-1.4	122.4+-1.0	93.9+-1.5	2
120	110	122	-	3
123.5	-	-	-	8
132	-	-	-	1
---------- pH				
7.81 to 8.00	7.33 to 7.52	-	-	5

(Adapted from Moscovitch, 1970)

1 Ulrich et al (1966)
2 Smith et al (1954)
3 Citron et al (1956)
4 Citron and Exley (1957)
5 Misrahy et al (1958)
6 Smith et al (1958)
7 Johnstone et al (1963)
8 Rauch (1964)
9 Schindler et al (1965)
10 Rodgers and Chou (1966)

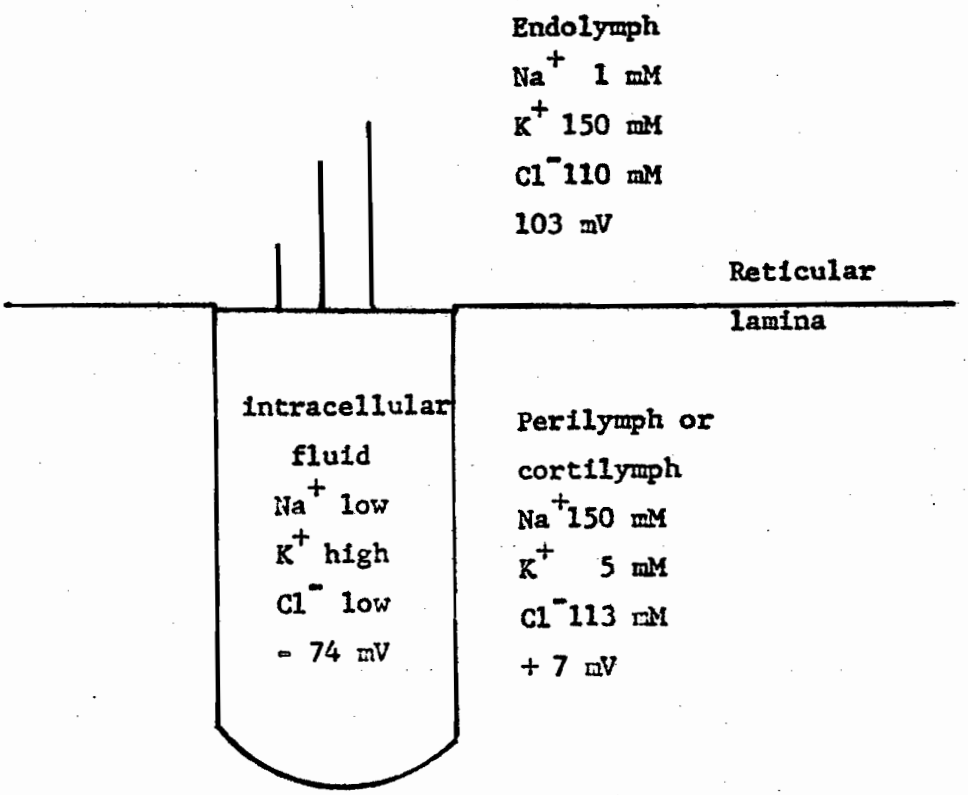

Figure:4.1.2.3 Internal and external environments of a cochlea hair cell. Adapted from Johnstone & Sellick (1972).

4.2 HAIR CELL EXPERIMENTAL DATA

The currently available data from hair cell experiments comes from guinea pig and non-mammalian sources: the hair cells in the flat basilar membrane of alligator lizard and the lateral line organ of animals such as catfish, frogs, and sea skates. Russell and Sellick (1977) recorded from guinea pig hair cells on the basal end of the cochlea. Using procion yellow in glass microelectrodes, hair cells were distinquished from supporting cells by post-mortem examination. The hair cells were found to have resting potentials of 80 to 90 millivolts and small depolarizing potentials of 0 to 1 millivolt at 74 dB SPL at characteristic frequency. The cells identified post-mortem under the microscope as hair cells had 34 to 35 mV resting potentials and positive receptor potentials between 5 and 17 mV at 74 dB SPL at characteristic frequency. They never found negative receptor potentials in a cell. Mulroy, Altman, Weiss, and Peake (1974) recorded intracellularly from the alligator lizard, Gerrhonotus multicarinatus, using fluorescent dye marking techniques to verify that the recording site was inside a hair cell. They found an average intracellular resting potential of -74 mV in a range of -25 to -125 mV. It is important to note that in the alligator lizard the anatomy of the middle ear and basilar

membrane is markedly different from mammals. The response of the hair cell is not a pure sine wave but similar to a sine wave plus a dc shift when the input at the ear drum is a pure sine wave. This may due to the shear force action on the cilia. Since the shape of the cilia array on the top of the hair cell has decreasing lengths in a "V" or "W" shape with the open side facing inward in the radial direction, may be the cilia array does the rectification. In fact, the only anatomical asymmetry, with respect to signal (physical response) between ear drum and hair cell is the cilia array. Mulroy et al (1974) showed an average intracellular response to a tone burst. It also had the form of a sine wave plus a dc shift and local smooth minimums.

Flock (1973) recorded intracellularly from the hair cells in the lateral line organs on the head of the catfish, Lota lota. He found intracellular potentials of -10 to -65mV and membrane resistances of 8 to 110 megohms, with a tendency for cells with a high membrane potential to have a high impedance. Using current pulses, a time constant of 0.2 msec was measured. These cells are cylindrical in shape with diameter 10 microns and length 25 microns, giving a surface area of 942 square microns. He remarks that a hair cell with a 1000 square micron surface area and time constant of 0.2 msec, would have a specific membrane

capacitance of about 0.3 micro Farad/sq cm, using an input resistance of 50 megohms. With the input impedance of the cells in the range of 10 to 100 megohms, the membrane resistivity is 100 to 1000 ohms*cm*cm.

Weiss, Mulroy, & Altmann (1974) report further work on the alligator lizard hair cells. A typical response is shown in figure:4.2. They state that displacement of the cilia toward the kinocilium (or toward the basal body of the missing kinocilium, as it is lost in mammals after birth) results in a depolarization of the hair cell and movement in the opposite direction causes hyperpolarization. This verifies the conjecture of Loewenstein and Wersall (1959), Flock and Wersall (1971), and Bekesy (1960) that the maximum sensitivity of the hair cells is achieved when the motion of the organ of Corti is radialward (away from the center of the cochlear helix toward the spiral lamina).

Russell and Sellick (1978) measured intracellular resistance changes by injecting sinusoidal current and measuring the potential change with a lock-in amplifier during exposure to a swept pure tone sound stimulus. They found receptor potentials in the order of 10 to 12 millivolts for approximately 40 to 90 dB SPL input amplitudes. By plotting receptor potential versus whole cell resistance change, they found the relationship to be

nearly a straight line with slope 0.62±0.18 millivolt/megohm and vertical intercept of zero. The range was 0 to 24 megohms.

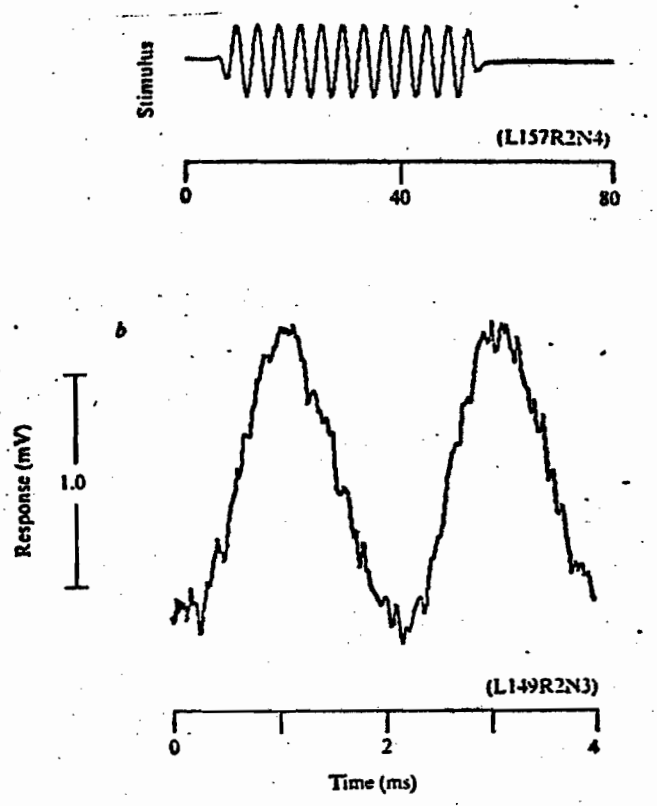

Figure:4.2 Typical response of an alligator lizard hair cell to a tone, recorded intracellulary and identified by dye marking post-experiment. The tone was 500 Hz at 73 dB SPL delivered at the external auditory meatus. The average response was computed from 310 individual responses sampled at 20 microsec. intervals. (From Mulroy et al, 1974)

4.3 THE HAIR CELL MODEL

The model of the hair cell used here consists of two membranes and three compartments. There is the receptor membrane at the top of the cell that separates the cell from scala media. The second membrane separates the interior from the extracellular space in the organ of Corti. The three compartments are scala media, the hair cell interior, and the organ of Corti extracellular space. Associated with each compartment there is a voltage: VSM, VHC, VOC, respectively for the fluid in scala media, the hair cell interior, and the organ of Corti extracellular space. The conceptual view point is that of current flow in the membranes. When the cuticular free region (CFR) is distorted due to the mechanical motion of the cilia, the permeability of the cuticular free membrane to sodium, potassium, and chloride is altered, resulting in a change in current flow through the top of the hair cell. The change in current flow through the CFR must be compensated by a change in current flow through the cell body (sides and bottom) membrane. The result of these currents is a change in the hair cell voltage, VHC.

The current through a membrane can be viewed as the sum of a distributive current due to the capacitance of the membrane and an ionic current (Hodgkin & Huxley, 1952;

Mackey, 1976). The ionic current is due to the electrochemical gradients and membrane permeabilities to the ions present. There is also the metabolic pump current. Thus the general membrane current is

$$I = A*Cm*V' + A*Gm*V + A*Jp$$

where A is the area of the membrane considered and Cm is the capacitance per unit area, and Jp is pump current per unit area. The time derivative of V is denoted by V', which is unambiguous here for no other derivatives are used in the hair cell model or analysis.

The total current, I_B, through the cell body is

$$I_B = A_B*C_{mB}*V_B' + A_B*G_{mB}*V_B + A_B*Jp$$

where A_B is the cell body membrane area, V_B is potential across the cell body membrane, C_{mB} and G_{mB} are respectively the capacitance and conductance per unit area.

The total current, I_T, through the cell top is

$$I_T = A_T*C_{mT}*V_T' + A_T*G_{mT}*V_T + g_r*V_T + A_T*Jp$$

where "T" denotes hair cell top and g_r is receptor conductance change in response to auditory stimulation. The pump current A_T*Jp at the cell top may be negligible compared to A_B*Jp. In any case, they both will drop out in the equilibrium condition.

Summing all the currents into the cell gives

$$I_B + I_T = 0$$

The model of the hair cell which I use is expressed graphically in figure:4.3. The transmembrane potential across the top of the cell, V_T, is

$$V_T = V_{HC} - V_{SM}$$

and for the cell body membrane

$$V_B = V_{HC} - V_{UC}$$

Substitution into the whole cell current conservation equation yields with some rearrangement

$$(A_B*C_{mB} + A_T*C_{mT})*VHC' + (A_B*G_{mB} + A_T*G_{mT})*VHC + g_r*(VHC-VSM)$$

$$=$$

$$A_B*C_{mT}*VUC' + A_T*C_{mT}*VSM' + A_B*G_{mB}*VUC + A_T*G_{mT}*VSM - (A_B+A_T)*Jp$$

This equation is called the hair cell complete equation.

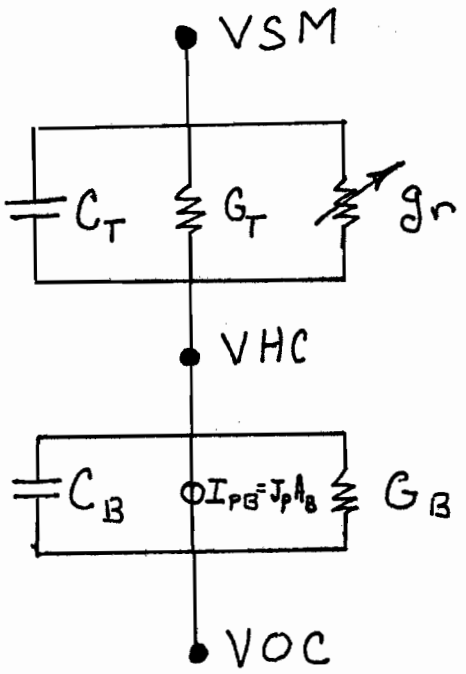

Figure:4.3 Hair cell circuit diagram. C is the capacitance per unit area of the cell membrane, the areas of the cell top and body are Atop and Abod, respectively. ACFR is the area of the cuticular free region, JCFR is the positive outward current density of the cuticular free region, JBOD is the positive outward current density of the cell body membrane and VtopO and VBbod are the equilibrium voltages for the top and body respectively. Jp is the membrane sodium-potassium pump.

4.4 REMAINING CONSTANTS

4.4.1 AREAS OF THE HAIR CELL MEMBRANES

There remains to specify the areas of the hair cell body ABOD, the top of the cell ATOP, and of the cuticular plate free region ACFR. The hair cells can be considered as cylinders shown in figure:4.4. Let WHC be the width of the hair cell and LHC be the length of the hair cell. Then the area of the body is the surface area of the cylinder without the top of the cell. Hence

$$ABOD = 2*pi*R*(LCH-R) + 2*pi*R^2$$

where R = WHC/2 and having considered the base of the cell as a half sphere as shown in figure:4.4.1. The area of the top is

$$ATOP = pi*R^2$$

From the multitude of pictures in Spoendlin (1966) and Engstrom et al (1966) it appears that the cuticular plate free region is an annulus between the cuticular plate region and the outer circumference of the top of the cell. If r is the radius of the cuticular plate and P is the fraction of the top of the cell which is cuticular plate free, then

$$ATOP - ACP = P*ATOP$$

Hence

$$pi*R^2 - pi*r^2 = P*pi*R^2$$

thus

$$P = 1 - (r/R)^2$$

It seems from the pictures cited which show the cuticular plate, that r/R = 0.9, giving P = 0.19. Therefore

ACPR = 0.19*ATOP

Mair (1973) in studies of the hereditary deafness of the white cat, made dimension measurements of normal cat hair cells. From his tables the width of the inner and outer hair cells are averaged and found to be

WIHC = 10.7 microns

WOHC = 4.7 microns

The lengths of the inner and outer hair cells are

LIHC = 29.9 microns

LOHC = 29.8 microns

The values of these dimensions are the average values for the adult, averaged over three coils. From these values, the areas are determined to be ABOD = 1005 sq. microns and ATOP = 89.9 sq. microns for inner hair cells. For outer hair cells, ATOP = 17.3 sq. microns and ABOD = 440 sq. microns.

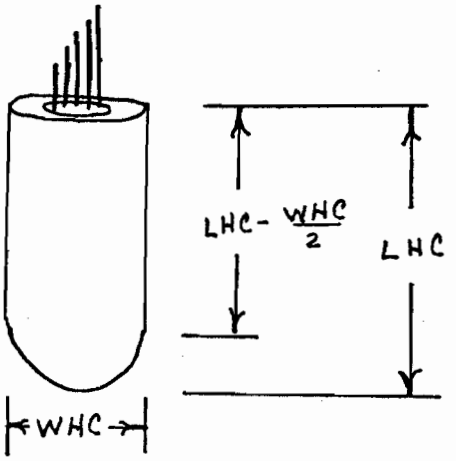

Figure:4.4.1 The dimensions of the hair cell labeled.

4.4.2 MEMBRANE CONDUCTANCES

The Hodgkin-Huxley (1952) equations for excitable neural membrane could be used to predict the membrane ionic current density and conductances. These equations are for squid giant axon membrane. However, these equations do not explicitly take into account different ionic gradients across a neural membrane. Also a hair cell does not have the same ion gradients across its membranes as does a typical neuron. Alternatively, there is the electrodiffusion theory, represented by the Goldman equation (Mackey,1975; Goldman,1943). Although the sodium conductance characteristics in the squid axon do not agree (Cole,1965) with electrodiffusion theory, potassium conductance does. As an explanation for passive properties of neural membrane particularly near equilibrium how well does the Goldman theory work as an approximation to ion conductances? I will examine the Goldman equation for this level of analysis as an approximation to ion conductances for membranes separating fluids with greatly differing ion concentrations.

To obtain the current density through the membranes, I use the electrodiffusivity formulation of passive ionic movement since the membranes are nonexcitable. Following Mackey & McNeel (1973) and Mackey (1975, Ch 5,6,7), the

current density of ions through a non-excitable membrane with the Goldman (1943) assumption of no charge inside the membrane and the deceleration of the ions due to collisions with the membrane being negligible, is

$$J = \frac{Q*Q*D*V}{t*K*T} * \frac{Ni*\exp(Q*V/K*T) - No}{\exp(Q*V/K*T) - 1}$$

where Q=charge on an ion (coulombs), D=diffusivity (cm*cm/sec), V=transmembrane voltage (volts, outside is the reference), Ni and No are the respective concentrations of the ion inside and outside the membrane (molecules/liter), t=membrane thickness (cm), K=Boltzman constant (Joule/deg Kelvin), and T=temperature (deg Kelvin). Using Z=valence of the ion, and e=charge on an electron, B=e/K*T, and P=D/t (permeability cm/sec), then

$$J = Q * \frac{Q}{K*T} * \frac{D}{t} * V * \frac{Ni*\exp(Z*B*V) - No}{\exp(Z*B*V) - 1}$$

$$= Z*Z*e*B*P*V * \frac{Ni*\exp(Z*B*V) - No}{\exp(Z*B*V) - 1}$$

The current density J is in amps per square cm. The neural membranes considered here have nonzero permeabilities only to sodium, potassium, and chloride. The net ionic current density JTOT is the sum of the current densities for sodium, potassium, and chloride.

$$JTOT = JNa + JK + JCl$$

Let PNa, PK, PCl denote the permeability of the membrane to

sodium, potassium, and chloride. Let NAi, NAo, Ki, Ko, CLi, CLo denote respectively the number densities (ions/liter) of sodium, potassium and chloride, inside and outside the membrane surface of the cell. Consequently, the total ionic current density becomes

$$J = e*B*V * \frac{T1*\exp(B*V) - T2}{\exp(B*V) - 1}$$

where

$$T1 = PNA*NAi + PK*Ki + PCL*CLo$$

$$T2 = PNA*NAo + PK*Ko + PCL*CLi$$

The current density through the cuticular free region, JCFR, and through the body membrane, JBOD, is given by

$$JCFR = e*B*VTOP * \frac{T1TOP*\exp(B*VTOP) - T2TOP}{\exp(B*VTOP) - 1}$$

$$JBOD = e*B*VBOD * \frac{T1BOD*\exp(B*VBOD) - T2BOD}{\exp(B*VBOD) - 1}$$

The permeabilities PNA, PK, and PCL are for the membranes at rest or unstressed. These permeabilities remain unchanged for the cell body membrane. However, for the top of the cell, the cuticular plate free region, the permeabilities change due to the stress on the membrane from the shear force on the cilia. In light of the decapsulated Pacinian corpuscle studies (Loewenstein, 1960) where the receptor potential is a linear function of stress for small displacements, it seems reasonable to change the permeabilities all by the same ratio during a stress of the

membrane constituting the cuticular plate free region (Goldman,1965).

From the experimental literature, it is seen that the cochlear nerve axons saturate (reach their maximum value of APs per second) at some sound pressure input level, say DBSAT, when the input frequency is equal to the characteristic (sound) frequency of the axon (Johnson, 1974; Sachs & Abbas, 1974). From chapter 3 the forces on the cuticular plate are available, F1 for the inner hair cells and F3 for the outer hair cells. In general, say the force on the cuticular plate is FC. Let FCMAX be the value of FC when the input SPL amplitude is DBSAT. The permeabilities are monotonic increasing with respect to FC, so as a first approximation use proportionality, thus for each permeability P_i,

$$P_i = P_{i0} + dP$$

where P_{i0} is the value for FC=0, dP is the (receptor) permeability change which is proportional to FC/FCMAX. Thus the permeabilities are changed by the same multiplier 1+(FC/FCMAX), and the permeability terms T1TOP and T2TOP become

```
T1TOP = (PNA*NAHC + PK*KHC + PCL*CLSM)*(1+Kp*(FC/FCMAX))
T2TOP = (PNA*NASM + PK*KSM + PCL*CLHC)*(1+Kp*(FC/FCMAX))
```

where Kp is the proportionality constant and where

NASM = number density of sodium in scala media
NAHC = number density of sodium in a hair cell
KSM = number density of potassium in scala media
KHC = number density of potassium in a hair cell
CLSM = number density of chloride in scala media
CLHC = number density of chloride in a hair cell

Since the membrane that surrounds the cell body is unchanged, T1BOD and T2BOD remain constant

T1BOD = PNA*NAHC + PK*KHC + PCL*CLOC

T2BOD = PNA*NAOC + PK*KOC + PCL*CLHC

where

NAOC = number density of sodium in organ of Corti
KOC = number density of potassium in organ of Corti
CLOC = number density of chloride in organ of Corti

Since not enough is known about the receptor region of the hair cell, except for anatomy, it is fruitless at this time to pursue the receptor conductances changes as changes in permeabilities. Thus Kp is left at zero and only the non receptor membrane conductances are examined.

The conductances per unit area for the cell body membrane, G_{mB}, and for the top, G_{mT}, are

$$G_{mB}=JBOD/VBOD$$

$$G_{mT}=JTOP/VTOP$$

The conductance for the hair cell body membrane is shown in figure:4.4.1.1. The conductance when v=0 (VHC=VHC0) is GVH0=5.2 picomho/sqmicron which corresponds to a resistivity value of 1919 ohm*cm^2. Permeability ratios for K,Na,Cl (1:0.06:0.02) were used from Woodward, Bianchi, and Erulkar (1969). Permeability for potassium taken to be $1.8*10^{-6}$ cm/sec (Hodgkin & Katz, 1949). A neuron with typical

intracellular ion concentrations (Na=32, K=160, Cl=11 milliM) and extracellular ion concentrations (Na=140, K=4.5, Cl=94 milliM) gives as a value of $G_m = G_{typ} = 2.6$ picomho/sqmicron. This is a resistivity value of 3.8 Kohms*cm^2. The values from the Goldman conductance for the hair cell top are shown in figure:4.4.1.2. The equilibrium conductance is 5.6 picomho/sqmicron. The upper family of three curves shows the membrane conductance at the hair cell top for different conditions: (1)Middle curve: equilibrium condition. (2)Top curve: increase of 10 mvolts in extracellular fluid (endolymph of SM). (3)Bottom curve: a decrease of 10 mvolts. The corresponding curves are plotted for a typical neuron in the lower three curves, with zero ECF potential (middle curve), increase of 10 mvolts (upper curve), and a decrease of 10 mvolts (lower curve). In the literature for comparison of neural membrane resistivity, R_m, the value of 1000 ohm*cm^2 is given for squid giant axon (Cole & Hodgkin, 1939; Cole & Barker, 1941a,b). Barrent and Crill (1974) found the range of 1777 to 2520 ohm*cm^2 for motoneurons. Rall (1959) analyzed whole neuron resistances, R_N, as seen by an electrode inserted in spinal motoneuron soma. He related experimentally obtained values with anatomical computed values and derived a formula relating R_N and R_m. He found that with R_m = 4000 ohm*cm^2, the whole

neuron resistances were best matched.

I will use R_m = 1000 ohm*cm^2 which is an upper range value from Flock (1973) and a compromise value with respect to this discussion. The corresponding conductance value is

$$G_m = 1/R_m = 10 \text{ picomho/sqmicron}$$

A really complete treatment would include the number of sodium pores, potassium pores, and chloride pores per unit area on the cell membrane. The value for the number of membrane pumps per unit area, would also be necessary for this treatment. After speculating this, I found that Stevens (1979) describes the neural membrane with typical numbers of ion specific pore and pump molecules per sqmicron. Even though ions per second are given for a pump site, and separate pore conductances are available, the number of these special membrane molecules vary widely. Unfortunately at this time a more precise value of hair cell membrane conductances is impossible.

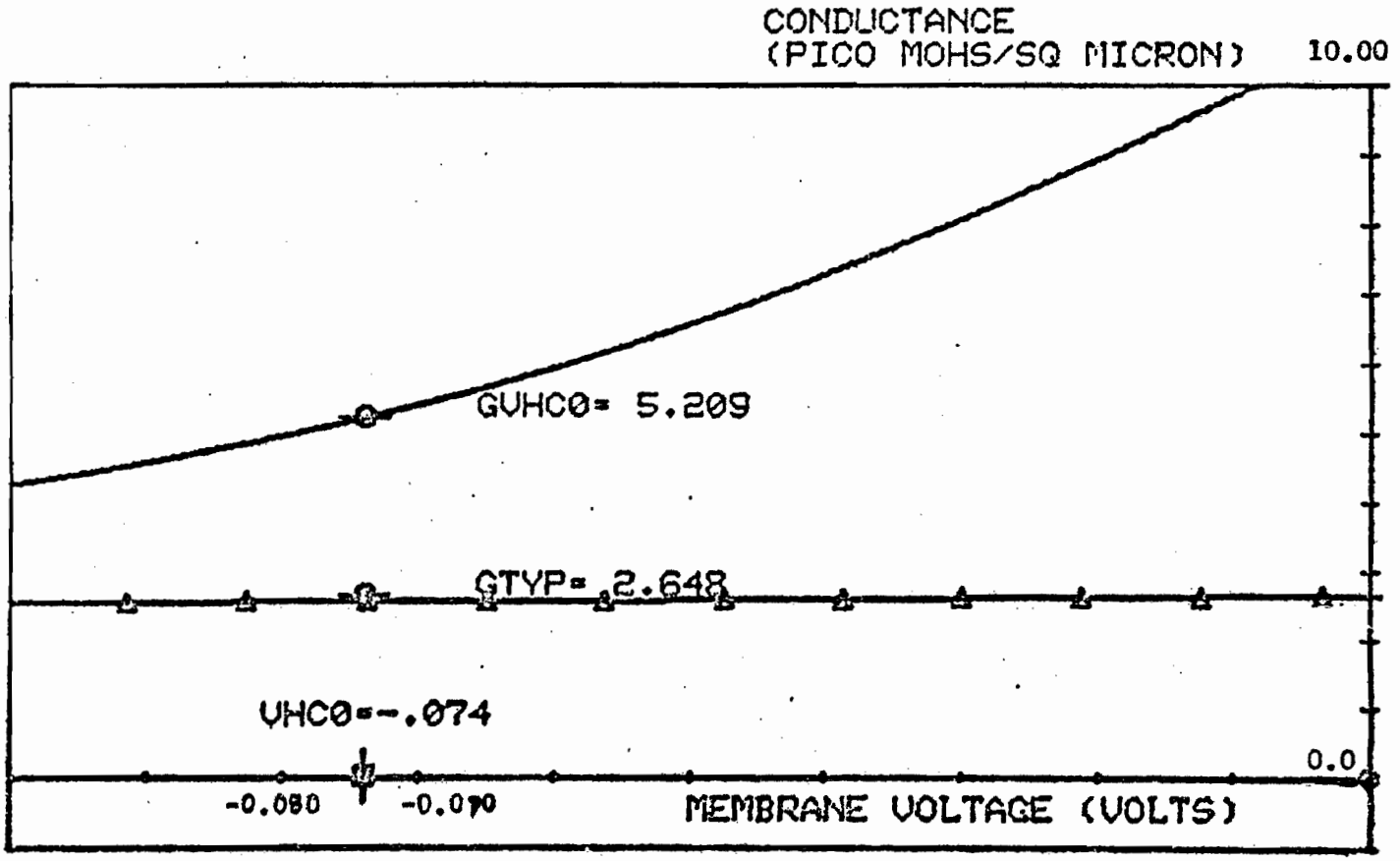

Figure:4.4.1.1 The lower curve is for a typical neuron with the usual intracellular and extracellular concentrations. The circled points, GVH0 and Gtyp values are potential value VBOD = VHC-VSM. See text for discussion.

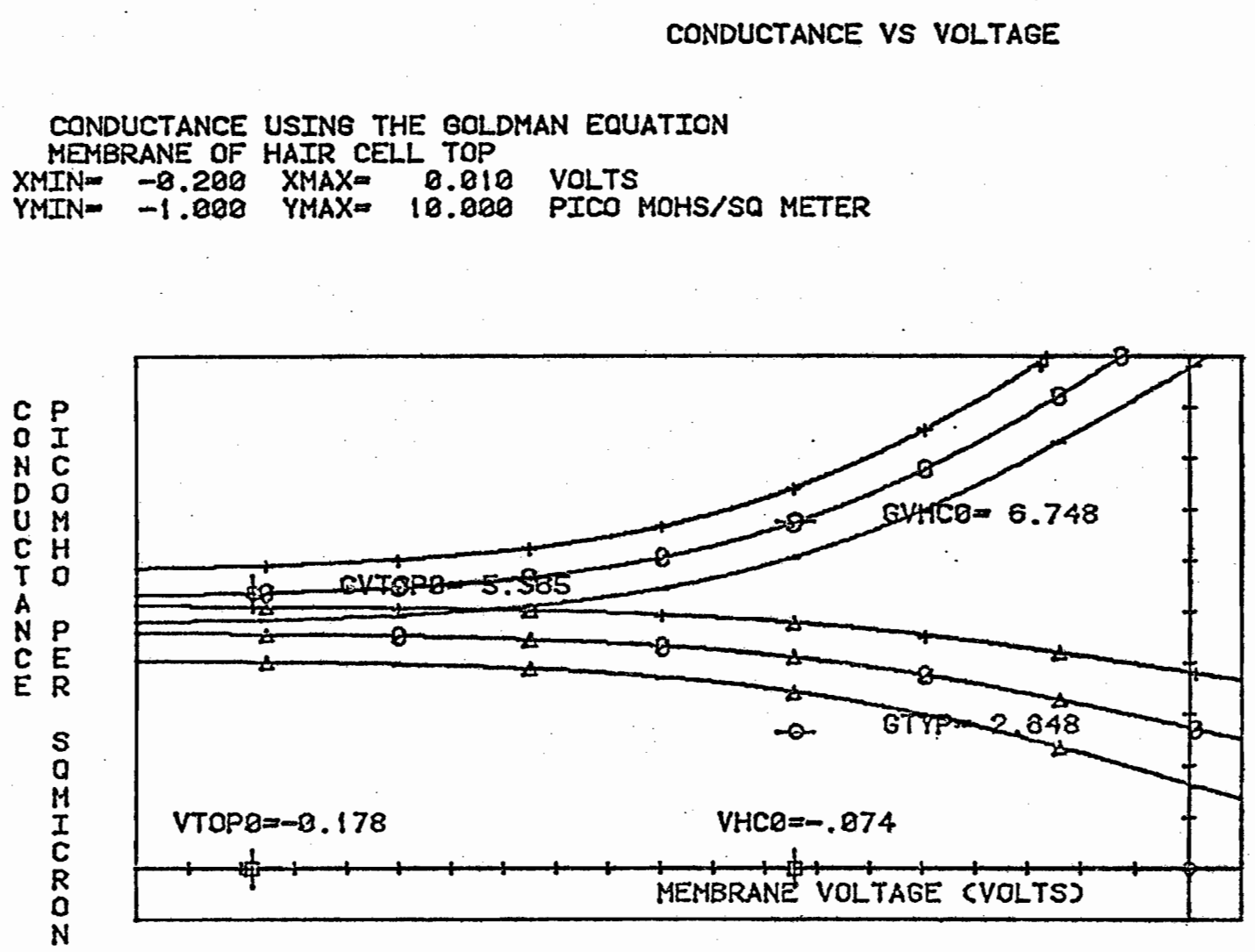

Figure:4.4.1.2 Conductance predicted from the Goldman equation for the hair cell top (non receptor concuctance). The curve with triangles is for a typical neuron with the usual intra- and extracellular concentrations. See text for discussion.

4.5 THE HAIR CELL IN SIMULATION FORM

Given the dynamic equilibrium equation for the hair cells which must be satisfied at all times, it is necessary to solve for VHC', the time derivative of the hair cell voltage. Let

$$C_B = A_B * C_{mB}$$

$$C_T = A_T * C_{mT} = A_{CFR} * C_{mT}$$

$$G_B = A_B * G_{mB}$$

$$G_T = A_T * G_{mT} = A_{CFR} * G_{mT}$$

then

$$(C_B + C_T)*VHC' + (G_B + G_T)*VHC + g_r*(VHC-VSM)$$

$$= C_B*VOC' + C_T*VSM' + G_B*VOC + G_T*VSM - (A_B + A_T)*Jp$$

and thus

$$VHC' = \frac{1}{C_B+C_T}\left|(G_B + G_T)*VHC + g_r*(VHC-VSM) - C_B*VOC' - C_T*VSM' - G_B*VOC - G_T*VSM + (A_B+A_T)*Jp\right|$$

For a dynamic time simulation, obviously

$$VHC = \int_0^{\Delta t} VHC'*dt$$

Note that the time derivatives VSM' and VOC' are in the expression for VHC'. They are not necessarily zero because of the cochlear microphonic produced by the ensemble of hair cells.

4.6 ANALYSIS

The hair cell dynamic equilibrium equation is nonlinear; however, it is possible to investigate the values of the parameters over the range of the input variables. The normal use of the hair cell is to produce the receptor potential, v, in response to receptor conductance change, g_r. What can be said about v in relation to g_r? What happens when the potential of the fluid extracellular to the hair cell is changed. The driving variable is not g_r, but VOC. What can be said about v with respect to VOC?

First, a simplification is made to the original hair cell equation. The hair cell potential is the sum of a resting potential, VHC0, and a receptor potential, v. Substitution into the whole cell current conservation equation equation and noting that

$$VHC' = (VHC0 + v)' = v'$$

yields with some rearrangement

$$(A_B*C_{mB} + A_T*C_{mT})*v' + (A_B*G_{mB} + A_T*G_{mT} + g_r)*v$$
$$+ (A_B*G_{mB} + A_T*G_{mT})*VHC0 + g_r*(VHC0 - VSM)$$
$$=$$
$$A_B*(C_{mB}*VOC' + G_{mB}*VOC) + A_T*(C_{mT}*VSM' + G_{mT}*VSM)$$
$$- (A_B*Jp + A_T*Jp)$$

This is called the hair cell complete equation.

When there is no auditory induced input to a hair cell,

$$g_r = 0, \quad v = v' = 0, \quad VSM' = VOC' = 0$$

and VSM and VOC are at resting values VSM0 and VOC0, respectively. This state gives the following equilibrium condition:

$$(A_B * G_{mB} + A_T * G_{mT}) * VHC0$$

$$=$$

$$A_B * G_{mB} * VOC0 + A_T * G_{mT} * VSM0 - (A_B * Jp + A_T * Jp)$$

Substituting this relation into the over all equation gives an equation for v and g_r about the resting point.

$$(A_B * C_{mB} + A_T * C_{mT}) * v' + (A_B * G_{mB} + A_T * G_{mT} + g_r) * v + (VHC0 - VSM) * g_r$$

$$=$$

$$A_B * C_{mB} * VOC' + A_T * C_{mT} * VSM' + A_B * G_{mB} * (VOC - VOC0) + A_T * G_{mT} * (VSM - VSM0)$$

Henceforth, this is called the hair cell equation, where the variables that change are v, VOC , and VSM , in response to a change in g_r.

4.6.1 RVHC VS RECEPTOR CONDUCTANCE

Now to analyze the hair cell equation for receptor voltage, v, versus receptor conductance, g_r. Assume that VSM, VSM', VOC, VOC' are near zero, to neglect cochlear microphics for this analysis. The hair cell equation becomes

$$(A_B*C_{mB} + A_T*C_{mT})*v' + (A_B*G_{mB} + A_T*G_{mT})*v + g_r*v + (VHC0-VSM0)*g_r = 0$$

Using C_B, C_T, G_B, G_T and rearranging gives

$$(C_B + C_T)*v' + [(G_B+G_T) + g_r]*v + (VHC0-VSM0)*g_r = 0$$

Using G_{mB} = 10 picomho/sqmicron (1000 ohm*cm^2), G_{mT} = 5.6 picomho/sqmicron from the Goldman equation, and an area of 440 sqmicrons, the whole cell resting conductance, G, is

$$G = G_B + G_T = A_B*G_{mB} + A_T*G_{mT}$$

$$= A_B*G_{mB} \quad \text{since } A_B >> A_T$$

$$= 4.4*10^{-9} \text{ mho}$$

Using

$$C_{mB} = C_{mT} = C_m = 0.3 \text{ microF/sqcm} = 0.3*10^{-14} \text{ F/sqmicron}$$

Thus, whole cell capacitance is

$$C = C_B + C_T = A_B*C_{mB} + A_T*C_{mT}$$

$$= A_B*C_{mB} \quad \text{since } A_B >> A_T$$

$$= 1.3*10^{-12} \text{ Farads}$$

Consequently, the hair cell equation becomes

$$C*v' + (G+g_r)*v = V_{T0}*g_r$$

where the driving voltage is

$$V_{T0} = -(VHC0 - VSM0)$$

$$= 0.177 \text{ volts}$$

The term g_r*v in $(G+g_r)*v$ makes the equation nonlinear.

What are the possibilities? They are

Case 1: $G << g_r$

Case 2: G and g_r are in the same range

Case 3: $G >> g_r$

4.6.1.1 CASE 1

When $G << g_r$, the hair cell equation becomes

$$C*v' + g_r*v = V_{TO}*g_r$$

thus

$$C*v' = (V_{TO} + v)*g_r$$

with the value of V_{TO} at 177 millivolts and v less than 10 millivolts (Weiss et al, 1974; Russell & Sellick, 1978), thus $V_{TO} >> v$. Consequently, the equation becomes

$$C*v' = V_{TO}*g_r$$

4.6.1.2 CASE 2

when G and g_r are in the same range, neither term can be neglected and the equation remains as

$$C*v' + (G + g_r)*v = V_{TO}*g_r$$

and is nonlinear since the product of input, g_r, and output, v, appear.

4.6.1.3 CASE 3

when $G >> g_r$, the hair cell equation becomes

$$C*v' + G*v = V_{TO}*g_r$$

Taking the Laplace transform of both sides gives

$$(C*s + G)*L[v] = V_{TO}*L[g_r]$$

thus the transfer function is

$$H(s) = \frac{L[v]}{L[g_r]} = \frac{V_{TO}}{C*s + G} = \frac{V_{TO}/C}{s + G/C}$$

where $V_{TO}/C = 1.3*10^{9}$ volts/Farad

and $G/C = 3.32*10^{3}$ Hertz

Thus, for this case, the hair cell is a low pass filter with a cut off frequency of 3.3 KHz and gain, K,

$$K = \frac{VSMO - VHCO}{C}$$

which is proportional to the voltage across the hair cell top. The frequency response curve is shown in figure:4.6.1.3.

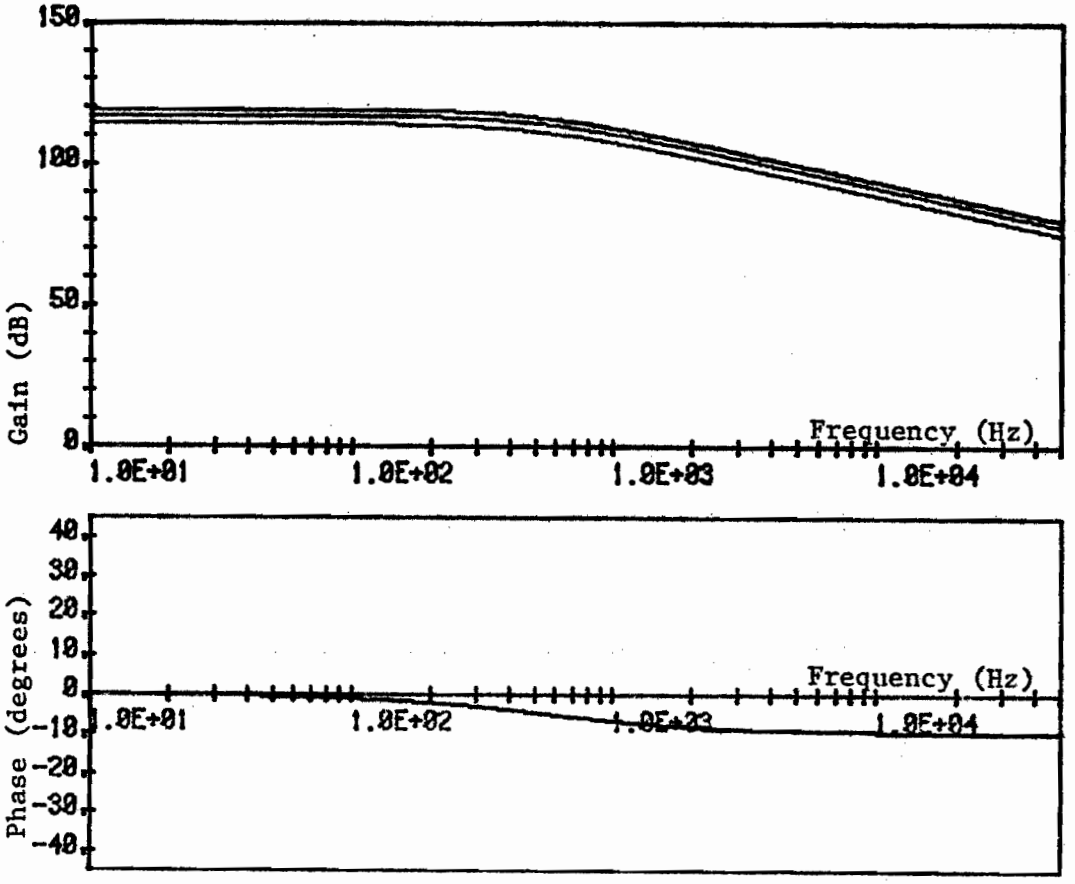

Figure:4.6.1.1 Bode plot of hair cell receptor voltage versus conductance change at the top of the cell. Top: gain in dB versus log(f). Bottom: phase in degrees versus log(f). The middle curve is for V_{TO} = VHCO-VSMO. The top curve is for an increase in V_T of 50 millivolts and the bottom curve is for a decrease of 50 millivolts.

4.6.2 RECEPTOR CONDUCTANCE RANGE

Which of the three cases for magnitude of G and G_r is true? The relative magnitudes are important since they determine whether or not the hair cell equation is linear. The whole cell conductance, G_c, is

$$G_c = A_B * G_{mB} + A_T * G_{mT} + g_r = G + g_r$$

whole cell resistance is thus

$$R_c = \frac{1}{G + g_r}$$

Resting whole cell conductance is

$$G_{c0} = A_B * G_{mB} + A_T * G_{mT} = G$$

and resting resistance is

$$R_{c0} = \frac{1}{G_{c0}}$$

Change in resistance, dR, is given by

$$dR = R_c - R_{c0} = \frac{1}{G_{c0} + g_r} - \frac{1}{G_{c0}}$$

Solving for g_r gives

$$g_r = G_{c0} * \frac{-1}{1 + 1/(dR * G_{c0})}$$

Russell and Sellick (1978) made measurements that can be used to evaluate g_r. Using their value for v/dR of 0.62 millivolt/megohm gives

v millvolt	dR megohm	g_r nanomho
0.0	0.0	0.0
1.0	-1.61	0.03
2.0	-3.22	0.06
5.0	-8.06	0.15
10.0	-16.1	0.29

Now since $G_{c0} = A_B * G_{mB} + A_T * G_{mT} = 4.4$ nanomho,

it is obvious that case 3 ($G >> g_r$) applies. Thus the hair cell equation is linear.

4.6.3 RVHC VS dR

In the Russell and Sellick (1978) paper, there is a graph for dc receptor voltage of a hair cell versus change in whole cell resistance. The graph is a straight line with slope of 0.62 mV/megohm and vertical intercept of zero. This section examines the model with respect to this data.

The hair cell equation from section:4.6.1.3 is

$$C*v' + G*v = V_{T0} * g_r$$

Since they used dc receptor potential, the equation is used with $v'=0$. Thus

$$v = \frac{V_{T0}}{G} * g_r$$

Now to find change in whole cell resistance, dR. Using the equation for g_r as a function of dR gives

$$g_r = \frac{-(G_{c0})^2 * dR}{1 + G_{c0} * dR}$$

Now $G_{c0} * dR << 1$, thus

$$\frac{v}{dR} = \frac{-V_{T0} * G_{c0}^2}{(G_{c0} + g_r)}$$

Thus the model predicts that v/dR is about 0.73 mV/megohm, when g_r is 0.29 nanomho (v=10 mV). This value agrees with the Russell and Sellick value, when their resistance change is in fact a decrease in resistance. Thus result supports the model.

4.6.4 RVHC VS VCC

What if the potential of the organ of Corti, VOC, changes as in the cochlear microphonic, or a pathological condition in the striae vascularis, or induced by a wire implanted in scala tympani for a prosthesis? The resulting relation of interest is the receptor voltage, v, versus VOC. Let v and g_r be as before and let

$$u = VOC - VOC0$$

$$w = VSM - VSM0$$

where VOC0 and VSM0 are the resting organ of Corti and scala media resting potentials. Noting that VOC'=u' and VSM'=w', then substituting into the hair cell complete equation gives

$$(A_B*C_{mB} + A_T*C_{mT})*V' + (A_B*G_{mB} + A_T*G_{mB})*v + (A_B*G_{mB} + A_T*G_{mT})*VHC0 + g_r*[VHC0 - (VSM+u)]$$

$$= A_B*[C_{mB}*u' + G_{mB}*(VOC0+u)] + A_T*[C_{mT}*w' + G_{mT}*(VSM0+w)] - (A_B*Jp + A_T*Jp)$$

For g_r=0, v=u=w=0, v'=u'=w'=0 thus

$$[A_B*G_{mB} + A_T*G_{mT}]*VHC0 = A_B*[G_{mB}*VOC0] + A_T*[G_{mT}*VSM0] - (A_B Jp + A_T*Jp)$$

Substituting this last equation into the previous one, gives

$$(A_B*C_{mB} + A_T*C_{mI})*v' + (A_B*G_{mB} + A_T*G_{mT} + g_r)*v + g_r*[VHC0 - (VSM0+w)]$$

=

$$A_B*[C_{mB}*u' + G_{mB}*u] + A_T*[C_{mT}*w' + G_{mT}*w]$$

and with rearrangement

$$(C_B + C_T)*v' - C_B*u' - C_T*w'$$

$$+ (G_B + G_T)*v - G_B*u - G_T*w + g_r*v$$

$$+ g_r*(VHC0-VSM0) + g_r*w = 0$$

For v=VHC-VHC0 versus u=VOC-VOC0, note that the voltage in scala tympani, VST, is assumed here to be approximately the same as VOC. This is the driving variable when stimulating the hair cells via cochlear implants. Assume that w=w'=0, as scala media is large and is held constant by the pump. Thus

$$(C_B+C_T)*v' - C_B*u' + (G_B+G_T)*v - G_B*u + g_r v$$

$$+ g_r*(VHC0-VSM0) = 0$$

Consider the case where an electrode in scala tympani drives the hair cell. Take VOC=VST, thus we want v=RVHC versus u=VOC-VOC0. Further, say that there there are no operable hair cell cilia as can occur in sensorineural hearing loss (Spoendlin,1976). The hair cell equation has $g_r=0$, thus

$$(C_B+C_T)*v' - C_B*u' + (G_B+G_T)*v - G_B*u = 0$$

and simplifies to

$$C*v' + G*v = C_B*u' + G_B*u$$

where $C = C_B + C_T$ and $G = G_B + G_T$.

Using the Laplace transform gives the transfer function

$$\frac{L[v]}{L[u]} = \frac{C_B*s + G_B}{C*s + G}$$

$$= \frac{m*s + n}{s + k}$$

where

$$m = C_B/C = C_B/(C_B + C_T) = 1$$

$$n = G_B/C = G_B/(C_B + C_T) = 3333 \quad 1/sec.$$

$$k = G/C = (G_B + G_T)/(C_B + C_T) = 3333 \quad 1/sec.$$

thus

$$\frac{L[v]}{L[u]} = \frac{s + n}{s + k}$$

which is a transfer function with unit gain.

4.7 CONCLUSION

In this chapter a quantitative model for an auditory hair cell was developed. A differential equation was derived which describes output, the receptor potential, as a function of the input, conductance at the receptor surface. The differential equation is non-linear. However, in the operating range of receptor conductance, it is linear. Using the Laplace transform, frequency plots were obtained.

The model suggests that the hair cell, operating in its lower range, is a low pass filter. The gain was found to be directly proportional to the voltage, V_T, across the receptor surface. Thus a change in voltage of the lymph in

scala media changes the gain.

When the hair cell cilia are damaged, as in sensorineural hearing loss, the conductance of the receptor surface does not properly change for normal auditory input. Rewriting the differential equation to use the voltage of the fluid surrounding the hair cell, VOC, the transfer function was obtained and found to have roughly unit gain.

Since the model is a quantitative model, it was possible to calculate the appropriate equation for comparison with the Russell and Sellick (1978) results. Particularly valuable is the fact that my model agrees very well with their measurements.

Angelborg,C. & Engstrom,H.(1973) The normal organ of Corti. In: Basic Mechanisms of Hearing. Moller,A.(ed.) Academic Press, N.Y. pp125-184.

Bekesy,G.von(1960) Experiments in Hearing. McGraw Hill, N.Y. 745P.

Billone,M.(1972) Mechanical stimulation of cochlear hair cells. Ph.D. Thesis. Northwestern Univ. 229P.

Citron,L., Exley,D. & Hallpike,C.S.(1956) Formation, circulation and chemical properties of the labyrinthine fluids. Brit. Med. Bull. 12:101-104.

Citron,L. & Exley,D.(1957) Recent work on the biochemistry of the labyrinthine fluids. Proc. Roy. Soc. Med. 50:697-701.

Cole,K.S.(1965) Electrodiffusion models for the membrane of giant squid axon. Physiol.Rev. 45:340.

Davis,H.(1961) Some principles of sensory receptor action. Physiol. Rev. 41:391-416.

Davis,H.(1965) A model for transducer action in the cochlea. In: Cold Spring Harbor Sympos. Quant. Biol. 30:181-190.

Engstrom,H. Ades,H.W. & Hawkins,J.E.(1962) Structure and functions of the sensory hairs of the inner ear. J. Acoust. Soc. Am. 34:1356-1363.

Flock,A., Jorgensen,J.M., & Russell,I.J.(1973) Passive electrical properties of hair cells and supporting cells in the lateral line canal organ. Acta Otolaryngol. 76:190-198.

Flock,A.(1975) Ion concentrations in Organ of Corti. J. Acoust. Soc. Am. Suppl. 2:47.

Flock,A.(1971) The lateral line organ mechanoreceptors. In: Fish Physiology.(ed. W.S. Hoar & D.J. Randall) Vol. 5, pp241-263. Academic Press, N.Y.

Harris,G.G., Frishkopf,L.S., & Flock,A.(1970) Receptor potentials from hair cells of the lateral line. Science 167:76-79.

Goldman,D.E.(1943) Potential, impedance, and rectification in membranes. J. Gen. Physiol. 27:37-60.

Goldman,D.E.(1965) The tranducer action of mechanoreceptor membranes. Cold Spring Harbor Symp. Quant. Biol. 30:59-68.

Hodgkin,A.L. & Huxley,A.F.(1952) A quantitative description of membrane current and its application to conduction and excitation in nerve. J.Physiol. 117:500.

Hodgkin,A.L. & Katz,B. (1949) The effect of sodium ions on the electrical activity of the giant axon of the squid. J.Physiol. 108:37.

Johnson,D.H.(1974) The response of single auditory-nerve fibers in the cat to single tones: Synchrony and average discharge rate. Ph.D. Thesis , M.I.T. Cambridge, Mass.

Johnstone,B.M.& Sellick,P.M.(1972) The peripheral auditory apparatus. Quart. Rev. Biophy. 5(1):1-58.

Johnstone,B.M., Schmidt,R.S. & Johnstone,B.M.(1963) Sodium and potassium in vertebrate cochlear endolymph as determined by flame microspectrophotometry. Comp. Biochem. Physiol. 9:335-341.

Lim,D.J.(1972) Fine morphology of the tectorial membrane. Its relationship to the organ of Corti. Arch. Otolaryngol. 96:199-215.

Lowenstein,O. & Wersall,J.(1959) Functional interpretation of the electron microscopic structure of the sensory hairs in the cristae of the elasmobranch Raja clavata in terms of directional sensitivity. Nature 184:1807.

Lowenstein,W.R.(1960) Biological transducers. Sci. Am., Aug. 1960.

Lowenstein,O.(1961) Problems concerning the mechanism of the hair cells of the vestibular receptors. Acta. Otolaryng.(Stockholm) Suppl. 163:56-58.

Lowenstein,O.(1966) Permeability of membrane junctions. Ann. N.Y. Acad. Sci. 137:441-472.

Mackey,M.C. & McNeel,M.L.(1973) Determinants of time-dependent membrane conductance. Biophys. J. 13:733-746.

Mackey,M.C.(1975) Ion Transport Through Biological Membranes. Springer-Verlag. N.Y. 240P.

Mair,I.W.(1973) Hereditary deafness in the white cat. Acta Otolaryngol.(Stockholm) Suppl. 314:1-48.

Malcolm,R.(1975) Action of Corti's organ and the cochlea: A new theory. Ann. N.Y. Acad. Sci. 247:219-231.

Misrahy,G.A., Hildreth,K.M., Shinabarger,E.W. & Gannon,W.J.(1958) Electrical properties of wall of endolymphatic space of the cochlea (guinea pig). Amer. J. Physiol. 194:396-402.

Moscovitch,D.H.(1971) The role of calcium in the cochlear transduction process in the guinea pig. Ph.D. Thesis, McGill University, Montreal, Canada. 229P.

Mulroy,M.J., Altman,D.W., Weiss,T.F. & Peake,W.T.(1975) Intracellular electric responses to sound in a vertebrate cochlea. Nature 249(5456):482-485.

Mulroy,M.J., Altman,D.W., Weiss,T.F. & Peake,W.T.(1974) Intracellular electric responses to sound in a vertebrate cochlea. Nature 249(5456):482-485.

Rauch,S.(1964) Biochemie der Hororgans: Einfuhrung in Methoden und Ergebnisse. G. Thieme, Stuttgart.

Rodgers,K. & Chou,J.T.-Y.(1966) Concentrations of inorganic ions in guinea-pig inner ear fluids. I. Concentrations of potassium and sodium in cochlear and utricular endolymph. II. Post-mortem changes in the ionic composition of utricular endolymph and perilymph. III. Phosphate content of utricular endolymph and perilymph. J. Laryngol. Otol. 80:778-790. 885-893.

Russell,I.J. & Sellick,P.M.(1977) Tuning properties of cochlear hair cells. Nature 267:858-860.

Russell,I.J. & Sellick,P.M.(1978) Intracellular studies of cochlear hair cells: Filling the gap between basilar membrane mechanics and neural excitation. In:

Evoked Electrical Activity in the Auditory Nervous System. Nauton,R.F. & Fernandez,C. (eds.) Academic Press, N.Y. pp113-139.

Sachs,M.B. & Abbas,P.J.(1974) Rate versus level functions for auditory-nerve fibers in cats: tone burst stimuli. J. Acoust. Soc. Am. 56(6):1835-1847.

Schindler,K. Schnieder,E.A., & Wullstein,H.L.(1965) Vergleichende bestimmung einiger elektrolyte und organischer substanzen in der perilymphe otosklerosekranker patienten. Acta Oto-Laryngol. 59:309-318.

Sellick,P.M. & Johnstone,B.M.(1972) The electrophysiology of the saccule. Pflug. Arch. Eur. J. Physiol. 366(1):28-34.

Smith,C.A., Davis,H., Deatherage,B.H. & Gessert,C.F.(1958) DC potentials of the membranous labyrinth. Amer. J. Physiol. 193:203-206.

Smith,C.A., Lowry,O.H. & Wu,M.-L.(1954) The electrolytes of the labyrinthine fluids. Laryngoscope 64:141-153.

Sohmer,H.S., Peake,W.T., & Weiss,T.F. (1971) Intracochlear potential recorded with micropipets. I. Correlations with micropipet location. J. Acoust. Soc. Am. 50:572-586.

Stevens,C.F. (1979) The neuron. Sci.Am. 241(3):54-65.

Tasaki,I.(1954) Nerve impulses in individual auditory nerve fibers of guinea pig. J. Neurophysiol. 17:97-122.

Ulrich,M.I., Mundie,J.R., & Margen,S.(1966) Biochemical properties of inner ear fluids: methods of microchemistry and fluid withdrawal. Wright-Patterson AFB, Ohio, Aerospace Medical Res. Labs., Tech. Rep. 65-177.

Wersall,J., Flock,A., & Lundquist,P.G.(1965) Structural basis for directional sensitivity in cochlear and vestibular sensory receptors. Cold Spring Harbor Symp. Quant. Biol.30:115-132.

CHAPTER 5: HAIR CELL AFFERENT SYNAPSE

CHAPTER 5
HAIR CELL AFFERENT SYNAPSE

5.0 INTRODUCTION

The synapses from cochlear hair cells to dendrites of the spiral ganglion neurons whose axons constitute the cochlear nerve are now analyzed. The literature on the hair cell anatomy (Engstrom, Ades, & Andersson, 1966; Spoendlin, 1966; Lorente de No, 1937; Dunn, 1975) agree that there are true synapses from the hair cells to the afferent dendrites of the spiral ganglion neurons. Those investigations with electron microscope pictures verify that the presynaptic regions resident in the hair cells contain vesicles. Vesicles are now generally accepted as containing quanta of neurotransmitter (e.g. Gage, 1976; Katz, 1962; Krnjevic, 1974; Eccles, 1964; Birks, Huxley, & Katz, 1960; MacIntosh, 1941; Birks, 1974). It is taken that the synapse is a true chemical synapse.

The literature on synapses is vast. For excellent reviews, see Katz (1962), Krnjevic (1974), Ginsborg (1967), Gage (1976), Bennet (1972) and Stevens (1979). The aim of this analysis is to develope a dynamic model of the synapse

as it applies to the case of the cochlear hair cell afferent synapses. The statistical quanta model (Katz,1962) is important but not practical for this kind of simulation where a deterministic model is needed.

5.1 ANATOMY OF THE HAIR CELL AFFERENT SYNAPSE

The afferent synapses of inner and outer hair cells of the cat cochlea (Spoendlin,1968) are shown in figures 5.1.1 and 5.1.2. They look like typical chemical synapses as described by Peters, Palay, and Webster (1970). They consist of three components: a presynaptic membrane, a postsynaptic element, and a synaptic cleft with a space of 20 to 40 nm. As in other chemical synapses, the presynaptic element contains an accumulation of synaptic vesicles; the pre- and postsynaptic membranes come into apposition with only a narrow interstice between them and with dark, filamentous or granular material condensed in the adjacent cytoplasm. The dense material is either limited to small areas, or may extend for the entire length of the junction. In the neuromuscular junction where radioactively labeled alpha-bungarotoxin has been applied, the postsynaptic densities are in aggregates of "hot spots" (Fambrough & Hartzell, 1972). The aggregation of vesicles in the presynaptic sites suggest that they represent sites for the

extrusion of the chemical transmitter into the synaptic cleft where it then acts on the postsynaptic membrane. Accordingly, Couteaux (1960) called these assemblages of synaptic vesicles and dense material the "active zones" of the synaptic junction.

Specifically, from measuring the pictures, I found the cochlear afferent synapses to have synaptic regions of 0.40 microns width in the electron microscope side views. The synaptic cleft has an intermembrane space of 0.16 micron.

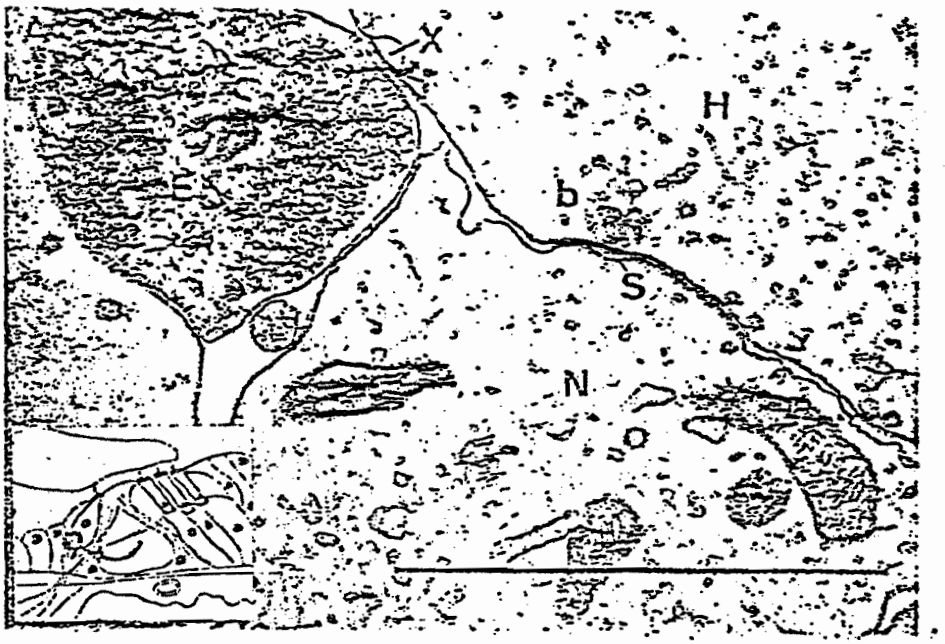

Figure:5.1.1 Afferent synapses of inner hair cells in cat cochlea. Spoendlin (1968). H denotes hair cell, N denotes afferent terminal and B denotes presynaptic bar.

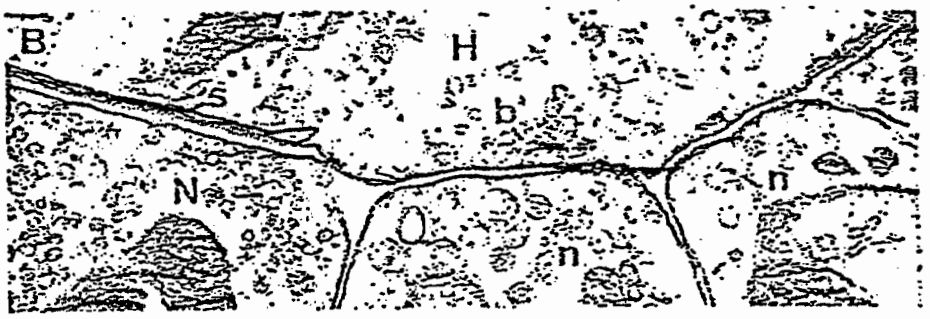

Figure:5.1.2 Afferent synapses of outer hair cells in cat cochlea. Spoendlin (1968). H denotes hair cell, n denotes afferent terminal, b denotes presynaptic bar, N denotes efferent terminal, and B denotes postsynaptic thickening.

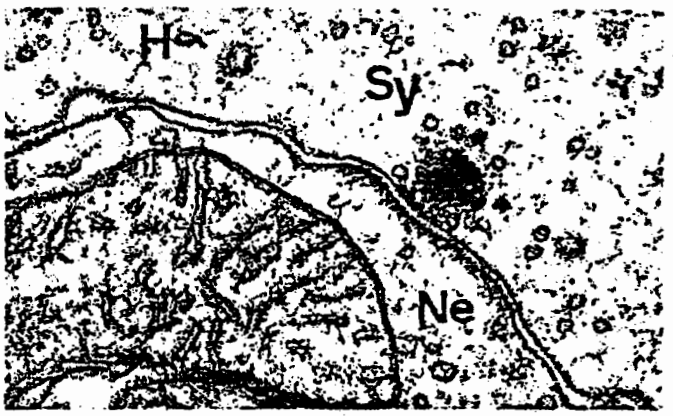

Figure:5.1.3 An inner hair afferent synapse showing a synaptic bar. Spoendlin (1974). H labels an inner hair cell, Sy denotes a synapse with synaptic bar and Ne labels a postsynaptic terminal.

Figure:5.1.3, from Spoendlin (1974), of an inner hair cell synapse, shows a synaptic bar on the presynaptic side, consisting of a dark rod surrounded by vesicles, presumably containing transmitter substance. Osborne and Thornhill (1975) find synaptic bars in hair cells of frog auditory papilla. Smith (1961) shows synaptic bars in rat cochlea hair cells. From my examination of the electron microscope pictures in the literature, there seems to be only one of these synaptic bars per synapse. I conjecture that this could be a physical structure responsible for the storage of the transmitter molecules. Synaptic bars are not seen at all synapses, presumably due to the necessity for the picture plane to intersect the plane of the synaptic bar, which does not always occur. Pappas and Waxman (1972) in reviewing the literature on synaptic structures, call them "synaptic ribbons" and note that they occur in receptor cells and other non-spike generating cells such as bipolar cells. Synaptic bars have been found in retinal receptors (Sjostrand, 1958; Dowling,1968). They were first seen in cochlear hair cells by Smith and Sjostrand (1961), lateral line hair cells (Hama, 1965), and retina bipolar cells (Dowling, 1968; Dowling & Boycott, 1966).

5.2 POSSIBLE TRANSMITTER

What is the transmitter at the afferent synapses from the hair cells to the dendrites of the spiral ganglion neurons whose axons form the cochlear nerve? Historically, in the literature there are a variety of reports which negate the possibility that the afferent transmitter is cholinergic or adrenergic. Spoendlin and Lichtensteiger (1961), Terayama, Holz & Beck (1966), Densert (1974) and Borg, Densert & Flock (1974), using various methods, have demonstrated that the sympathetic nerve endings in the region of the osseous spiral lamina contain noradrenaline. Densert (1974) showed adrenergic nerve terminals around radiating nerve fibers in rabbit spiral lamina and that this innervation originated in the ipsilateral superior cervical ganglion. Flock & Russell (1973), Fex (1967), Russell (1971) and Flock & Russell (1971) have evidence that acetylcholine is the efferent transmitter having used curare to block inhibitory postsynaptic potentials in hair cells and ensuing inhibition of afferent discharges. Hilding & Wersall (1962), Iurato et al (1971), Russell (1971), and Jasser & Guith (1973) have found both acetycholine esterase and choline acetyltransferase in the efferent fibers. In these studies the synapses of the hair cells to the afferent dendrites were examined and were found to have no signs of

histological or physiological changes that would suggest the nature of the afferent transmitter.

The first evidence of any kind which suggested that the afferent transmitter was gamma-aminobutyric acid (GABA), arose when Flock & Lam (1974) investigated possible neurotransmitters in the inner ear and lateral line, especially at the afferent synapse. They used the following preparations: (1) the basilar papilla of the bullfrog (Rana catesbeiana) which have only afferent innervation, (2) the lateral line canal organ of a teleost fish (toadfish, Opsanus tau) with previously identified and studied afferent and efferent innervations, and (3) the crista ampullaris of the semicircular canal in the skate (Raja ocelatta) which has both afferent and efferent innervations. Their method was based on the accepted fact that the neurons which use a particular transmitter can synthesis and store the transmitter in high concentrations (Kravitz, 1967). Tissues were incubated in a medium containing radioactive precursors of noradrenaline, dopamine, GABA, acetylcholine and serotonin. Then tissue extracts were fractionated by high-voltage electrophoresis and the radioactive products were identified. The results seem so unambiguous and convincing, they are presented in table 5.2, where the numbers are counts per minute of radioactivity. The data

suggests that the afferent transmitter is GABA.

Incubations	^{3}H-Noradrenaline	^{3}H-Dopamine	^{3}H-GABA	^{3}H-Acetylcholine
Frog basilar papillae	30 ± 26	32 ± 18	562 ± 85*	49 ± 15
Frog medium	32 ± 20	35 ± 29	74 ± 39	55 ± 20
Toadfish lateral line organs	30 ± 18	15 ± 9	2,350 ± 340*	536 ± 81*
Toadfish medium	28 ± 15	16 ± 10	122 ± 56	53 ± 27
Skate semicircular canal ampullae	33 ± 22	26 ± 16	1,252 ± 315*	145 ± 45*
Skate medium	30 ± 18	26 ± 16	65 ± 35	26 ± 16
Medium without incubation	29 ± 6	18 ± 8	56 ± 25	28 ± 15

The tissues were incubated in media containing ^{3}H-tyrosine, ^{3}H-glutamate and ^{3}H-choline for 16 h. The numbers represent means ± s of radioactive c.p.m. for 10 µl homogenate or medium for three experiments.
* Value indicates that the synthesis in tissue is significantly different from background.

Table:5.2 Candidates for hair cell afferent synaptic transmitter. Flock (1974).

Flock and Goldstein (1973), using an isolated preparation, recorded from single nerve fibers innervating the crista ampularis of the skate Raja erinacea and Raja ocellata. They found units which showed tonic responses to excitatory displacements of the cupula with elevated firing rates lasting several minutes and strong phasic components lasting less than 5 seconds. Other units showed only phasic responses. They further state that step displacements opposite to the excitatory direction were always suppressive with tonic units requiring up to 10 minutes to regain their full spontaneous rate and sensitivity to small test displacements in the excitatory direction. Flock and Lam (1974) state that they used this prepartion with picrotoxin, a specific blocking agent for synapses transmitting GABA, and found that it blocks spontaneous as well as evoked discharge in the sensory nerve fibres, at concentrations of $5*10^{-5}$ to 10^{-6} M. Goldstein (personal communication, 1976) stated that these picrotoxin results were not repeatable in an intact animal. I wonder if the Deiter's cells around the base of the cell where the synapses occur could be blocking the effect of picrotoxin to penetrate to the synaptic regions, especially since the mechanism of picrotoxin action on blocking GABA inhibition is not understood (Krnjevic, personal communication, 1976). There is the distinct

possibility since the hair cell to afferent dendrite is excitatory (increase in sound pressure level for the cochlea or increase in cupula deflection for the lateral line organ causes an increase in AP discharge rate in the afferent fibers), that the usage of picrotoxin or of bicuculin, which block the inhibitory effect of GABA in CNS, would produce a distinctly different effect at these synapses.

The criteria for indentification of transmitters has been discussed by Werman (1966), McLennan (1970), Phillis (1970) and Krnjevic (1974). Krnjevic (1974) states: "to prove that a substance is a transmitter or the transmitter at a particular junction requires the demonstration that its action on the postsynaptic cell is in every respect identical with the synaptic action and that it is released in adequate amounts by activity of the presynaptic nerve endings." For the afferent synapse of the hair cells, no substance has been proven to be the transmitter. The presence of GABA at the hair cell region of the cochlea is helpful, but not sufficient to prove that it is the transmitter.

It appears that GABA is removed from the synaptic cleft by uptake from presynaptic and postsynaptic neurons and glial cells (Bennett, Logan, & Synder, 1972; DeFeudis, 1972; Kuriyama, Weinstein & Roberts, 1969; Martin,

Wickegren, & Beranek, 1970; Varon, Weinstein, Baxter, & Roberts, 1965). In fact, ever since the first reports that GABA is an inhibitory transmitter in the brain, it has been clear that intracellular uptake is the most significant method of removal of GABA from extracellular space (Elliot & von Belder, 1958; Krnjevic & Phillis, 1963; Krnjevic, 1974). In agreement with this removal story, Kuriyama & Kimura(1976) report 1.1 nano-moles/mg dry weight of GABA in the spiral ganglion of guinea pig compared to below detectable amounts in the organ of Corti. It is interesting that Tachibana and Kuriyama (1974) found correspondingly high levels of GABA in the dorsal part of the cochlear nucleus compared to the ventral part. The exposure of the animal to high-frequency large amplitude sound (4kHz, 90 dB, 10min.) caused a 30% to 40% increase in the concentration of GABA in the dorsal cochlear nucleus (Kuriyama & Kimura, 1976). Lorente de No (1933) first reported a pathway of fibers from the interior colliculus to the dorsal cochlear nucleus and Whitfield & Comis (1966) report strong depression in the discharge rate of neurons in the cochlear nucleus. All of this evidence correlates with the Tachibana & Kuriyama (1974) report of a high concentration of GABA in the inferior colliculus.

If GABA is the afferent excitatory transmitter from

hair cells to dendrites of the spiral ganglion neurons, how can it act in an excitatory manner when it is invariably inhibitory in the central nervous system? There are several interesting pieces of literature on synapses and/or GABA, e.g., Roberts, Chase, & Tower (1976); Andersen et al(1970); and Krnjevic (1974). In the cortex, where GABA works as an inhibitor, there is agreement that the transmitter effect is on the chloride permeability of the postsynaptic neuron, (Krnjevic, personal communication 1976). The essential and most prominent feature of the prevalent type of postsynaptic inhibition is an increase in the anionic permeability of the neuronal membrane, which tends to "clamp" the membrane potential close to the equilibrium level for Cl^- (E_{Cl}). Since E_{Cl} is usually more negative than the resting potential, presumably due to an outward active transport of Cl^-, this clamping action impedes depolarization and thus inhibits the generation of action potentials by excitatory inputs. Dreifuss, Kelly, & Krnjevic (1969) show good data where the iontophoretic application of GABA causes a hyperpolarization and an increase in membrane negativity of neurons in the cerebral cortex of the cat. Direct evidence that GABA raises the membrane conductance has been obtained in neurons of the mammalian cerebral cortex (Krnjevic & Schwartz, 1966, 1967; Dreifuss, Kelly & Krnjevic, 1969;

and Kelly & Krnjevic, 1969), Deiters' nucleus (Obata, Takada & Shinozaki, 1970; tenBruggencate, & Engberg, 1971), sympathetic ganglion (Adams & Brown, 1973), spinal interneurons of the lamprey (Martin, Wickelgren, & Beranek, 1970), Purkinje cells of frog cerebellum (Woodward, Hoffer, Siggins, & Oliver, 1971), and Mauthner cells in the medulla of goldfish (Diamon, Roper, & Yasargil, 1973).

It has been known for some time that GABA depolarizes primary afferent terminals to the spinal cord (Eccles, Schmidt, & Willis, 1963; Tebecis & Phillis, 1969; Davidson & Southwick, 1971) and that this depolarization is blocked by picrotoxin and bicuculine (Davidoff, 1972; Barker & Nicoll, 1973) and by drugs which antagonize presynaptic inhibition (Eccles, Schmidt, & willis, 1963; Schmidt, 1963; Curtis, Duggan, Felix & Johnston, 1971; Levy, Repkin & Anderson, 1971; Davidoff, 1972). Accordingly, these investigations provide good evidence that the transmitter mediating presynaptic inhibition is GABA. Nishi, Minota, & Karczmar (1974) provide direct evidence that the GABA mediated depolarization of primary afferent neurons is due mainly to an increased chloride conductance; finding an equilibrium potential for the GABA depolarization of E_{GABA}=-33.7 mv, upon replacement of the extracellular chloride with and without GABA antagonists. As the GABA

depolarization appears to be dependent upon the change in chloride conductance E_{GABA} should be nearly equal to the equilibrium potential for chloride ions, which is markedly lower than the resting membrane potential (-60 to -75 mv). To provide this equilibruim potential for chloride ions, Nishi, Minota & Karczmar postulate the existance of a chloride pump which maintains the intracellular concentration of chloride at about 24.2 mM, which they measured by using a chloride electrode. Lux (1971) showed the blocking of active extrusion of chloride in motor neurons which normally maintain a high ionic gradient for hyperpolarizing inhibition; the blocking was achieved using an infusion of ammonium salts. Llinas, Baker & Precht (1974) verified this in the cat, testing the effect of ammonium acetate on the inhibitory action of vestibular nerve stimulation on ipsilateral trochlear motor neurons. Barker, Nicoll, and Padjen (1978) and Nicoll and Padjen (1978) report that the GABA response at all regions of the primary afferents is due to primarily an outward chloride current. Adams & Brown (1973) report a reversal potential for GABA (E_{GABA}) of about -42 mV, for the isolated rat superior cervical ganglia neurons using conventional intracellular recording techniques. D.A. Brown (personal communication, 1976) has gone on with this work and concurs

with the evidence for a chloride pump that maintains the intracellular chloride concentration at about 25 mM which agrees with Woodward, Bianchi, & Frulkar (1969) and Nicoll & Padjen (in preparation). Scruggs & Landowne (1975) have evidence for the existance of an inwardly directed active transport mechanism for chloride ions in the squid axon membrane using radioactively labeled chloride ions. Keynes (1963) using dinitrophenol showed blockage of an inward transport of chloride in the squid giant axon. It is noteworthy that in these cases the effect on the postsynaptic membrane is depolarization of the membrane to the value of E(GABA).

Since, (1) the synpase from hair cell to dendrite lacks solid evidence for identification of the afferent transmitter, and (2) the number of neurotransmitters or candidates for neurotransmitters has increased remarkably in the past few years, it is therefore unsound to choose an actual transmitter. A safe path is to use typical numbers for the parameters. In this phenomenon it is the structure of binding of transmitter with receptor sites and pore conductance channel opening which determine the function of the synapse.

5.3 THE SYNAPSE MODEL

The physiological block diagram of the synapse is shown in figure:5.3. The presynaptic site, in this case on a hair cell, incurs a change in receptor voltage. This presynaptic voltage change induces release of quanta of transmitter into the intersynaptic cleft. The transmitter molecules in the synaptic cleft interact with the receptor sites on the postsynaptic membrane. The postsynaptic receptor sites then cause conductance changes in the postsynaptic button of the afferent dendrite.

5.3.1 TRANSMITTER RELEASE

The starting point is the release of transmitter. Katz (1962) plotted the relation between frequency of miniature end plate potentials (mepps) and depolarization of an axon presynaptic terminal for the rat diaphragm neuromuscular junction, based on the work of Liley (1956) in which he changed the extracellular concentration of potassium causing changes in presynaptic transmembrane voltage. I fitted a function to this data and found it has the form

$$R = e^{b*V}$$

where R is the release rate of transmitter (quanta/sec). V is the presynaptic depolarization voltage (millivolts), and b=0.161 (1/millivolts). Hubbard et al (1967) re-did this

work in more detail and found a marked decrease in the slope of the curve. They measured the mean mepp frequency 2 to 7 minutes after increasing the extracellular potassium concentration at $38^{o}C$, compared to Liley who made the measurements 20 minutes later at $38^{o}C$. The difference is mainly in the slope of the line on a log-linear plot. On fitting a function to their data, it had the form

$$R = A*e^{b*V}$$

where A=3.831 (mepps/sec) and b=0.0863 (1/mV). This is shown in figure:5.3.1. Hubbard et al (1967) showed the difference to be due to osmotic effects of the potassium used to depolarize the presynaptic terminal.

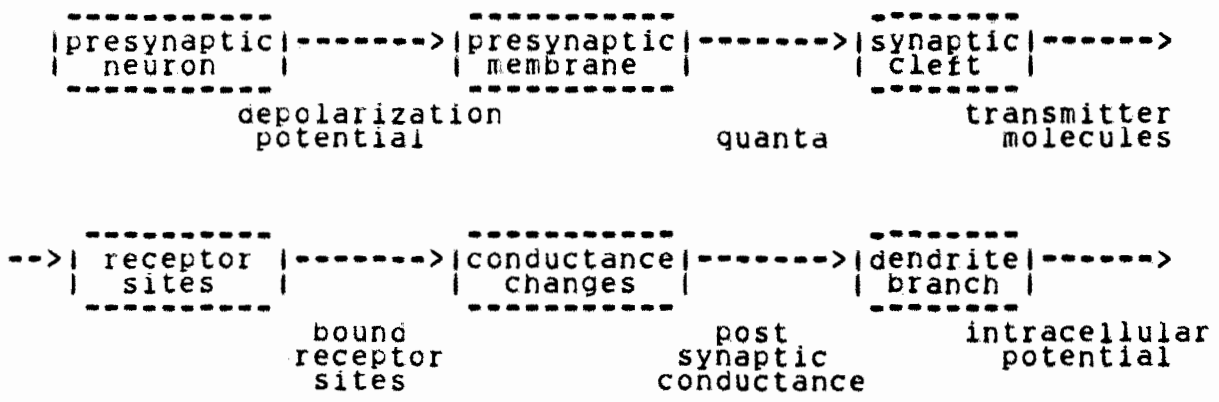

Figure:5.3: Physiological block diagram of the synapse.

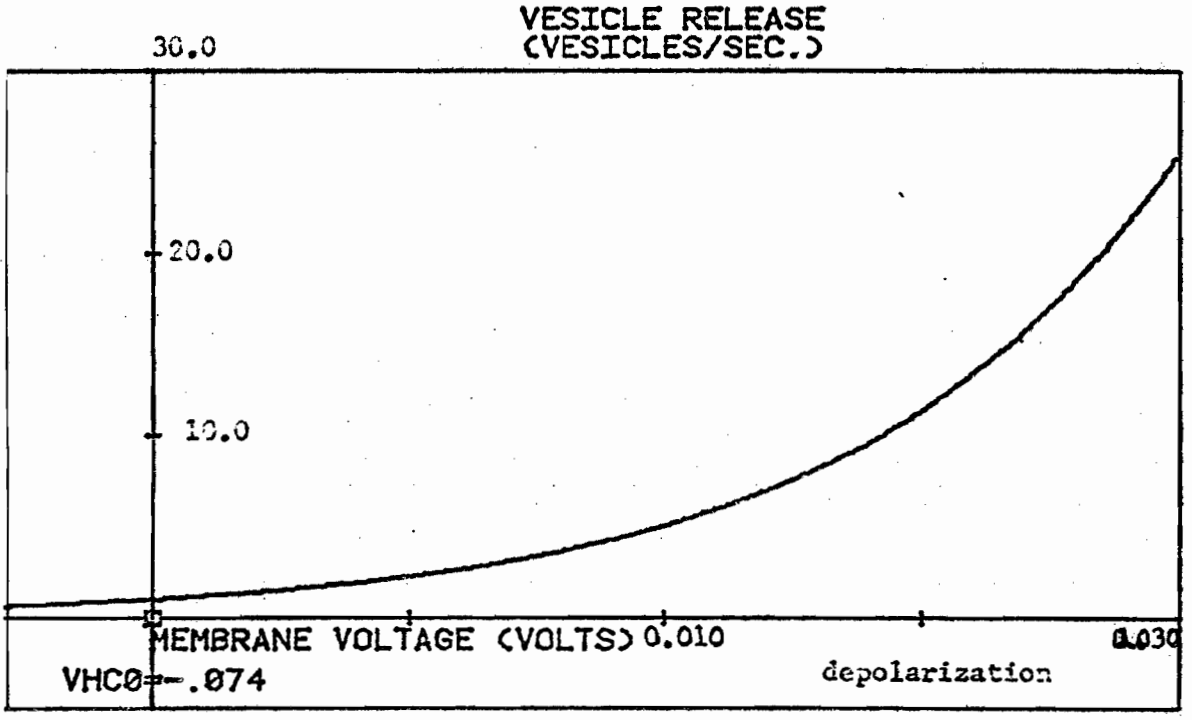

Figure:5.3.1. Transmitter release versus presynaptic membrane voltage. See text.

Krnjevic and Whittaker (1965) analyzed the fractional components of cat cortex, using subcellular fractions containing synaptosomes, synaptic vesicles and soluble cytoplasmic constituents. They found 1.8 n-mole of GABA/ml. with 8.7 ml.of that fraction derived from 1.0 g. of cortex. Whittaker & Sheridan (1965), in the same lab using the same technique, found 3.8×10^{12} vesicles/g. Thus the number of molecules of GABA per vesicle, NMGV is given by

$$NMGV = \frac{1.8*10^{-9}\ (\text{mole/ml})*[8.7(\text{ml/g})]}{3.8*10^{12}\ (\text{vesicles/g})}$$

$$= 4.1*10^{-21}\ \text{mole/vesicle}$$

$$= [4.1*10^{-21}\ (\text{mole/vs.})]*[6.0255*10^{23}\ (\text{molec./mole})]$$

$$= 2.48*10^{3}\ \text{molecules/vesicle}$$

Whittaker (1965) calculates for acetylcholine, based on his best figures for cerebral cortical vesicle preparation, that the number of molecules of ACH per vesicle is

$$NMAV = \frac{0.75*10^{-9}\ (\text{moles/ml})}{1.8\times10^{12}\ (\text{vesicles/ml})}$$

$$= 4.17*10^{-22}\ (\text{moles/vesicle})$$

$$= 250\ (\text{molecules/vesicle})$$

MacIntosh (1959) estimates 900 molecules/vesicle which is an early low estimate in the literature for ACH and the highest is 10^{5} from Krnjevic and Mitchel (1961). Whittaker (1965)

calculates for a sphere of inside diameter 310 Å (the inside diameter of a vesicle of ACH) that it will contain about $1.5x10^{3}$ molecules of ACH if filled with an isotonic (0.16M) solution and about $5x10^{4}$ molecules if filled with solid acetylcholine chloride. The average is given as the 250 molecules/vesicle figure, since it is based on a large number of vesicles in cortex slab. In this model, I use

$$NMTV = 4.17*10^{-22} \text{ (moles/vesicle)}$$

$$= 250 \text{ (molecules/vesicle)}$$

The transmitter molecules from the presynaptic site are released into the intersynaptic cleft. From figure:5.1.1 the diameter of the synaptic cleft is $4.86*10^{-1}$ micron, with a thickness of $1.62*10^{-2}$ micron. If the intersynaptic volume is taken to be a cylinder of diameter D and thickness H, then the intersynaptic volume, ISV is

$$ISV = pi*(D/2)^{2}*H$$

$$= 3.04*10^{-18} \text{ liter}$$

The concentration in the intersynaptic cleft of transmitter from one vesicle is

$$CONCT = NMTV/(ISV*AN)$$

$$= 1.365*10^{-4} \text{ mole/liter}$$

where AN is Avogadro's number.

5.3.2 POSTSYNAPTIC RECEPTOR

The literature on the binding of transmitters with the receptor sites on synaptosomes indicates that it obeys a typical rate kinetic model of reaction (Harrington, 1973; Leibovic & Sabah, 1969). Young, Enna, Zukin, and Snyder (1976), using GABA as the ligand, studied measured sodium-dependent and independent binding to crude synaptic membrane fractions of mammalian brain. They found the dissociation constant, K_D =1.2 micro molar for sodium dependent binding and K_D= 0.37 micro molar for sodium independent binding. A big distinction for the two forms of binding is that sodium-independent binding is sensitive to inhibition by bicuculline, whereas the dependent form is not. Furthermore, the sodium-dependent binding is very susceptible to inactivation by low temperatures. The most potent inhibitors of sodium-independent GABA binding are 3-amino propane sulfonic acid, imidazoli acetic acid, and 3 hydroxy GABA, all of which are potent activators of post synaptic GABA receptors in-vivo and are generally as potent neurophysiologically as they are as inhibitors of sodium-independent GABA binding. Amino-propane-sulfonic acid is more potent than GABA neurophysiologically and about 30% more potent than GABA in inhibiting sodium-independent

GABA binding. 3-hydroxy GABA is about half as effective as GABA itself both neurophysiologically and in inhibiting sodium-independent GABA binding. Enna and Synder (1975) have considered these differences and kinetic studies and have made the strong case that sodium-dependent GABA binding involves uptake sites for the GABA accumulating system of glia and non-synaptic receptor sites, whereas the sodium-independent binding is associated with the GABA receptor sites of the postsynaptic membrane. Enna and Synder found the rate constant for the sodium-dependent (nonreceptor site uptake) to be $6*10^{-7}\ M^{-1}\ min^{-1}$.

The reaction of transmitter (T) with receptor molecules (RM) is depicted by the reaction

$$T + RM \underset{K_2}{\overset{K_1}{\rightleftharpoons}} T*RM$$

The kinetics are described by the rate of change of the concentration of bound receptor sites CBRS, related to the concentration of transmitter, CONCT, and the concentration of unbound receptor sites, CRS, (Mahler & Cordes, 1966).

$$D_t CBRS = K_1*CONCT*CRS - K_2*CBRS$$

Young, Enna, Zukin, & Synder (1976) have found that the actual rate constants for the sodium-independent binding are so rapid even at $4^{o}C$ that they cannot be measured with present techniques. Consequently, the GABA in the

intersynaptic cleft is in equilibrium with the receptor molecules. In this model, I assume that this is the case. At equilibrium, with $K_D = k_2/k_1$

$$KD = \frac{CONCI * CRS}{CBRS}$$

Multiplying this fraction by AN*ISV/AN*ISV, where $AN=6.0255*10^{23}$ (molecules/gm.molec.wt.) which is Avogadro's number and $ISV=3.04*10^{-18}$, the intersynaptic cleft volume,

$$KD = \frac{CONCI*NUBRS}{NBRS}$$

where NUBRS is the number of unbound receptor sites and NBRS is the number of bound receptor sites. Letting NTRS be the total number of receptor sites, and solving for the number of bound receptor sites gives

$$NBRS = \frac{CONCI*NTRS}{KD + CONCI} \quad \text{(molecules)}$$

The concentration of transmitter in the intersynaptic cleft, CONCI, is given by

$$D_t CONCI = (NMGV/ISV)*D_t Q - CONCI*RRI$$

(moles/(liter*sec))

where $D_t Q = dQ/dt$ is the arrival rate of quanta due to presynaptic release and RRI is the removal rate of transmitter by the membranes surrounding the synapse. The value of RRI is the value of the sodium-dependent uptake of transmitter by synaptosomes (Enna & Synder, 1975)

$$RRTK = 6*10^{-7} \text{ /M*min}$$

$$= 10^{-8} \text{ mole}^{-1} * \text{sec}^{-1} * \text{liter}$$

$$RRT = RRTK * conc(T) * conc(Na)$$

where conc(Na) = concentration of sodium in ECF, in this case Corti's Organ. Namba & Grob (1967) give $2.7 * 10^{8}$ molecules/msec as the removal rate for acetylcholine at the neuromuscular junction.

The only number left to find in this development of the synapse model is the total number of receptor molecules on the postsynaptic membrane. In Electrophorus electroplax, a density of $3*10^{4}$ receptors/micron^{2} has been calculated from autoradiographic studies with alpha-bungarotosin (Bourgeois, Ryter, Menez, Fromageot Boquet, & Changeux, 1972). A lower figure is $2.5*10^{3}$ /micron^{2} for this in which affinity labels were used to count receptors (Karlin, Prives, Deal & Winnik, 1971). A density of 10^{3} to 10^{4} /micron^{2} has been reported for active centers of acetylcholinesterase molecules associated with subsynaptic membrane (Banard, Wieckowski, & Chiu, 1971; Meunier, Olsen, Menez, Fromageot, Boquet, & Changeux, 1972; Miledi, Molinoff & Potter, 1971; Porter, Chiu, Wieckowski & Barnard, 1973; Potter, 1973; Saltpeter, Plattner & Rodgers, 1972). On the assumption that one alpha-bungarotoxin molecule binds to each receptor, 10^{7} acetylcholine receptors per end plate for rat and frog

tissue has been obtained from autoradiographs of muscles exposed to tritiated alpha-bungarotoxin (Barnard, wieckowski, & Chiu, 1971; Fambrough & Hartzell, 1972; Porter et al 1973a,b; Barnard & Chiu, 1973). Porter et al (1973) report that alpha-bungarotoxin binding membrane fragments from Torpedo electric tissue are covered with rounded units 6 to 7 nm in diameter, with a density of about 10^4 /micron^2. These were sometimes in hexagonal arrays in which the center to center distance was 8 to 9 nm. Each unit appeared to composed of subunits (usually 6, occasionally 5), each 2 to 2.5 nm in diameter. It was concluded that the observed units and subunits were "receptor-ionophore components" with an estimated length of 9 to 14 nm. This is further substantiated by Potter (1974).

Rosenbluth (1973a,b) using the electron microscope has revealed that insect and leech neuromuscular junctions show a series of concave patches about 0.3 micron in diameter and outer surfaces of the membrane in these patches appear coated, the outer coating consisting of hexagonal arrays of projections. These projections are about 15 nm apart, thickened at their tips, and project about 20 nm into the synaptic cleft. Their density is about 10^4 /micron^2 in the concave patches. Such clearly defined arrays of projections are more prominent in annelides than in other phyla where

they can be seen only with difficulty (Rosenbluth, 1973b). These presumed receptors are aggregated in "hot spots" rather than being evenly distributed over the subsynaptic membrane. In frog motor end plate there are dense aggregations of particles with a density of 7500/micron^2 on the "juxtaneural lips" of junctional folds (Peper, Dreyer, Sandri, Akert & Moor, 1974). The density of these hot spots is close to the values quoted for average receptor density over the whole subsynaptic membrane. If the projections and particles are true receptors, the total number of receptors may be lower than estimated from alpha-bungarotoxin binding.

For the purpose of this model, the density of transmitter receptor sites is taken to be 10^4/micron^2 with a previously measured diameter of the afferent postsynaptic receptor region of $4.85*10^{-1}$ micron, and considering the synaptic receptor region to be a circle, the total number of receptor sites is

$$NTRS = pi*(4.85*10^{-1}\ \text{micron}/2)^2 * 10^4/\text{micron}^2$$

$$= 1.847*10^3 \text{ receptor molecules}$$

5.3.3 RECEPTOR SITE CHANNELS

The consensus in the literature on postsynaptic receptor sites of chemically mediated synapses is that the receptor site works by a transmitter molecule combining with a receptor site molecule which induces a conformational change thus opening a pore in the postsynaptic membrane allowing an ionic current through the membrane (Smythies, Benington, Bradley, Bridgers & Morin, 1974; Armstrong, 1975; Whittaker, 1965; Katz & Miledi, 1972; Katz, 1962; Gage, 1976; Young, Enna, Zukin & Snyder, 1976; Enna & Snyder, 1975; Magledy & Stevens, 1972). There are pictures of the pores in the receptor sites of the postsynaptic membrane associated with the electroplaques of the ray Narcine Brazilliensis (Allen, Chang & Potter, 1975). Glutaraldehyde fixed freeze-cleaved tissue showed particles with a central 20Å pit protruding from the pre and postsynaptic membranes with a diameter of about 90 Å and packing density of about 5000/micron^2. They claim that these pores are the ion channels for the receptor sites. The receptor for acetylcholine from electric tissue of Torpedo californica and Electrophorus electricus has been purified (Weill, et al, 1974; MacNamee, et al, 1975; Valderrama, et al, 1976). Smythies, Benington, Bradley, Bridgers & Morin (1974) have proposed a molecular structure

for the sodium channel in the nerve membrane. The relevant feature is a 3X5 Å rectangular pore for the passage of sodium whereby the molecular structure recognizes $Na^+.6H_2O$, removes $5H_2O$ and transmits $Na^+.1H_2O$ through the channel.

The literature on nerve membranes indicates that the pores in the nerve membrane are ion selective, if the vast amount of experimental data is to make sense. For a good review of this, see Hille (1970) or Armstrong (1975). It is not the object of this work to discuss the evidence for ion selective pores. Since, (1) the giant squid axon and the frog muscle fiber have their ionic currents during an action potential mediated by changing sodium, potassium and leakage conductance, and (2) nerve toxins such as tetrodotoxin, saxitoxin, and tetra-ethylammonium ions selectively interfere with the conductances, thus estimates are available for conductance per sodium and per potassium pore. A summary of the literature's estimates of conductance per sodium pore is given in table:5.3.3.

For comparison, potassium conductance per pore measurements are given by Armstrong (1966,1974) using TEA on giant squid axon as 1 to 3 nano mho; Katz and Meledi (1973) give 0.3 nano mho. There seem to be no estimates for chloride channels available in the literature.

Pore density (pores/μm^2)	Pore conductance (mho)
200	0.8×10^{-11}
200–300	$0.5–0.8 \times 10^{-11}$
400	0.4×10^{-11}
< 13	$> 10^{-10}$
49	3×10^{-11}
75	2×10^{-11}
36	4×10^{-11}
2.5	6×10^{-10}
27	6×10^{-11}
16	9×10^{-11}

Table:5.3.3 Estimates of Na pore density and conductance. Adapted from Armstrong (1975).

5.4 VERIFICATION OF MODEL

5.4.1 TRANSMITTER RELEASE

How can the functional relationship of transmitter release due to presynaptic voltage change be verified? If the number of quanta released at a synapse due to the arrival of a normal presynaptic action potential were known, a means of verifying the transmitter release function would be available.

Zorychta (1974) recorded unitary synaptic potentials from cat spinal motorneurons innvervated by the triceps surae nerve (TS). The preparation used an intracellular recording electrode (R_1) in the motorneuron, a hook recording electrode (R_2) under a finely dissected filament from the dorsal root of TS, a stimulating electrode (S_1) under the entire nerve and a stimulating electrode (S_2) under finely dissected brancnes of the TS nerve. All afferent fibers entering the lumbosacral spinal cord were severed except the small filament on R2. Stimulation of the entire TS nerve at S1 excited all TS motorneurons antidromically via their axons in the intact ventral roots. An AP in a neuron impaled by the microelectrode R1 identified it as a TS motor neuron. The stimulus excited several axons in the dorsal root filament producing a burst

of action potentials recorded at R2. Stimulation at S2 then evoked a single action potential in the dorsal root filament at R2 and a unitary EPSP at R1, if the TS motoneuron is innervated by the single fiber. Thus the preparation allowed the recording of the postsynaptic potentials from single action potentials arriving from the dorsal root of the TS nerve. The mean quantum content of the postsynaptic unitary potentials was determined by the method of failures and fitting the amplitude histogram to a Poisson distribution. She found that the average mean quantum content in 41 motor neurons was 2.38, with a range of 1.01 to 5.19. The average unit potential was 0.118 mvolts, with a range of 0.059 to 0.273 mvolts.

This experimental result provides a means of verifying the transmitter release function. Coombs, Eccles and Fatt (1955) show motor neuron action potentials with a 60 mV. maximum at 1.6 msec. after start of the AP. Cortical neurons show the maximum amplitude occurring at 150 microsec. (winslow, 1972). Presynaptic spike potentials recorded from the abnormally large synapse in the stellate ganglion of Loligo pealii (Hagiwara & Tasaki,1958) show the maximum occurring at 0.2 millisec. after the start of the rising phase. Auerbach and Bennet (1969) show presynaptic spikes in the Mauthner fiber, the giant fiber synapse of the

hatchet fish which has chemically mediated transmission. Those presynaptic spikes have maximums occurring at about 0.2 msec. with the synaptic delay being 50 microsecs. Using the Loligo pealii synapse a curve was fitted to the presynaptic action potential:

$$V(T) = M*\exp(at)*\sin(2*pi*f)*(U(t)-U(t-t_0))$$

where a=-108357 (1/sec.), f=11,250 Hz $t_0 = 2/f$, and M=90 mvolts. It is shown in figure:5.4.1.1. The total quanta released during an action potential can now be given by

$$Q = \int_0^{/\backslash t} A*e^{b*V(t)}\,dt$$

Observe that quantal release is dependent on the positive going portion of the AP and the negative recovery phase has no affect on release. Release is most sensitive to the maximum value of the AP. Using Liley's original curve it was found that AP maximums of 60, 70, 80, 85, 90 millivolts yieled total quantal release values of 0.16, 1.4, 3.4, 7.4, 16.0, respectively, shown in figure:5.4.1.2. Note that this agrees well with Zorychta's (1974) experimental range of 1.01 to 5.19 quantal content per action potential.

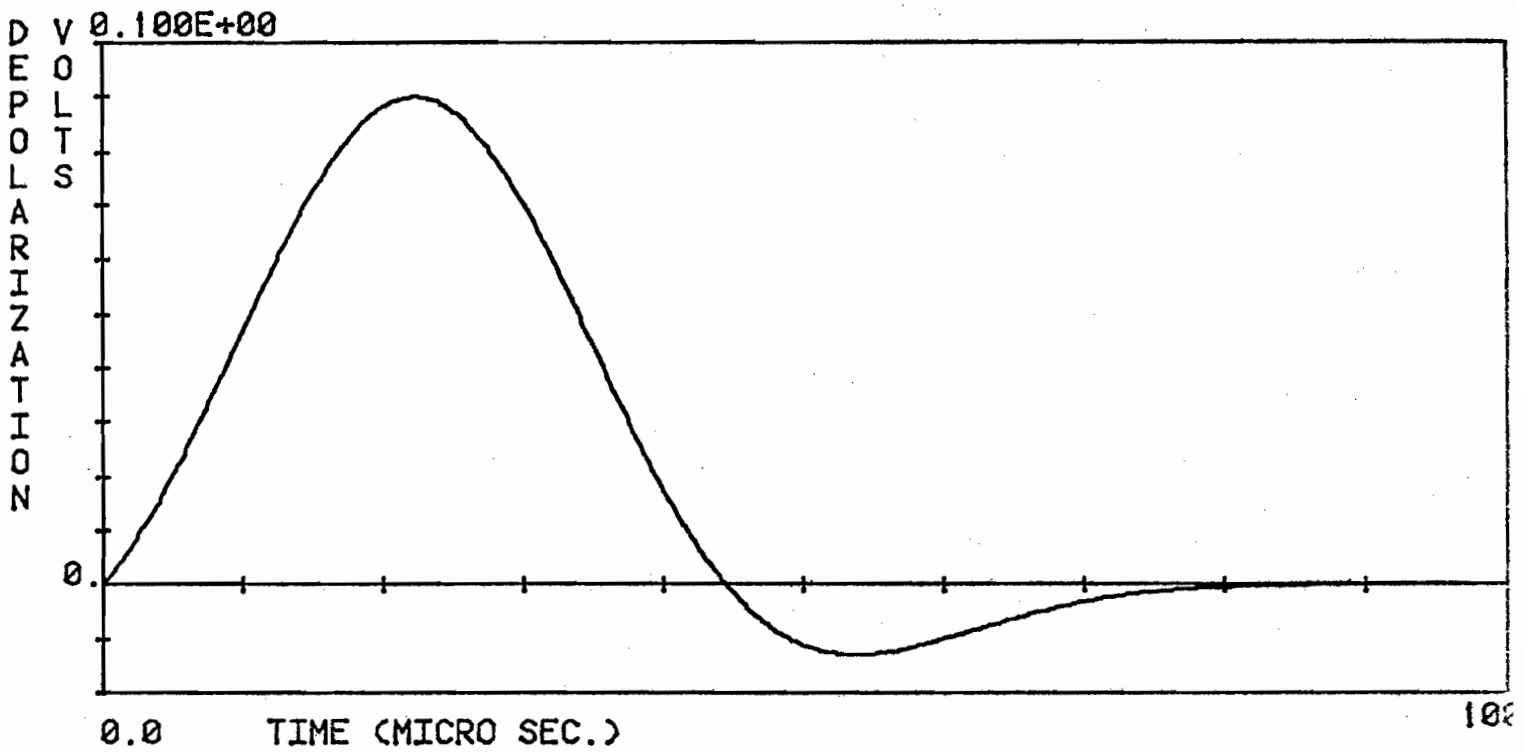

Figure:5.4.1.1 An action potential in the presynaptic terminal of the Mauther fiber of Loligo pealii fitted using the function described in the text.

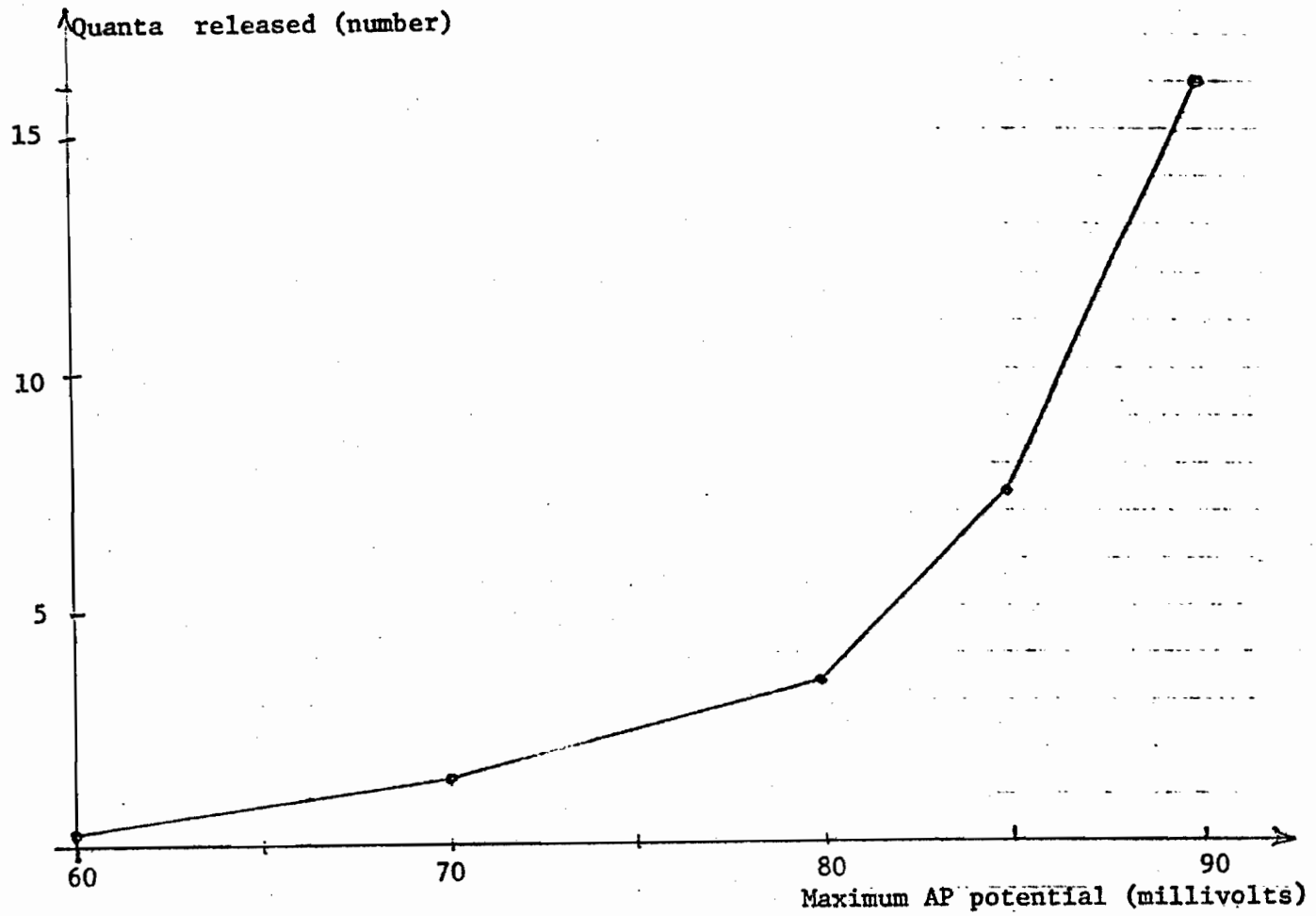

Figure:5.4.1.2 Total quanta (number) released per action potential versus AP maximum voltage (millivolts).

5.4.2 POSTSYNAPTIC CONDUCTANCE

The maximum conductance for a synapse occurs when all the postsynaptic pores are open. The number of postsynaptic receptor site molecules, which equals the maximum number of available pores, was previously calculated as $1.386*10^{3}$. Using an average pore conductance of 10^{-11} mho per pore, the maximum conductance for the postsynaptic membrane of the synapse is $1.4*10^{-8}$ mho. It turns out that this is exactly in the conductance range which affects the dendrite, resulting in a millivolt range response at the AP generating site, as shown in the dendrite study of chapter 6.

5.4.3 LUMPED POSTSYNAPTIC COMPARTMENT

Consider one long compartment with lumped membrane parameters and synaptic conductance G_s. For a dendrite of length L, radius r, the membrane area is $A=2*pi*r*L$, thus the total membrane resistance is $G=A*G_m$, where $G = 1/(A*R_m)$. Membrane capacitance is $C=A*C_m$. The resting transmembrane potential K at the synapse is $(V_r-W_e)-E_{Na}$, where $V_r=-68.6$ mvolts is the membrane resting potential. W_e is the external static potential (zero for extracellular fluid and +7mV for organ of Corti lymph). The equation is

$$C*D_t V = -VG - (V + K)*G_s$$

where $G = 1/A*R_m$. This is the same as the compartment equation in chapter 6, but without the longitudinal current.

Using diameter of 1 micron, l=100micron, $C_m = 1.3*10^{-6}$ F/Cm^2, $R_m = 1000 ohm*cm^2$ then $C = 2.04*10^{-12}$ F and $G = 1.571*10^{-9}$ mho. For further details see section 3 on dendrite compartment in the next chapter.

5.5 THE SYNAPSE IN SIMULATION FORM

To summarize the equations that describe the synapse, they are presented here in sequential form as they appear in the simulation. The number of quanta, Q, released per second is given by

$$D_t Q = R = A*e^{b*V}$$

where A=3.831 (quanta/sec), b=0.0863 (1/millivolts) and V is the receptor voltage of the hair cell. The number of molecules of transmitter per quanta is

$$NMTV = 250 \text{ (molecules/quanta)}$$

The volume of the intersynaptic cleft is

$$ISV = 3.04*10^{-18} \text{ liter} = 3.04*10^{-21} M^3$$

The predicted rate of change of the concentration of transmitter, CONCT is given by

$$D_t CONCT = \left| \frac{NMIV}{ISV*AN} * D_t Q \right| - CONCT*RRT$$

where RRT is the removal rate of the transmitter by the surrounding cells and $RRT = 10^{-8}$ (1/sec)

The concentration of transmitter at any moment in time is given by

$$CONCT(t) = \int_0^t (D_t CONCT)dt$$

and is shown in figure:5.5.1. The number of bound receptor sites is given by

$$NBRS = \frac{CONCT*NTRS}{KD + CONCT}$$

where the total number of receptor sites is $NTRS=1.847*10^{3}$ sites and the dissociation constant for transmitter binding with receptor sites is

$KD = 1.2*10^{-6}$ (mole/liter)

The predicted fraction of bound receptor sites R = NBRS/NTRS versus transmitter concentration is now easily computed and is shown in figure:5.5.2.

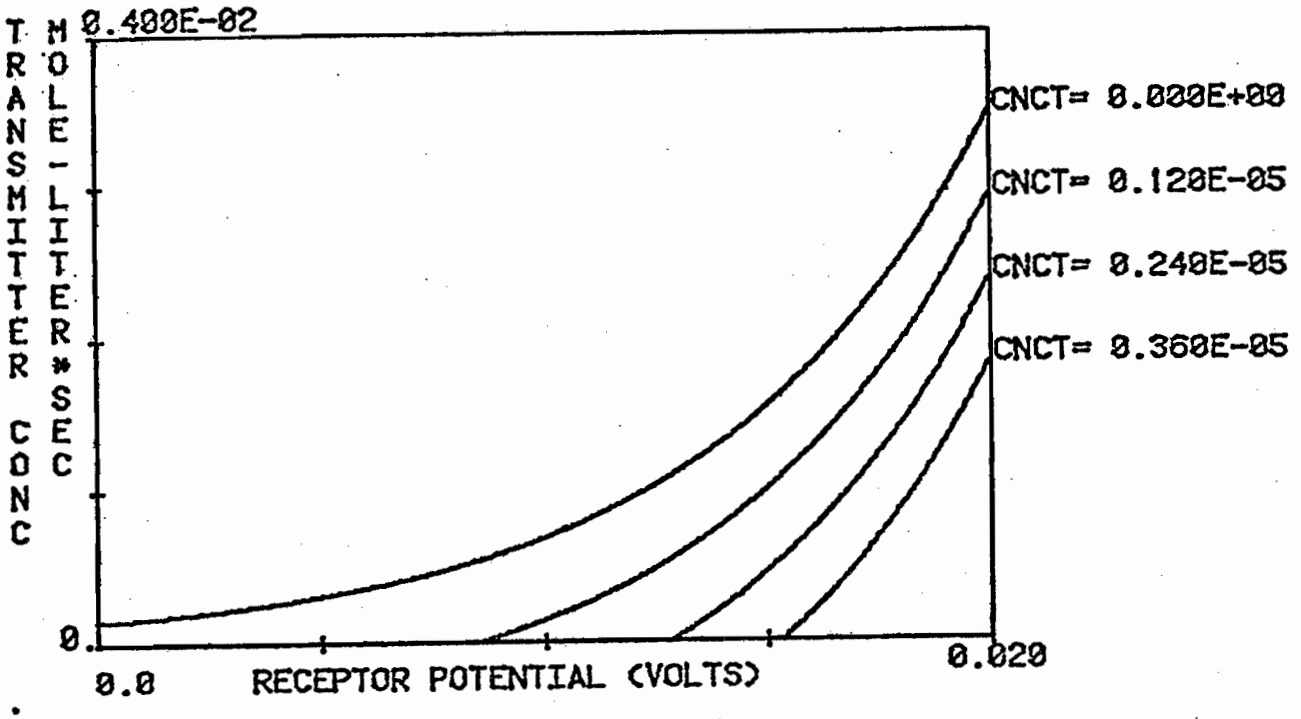

Figure:5.5.1 Rate of change of transmitter concentration in synaptic cleft for steady state presynaptic depolarization at various initial transmitter concentrations.

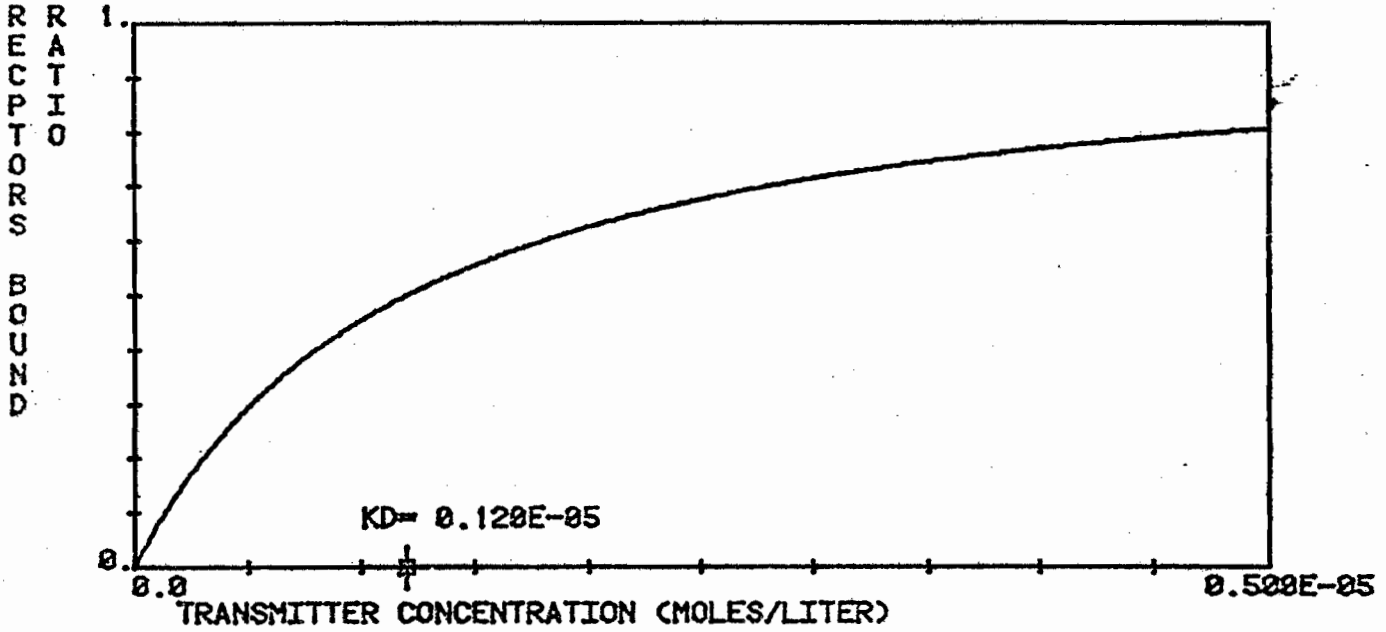

Figure:5.5.2 Fraction of bound receptor sites versus transmitter concentration in the synaptic cleft.

5.6 CONCLUSION

It was shown that an excitory synapse can be described by an input-output equation, using the physiological variables, presynaptic depolarization voltage and postsynaptic conductance. The model predicted that for an action potential voltage waveform as input depolarization voltage, the number of vesicles released agrees with the number of mepps measured by Zorychta (1974) in spinal motor neurons on arrival of an AP. The synapse model predicts a postsynaptic conductance change of 10^{-8} mhos for an excitory synapse which causes a millivolt change in dendrite receptor depolarization at the AP generating site. The usefulness of this model is that it combines the actual quanta release rate with a kinetic binding model for receptor sites to produce postsynaptic conductance as a function of presynaptic depolarization per individual synapse.

EFERENCES: CHAPTER 5

Adams,P.R. & Brown,D.A. (1973) Action of gamma-aminobutyric acid (GABA) on rat sympathetic ganglion cells. Br. J. Pharmacol. 47:639-640P.

Allen,T. Chang,R., & Potter,L.T. (1975) Acetylcholine receptor and Na.K.ATPase from electroplaques of Narcine Brazilliensis. Pharmacol. Fed. Proc. 34:738.

Andersen,E.G., Haas,H.L., & Hosli,L. (1970) Interaction of histamines, imidazole acetic acid, and convulsants on brain stem neurons. Experientia 28:741.

Armstrong,C.M. (1966) Time course of TEA-induced anomalous rectification in squid giant axon. J. Gen. Physiol. 50:491-503.

Armstrong,C.M. (1974) K pores of nerve and muscle membrane. In: A Series of Advances. vol. 3. Eisenman,G. (ed.) Marcel Dekker. N.Y.

Armstrong,C.M. (1975) Ionic pores, gates, and gating currents. Quart. Rev. Biophys. 7(2):179-210.

Auerbach,A.A. & Bennet,M.V.L. (1969) Chemically mediated transmission at a giant fiber synapse in the central nervous system of a vertebrate. J. Gen. Physiol. 53:183.

Barnard,E.A., Wieckowski,J. & Chiu,T.H. (1971) Cholinergic receptor molecules and cholinesterase molecules at mouse skeletal muscle junctions. Nature 243:207-209.

Barker,J.L. & Nicoll,R.A. (1973) The pharmacology and ionic dependency of amino acid responses in the frog spinal cord. J. Physiol. (Lond.) 228:259-277.

Barker,J.L., Nicoll,R.A. & Padjen,A. (1975a) Studies on convulsions in the isolated frog spinal cord. I: Antagonism of amino acid responses. J. Physiol. 245:521-536.

Barker,J.L., Nicoll,R.A. & Padjen,A. (1975b) Studies on convulsions in the isolated frog spinal cord. II: Effects on root potentials. J. Physiol. 245:537-548.

Barker,J.L., Nicoll,R.A. & Padjen,A. (in prep.) Factors underlying the genesis of dorsal root potentials in the frog spinal cord.

Bennett,J.P., Logan,W.J. & Synder,S.H. (1972) Amino acid neurotransmitter candidates: sodium-dependent high-affinity uptake by unique synaptosomal fractions. Science 178:997-999.

Bennet,M.V.L. (1972) Comparison of electrically and chemically mediated synaptic transmission. In: Structure and Function of Synapses. G.D.Pappas & D.P.Purpura (eds.) Raven Pub. N.Y. pp221-256.

Birks,R.I. (1975) The relationship of transmitter release and storage to fine structure in a sympathetic ganglion. J. Neurocytol. 3:133-160.

Birks,R., Huxley,H.E. & Katz,B. (1960) The fine structure of the neuromuscular junction of the frog. J. Physiol. (Lond.) 150:134-144.

Borg,E., Densert,O., & Flock,A., (1974) Synaptic vesicles in the cochlea. Acta Otolaryngol. 78:321-332.

Bourgeois,J.-P., Ryter,A., Menex,A., Fromageot,P., Boquet,P. Changeux,J.-P. (1972) Localization of the cholinergic receptor protein in Electrophorus electroplax by high resolution autoradiography. Fed European Biochem. Soc. Letters 25:127-133.

Brown, D.A. (personal communication, 1976)

Coombs,J.S., Eccles,J.C., & Fatt,P., (1955) The electrical properties of the motoneurone membrane. J. Physiol. 130:291-325.

Coombs,J.S., Eccles,J.C., & Fatt,P., (1959) The electrical constants of the motoneurone membrane. J. Physiol. 145:505-528.

Couteaux,R. (1960) Motor end-plate structure. In: The Structure and Function of Muscle. Bourne,G.H. (ed.) Academic . N.Y. vol 1. 337-380.

Curtis,D.R. & Johnston,G.A.R. (1974) Amino acid transmitters iin the mammalian central nervous system. Rev. Physiol. Biochem. Exp. Pharmacol. 69:97-188.

Curtis,D.R., Duggan,A.W., Felix,D. & Johnston,G.A.R. (1971) Bicuculline, an antagonist of GABA and synaptic inhibition in the spinal cord of the cat. Brain Res. 32:69-96.

Davidoff,R.A. (1972) The effects of bicuculline on the isolated spinal cord of the frog. Exptl. Neurol 35:179-193.

Davidson,N. & Southwick,C.A.P. (1971) Amino acids and presynaptic inhibition in the rat cuneate nucleus. J. Physiol. (Lond.) 219:689-708.

DeFeudis,F.V. (1972) Binding 3H-acetylcholine and 14C-gamma-aminobutyric acid to subcellular fractions of the brains of differentially-housed mice. Neuropharmacology 11:879-888.

Densert,O., & Flock,A. (1974) An electron-microscopic study of adrenergic innervation in the cochlea. Acta Oto-Laryngol. 77(3):185.

Densert,O. (1974) Adrenergic innervation in the rabbit cochlea. Acta Otolaryngol. 78:345-356.

Diamond,J., Roper,S. & Yasargil,G.M. (1973) The membrane effects and sensitivity to strychnine, of neural inhibition of the Mauthner cell, and its inhibition by glycine and GAGA.. J. Physiol. 232:87-111.

Dowling,J.E. (1968) Synaptic organization of the frog: an electron microscopic analysis comparing the retinas of frogs and primates. Proc. Roy. Soc. (Lond.) 170B:205-228.

Dowling,J.E. & Boycott,B.B. (1966) Neural connections of the retina: fine structure of the inner plexiform layer. Cold Spring Harbor Symp. Quant. Biol. 30:393-402.

Dreifuss,J.J., Kelly,J.S. & Krnjevic,K. (1969) Cortical inhibition and gamma-aminobutyric acid. Exptl. Brain. Res. 9:137-154.

Dunn,R.A. (1975) Innervation patterns and synaptic morphology in the cochlea of the cat. Anat. Rec. 181(2):348A.

Eccles,J.C. (1964) The Physiology of Synapses. Springer-Verlag, Berlin.

Eccles,J.C., Schmidt,R. & Willis,W.D. (1963) Pharmacological studies on presynaptic inhibition. J. Physiol. (Lond.) 168:500-530.

Elliot,K.A.C. von Gelder,J. (1958) Occlusion and metabolism of gamma aminobutyric acid by brain tissue. J. Neurochem. 3:28-40.

Engstrom,H. Ades,H.W., & Andersson,A., (1966) Structural pattern of the organ of Corti. Almquist & Wiksell, Stockholm. 172P.

Enna,S.J. & Synder,S.H. (1975) Properties of gamm-amminobutyric acid (GABA) receptor binding in rat brain synaptic membrane. Brain Res. 100(1):81-97.

Fambrough,D.M. & Hartzell,H.C. (1972) The acetylcholine receptors: number and distribution at neuromuscular junctions in rat diaphragm. Science 176:189-191.

Fex,J. (1967) Calcium action at an inhibitory synapse. Nature 213:1233-1234.

Flock,A. & Goldstein,M. (1973) Preliminary studies of the skates's semicircular canal. Biol. Bull. 145:433.

Flock,A. & Lam,D.M.K., (1974) Neurotransmitter synthesis in inner ear and lateral line sense organs. Nature 249(5453):142-144.

Flock,A., Jorgensen,J.M., & Russell,I., (1971) Efferent nerve fibers: Postsynaptic action on hair cells. Nature New Bio. 243:89-91.

Flock,A., Jorgensen,J.M., & Russell,I., (1973) Passive electrical properties of hair cells and supporting cells the lateral line canal organ. Acta Otolaryngol. 76:190-198.

Gage,P.W. (1976) Generation of end-plate potentials. Physiol. Rev. 56(1):177-239.

Ginsborg,B.L. (1967) Ion movements in junctional transmission. Pharmacol. Rev. 10(3):280-316.

Goldstein,M. (Personal Communication, 1976)

Hagiwara,S. & Tasaki,I.(1958) A study of the mechanism of impulse transmission across the giant synapse of the squid. J. Physiol. 143:114.

Hall,Z.W. (1972) Release of neurotransmitters and their interaction with receptors. Ann. Rev. Biochem. 41:925-952.

Hama,K. (1965) Some observations on the fine structure of the lateral line organ of the Japanese sea eel Lyncozymba nystromi. J. Cell Biol. 24:193-210.

Harrington,L. (1973) A linear dose-response curve at the motor endplate. J. Gen. Physiol. 62:58-76.

Hilding,D. & Wersall,J. (1962) Cholinesterase and its relation to the nerve endings in the inner ear. Acta Otolaryngol. 55:205-217.

Hille,B. (1970) Ionic channels in nerve membranes. Prog. in Biophys. & Molec. Biol. 21:1-32.

Hubbard,J.I., Llinas,R. & Quastel,D.M.J. (1967) Electrophysiological Analysis of Synaptic Transmission. Edward Arnold, London.

Iurato,S., Luciano,L, Pannese,E., & Reale,E (1971) Histochemical localization of acetycholinesterase (AChE) activity in the inner ear. Aca Oto-laryngol. Suppl. 279:1-50.

Jasser,A. & Gluth,P. (1973) Synthesis of acetylcholine by the olivocochlear bundle. J. Neurochem. 20:45-53.

Karlin,A., Prives,J., Deal,W. & Winnik,M. (1971) Counting acetylcholine receptors in the electroplax. In: Molecular Properties of Drug Receptors. Porter,R. & O'Connor,M. (eds.) Churchill. London. pp247-261.

Katz,B. (1962) The transmission of impulses from nerve to muscle and the subcellular unit synaptic action. Proc. Roy. Soc. 155(B):455-477.

Katz,B. & Miledi,R. (1972) The statistical nature of the acetycholine potential and its molecular components. J. Physiol. 234:665-699.

Katz,B. & Meledi,R.(1973) The binding of Acetylcholine to receptors and its removal from the synaptic cleft. J. Physiol. (Lond.) 231:549-574.

Kelly,J.S. & Krnjevic,K. (1969) The action of glycine on cortical neurones. Exp. Brain Res. 9:137-336.

Keynes,R.D. (1963) Chloride in the squid giant axon. J. Physiol. 169:690-705.

Kravitz,E.A. (1967) Acetylcholine, gamma-aminobutyric acid, and glutamic acid: Physiological and chemical studies related to their roles as neurotransmitter agents. In: The Neurosciences. A Study Program. (ed. Quarton,G., Melnechuk,T. & Schmitt,F.) Rockefeller Univ. Press. N.Y. p433.

Krnjevic,K. (1974) Chemical nature of synaptic transmission in vertebrates. Physiol. Rev. 54:418-540.

Krnjevic,K. (personal communication, 1976)

Krnjevic,K. & Mitchel,J.F., (1961) The release of acetylcholine in the isolated rat diaphragm. J. Physiol. (London) 155:246-262.

Krnjevic,K. & Phillis,J.W. (1963) Iontophoretic studies of neurones in the cerebral cortex. J. Physiol. 165:274-304.

Krnjevic,K. & Schwartz,S. (1966) Is gamma-aminobutyric acid an inhibitory transmitter? Nature (Lond.) 211:1372-1374.

Krnjevic,K. & Schwartz,S. (1967) The action of gamma-aminobutyric acid on cortical neurones. Expl. Brain Res. 3:320-336.

Krnjevic,K., & Whittaker,V.P. (1965) Excitation and depression of cortical neurones by brain fractions released from micropipettes. J. Physiol. 179:298-322.

Kuriyama,K., Weinstein,H. & Roberts,E. (1969) Uptake of gamma-aminobutyric acid by mitochondrial and synaptosomal fractions from mouse brain. Brain Res. 16:479-492.

Kuriyama,K. & Kimura,H. (1976) Distribution and possible functional roles of GABA in the retina, lower auditory pathway, and hypothalamus. In: GABA in Nervous System Function. Roberts,E., Chase,T.N., & Tower,D.B. Raven Press, N.Y. pp203-216.

Leibovic,K.N. & Sabah,N.H. (1969) On synaptic transmission, neural signals and psychophysiological phenomena. In: Information Processing in the Nervous System. Leibovic,K.N. (ed.) Springer-Verlag. N.Y. pp272-292.

Levy,R.A., Repkin,A.H. & Anderson,E.G. (1971) The effect of bicuculline on primary afferent terminal excitability. Brain Res. 32:261-265.

Liley,A.W. (1956) The effects of presynaptic polarization on the spontaneous activity at the mammalian neuromuscular junction. J. Physiol. (Lond.) 134:427-443.

Llinas,R., Baker,R., & Precht,W. (1974) Blockage of inhibition by ammonium acetate action on chloride pump in cat trochlear motoneurons. J. Neurophysiol. 37:522-532.

Lorente de No,R., (1933) Anatomy of the eighth nerve I.:The central projection of the nerve endings of the internal ear. Laryngoscope. 43:327-350.

Lorente de No,R. (1937) The sensory endings in the cochlea. Laryngoscope 47:373-377.

Lux,H.D. (1971) Ammonium and chloride extrusion: Hyperpolarizing synaptic inhibition in spinal motoneurons. Science 173:555-557.

MacIntosh,F.C. (1941) The distribution of acetylcholine in the peripheral and the central nervous system. J. Physiol. (Lond.) 99:436-442.

MacIntosh,F.C. (1959) Formation, storage, and release of acetylcholine at nerve endings. Can. J. Biochem. Physiol. 37:342-356.

Magleby,K.L. & Stevens,C.F. (1972) The effect of voltage on the time course of end-plate currents. J. Physiol . 223:151-171.

Mahler,H.R., & Cordes,E.H., (1966) Biological Chemistry. Harper & Row, N.Y. 872P.

Martin,A.R. Wickelgren,W.O. & Beranek,R. (1970) Effects of iontophoretically applied drugs on spinal interneurones of the lamprey. J. Physiol. 207:653-665.

McLennan,H. (1970) Synaptic Transmission, 2nd Ed. Saunders. London.

McNamee,M.G., Weill,C.L., & Karlin,A. (1975) Purification of acetylcholine receptor from Torpedo californica and its incorporation into phospholipid vesicles. Ann. N.Y. Acad. Sci. 264:175-182.

Meunier,J.-C., Olsen,R.W., Menex,A., Fromageot,P., Boquet,P. Changeux,J.-P. (1972) Some physical properties of the cholinergic receptor protein from Electrophorus electricus revealed by a tritiated toxin from Naja nigriocollis venom. Biochemistry 11:1200-1210.

Miledi,R., Molinoff,P. & Potter,L.T. (1971) Isolation of the cholinergic receptor protein of Torpedo electric tissue. Nature 229:554-557.

Miledi,R. & Potter,L.T. (1971) Acetylcholine receptors in muscle fibres. Nature 233:599-603.

Namba,T. & Grob,D. (1967) Cholinergic receptors in skeletal muscle: isolation and properties of muscle ribonucleoprotein and affinity for d-tubocurarine and acetylcholine, and binding activity of the subneural apparatus of motor end plates with divalent metal ions. Ann. N.Y. Acad. Sci. 144:772-802.

Nicoll,R.A., Padjen,A. (in prep.) The distribution and the ionic requirements of responses evoked by amino acids in the primary afferents of the frog.

Nishi,S. Minota,S. & Karczmar,A.G. (1974) Primary afferent neurones: The ionic mechanisms of GABA-mediated depolarization. Neuropharmacology 13:215-219.

Obata,K. Takada,K. & Shinozaki,H. (1970) Further study on pharmacological properties of the cerebellar-induced inhibition of Deiter' neurones. Exp. Brain Res. 11:327-342.

Osborne,M.P. & Thornhill,R.A. (1972) The effect of monoamine depleting drugs upon the synaptic bars in the inner ear of the bull frog (Rana catesbeiana). Z. Selforschung 127:347.

Padjen,A. Nicoll,R.A., & Barker,J.L. (1973) Synaptic potentials in the isolated frog spinal cord studied with the gap technique. J. Gen. Physiol. 61:270-271.

Pappas,G.D. & Waxman,S.G. (1972) Synaptic fine structure--morphological correlates of chemical and electronic transmission. In: Structure and Function of Synapses. G.D.Pappas & D.P.Purpura (eds.) Raven Pub.. N.Y. pp1-49.

Peters,A., Palay,S.L., & Webster,H.deF.(1970) The Fine Structure of the Nervous System. Harper & Row, N.Y. 198P.

Phillis,J.W. (1970) The Pharmacology of Synapses. Pergamon. N.Y.

Porter,C.W., Barnard,E.A. & Chiu,T.H. (1973) The ultrastructural localization and quantitation of cholinergic receptors at the mouse motor endplate. J. Membrane Biol. 14:383-402.

Porter,C.W., Chiu,T.H., Wieckowski,J. & Barnard,E.A. (1973) Types and locations of cholinergic receptor-like molecules in muscle fibres. Nature 241:3-7.

Potter,L.T. (1973) Acetylcholine receptors in vertebrate skeletal muscles and electric tissue. In: Drug Receptors; a Symposium. Rang,H.P. (ed.) Macmillan. London. pp295-312.

Potter,L.T. (1974) Synthesis, storage & release of C14 acetylcholine isolated rat diaphragm muscle. J. Physiol. London 20B:145-166.

Roberts,E., Chase,T.N., & Tower,D.B., Eds. (1976) GABA in Nervous System Function Kroc Foundation Series, Vol. 5, Raven Press. N.Y. 554P.

Rosenbluth,J. (1973a) Membrane specialization at an insect myoneural junction. J. Cell Biol. 59:143-149.

Rosenbluth,J. (1973b) Postjunctional membrane specialization at cholinergic myoneural junctions in the leech. J. Comp. Neurol. 151:399-406.

Russell,I. (1971) The pharmacology of efferent synapses in the lateral line of Xenopus laevis. Exp. Biol. 54:643-658.

Salpeter,M.M., Plattner,H. & Rodgers,A.W. (1972) Quantitative assay of esterases in end plates of mouse diaphragm by electron microscope autoradiography. J. Histochem. Cytochem. 20:1059-1068.

Scruggs,V. & Landowne,D. (1975) The temperature dependence of chloride fluxes in the squid giant axon. Biophys. J. 15:126a.

Seite,R., Mei,N. & Vuillet-Luciani,J. (1972) Influence de la duree de la stimulation electrique sur l'organisation ultrastructurale des inclusions nucleaires des neurones sympathiques. J.Physiol. (Paris) 65(Suppl. 1):165A.

Sjostrand,F.S. (1958) Ultrastructure of retinal rod synapses of the guinea pig eye as revealed by three-dimensional reconstructions from serial section. J. Ultrastruct. Res. 2:122-170.

Smith,C.A. (1961) Innervation pattern of the cochlea: The inner hair cell. Ann. Otol. Rhinol. Laryngol. 70:504.

Smith,C.A. & Sjostrand,F.S. (1961) Structure of the nerve endings on the external hair cells of the guinea pig cochlea as studied by serial sections. J. Ultrastruc. Res. 5:523.

Smythies,J.R., Benington,F., Morin,R.D. (1975) The action of the alkaloids from yew (Taxus baccata) on the action potenial in the Xenopus medullated axon. Experientia 31(3):337-8.

Spoendlin,H. (1966) The organization of the cochlear receptor. Adv. Oto-Rhinolaryng. (Fortschitte der Hals-Nasen-Ohrenheilkunde) Vol. 13. 227P.

Spoendlin,H. (1968) Ultrastructure and peripheral innervation pattern of the receptor in relation to the first coding of the acoustic message. In: Hearing Mechanisms in Vertebrates. A.V.S. deReeuck & J. Knight (eds.) Churchill Press. London. pp89-119.

Spoendlin,H. (1974) Neuroanatomy of the cochlea. In: Facts and Models in Hearing, Zwicker,E. & Terhardt,E. (eds.) Springer-Verlag, N.Y. pp18-36.

Spoendlin,H. & Lichtensteiger,W. (1966) The adrenergic innervation of the labyrinth. Acta Otolaryngol. 61:421.

Tachibana,M. & Kuriyama,K. (1974) Gamma-aminobutyric acid in the lower auditory pathway of the guinea pig. Brain Res. 69:370-374.

Tebecis,A.K., & Phillis,J.W. (1969) The use of convulsants in studying possible functions of amino acids in the toad spinal cord. Comp. Biochem. Physiol. 28:1303-1315.

ten Bruggencate,G. & Engberg,I. (1971) Iontophoretic studies in Deiters' nucleus of the inhibitory actions of GABA and related amino acids and the interactions of strychnine and picrotoxin. Brain Res. 25:431-448.

Terayama,Y., Holz,E., & Beck,C.(1966) Adrenergic innervation of the cochlea. Ann. Otl. 75:69.

Valderrama,R. Weill,C.L., McNamee,M., et al (1976) Isolation and properties of acetylcholine receptors from Electrophorus and Torpedo. Ann. N.Y. Acad. Sci. 274:108-115.

Varon,S. Weinstein,H., Baxter,C.F. & Roberts,E. (1965) Uptake and metabolism of exogenous gamma-aminobutyric acid by subcellular particles in a sodium-containing medium. Biochem. Pharmacol. 14:1755-1764.

Weill,C.L., McNamee,M.G., & Karlin, (1974) Affinity-labeling of purified acetylcholine receptor from Torpedo californica. Biochem. Biophys. Res. Commun. 61(3):997-1003.

Werman,R. (1966) Criterion for identification of a central nervous system transmitter. Comp. Biochem. Physiol. 18:745.

Whitfield,I.C. & Comis,S.D. (1966) A micro-tap for drug application to single neurones. Final Rep. (Part 1), Sept. 1966. Af EOAR Grant 63-115. Neurocommunications Res. Unit, U. of Birmingham, England.

Whittaker,V.P. (1965) The application of subcellular fractionation techniques to the study of brain function. Progr. Biophys. 15:39-96.

Whittaker,V.P. & Sheridan,M. (1965) The morphology and acetycholine content of isolated cerebral cortical synaptic vesicles. J. Neurochem.

Winslow,J.L. (1972) In vivo neural network recording. M.Sc. Thesis, McGill Univ., Montreal.

Woodward,J.K., Bianchi,C.P. & Frulkar,S.D. (1969) Electrolyte distribution in rabbit superior cervical ganglion. J. Neurochem. 16:289-299.

Woodward,D.J. Hoffer,B.J., Siggins,G.R. & Oliver,A.P. (1971) Inhibition of Purkinje cells in the frog cerebellum, II. Evidence for GABA as the inhibitory transmitter. Brain Res. 33:91-100.

Young,A.B., Enna,S.J., Zukin,S.R., & Synder,S.H. (1976) Synaptic GABA receptor in mammalian CNS. In: GABA in Nervous System Function. Roberts,E., Chase,T.N., & Tower,D.B. Raven Press, N.Y. pp305-318.

Zorychta,E. (1974) An intracellular study of the actions of anesthetics on spinal monosynaptic transmission. Ph.D. Thesis. McGill University. Montreal, Canada. 150P.

CHAPTER 6: COCHLEAR DENDRITES

CHAPTER 6
COCHLEAR DENDRITES

6.1 INTRODUCTION

6.1.1 THE PROBLEM

6.1.1.1 STATEMENT

In the mammalian cochlea the hair cells innervate bipolar neurons whose axons constitute the afferent portion of the cochlear nerve. There are two kinds of afferent dendrites. The inner hair cells innervate one type which becomes an afferent axon of the cochlear nerve. The outer hair cells innervate a second type of dendrite which also becomes an axon in the nerve. The first type of dendrite is a straight unbranched fiber from one inner hair cell to its axon. The second type has the shape of a lady's long handled comb with typically ten teeth, where each one of the ten branches is innervated by one outer hair cell (Spoendlin,1974). What are the functional purposes of these two types? Looking at the preceding step with respect to signal processing, Dallos et al (1972b,73) report that an inner hair cell's receptor potential is proportional to basilar membrane velocity, whereas an outer hair cell receptor potential is proportional to displacement.

If this is the major reason for the two hair cell and dendrite types, then why are the dendrites so different in shape? The ensuing analysis and simulations are designed to sort out this problem. With increasing interest in cochlear implant prosthesis technology, what effect do changes of cochlear gross potentials have on the auditory signals as they exist in the afferent dendrites?

Almost all nervous system regions have complicated interconnections of their neurons. To predict how neurons interact via their synaptic connections, it is necessary to describe neuron responses to synaptic inputs from multiple precursor neurons. To answer this and provide an analysis of the "cochlear two type dendrite question", the following problem must also be solved. Is it possible to extend Rall's (1962a,b) work on highly regular symmetric dendrites with stringent requirements on branch diameters to irregular asymmetric dendrites with unrestricted branch diameters and unrestricted branching?

6.1.1.2 CONJECTURES

What are the possible reasons for the structural differences between the inner and outer dendrites? A major tenet of biology is that structure and function correspond and that structure determines function. The possible conjectures

for the differences are discussed as follows. The underlying concept is that the basilar membrane frequency response is organized with respect to position on the membrane with highest frequency at the basal end of the cochlea and lowest frequency at the apex (Bekesy,1949,60; Johnstone and Boyle,1967; Rhode,1971)

Since the outer dendrites receive synaptic input from outer hair cells over a distance on the basilar membrane which corresponds to a frequency band, could these dendrites be frequency band detectors? The possible usefulness could arise in the detection of vocalizations with large variation in the component frequencies.

Since inner dendrites come from one inner hair cell and frequency is localized on the basilar membrane, inner hair cells and inner dendrites are optimally tuned to a narrow frequency band of sound input, based on only basilar membrane localization. The outer dendrites traverse two hundred microns apically along the cochlear partition while receiving inputs from approximately 10 outer hair cells. The apicalward direction corresponds to decreasing frequency on the basilar membrane. Pyschophysical data supports this. Mammalian distress vocalizations reported in the literature consist mainly of downsweeps in frequency (Winter et al, 1966; Worden & Galambos, 1972).

The neural response of a cochlear axon is sharper than the basilar membrane with respect to sound input frequency (Evans & Wilson, 1973; Wilson, 1974; Duhifus, 1976, Inselberg, 1978). Could cochlear microphonic potentials contribute to the frequency sharpening of the cochlear response? It was suggested by Manley (1977) that the gross potentials generated by the hair cells influence the neural tuning curves and the role of the outer dendrites is merely to provide a trophic affect on the outer hair cells. Since dennervated neurons atrophy, this conjecture is possible, but not probable on the basis of Nature's parsimony of structure.

6.1.2 STRATEGY

To analyze the response of cochlear dendrites without the influence of hair cells, transmitter release, and dynamic cochlear potentials, it is preferable to utilize a simulation rather than an experimental study. With an accurate simulation, frequency sweep experiments can be performed that are impractical to do while recording from a single cochlear nerve axon due to the necessity of holding the same axon for a long time. It is also possible to influence the dendrite by changing the extracellular potential without affecting the synapse and hair cell response. This is important because the cochlear gross dynamic potentials are determined by the hair

cells.

In a biological system, as in any system, structure determines function. This principal is particularly important because it is the geometry of the dendrites that determine response when properties of dendritic membrane are used. Thus the well understood passive neural membrane is taken as the starting point. A simulation model is then developed, based on the geometry of the dendrites and arrangement of synaptic inputs.

6.2 COCHLEAR DENDRITE GEOMETRY

6.2.0 ORIENTATION

The afferent synapses from the hair cells transmit their signal to the dendrites of the spiral ganglion neurons whose axons constitute the cochlear nerve (Lorente de No, 1935,1937; Cajal,1909; Gacek 1967). The cat cochlear nerve has 50,000 axons in it (Gacek & Rasmussen,1961). The dendrites are organized as to position along the spiral arc of the cochlea and as to one of two types based on analysis in the cat per Spoendlin (1979,74,73,72,71a,71b,70b,69,66,63). As summarized by Spoendlin (1973), class one dendrites are innervated by one and only one inner hair cell (95% of the axons in the nerve). Class two dendrites run for about 600 to 700 microns under the outer hair cells going in the apical direction. In the first 200 microns (I prefer to designate direction according to signal movement) each dendrite receives a dendrite branch from each outer hair cell for about 10 hair cells. This was confirmed in cat by Perkins and Morest (1975) and noted by Dunn (1975) After the 600 to 700 microns, these outer hair cell dendrites cross the tunnel of Corti as lower tunnel crossing fibers (also referred to as basilar tunnel crossing fibers) and enter the habenula perforata as one type two dendrite per perforata hole. The geometry is shown in figure:6.2.0.

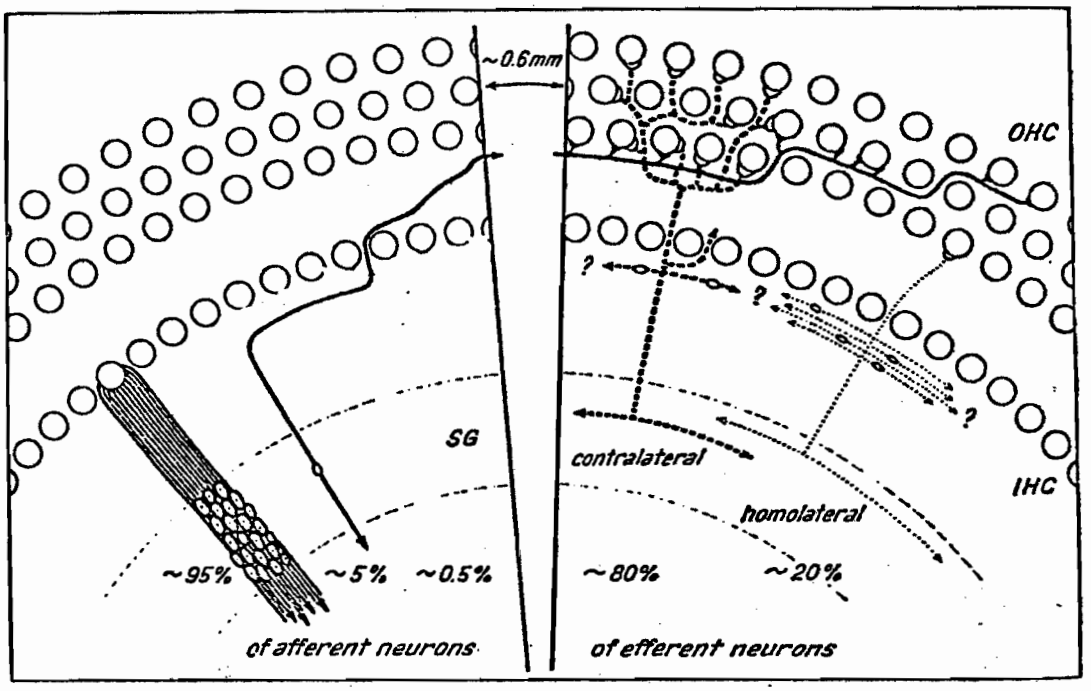

Figure:6.2.0 Horizontal innervation schema of the organ of Corti with the different types of afferent neurons shown on the left and efferent neurons shown on the right, with their corresponding approximate percentages. From Spoendlin (1971) and updated from Spoendlin (1973).

6.2.1 INNER HAIR CELL DENDRITES

The dendrites from the inner hair cells receive a synaptic input from one and only inner hair cell, with one inner hair cell synaptically transmitting to 20 dendrites. The diameter of the dendrite from the synapse to the habenula perforata is 1 micron. The distance from the postsynaptic region to the end of the satellite cell surrounding the dendrites after they enter the habenula perforata is 30 microns. The myelin sheath around the fibers starts just after the proximal end of the satellite cell. The satellite cell is depicted in figure:6.2.3.1. The value of 30 microns is the average of my estimates for the distance from Smith (1961,fig.1 and fig.2), the sum of parameters h and g for the organ of Corti as determined by Billone(1972), and Ades and Engstrom (1972,fig.1a,1b). From these same pictures, the narrow part of the dendrite at the satellite cell where the dendrite passes through the habenula perforata hole is estimated to be 5 microns. These dimensions are summarized in figure:6.2.1.

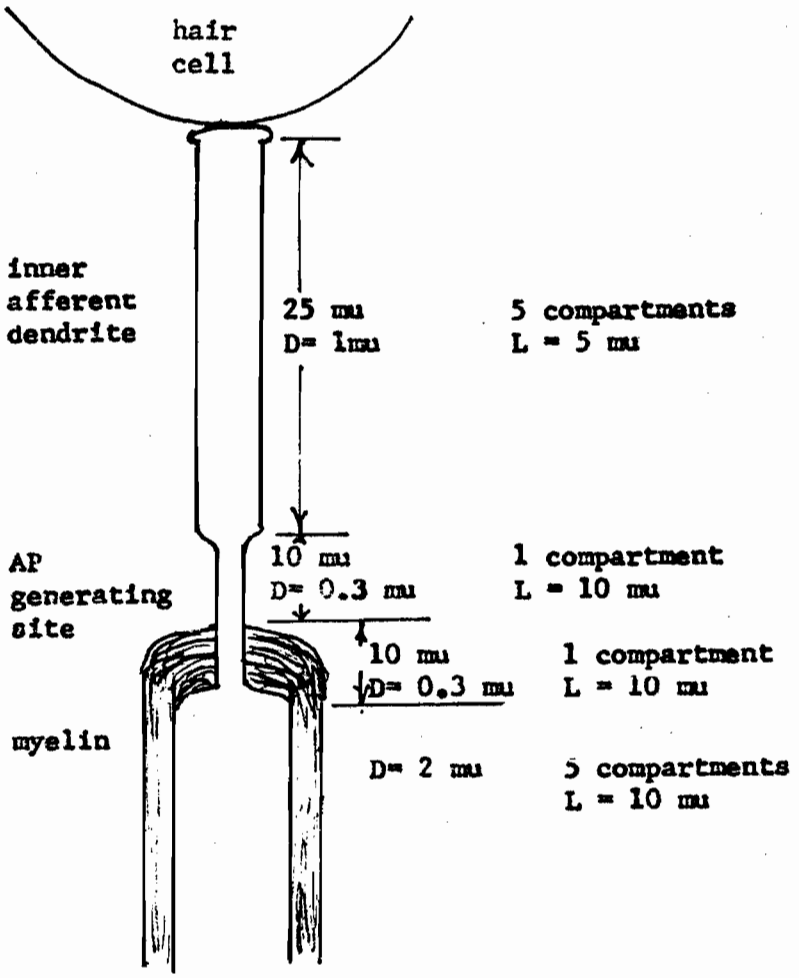

Figure:6.2.1 Inner dendrite dimensions.

6.2.2 OUTER HAIR CELL DENDRITES

The outer dendrites are those which receive input from the outer hair cells. They start at a hair cell and run for about 200 microns receiving synaptic input from about 10 outer hair cells with each outer hair cell making synaptic contact to 4 dendrites. After the dendrite has run for 600 to 700 microns in an apical direction it crosses the tunnel of Corti as a lower tunnel crossing fiber and enters the habenula perforata with the dendrites from the nearest inner hair cell. The diameter of the section of dendrite from the hair cell afferent synapse to the main dendrite (these are sometimes called outer spiral fibers) is 0.2 microns and this section is about 10 microns long (Engstrom, Ades, and Andersson 1966, fig. 75 and 76). The diameter of the main body is 0.5 microns. The length of the section crossing the tunnel of Corti is estimated to be 80 microns, thence for 5 microns to the proximal side of the satellite cell after the habenula perforata (Engstrom, Ades, and Andersson 1966, fig. 49). According to Spoendlin (1974) these fibers (spiral ganglion type II) remain unmyelinated with a monopolar soma. As of now, there is one report in the literature (Spoendlin, 1979) that the axons from these dendrites taper off as unmyelinated axons after the soma and do not continue in the nerve as

proper afferent axons. These dimensions are summarized in figure:6.2.2.

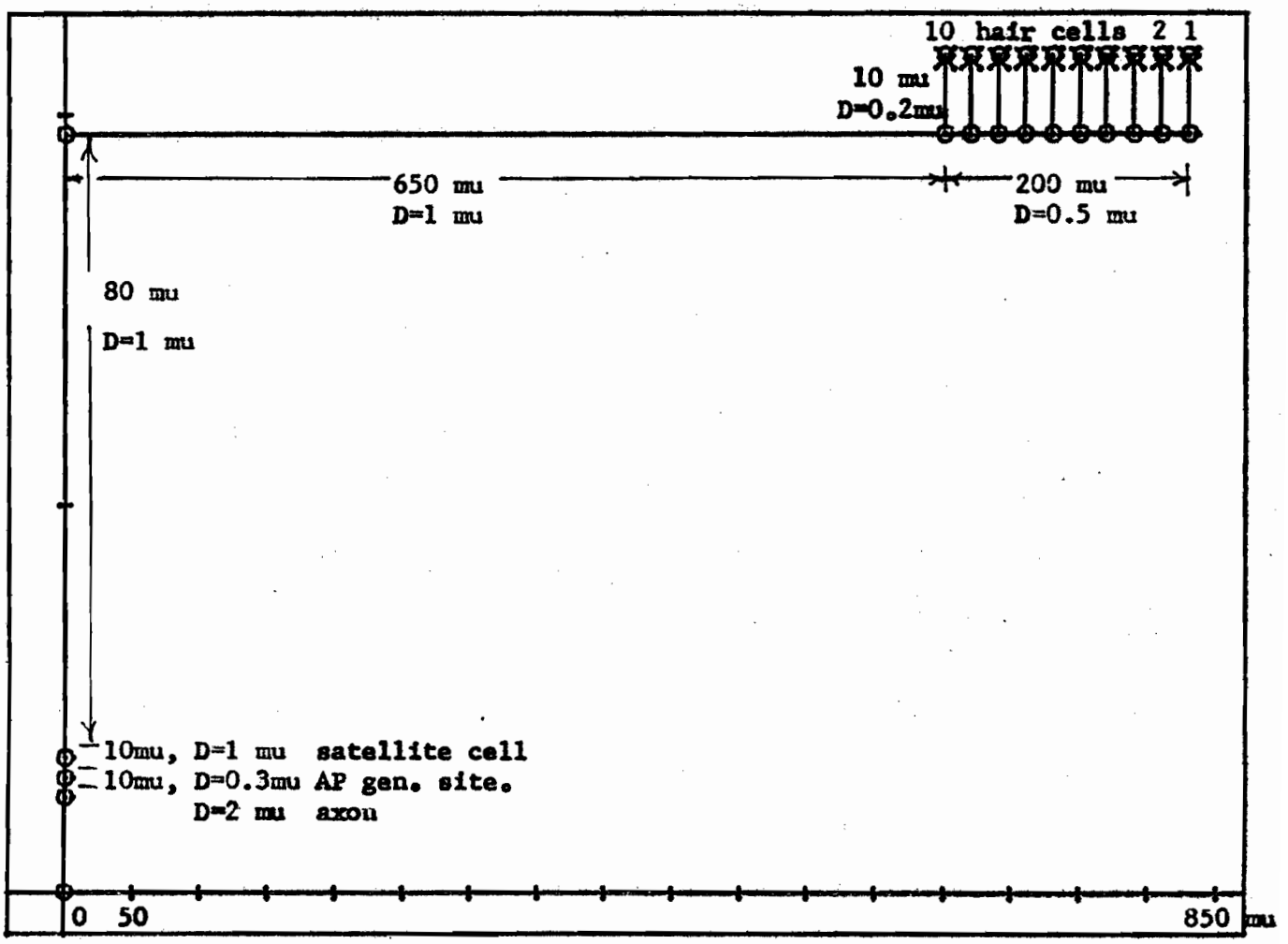

Figure:6.2.2 Outer dendrite dimensions.

6.2.3 AP GENERATING SITE

The anatomy of the AP generating site is shown in figure:6.2.3.1 with the satelite cell surrounding the constricture of a cochlear afferent dendrite. Between the satellite cell and the start of the myelin for the inner dendrites (Spoendlin, 1974), I assume that the constricture is present and the enlargement to 2 mu occurs just before the myelin sheath. Spoendlin was unclear about this and the literature does not provide an appropriate picture to ascertain this dimension. Spoendlin (1974) states that the outer afferent dendrites (Spoendlin type II) are unmyelinated. It was not specifically stated, but I assume that the enlargement of the constricture to 2 mu also applies to the outer dendrites.

The geometry for this model takes the constricture to be 10 mu in length and 0.3 mu in diameter. The specific resistance for the dendritic membrane with surrounding satelite cell is assumed to be, for myelinated axon, $1.6*10^{5}$ $ohm*cm^{2}$ and the myelin specific capacitance is $2.5*10^{-9}$ F/cm^{2} (Stampfli, 1954), since this compartment is surrounded by the satellite cell (Spoendlin, 1974). I assume from Spoendlin (1974, figure 7) that the gap between the satellite cell and the Schwann cells is like a node of Ranvier where APs are

generated. I approximate the length of the gap to be 0.70 mu which is the length of a gap with diameter 0.3 mu with a decaying exponential fitted to the gap length versus gap diameter data of Hess and Young (1952), shown in figure:6.2.3.2.

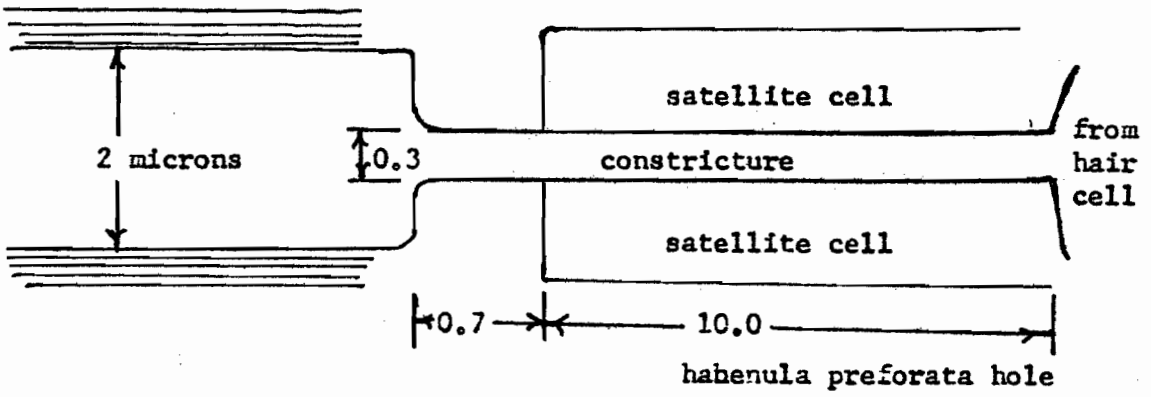

Figure:6.2.3.1 Anatomy of action potential generating site for afferent axons from the cochlea. The dimensions are in microns.

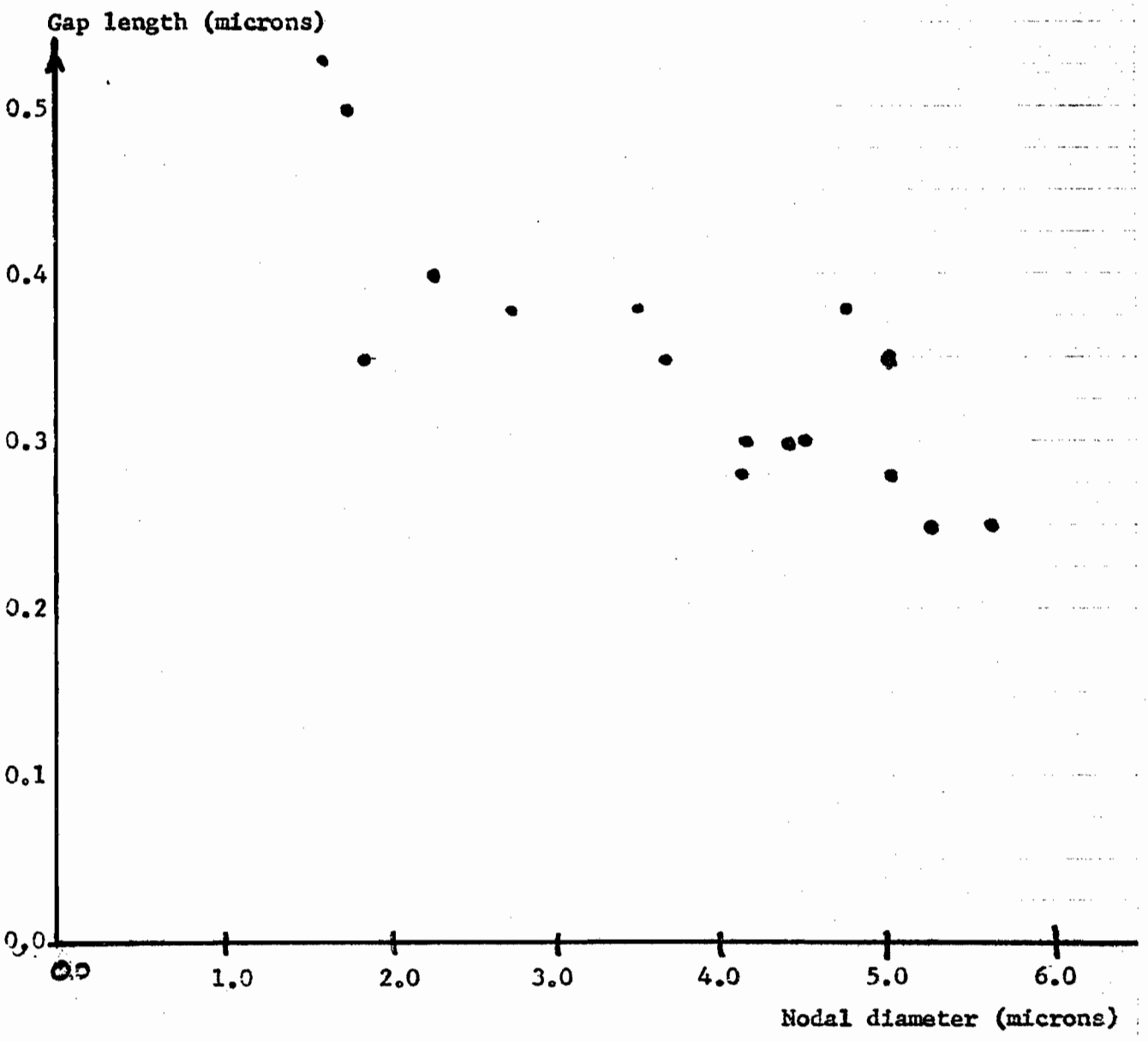

Figure:6.2.3.2 Node of Ranvier gap length versus gap diameter. See text for discussion.

6.3 DENDRITE ANALYSIS

6.3.1 REVIEW

In a series of papers, Rall(1959,1960,1962a,1962b) developed various versions of models for dendritic trees. His approach treated the dendritic membrane as an electrically passive membrane that does not generate an action potential. He then derived equations for the transmembrane voltage as a function of time and actual position along the dendrite. The dendritic trees which possessed a regular symmetric branching pattern and a branch diameter property were shown to be functionally identical to an equivalent cylinder type of dendrite when excitatory or inhibitory synapses were activated at the same electrotonic distances from the soma.

The requirement on the branching is that the sum of the diameters to the 3/2 power of each of the daughter branches at each bifurcation be equal to the parent branch diameter to 3/2 power (Rall, 1962a). Although this property and symmetry of branching allow analysis as an equivalent cylinder, dendrites in general do not satisfy these properties.

There are severe limitations on these models, quite apart from the computational complexity required to produced descriptions of their behavior, since they are in closed analytic form. The limitations are summarized as follows:
(1)All terminal branches must be assumed to end with the same

electrotonic distance from the soma, i.e., the same z=x/L value, where L is the space constant. (2)The spatio-temporal patterns of excitation or inhibition in the equivalent cylinder can represent only those dendritic tree disturbances which can be assumed to be the same in all parts of the tree corresponding to a given z value. (3)The constraint on the branch diameters that allows the equivalent cylinder development is obviously not fulfilled by all dendritic trees.

As a result of the limitations on the first models, Rall(1964) developed a compartmental model for dendrites. The point of this type of model is to treat each cylindrical region of the considered dendrite as a compartment. The transmembrane voltage of each compartment is considered as a function of the currents entering and leaving the compartment. The currents are of three types: those entering the compartment in the longitudinal direction, those leaving in the longitudinal direction, and the current through the membrane (in the radial direction).

This compartmental model of Rall was developed with normalized variables and a somewhat imprecise description of synapses on the dendrite. To make a model of dendrites that is more applicable to a real dendrite structure, I use a different model for a general dendritic compartment, with a direct synaptic input structure.

Rall (1964) collapsed a radially symmetric fan shaped dendrite into one long dendrite with equivalent cylinders and simulated it with ten compartments to ascertain the importance of synaptic location. This equivalence works only when the sum of the 3/2 powers of the diameters of the branches is constant, which is an idealization for which there is insufficient evidence. Dendrites are usually nonsymmetric and the 3/2 power conjecture most likely is too severe for Mother Nature. The simulation for a small number of compartments was probably due to the technical limitations of numerical integration and computer speed at that time. The methods employed in this investigation permit large numbers of compartments with greatly different properties.

6.3.2 A PATCH OF DENDRITIC MEMBRANE

A small homogeneous region of dendritic membrane without synapses is functionally described by the equivalent circuit in figure:6.3.2. This equivalent circuit is a generalization of the models proposed by Fatt and Katz (1953) and Fatt (1955). This equivalent circuit originates from the papers of Hodgkin and Katz (1949), Fatt and Katz (1951), and Hodgkin and Huxley (1952). It is similar to that used by Rall. The variables are defined as:

V = response voltage of the intracellular medium (volts)
We = voltage of the extracellular medium (volts)
Vr = resting membrane voltage (volts)
Vm = transmembrane voltage (volts)
Cm = capacitance per unit area (farads/cm*cm)
Gm = resting membrane conductance (mho/cm*cm)
Rm = resting membrane resistance density (ohm*cm*cm)
= 1/Gr
Jm = transmembrane current density (amps/cm*cm)

The essential feature of this model is that the membrane resting conductance Gm is assumed to remain constant and the ionic conducting pathway contains the transmembrane potential Vm in series. The net membrane potential is Vm = (V + Vr) - we, where Vr is the resting membrane electromotive force for no net current (Jm=0), V is the response voltage and We is the external potential. If the equation for Jm, the membrane current density, is written for the equivalent circuit in figure:6.3.2 using Vm = V + Vr - We, and noting that $D_t V_m = D_t V$, (D_t is the first derivative operator with respect to time t, likewise D_{xx} denotes the derivative operator with respect to x twice)

$$Jm = Cm*D_t V + Gr*(V + (Vr - We))$$

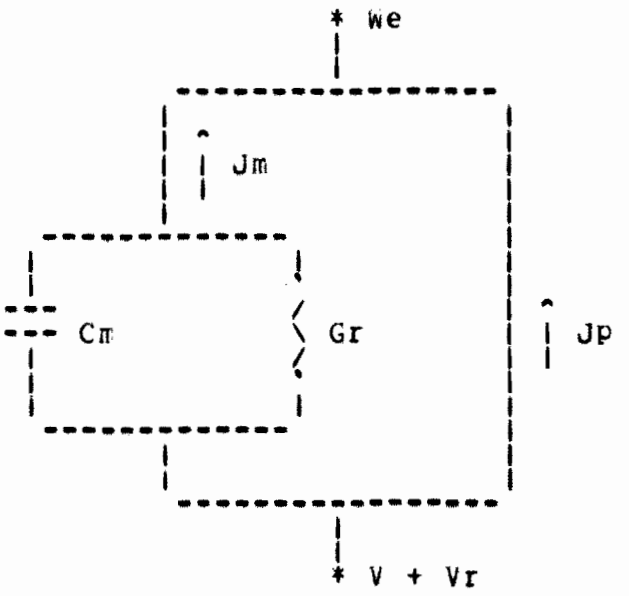

Figure:6.3.2 A region of dendritic membrane. V is the dendrite response potential, Vr is the internal resting potential, We is the extracellular potential, Cm is capacitance per unit area, Gr is conductance per unit area and Jm is current density per unit area, and Jp is the membrane pump current density.

6.3.3 SYNAPSES

The transmitter from cochlear hair cells to dendrites is excitatory. Increased sound pressure at the ear drum increases the hair cell receptor potential (Russell & Sellick, 1977) and increased AP frequencies in the cochlear nerve (Kiang et al, 1967). There are no known receptor cells which release an inhibitory transmitter. During synaptic excitation, membrane permeability increases for one or both of the principal monovalent cations, Na^+ and K^+ (Eccles,1964; Katz,1966). For the purpose of this simulation, the affected ion is taken to be sodium with an equilibrium potential of 50 mv (Curtis et al, 1972). The choice of affected ion is not dramatically important.

Consider what an active synapse does to the dendritic compartment. The output from a synapse is an ionic current (postive outward) through the postsynaptic receptor sites on the dendritic membrane. The current originates from the electrochemical gradient across the membrane and the opening of an ion selective pore. Thus the current at a synapse, Isyn, is

$$\begin{aligned} Isyn &= NBRS*Ipore \\ &= NBRS*Jion*Apore \end{aligned}$$

where NBRS is the number of bound receptor sites or number of pores open, Ipore is the current through one pore, Jion is the

current density from the Goldman equation for the selective ion, Apore is the effective area of a pore. It should be noted that for the i-th synapse, $Isyn_i$ is for only that synapse and Ipore, the current per pore, is based on the consideration of the mode of action of the transmitter at that synapse. Accordingly, $Ipore_i$ is evaluated for the ion(s) utilized. As a result of this treatment of the synaptic input, the fact that a particular synapse is excitatory or inhibitory is immaterial; $Isyn_i$ just makes its contribution to the equation for the compartment.

The maximum conductance of the synapse occurs when all the postsynaptic receptor ion pores are open. Based on the discussion in the synapse chapter, the number of postsynaptic receptor site molecules which equals the maximum number of available pores is 1386. From Armstrong's (1975) data, the pore conductance ranges around 10^{-11} mho per pore. Thus the maximum synaptic conductance is taken to be $Gsm = 1.4*10^{-8}$ mho.

The input to the post synaptic dendrite is taken to be

$$Gs(t) = Gsm*CS(t)$$

The function CS(t) is a continuous pulse, all of whose derivatives are continuous, and

$$CS(t) = \begin{cases} 0, & t < Ton \\ 0.5*(-1 + \cos(w*(t-Ton)), & Ton \leq t < Toff \\ 0, & Toff \leq t \end{cases}$$

where w = 2*pi/2*R, R being the rise and fall time of the pulse, and Ton and Toff are respectively the onset and offset times of the pulse. The synaptic current for a compartment is thus

$$Is(t) = Gs(t)*(Vm - Ena) = Gs(t)*(V + (Vr - U))$$

where U = We + Ena.

6.3.4 A GENERAL COMPARTMENT

The model for a general dendritic compartment is developed in this section. Consider the cylindrical piece of dendrite depicted in figure:6.3.4. The appropriate variables are:

A_i = exposed cylindrical surface area through which the membrane current passes

= 2*pi*r*dx (cm*cm)

Cm_i = capacitance per unit area of i-th compartment (farads/cm*cm)

Gm_i = conductance per unit area of i-th compartment (mho/cm*cm)

C_i = capacitance of the i-th compartment (farads)

= $A_i * Cm_i$

J_i = ionic membrane current density leaving compartment (amps/cm*cm)

Im_i = total ionic current leaving dendrite compartment through the membrane (amps)

$= A_i * J_i$

W_i = internal potential for i-th compartment

V_i = response potential for i-th compartment

Vm_i = transmembrane voltage drop from inside to outside of the i-th compartment (volts)

$= w_i - We$

$= V_i + Vr - We$

IL_{ji} = net longitudinal current from i-th to j-th compartment

$= g_{ij}(w_i - w_j)$

g_{ij} = conductance from i-th to j-th compartment

$= g_{ji}$

Jp = constant membrane pump current density

$Ip_i = A_i * Jp$

The longitudinal current from the j-th to the i-th compartment is

$$I_{ij} = GL_{ij} * (w_j - w_i) = GL_{ij} * (V_j - V_i)$$

The length dx is taken as the distance between centers of the compartments. Thus, for adjacent compartments with the same radii and centers dx apart, using axoplasmic resistivity, AR, the longitudinal conductance is

$$G_{ij} = G_{ji} = pi * r * r / AR * dx \qquad \text{(mho)}$$

The synaptic current is now

$$Is(t) = Gs(t)*(V_i + U)$$

Consider the positive direction of the currents as indicated by the arrows in figure:6.3.4; the dynamic equilibrium equation is

$$Im + Ip + Is = \sum_{j \text{ in } B_i} IL_{ij}$$

where B_i is the set of compartments connected to the i-th compartment. Substitution gives

$$A_i*C_i*D_t V_i + Gm_i*(V_i + Vr - We) + Ip + Gs(t)*(V_i + Vr - U)$$

$$= \sum_{j \text{ in } B_i} GL_{ji}*(V_j - V_i)$$

Examining the equilibrium current through the membrane with no synapses active, $D_t V_i = 0$ and $V_i = 0$, thus

$$Gm_i*(Vr-We) + Ip = 0.$$

Solving for the time derivative gives

$$D_t V_i = (1/(A_i*C_i))*\left[-Gm_i - \sum_{ij} GL_{ij} - Gs(t) \right]*V_i + \left[\sum_{ij} GL_{ij}*V_j - Gs(t)*(Vr - U) \right]*(1/A_i*C_i)$$

as the equation for the general compartment with a synapse.

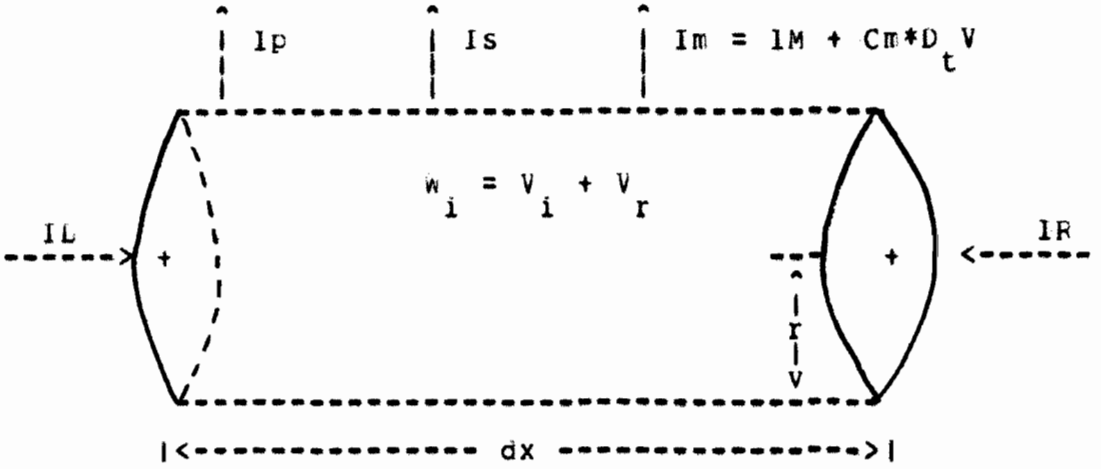

Figure:6.3.4 A compartment in a uniform segment of dendrite with radius r, length dx, conductance per unit area Gm, and capacitance per unit area Cm. The current from the left neighboring compartment is IL and the right neighboring compartment is IR. The pump current is Ip, the synaptic current (if there is one) is Is, the membrane current density is Im, and the diffusion current is IM.

6.3.5 IN PDE FORM

The compartment formulation is equivalent to a partial differential equation governing a piece of dendrite at a point in space and time (x,t), with synapses and pump current. Consider a compartment for an unbranched segment with the same size compartment on each side as in figure:6.3.4. The dynamic equilibrium equation is

$$-IM - A_i Cm*D_t V_i + IL + IR - Is - Ip = 0$$

where

IM = membrane current

$= (V_i + Vo)*Gm$

Vo = Vr - we

$IL = (V_{i-1} - V_i)*GL_{i-1,i}$

$IR = (V_{i+1} - V_i)*GR_{i,i+1}$

Is = synaptic current

$= (V_i + Vo)*Gs$

$= (V_i + Vr - U)*Gs$

Ip = Jp*2*pi*r*dx

rearranging gives

$$A_i*Cm*D_t V_i = -IM + IL + IR - Is - Ip$$

substituting, dividing by dx, and some rearranging gives

$$2*pi*r*Cm_i*D_t V_i = (V_{i+1} - 2V_i + V_{i-1})/(dx)^2]*(pi*r^2/AR) - (V_i + Vo)*(pi*2*r/Rm) - (V_i + Vo - Ena)*Gs/dx - Jp*2*pi*r$$

where

$$RL = AR*dx/pi*r^2$$

$$GL = 1/RL$$

$$A = pi*2*r*dx$$

$$Rm_i = 1/Gm_i$$

Multiplying through by Rm/(2*pi*r) gives

$$TD_t V_i = m^2*[(V_{i+1} - 2V_i + V_{i-1})/(dx)^2] - V_i - V_o - (Gs/dx)*(V_i + Vo - Ena)Rm/2*pi*r - J_p*Rm$$

where the time constant is T=Rm*Cm and the space constant is $m=(Rm*r/2*AR)^{1/2}$. Note that for an inactive synapse (Gs=0), the response voltage V_i is zero, thus

$$Vo + Jp*r*Rm/2 = 0$$

Letting dx go to zero and noting that Gs is really a function g(x,t) which is nonzero only at the synapse location, the result is

$$T*D_t V = M^2*D_{xx} V - V - D_x g(x,t)*[(V + Vo - Ena)*Rm/(2*pi*R)$$

Except for the synapse, this is what Hodgkin and Rushton (1946) used to describe the transient distribution of membrane potential along a cylindrical structure of passive nerve membrane. This was also used by Rall except for synapses.

6.3.6 IN SYSTEM FORM

6.3.6.1 THE EQUATIONS

To examine the properties of a dendrite as a system it is necessary to write the compartmental equations in matrix form. The general compartment equation is

$$D_t V_i = \frac{1}{A_i * C_i} \left| -Gm_i - \sum_{j \text{ in } B_i} GL_{ij} - GS(t) \right| * V_i$$

$$+ \left| \sum_{j \text{ in } B_i} (GL_{ij} * V_j) - GS(t) * (Vr - we - E_{Na}) - Gm_i * (Vr - we) + Ip \right|$$

Let

$$K_i(t) = \left| -Gm - \sum_{j \text{ in } B_i} GL_{ij} - GS(t) \right| * (1/A_i * C_i)$$

$$Vs = Vr - we - E_{Na}$$

$$G_{ij} = \frac{GL_{ij}}{A_i * C_i}$$

and recall that $Gm_i * (Vr - we) + Ip = 0$ at equilibrium with no synaptic input. Thus the equation for the general compartment becomes

$$D_t V_i = K_i(t) * V_i + \sum_{j \text{ in } B_i} G_{ij} * V_j - GS_i(t) * (Vs / A_i * C_i)$$

Thus

$$D_t \underline{V} = (\underline{M} - \underline{I} * \underline{S}) * \underline{V} - \underline{Vs} * \underline{S} = \underline{A}(t) * \underline{V}(t) - \underline{Vs} * S(t)$$

where

$$M_{ij} = \begin{cases} (-Gm_i - GL_{ij})/A_i*C_i & \text{if } i = j \\ G_{ij} & \text{if } i \neq j \end{cases}$$

$$S_i(t) = \begin{cases} GS_i(t)/(A_i*C_i) & \text{for synapse S on compartment i} \\ 0 & \text{for no synapse on compartment i} \end{cases}$$

and

$$\underline{A}(t) = \underline{M} - \underline{I}*\underline{S}(t)$$

$\underline{I}$ = the identity matrix

6.3.6.2 PROPERTIES

Noting that the synapse vector $\underline{S}$ has time varying elements, the system is linear with time varying coefficients, by definition. Although the function $GS_i(t)$ for synaptic conductance is a result of several hundred ionic pores opening and closing along with the release of quanta from the presynaptic region (Katz,1966,69), the time course of the conduction is continuous as the action of the pores is summed (Katz and Melidi, 1967). Consequently, the system matrix $\underline{A}(t)$ is continuous. It is also bounded as the conductances are the only nonconstants and they are bounded. It can be shown that the system is stable and bounded for

bounded input (Ch 8, D'Angelo, 1970). This is not suprising since the system originates from a type of partial differential equation which without the synapses is well known to be stable (Wiley, 1960).

Since Gm_i, GL_{ij}, A_i, and C_i are all positive nonzero, the diagonal terms of $\underline{A}(t)$ are strictly negative and the off diagonal terms are positive. There is a strictly dominant diagonal,

$$ABS(A_{ii}) > ROW_i = \sum_{j \neq i} ABS(A_{ij})$$

$$ABS(A_{ii}) > COL_j = \sum_{i \neq j} ABS(A_{ij})$$

and the column and row sums are nonpositive. Thus the eigenvalues are nonpositive reals, (Hearon, 1963).

6.3.6.3 SOLUTIONS

The solution to the partial differential equation in an analytical form is impossible because of the multiple synapses, irregular geometry, and the nonlinear time varying synaptic conductances. An analytical solution to the discretized form, the compartmental formulation, is impractical because of the time varying coefficients. To quote Zadeh and Desoer (1963,p377)

"... we have little to say about computational

techniques because, except for a few special cases of some practical interest, the only effective means for computing the responses of time-varying systems is the digital computer."

6.3.7 CONSTANTS

The value of axoplasmic resistivity is taken to be AR=60 ohm*cm and the membrane capacitance Cm, is taken as 1.33 micro farads per sq cm from crustacean nerve fiber (Hodgkin and Rushton, 1946). The dendrite resting potential is taken from the superior cervical ganglion because the ionic environment is similar to that of the cochlear dendrites, Vr=-68.8 mv (Woodward, Bianchi, and Erulkar, 1969). The potential of the fluid surrrounding the dendrites is the fluid in scala media, We=7 mv (Weiss, Peake, and Sohmer, 1969).

Membrane conductance is the inverse of membrane resistivity for which there is a range of values in the literature. The value of 1000 ohm*sqcm is given for the giant squid axon (Cole and Hodgkin, 1939; Cole and Baker, 1941a,b). Using dye injected motoneurons, Barrett and Crill (1974) give the range as 1777 to 2520 ohm*sqcm.

Rall (1959) analyzed whole neuron resistance R_N as seen by an electrode inserted in the soma. Based on matching physiologically obtained whole neuron resistances with

anatomical measurements and a derived formula for the ratio of R_N and R_m, he found that for R_m=4000 ohm*sqcm, the whole neuron resistances were best matched. This value seems to be under emphasized in the literature. This value is used for the dendritic membrane. Thus the time constant $\tau = R_m * C_m$ has the value of 5.33 millisec.

The space constant $m=(Rm*r/2*AR)^{1/2}$ is dependent on membrane resistivity and radius r of the dendrite. A plot of the space constant of resistivity is shown in figure:6.3.7. Notice that the value falls off sharply with decreasing diameter. For a dendrite diameter of 1 micron, the space constant is 1.44 microns, when membrane resistivity R_m=500 ohm*sqcm, compared with the value 408 mu when R_m=4000 ohm*sqcm. This is significant when the length of the inner dendrite is 30 microns as compared with 985 mu for the outer dendrites.

The core conductance for a piece of dendrite is the conductance from the j-th to the i-th compartment. Let AR be the specific resistivity of the intracellular medium (ohm*cm). The resistance per unit length for a circular cylinder with radius r is

$$AR/pi*r^2 \quad \text{(ohm/cm)}$$

The conductance for a cylinder of radius r and length dx is

$$g = pi*r^2/AR*dx \quad \text{(mho)}$$

The length dx is taken as the distance between centers of the compartments, thus for adjacent compartments with the same radii and centers dx apart

$$g_{ij} = pi*r^2/AR*dx$$

For dendrite diameter of one micron and typical simulation length of compartments 1, 2.5, and 10 microns, values of g_{ij} are 13.1, 5.24, 1.31 $*10^{-11}$ mho respectively, which correspond to 7.64, 19.1, and 7.64 $*10^{9}$ ohms in resistance. So for a potential drop of a millivolt from one compartment to the next separated by 2.5 microns, the current is $5.24*10^{-14}$ amps.

For adjacent compartments of length dx_i, dx_j, and radii r_i, r_j, respectively, the conductance used is the inverse of the sum of the one-half resistances contributed by each compartment, thus

$$G_{ij} = \left[\frac{pi*(r_i)^2}{2*AR*dx_i} + \frac{pi*(r_j)^2}{2*AR*dx_j} \right]^{-1}$$

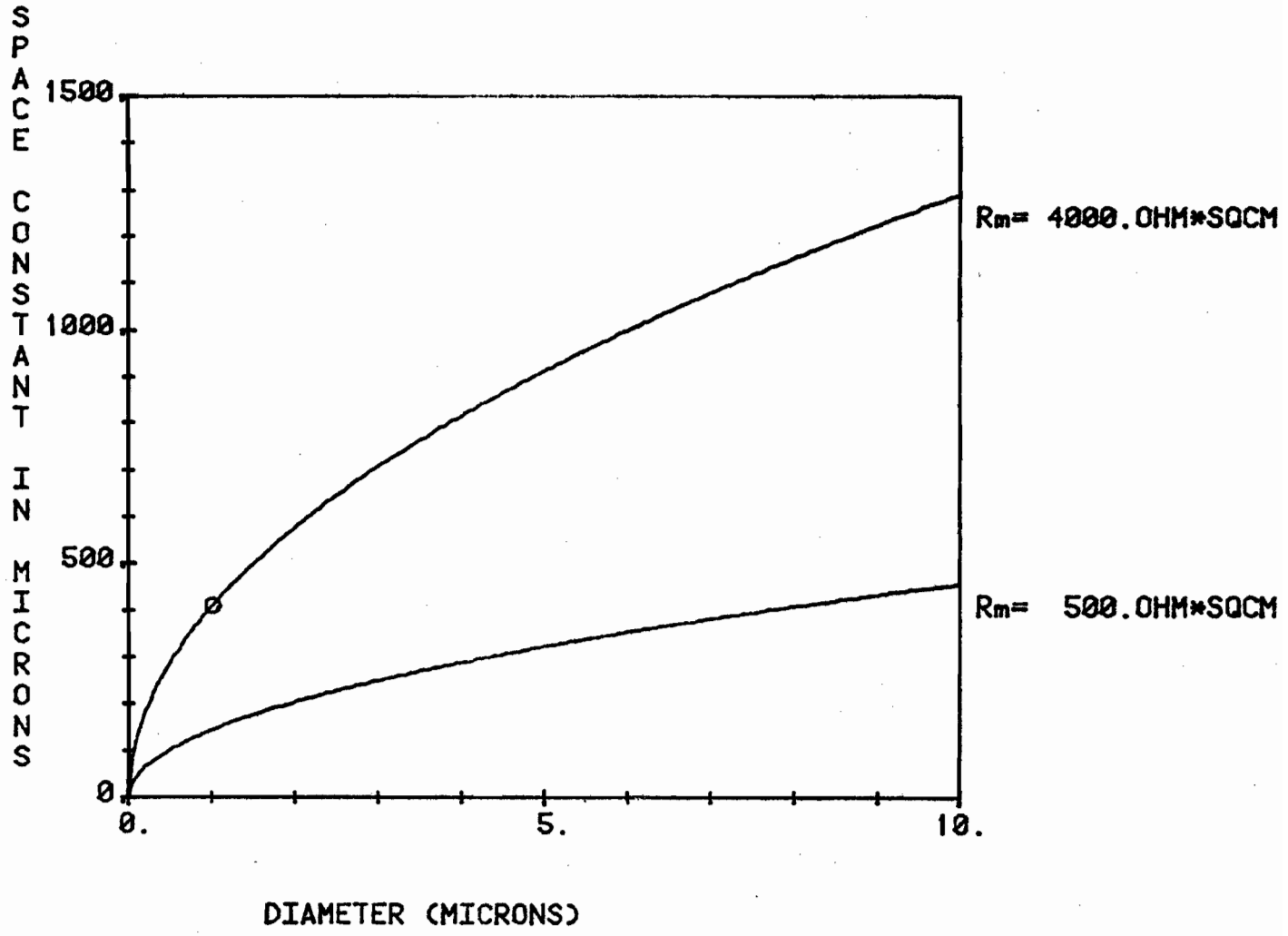

Figure:**6.3.1** Dendrite space constant $m = [(R_m * r)/(2*AR)]^{1/2}$ $= 204 * r^{1/2}$ versus diameter.

6.4 SIMULATION METHODS

6.4.1 REQUIREMENTS

The requirements for the simulation of the dendrites turn out to be rather stringent, if the results are to be of any use. Starting at the begining, the normal physiological input signal at synapses is a time varying signal which is not in any way a constant or a sine wave. This means that the simulation must be a dynamic as opposed to a steady state simulation or solution.

The simulation must allow for multiple synapses and different signal inputs to be able to mimic the real thing. This is also necessary to investigate the response to different inputs.

The simulation must allow for easy alteration of constants. This is to allow the usual adjustment of constants to ascertain their importance.

The simulation program must run in a reasonable length of time.

Compartment voltages versus location for each time step of the input signals at the synapses, must be obtainable. This is necessary to plot the simulation results versus time.

The constants must be input in a physiological form. The same applies to the dendrite geometries to which the

simulation is applied.

The absolute accuracy must be in the order of 0.0001 volts, because the dendrite voltages are typically in millivolts. The relative accuracy should be at least 99 % to give the simulation validity. With respect to the numerical stability of the numerical solution, the absolute and relative accuracies must be much better than these numbers. More will be said about this in the integration methods.

The simulation program must fit into 32,736 = 32K - 32 computer words of memory. This is the size of program which the Digital Equipment Corporation's PDP 11-70 computer with the RSX 11M operating system allows (RSX-11M Task Builder Reference Manual, 1978). For programs of memory size requirement greater than 32K, an overlay structure is used. When overlays are used, the running time is increased by the time spent in transferring subprograms between memory and disk. For many time steps or small delta t (about 10^{-14} sec) this is a heavy requirement when it comes to wanting reasonable length runs of a program. It is, therefore, a stringent requirement for the simulation program.

The variables in the simulation should be in double precision to increase the accuracy of the simulation. Double precision on the PDP 11-70 with the FORTRAN compiler

requires four computer words of memory per variable. To simulate a cochlear outer dendrite and dendrites in general it is required to have in the order of say one hundred compartments. Each one compartment requires the variables: voltage, derivative of voltage, longitudinal conductance, etc. Concomitant with the compartmental variables, work space is required by the integration routine. As a result, usage of computer memory becomes large. So variables for the compartments must be used efficiently.

Using direct numerical integration methods, the simulation equations are solved for the derivatives of the state variables, the compartment voltages in this case. From examination of the equation for the general compartment, it is clear that different size compartments will have different values for their membrane capacitance ($A_i * C_i$) and longitudinal conductance (GL_{ij}=pi*r*r/AR*dx). As a result the derivative magnitude will different greatly for different size compartments, especially since the length of the compartments can differ by almost two magnitudes due to the branch pieces compared to the long pieces of dendrite. Thus the system Jacobian

$$J_{ij} = D_{V_j} (D_t V_i)$$

can have elements that differ greatly in magnitude and pose a stability problem (Houwen,1971b). The simulation method

must take this into account.

One could scale time and reduce the spectral radius by scaling constants; however, this causes a proportional increase in the number of time steps needed to compute the integrals over an actual interval of time. So in the simulation, it is better if variables are left unscaled, because there is no net saving in the number of time steps required.

6.4.2 FORMULATIONS

6.4.2.1 COMPARTMENTAL FORMULATION

The compartmental formulation is the one presented previously when describing the general compartment. The dendrite is divided into compartments and the equation for that compartment is the dynamic equilibrium condition for the currents in and out of the compartment including synapses, if there are any on that compartment. With the dendrite divided into compartments, it is then described by a system of differential equations. Each of the equations is solved for its time derivative, giving a system formulation with compartmental voltages as the state variables. At each time step the derivative is evaluated by a direct numerical technique, about which more will be said under integration methods. The new values for the state variables are then inserted into the equations, evaluating the derivatives, etc.

If the compartment formulation is done naively, it consumes a large amount of computer memory, as is done in most compartment simulations. Usually constants are assigned to each compartment and the equation set up for each compartment. The constants and variables for each compartment constitute a large memory requirement. This is the way standard compartment simulations are done.

The solution to reducing the memory requirement is to classify the compartments by type, based on length, diameter, membrane conductance per unit area, membrane capacitance per unit area, and whether it is a simple compartment connected to two neighboring compartments or is a branching compartment connected to three or more neighboring compartments. Thus for each compartment, only the following variables are required: voltage, time derivative of voltage, type, number of the compartments to which it is connected, and number of the synapse if there is one that innervates the compartment. This scheme provides the minimal choice of variables possible for the simulation using the compartmental formulation.

The success of the method is then linked to the integration method used. This depends on the accuracy and stability of the method along with the running time of the program.

6.4.2.2 FINITE DIFFERENCE METHODS

A finite difference method starts with the partial differential equation and converts it into a discrete form by evaluation of the equation at each point in space and time, marching out the solution in time. In the dendrite case, the spatial coordinate is distance along the dendrite.

Finite difference methods have been used for partial differential equations for some time. A good description is found in Smith (1969).

The dendrite equation without synapses is of the parabolic type of partial differential equation and what follows is adapted from Smith (1969). To calculate the values of a parabolic PDE the spatial variables are covered by a regular mesh. The equation is evaluated for each grid point. The derivatives are replaced by forward difference expressions in the explicit methods. For convergence it is necessary that

$$[(dt/\tau)/(dx/lambda)] < 1/2$$

where τ is the time constant and lambda is the space constant. For a dendrite with τ = 0.65 msec., lambda = 144.3 microns, and dx in the order of 1 micron at the smallest part of the dendrite, this means that the time step must be $dt < 10.0^{-8}$ sec. This is irrespective of the rate of change of the synaptic conductances which also determines the allowable time step.

The Crank-Nicolson implicit method replaces the second spatial derivative by the mean of the difference approximations at the t and t+dt time steps, then solves for the value of the dependent variable at t+dt. The time step allowable is smaller but still in the same order of

magnitude.

The weighted average of the second spatial derivative difference approximations at the t and t+dt time steps along with a fully implicit backward time difference method can be unconditionally valid (stable and convergent), but accuracy is reduced.

The problem with finite difference methods is that putting in branching compartments is somewhat clumsy, particularly for the implicit methods. Also changing the geometry of the dendrites necessitates rearranging the computational scheme each time. These methods are more readily applicable to static regular unbranched geometries. A further problem is that in these methods it is not obvious what the time step should be for time varying boundary coefficients as is the case for the terms involving a synapse.

The standard improvements of the finite difference method, the iterative point methods such as the Jacobi and Gauss-Seidel method, successive over-relaxation, or extrapolated Liebmann do not solve the problems which pertain to the dendrite equation simulation.

6.4.2.3 FINITE ELEMENT METHOD

The finite element method has its origin in structural and continuum mechanics problems. For a treatment of its application to those areas, the reader is referred to Zienkiewicz (1967). For those applications it is usually sufficient to have a steady state static solution, so dynamic solutions using the finite element method are normally ignored. A quite understandable treatment of the finite element method, which is not embedded in the usual structural mechanics, and which discusses dynamic solutions is found in Myers (1971). The method is applied to the dendrite problem, noting that dendrites appear as line segments, not planar regions.

Given a partial differential equation with driving function D(x,t)

$$\sum_{n=0}^{N} A_n * \frac{D^n U}{Dx^n} + \sum_{m=0}^{N} B_m * \frac{D^m U}{Dt^m} + D(x,t) = 0$$

It can be shown (Myers,1971; Weinstock,1952) that for a functional

$F(x,t,u(x,t),u'(x,t),...)$ where $u' = du/dx$

such that the Euler Lagrange equation is satisfied

$$D_u F - D_u (D_{u'} F) = 0$$

and is equivalent to the original partial differential equation, then the function u(x,t) which minimizes the integral

$$I = \int_{x \text{ in } R} F(x,t,u(x,t),u'(x,t),...)dx$$

is a solution of the original partial differential equation on the region R. The region R is the dendrite.

Now the method becomes:

(1) Find the functional F by rearranging the orginal PDE to have the form of the Euler Lagrange equation

(2) Find the expression for the integral I

(3) Divide the region of interest R into subregions

For dendrites, R_i is a compartment's length interval

$$R = \bigcup_{i=1}^{N} R_i$$

(4) Rewrite the integral as a sum of integrals on the subregions (finite elements)

$$I = \sum_{i=1}^{N} \int_{x \text{ in } R_i} F(x,t,u(x,t),u'(x,t),...)dx$$

(5) Given values of u on the boundary of the subregions R_i (elements) approximate u(x,t) on each element R_i by some approximating function f_i. For a dendrite, the boundary of an element R_i is its set of end points $\{x_{i,1}, x_{i,2}\}$. For a "1" or "Y" junction, the boundary is $\{x_{i,1}, x_{i,2}, x_{i,3}\}$.

$$u(x,t) = f_i(X_{i,1}, X_{i,2}, \ldots, X_{i,N}) \qquad x \text{ in } R_i$$

on the regions

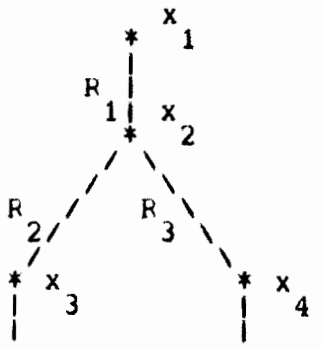

(6) Evaluate the subintegrals using the approximating functions for u(x,t) on each of the subregions.

(7) Obtain the integral

$$I = \sum_{i=1}^{N} \int_{x \text{ in } R_i} F\,dx$$

where F on each R_i is computed using the f_i's

(8) To minimize I by setting

$$\frac{d}{dU} \underline{I} = \underline{0}$$

where the differentiation is with respect to the nodal values,

$$\underline{U} = (U_1, U_2, \ldots, U_N)$$

(9) Thus it only remains to solve for $\underline{U}$, the values at the nodes at each moment in time. Since the equation in step 8 is a big matrix equation, the solution is typically done using Gaussian elimination with or without refinement of the solution.

The power of the finite element method is based on two major points. First, it can specifically cope with irregular geometries, via the region R_i, i=1,2,...,N assignment. This is done by first specifying the nodal points x_i; i=1,2,...,N, in and on the border of spatial region of interest R. Then the elements (subregions) are specified by designating which nodal points constitute their polygonal boundaries. For a two dimensional region, typically triangular elements are used. For a dendrite, an element is a line segment.

Secondly, the method of approximating a time derivative is usually algebraic, in that one replaces the time derivative of each U_i by a difference approximation, then solve for the U_i's. This eliminates the need for a direct

integration subprogram, but then a big matrix must be solved at each time step.

A finite element formulation was actually done for dendrites and I found that the final integral minimizing equation of step 8 took the form

$$\underline{I} = \underline{C}*\dot{\underline{V}} + \underline{H}*\underline{V} + \underline{K}*\underline{V} + \underline{Hs}*\underline{V} = \underline{0}$$

where vector $\underline{V}$ contains the voltages at the nodal points. In the case of the dendrites, the nodal points are the end points of the intervals (elements) along the dendrites. $\underline{C}$ is the global capacitance matrix, $\underline{H}$ is the global membrane conduction matrix, $\underline{K}$ is the global longitudinal conductance matrix, and $\underline{Hs}$ is the global synaptic conductance matrix. Thus at each time step the following equation must be solved.

$$\underline{C}*\dot{\underline{V}} = -(\underline{H} + \underline{K} + \underline{Hs})*\underline{V}$$

Since the conductances at the synapses vary with time and are the driving functions to the system, the matrix $(-\underline{H} - \underline{K} - \underline{Hs})$ must be altered at each time step because the values of $\underline{Hs}$ change. In finite element lingo this is called a partial reassembly of the global system matrix.

The matrices $\underline{C}$, $\underline{H}$, and $\underline{K}$ are sparse with a band width of three, except for the terms off the main diagonal which are due to the branching geometry of the dendrite. The matrix $\underline{Hs}$ is also sparse. Unless special subprograms are

developed to manipulate these irregularly sparse matrices, they consume a large amount of computer memory. For say one hundred elements this means that a 100X100 matrix is required. A 10,000 real variable array is definitely out of the question for a 32K program. I actually wrote a finite element program with the matrix as a random access unformatted disk file, but the program ran too slowly to be practical. To change geometries, a new scheme, hence subprograms would be necessary to handle the sparse matrices, if they were to reside in main memory. Clearly, the finite element method for simulating dendrites is only practical for a computer with a very large amount of available memory. Also it is impossible to use larger dendrites, which is necessary for further applications.

6.4.3 INTEGRATION METHODS

6.4.3.0 INTRODUCTION

An overall survey of numerical integration methods is given by Parlette (1978). Detailed discussion of integrations routines is found in Carnahan, Luther and Wilkes (1969). Running time evaluations can be found in Hull, Enright, Fellen and Sedgwick (1972). An evaluation of the numerical methods considered is given.

6.4.3.1 FLAP

One of the simplest time simulation systems to use is FLAP, developed by Elliot (1972). It is a skeletal program that provides the framework for a dynamic simulation. The available subroutines contain time delays, saturation elements, hysteresis elements, and integration operators. The integration subroutine uses a predictor-corrector scheme with iterations.

It is unsuitable for the dendrite simulation for the following reasons. There is no accuracy or stability error checking. This is important in large systems of equations because the elements of the Jacobian can have large differences in their values. To increase the accuracy of the solution, the time step is reduced or the number of iterations per time step is increased. This means that the run time of the program increases as a product of the time steps and iterations, rather than linearly as the number of time steps increase. The requirement for five times the number of equations and variables as work space significantly limits the size of the system to which FLAP is applicable.

6.4.3.2 ADAMS-PECE DE

Shampine and Gordon (1975) describe the Adams-Pece differential equation subprogram which is very fast. It is an adaptive method which works by either interpolating or integrating between points in time according to the accuracy tolerance specified upon initialization. The major problem with this algorithm is that it requires 124+(21*NEQS) words of memory where NEQS is number of equations. This is obviously out of the question for simulation of partial differential equations for more than a few spatial locations.

6.4.3.3 GEER'S METHOD

Geer's method (Geer, 1971a,71b) as found in the IMSL (1975) collection of numerical programs is an adaptive method for stiff differential equations. Stiff differential equations have eigenvalues with a negative real part and are located in widely separated clusters in the complex plane (Houwen,1971b). Numerical integration methods which work on stiff systems also work on systems whose Jacobian matrix contains elements with greatly different magnitudes, as arise from partial differential equations (Houwen,1971a,b). The problem with this method is that it requires a work area of dimension NEQS*(NEQS+17). This memory requirement makes

the method untenable for the dendrite equations.

6.4.3.4 INDIRECT METHODS

Indirect methods are presented to make the survey complete. The idea is to solve the state-variable equations for the first derivatives and substitute a finite difference approximation, then solve for the value of the variable at the next time step. For systems of equations with a Jacobian that has widely varying magnitudes of the elements, this scheme is not really practical because there is no ready way to implement accuracy and stability checks using the value of the derivatives. In addition, a change of the geometry of a dendrite for a simulation requires reprogramming.

6.4.3.5 WYNN-LAU-HOUWEN ARK

6.4.3.5.1 INTRODUCTION

This method is a stabilized adaptive Runge-Kutta method with limited storage requirements for the integration of very large sets of differential equations such as those originating from partial differential equations. Although methods for integrating stiff systems of ordinary differential equations (Liniger,1970) and methods with

extended stability regions (Lawson,1966) have appeared in the differential equation literature, these methods are not suitable for partial differential equations for they are not designed with limited storage as a criterion.

Houwen(1971b) surveys the stabilized Runge-Kutta methods. The majority of literature on the Runge-Kutta methods is devoted to increasing the order of accuracy, while relatively little attention is devoted to improving the stability of these methods. When standard Runge-Kutta methods are applied to stiff equations or partial differential equations, it is the severe stability conditions which make them unattractive to be used for numerical integration in these problems.

6.4.3.5.2 STABILIZED RUNGE-KUTTA FORMULAE

Say it is required to find the numerical solution of the set of simultaneous first-order differential equations

$$\frac{d\underline{y}}{dt} = \underline{f}(x,\underline{y}(x))$$

with the initial condition $\underline{y}(x_0) = \underline{y}0$.

Following Wynn (1978), consider the N-th order Runge-Kutta scheme

$$\underline{y}^{(n+1)} = \underline{y}^{(n)} + \sum_{j=0}^{N-1} \theta_j \underline{k}^{(j)}$$

$$\underline{k}^{(j)} = h_n * \underline{f}(x_n + M_j h_n, \underline{y}^{(n)} + \sum_{e=0}^{j-1} L_{j,e} * \underline{k}^{(e)})$$

for $j = 1,2,\ldots,N-1$

where $h_n = x_{n+1} - x_n$ and $\underline{y}^{(n)} = \underline{y}(x_n)$

It is assumed that $\underline{f}$ is a suitable differentiable function. For the dendrite discretized partial differential equation $\underline{f}$ is a function with all its derivatives existant and continuous. Thus $\underline{y}^{(n+1)}$ may be expressed as the sum of a power series in the variable h_n, with coefficients involving the derivates $\underline{y}^{(n)}$.

$$\underline{y}^{(n+1)} = \underline{y}^{(n)} + b_1 D \underline{y}^{(n)} h_n + b_2 D^2 \underline{y}^{(n)} h_n$$

$$+ b_3 D^3 y^{(n)} h_n^3 + 0.5 * b_{3,1} [D^3 y^{(n)} - \underline{J}^{(n)} D^2 y^{(n)}] * h_n^3 + \ldots$$

where D is the derivative with respect to x and $\underline{J}^{(n)}$ is the system Jacobian at the n-th time step whose elements are the i,j-th partial derivatives

$$\frac{D f_i(x_n, \underline{y}^{(n)}(x))}{D y_j^{(n)}(x)} \quad ; \quad i,j = 1,2,3,\ldots,N$$

Expanding each of the $\underline{k}^{(j)}$ in the previous equation for $\underline{y}^{(n+1)}$ in ascending powers of h_n, it is found that the $\underline{B}$, $\underline{M}$, and $\underline{L}$ of the previous equation and the b's of the latter

equation are related as follows:

$$b_1 = \sum_{j=0}^{N-1} \theta_j$$

$$b_2 = \sum_{j=1}^{N-1} \theta_j M_j$$

$$b_3 = \sum_{j=2}^{N-1} \theta_j \sum_{e=1}^{j-1} L_{j,e} M_e$$

$$b_{3,1} = \sum_{j=1}^{N-1} \theta_j M_j^2$$

$$b_4 = \sum_{j=3}^{N-1} \theta_j \sum_{e=2}^{j-1} L_{j,e} \sum_{i=1}^{e-1} L_{e,i} M_i$$

$$b_{4,1} = \sum_{j=1}^{N-1} \theta_j \sum_{e=1}^{j-1} L_{j,e} M_e^2$$

$$b_{4,2} = \sum_{j=2}^{N-1} \theta_j M_j \sum_{e=1}^{j-1} L_{j,e} M_e$$

$$b_{4,3} = \sum_{j=1}^{N-1} \theta_j M_j^2$$

Now by imposing conditions on the b's, thus θ, M, and

L are found. One such condition comes from the agreement between the Runge-Kutta expression and Taylor series expansion of $\underline{y}(x_n + h_n)$ in ascending powers of h_n, given that $\underline{y}$ satisfies the original set of equations. When the agreement continues up to and including the term for $(h_n)^r$, the scheme is said to r-th order exact.

Accordingly, the b's have the following values

r	b_1	b_2	b_3	$b_{3,1}$	b_4	$b_{4,1}$	$b_{4,2}$	$b_{4,3}$
1	1							
2	1	1/2						
3	1	1/2	1/6	1/3				
4	1	1/2	1/6	1/3	1/24	1/12	1/8	1/4

A second condition is for stability. Let $\underline{\hat{y}}^{(n+1)}$ be the vector produced by the Runge-Kutta scheme from the vector $\underline{\hat{y}}^{(n)}$ and likewise

$$\underline{\hat{y}}(n+1) \quad \text{from} \quad \underline{\hat{y}}(n)$$

where the error

$$\underline{e}^{(n)} = \underline{\hat{y}}^{(n)} - \underline{\hat{y}}^{(n)}$$

is small. Then

$$\underline{\hat{y}}^{(n+1)} - \underline{\hat{y}}^{(n+1)} = P_N(h_n \underline{J}^{(n)})*\underline{e}^{(n)} + \mathcal{O}(\underline{e}^{(n)})^2$$

as $e^{(n)} \to 0$, where

$$P_N = 1 + B_1 z + B_2 z + \ldots + B_N z^N .$$

The scheme is stable if $|P_N(h_n d)| \leq 1$ for all eigenvalues d of $\underline{J}^{(n)}$ in the closed left half-plane $\mathrm{Re}(d) \leq 0$.

If all the deltas are very small, then a relatively large step size h_n is possible without violating the above

stability condition. For this type of differential equation, it is possible to choose the b's and, by implication, the $\underline{B}$, $\underline{M}$, and $\underline{L}$ to ensure the r-th order exactness for the highest possible value of r. When the deltas are not all small, which occurs for stiff equations and many systems arising from the numerical solution of partial differential equations, it is better to sacrifice a certain degree of exactness in lieu of stability. The solution is to work with a stability polynomial whose first few coefficients B_i are fixed, ensuring a certain degree of exactness, and determine the remaining coefficients B_i in such a way that the stability condition $|P_N(h_n d)| \leq 1$ is satisfied for the largest possible step size h_n.

Using the spectral radius $d(\underline{J})$ of $\underline{J}(x)$ with respect to its eigenvalues in the closed left half-plane, stability polynomials $P_n(z)$ are constructed such that the associated Runge-Kutta scheme is stable if the step size in $\underline{x}$, h, satisfies the inequality

$$H \leq B(n)/d(\underline{J}).$$

B(n) is a constant associated with the polynomial $P_n(z)$ in question. In each case $P_n(z)$ has been determined so that B(n) assumes its maximum value. Such polynomials $P_n(z)$ and associated constants B(n), together with the types of equations (i.e., those for which the eigenvalues in the

closed left half-plane $Re(\sigma) \leq 0$ of the associated Jacobian matrix $J(x)$ are all pure real or all pure imaginary) to which they refer, and the order r of exactness of the polynomial in question are presented in the following table.

n	B_1	B_2	B_3	B_4	B_5	B(n)	type	r
3	1	1/2	1/4			2	imag	2
4	1	1/2	1/6	1/24		$2^{3/2}$	imag	3
4	1	5/32	1/128	1/8192		32	real	1
4	1	1/2	.078	.0036		12	real	2
4	1	1/2	1/6	.0185		6	real	2
5	1	1/2	3/16	1/32	1/128	4	imag	2

6.4.3.5.3 ARK

6.4.3.5.3.1 REMARKS

The subroutine ARK is the adaptive Runge-Kutta method which utilizes the algorithm decribed in the preceding section. In programming, the emphasis is on limited storage requirements. It requires 4961+(2*NEQS*4) computer words of storage when compiled with DEC's FORTRAN IV+ compiler which optimizes for speed and storage, where NEQS is the number of equations and the 4 is for four computer words per double precison real number. Considering that the subprogram uses double precision, this is a remarkably low amount of memory

required.

6.4.3.5.3.2 HISTORY

The original routine was written in ALGOL by Houwen (1971a). It was later translated into FORTRAN by Wynn and Lau (1978). With some improvements, that is the version I used in the simulation. The improvements make initialization easier and deal with overflows in debugging.

6.4.3.5.3.3 USAGE OF ARK

The subprogram is called by the following statement.

CALL ARK(T,TE,N1,NL,Y,DERIVA,DATA,OUT)

The integration is to be done over the interval T to TE, N1 is the first derivative to be integrated and NL is the last, Y is the name of the array containing the derivatives, DERIVA is the name of the logical function subprogram which evaluates the derivatives, DATA is a utility data array, and OUT is the name of a logical function subprogram which is called at the end of each integration step as a monitoring device and in which the step size is changed if needed.

The user provides in the array DATA(I), I=1,2,3,4 the values of n, r, B(n), and an upper bound for the spectral radius which holds for the interval of integration [T,TE]. The minimum step size used by ARK when integrating over the

interval [T,TE] is specified by the user in DATA(5). The absolute and relative tolerances permissable are provided in DATA(6) and DATA(7). If the tolerances are both negative, then ARK integrates with constant step size equal to the minimum step size, rather than reducing it as required by stability analysis.

The number of integration steps performed is returned in DATA(8), which should be set to zero prior to the first call and not changed for further intervals.

6.5 DENDRITE SIMULATION

6.5.1 THE METHOD OF CHOICE

The method of choice is the compartmental formulation with a direct integration technique.

The most influential requirement in choosing the compartment formulation is the need to handle large variations in dendritic shape with different parameters and whatever branching topology the dendrite posseses. The finite element method also fulfills this criterion; but it is eliminated on the basis of the undue amount of memory required and the fact that it has a lot of computational overhead.

The only available integration technique that allows for large variation in elements of the system Jacobian,

which is designed for minimal storage, is the Wynn-Lau-Houwen stabilized adaptive Runge-Kutta technique. Using a direct integration method has the advantage that the dendrite geometry is changable without changing the simulation equations and subsequent program code. That is because the simulation program which uses compartments sees the branching geometry in the form of compartment connection vectors.

A large number of compartments are necessary for the cochlear outer dendrite because there are short branches between the main dendrite and the hair cell synapses. The distance between the branching junctions is small compared to the long portion of the dendrite. Thus, it is a problem of scale in the choice of dendrite compartment size. To obtain an accurate numerical solution, the discretization of the length coordinate is to be at least as small as the length of the branch segments between connections. The long unbranched segments can be discretized with long compartments, to reduce the number of compartments. Thus, to preserve the geometry accurately and not have a very large number of compartments, it is necessary to have compartments of greatly different sizes. This difference in sizes causes greatly different time constants in the system of compartmental equations. Furthermore, the dendrite is

connected to the AP generating site and the axon is treated as neural membrane but with different membrane resistance and capacitance. Again this leads to compartment equations with different time constants. Therefore the large number of compartments is necessary in this analysis.

The simulation program ARKDEN is described below since no available general compartment program is suitable for the simulation with large numbers of compartments and greatly different magnitude of elements in the system Jacobian.

6.5.2 ARKDEN

6.5.2.1 ORGANIZATION

The simulation program is called ARKDEN for adaptive Runge-Kutta dendrite. The program is designed to allow for different dendrite topologies and parameters.

First, in the main program the standard simulation parameters are initialized. The parameters specific to the particular run are read in from a disk file to facilitate changes in them. These parameters are the simulation time interval TMAX, delta t DELT, synaptic signal parameters Ton, Toff, Tduration, Trise, and maximum synaptic conductance SYNSCL. The second of the two input files is a file containing a description of the particular dendrite to be simulated. It consists of two parts: (1)the compartment type parameters and (2)the compartment list with type, connections, and synapse number.

As part of the memory conservation drive, the compartments are classified as to type; then when a compartment parameter is needed it is accessed according to type. This scheme reduces the compartment variables required by a factor of five.

The synapse delays, compartment voltages, and program statistics are initialized. A call is made to ARKINT which

initializes the integration subprogram ARK by setting up the spectral radius, the degree of exactness, the minimum step size used in the integration from T to T+DELT and some other book keeping parameters.

In the main time loop a call is made to ARK, passing: the compartment voltages, time, book keeping parameters, the subprogram name ARKDRV which evaluates the derivatives when called by ARK, and the subprogram ARKOUT which changes the minimum step size if needed. The only other thing which the main time loop in the main program does is to save the synapse conductances and compartment voltages per time step for specialized plotting. A complete space-time response of the dendrite in its entirety can be obtained as the program runs if the user wishes.

When the program passes through each time step as called from the main, the statistics (number of derivative evaluations and integrations steps performed in integrating from T to T+DELT) and any errors encountered are reported. Due to the way the simulation program is organized in conjunction with the integration subprogram ARK, much of the work is done in the subroutines called by ARK. The major subprograms are described below.

6.5.2.2 MAJOR SUBPROGRAMS

6.5.2.2.1 DENPRP

The subroutine DENPRP reads in the dendrite compartment type parameters and dendrite branching topology. The file containing the dendrite specifications has in its first part, one line per compartment type. Each line gives the type IT, conductance per unit area GMA (mho/sq.micron), capacitance CPA (F/sq.micron), diameter DIAM (microns), and compartment length RLEN (microns). A compartment type of zero, IT=0, designates that there are no more types. After the parameters are read in for each type of compartment, the following new parameters are calculated: the longitudinal resistance of half the compartment

RESHLF(IT) = 0.5*AR*RLEN/(PI*(R**2))

the membrane area AREA = PI*DIAM*RLEN. If the type IT=1, that of an end compartment with a synapse, then the area is halved because it is connected only to one other compartment. If the type IT=3, that of a compartment connected to three other compartments, then the area is multiplied by 1.5 since it has a symmetric "T" shape. The compartment membrane conductance is then GM(IT)=AREA*GMA, and the compartment membrane capacitance is AC(IT)=AREA*CPA.

The second part of the dendrite specification file has

one line per compartment. These lines contain IC, IT, IC1, IC2, IC3, IS, where IC is the compartment number and IT is the type. The connecting compartments to IC are IC1, IC2, and IC3. IS is the number of the synapse connected to the compartment. If IT=1, an end synaptic compartment, then IC2=IC3=0. If IT=2, a typical compartment connected to only two others without synapse, then IC3=0 and IS=0. If IT=10, a termination compartment in the connecting axon, then IC2=IC3=IS=0. The end of the compartments is designated by the last line containing IC=0.

6.5.2.2.2 DENPRM

This subroutine reads in the simulation parameters particular to a specitic simulation run. The parameters read in and passed to the main are: Vr, the dendrite internal resting voltage; we, the external potential; Ena, the equilibrium or driving potential for sodium used at the synapses; F, the frequency of occurrence of the synaptic pulses; TMAX the simulation time interval; DELT, the time step for evaluation of the compartment voltages; TON, the on time for one synaptic pulse; TDUR, the duration of synaptic pulse; TRISE, the rise time for synaptic pulse; TDELAY, the delay time for the synaptic pulses; and SYNSCL, the maximum synaptic conductance value.

6.5.2.2.3 ISYN

This function subprogram finds, in a data table, which synapse is connected to which compartment. It is entered with IC the compartment number and returns the synapse number ISYN.

6.5.2.2.4 GSYNFN

This function subprogram evaluates the synaptic conductance signal for the IS-th synapse at time T. It looks up the delay for the IS-th synapse and shifts time by this amount. The value returned is

GSYN = SYNSCL*WINDOW(IS,TON,TOF,TRISE)

where IS is the shifted time. WINDOW is a continuous pulse with all derivatives continuous. The arguments are: onset time TON, off time TOF, with rise and fall time TRISE.

6.5.2.2.5 ARKOUT

This subprogram changes the minimum time step used by ARK to integrate from T to T+DELT. The minimum time step is reduced by the factor REDUCE, typically 0.1. When it is reduced, a message is printed on the terminal or output file, specified by LUNOUT.

6.5.2.2.6 ARKDRV

This subprogram is a logical function subprogram. It enters with the compartment voltages in the array V, transfers them to the array VP, and returns with dV/dt in the array V. For successful evaluation of the derivatives ARKDRV returns the value true, otherwise it is false.

For each compartment IC, it evaluates the type IT=TYPE(IC), then goes to the appropriate section of code to compute dVi/dt for i=IC. For each of the compartments connected to IC, ITL=TYPE(ICON(IC,i)), which is the type of the i-th neighboring compartment connected to the IC-compartment, is evaluated. The conductance from the IC-th to the ICON(IC,j)-th compartment is

$$GL(j) = 1.0/[RESHLF(IT) + RESHLF(ITL)]$$

where RESHLF(IT) is half the longitudinal resistance for the compartment of the IT-th type. It then evaluates the total input current for the compartment.

$$CURR = -GM(IT) - \left[\sum_{J=1}^{NIC} GL(J)\right] - GS*VP(IC)$$

$$+\left[\sum_{J=1}^{NIC} GL(J)*VP(ICON(IC,I))\right] - GS*(VRMWE-Ena)$$

where GS=GSYNFN(T,IS) and NIC is the number of compartments

connected to the IC-th compartment. Then the derivative is evaluated as

$$D_t V_i = \begin{cases} CURR/AC(IT), & \text{if } ABS(CURR) \le (1.0E+36)*AC(IT) \\ 0.0, & \text{if } ABS(CURR) \le (1.0E-36)*AC(IT) \\ 1.0E+36, & \text{if } ABS(CURR) > (1.0E+36)*AC(IT) \end{cases}$$

6.5.3 SPECTRAL RADIUS AND TIME STEP SIZE

It can be shown for the adaptive Runge-Kutta method employed in this simulation that the integration scheme is stable if the time step size $dt<[B(n)/s(\underline{J})]$, where $s(\underline{J})$ is the spectral radius and B(n) is a constant associated with the stability polynomial and degree of exactness (Wynn,1978). Since the system of equations obtained from the discretized partial differential equation in compartment form has real eigenvalues, as previously shown, B(n) has values 32,12,6, respectively, for degree of exactness 1,2,3. The spectral radius $s(\underline{J})$ is the L_1 norm of the system Jacobian $\underline{J}$.

$$s(\underline{J}) = \sum_{i=1}^{N} \sum_{j=1}^{N} |J_{ij}|$$

Given the system of differential equations

$$D_t V_i = F_i(t,V(t),GS(t)) \; ; \quad i=1,2,\ldots,N$$

the system Jacobian is the matrix $\underline{J} = [J_{ij}]$, where

$$J_{ij} = \frac{\partial}{\partial V_j} F_i$$

For the dendrite system of equations,

$$J_{ij} = \frac{1}{A_i * C_i} \left[Gm_i - \left[\sum_{i,j} GL_{ij} \right] - GS(t) \right] \qquad \text{for } i=j$$

$$\frac{1}{A_i * C_i} * GL_{ij} \qquad \text{for } i \neq j$$

The maximum value of the minimum time step allowed is dependent on the degree of exactness.

6.6 PARTIAL ANALYTICAL SOLUTIONS

6.6.1 THE PROBLEM

For a check of the numerical method, consider a straight dendrite with one synapse at the end as depicted in figure:6.6.1. The dendrite equation for voltage change from resting potential is a function of location x and time t, V(x,t), and obeys the partial differential equation

$$m^2 D_{xx} V - V = \tau D_t V$$

where D_{xx} is the second partial derivative operator with respect to x, and D_t is the first partial derivative operator with respect to time t. The space constant is m and time constant is τ. How does the synapse affect V(x,t)? Recall the compartment equation

$$A_i C_i D_t V_i = -IM_i + IL_i + IR_i + Is_i - Ip_i$$

where IM_i, IL_i, IR_i, Is_i, Ip_i are, respectively, the conductive membrane currents, the longitudinal current from the left compartment, the longitudinal current from the right, the synaptic current, and the pump current. The compartment membrane area is A_i, the capacitance per unit area is C_i, and interior compartment voltage is V_i.

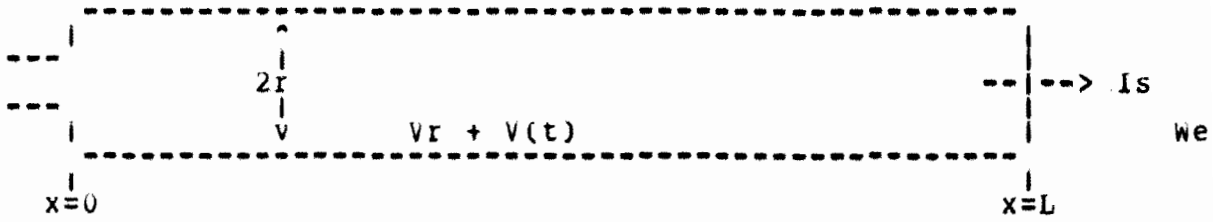

Figure:6.6.1 The simple straight dendrite. The response voltage is V(t), resting potential is Vr, external potential is we, radius is r, length is L, and synaptic current is Is. The action potential site is at x=0.

For the synapse at x=L, IR=-Is and for the synapse at x=0, IL=Is. The general i-th compartment of length dx has

$$IR_i = (V_{i+1} - V_i)*(pi*r^2/dx*AR)$$

$$IL_i = -(V_{i-1} - V_i)*(pi*r^2/dx*AR)$$

Taking the limit as dx goes to zero gives

$$IR = +D_x V*(pi*R^2/AR)$$

$$IL = -D_x V*(pi*R^2/AR)$$

The synaptic current (positive is outward from compartment) for synaptic conductance g(t) is

$$Is = g(t)*(V + Vr - we - Ep)$$

where Vr is the internal resting potential, We is the external potential. At the synapse the longitudinal current equals the synaptic current, thus the boundary condition at x=L is

$$D_x V(L,t) = -(AR/(pi*r^2)*g(t)*(V_{x=L} + K)$$

where K = Vr-we. The boundary condition at x=0 is

$$D_x V(0,t) = 0$$

since there is a constricture at the spike generating site which limits longitudinal current flow. The diameter for the AP generating site on the cochlear afferent neurons is 1/2 that of the dendrite diameter which causes the longitudinal conductance to be 1/4 that of the dendrite. The alternative choices for other boundary conditions as x becomes large are:

(1) $V(x,t) = 0$, as x becomes large

(2) $V(x,t) = FH(x,t)$, at x=L

(3) $D_x V(x,t) = 0$, at x=L

where FH(x,t) is the voltage given by the Frankenhauser, Hodgkin & Huxley equation (1964); that is, use action potential generation with threshold. Setting V to 0 as x becomes large clamps the end voltage at zero. Using the FH equations for voltage introduces a complicated boundary condition which is nonlinear and far too complicated for available analytical solutions. Furthermore, it is unnecessarily complicated for the initial simulation studies of these dendrites. Setting the first spatial derivative to zero in no way constrains the voltage value at x=L.

Since the partial differential equation is of second order, only two boundary conditions are required. The equation is of the parabolic type and has the form of the heat equation for a rod with radiation into its environment (Myers, 1971).

As is typically done in these problems, let $V=u*\exp(-t/\tau)$ and $y=(x/L)$. Thus, with $a=(m/L)^2\tau$ and $K=AR/\pi*r^2$, the partial differential equation becomes

$$a*D_{yy}u = D_t u$$

and the boundary conditions become

at y=1: $D_y u = -k*L*g(t)*(u + K*\exp(t/\tau))$

at y=0: $D_y u = 0$

with initial conditon

at t=0: $u(x,0) = V(x,0) = f(x)$.

Now the boundary condition at y=1 fails the homogeneous condition "c*u(x,t) is a solution when u(x,t) is a solution and c is constant". This is due to the term containing K. The g(t)*u(1,t) term causes a problem because the conductance g(t)*u makes a time varying boundary condition. Consequently, a complete analytic solution is unavailable. Thus, the comparison of the numerical solution with an analytical solution proceeds with limitations. Obviously, if an analytic solution for the "unweakened" or "complete" equations were available, the numerical solution would not be required.

6.6.2 NONLINEARITY

When a straight dendrite with one synapse at x=L is considered as a system, the input is synaptic conductance g(t) and output is the response voltage V(x,t) at x=0. The partial differential equation with boundary conditions is a system of simultaneous differential equations that the solution must satisfy

$$m^2 D_{xx} V - V = \tau D_t$$

$$D_x V = -K*g(t)*(V(L,t) + K), \qquad \text{at } x=L$$

$$D_x V = 0 \qquad \text{at } x=0$$

The partial differential equation is linear in the sense that if V_1 and V_2 are solutions, then so is $aV_1 + bV_2$, for constants a and b. Note that the boundary condition is not linear in this sense.

The response of the system is not linear with respect to input g(t) in the following sense. If $g_1(t)$ produces response $V_1(t)$ and $g_2(t)$ produces response $V_2(t)$, then the system is linear if $ag_1(t)+bg_2(t)$ produces response $aV_1(t)+bV_2(t)$. Clearly the synapse boundary condition does not satisfy this requirement. It should be noted also, that this nonlinearity is for any kind of input g(t).

A somewhat simpler condition for a system to be linear, which is equivalent to the condition in the last paragraph, is the following (Hardy & Wright, 1960). If $g_1(t)$ produces response $V_1(t)$ and $g_2(t)$ produces response $V_2(t)$, then $g_1(t)-g_2(t)$ produces $V_1(t)-V_2(t)$. This equivalent condition can be used to state how "badly non-linear" is the simple dendrite with synapse. Let $g=g_1-g_2$ and $V=V_1-V_2$. Substitute these into the synaptic boundary condition. The requirement for linearity is

$$g_2*(V_1-2V_2) + g_1*V_2 = 0$$

for all g_1 and g_2. It cannot hold even when $g_2=a*g_1$, for constant a.

6.6.3 MODIFIED BOUNDARY CONDITIONS

A solution of a partial differential equation with boundary conditions and initial condition is, in fact, a solution to a system of simultaneous differential equations. Since the partial differential equation is linear and the boundary condition for the synapse causes the difficulty, the course of action is to modify the boundary condition in some way.

6.6.3.1 VOLTAGE VARYING END

One of the simplest ways of changing the boundary condition to obtain a means of checking the numerical method is to specify no current flow at x=0 and set the response potential at x=L to P(t). The untransformed version of the problem becomes

$$D_t V = Q D_{xx} - V/\tau \qquad \text{where } Q = m^2/\tau$$

$$D_x V = 0 \qquad \text{at } x=0$$

$$V(x,t) = P(t) \qquad \text{at } x=L$$

A solution to this problem is given directly, Carslaw and Jaeger (1959,sec.4.7).

$$V(x,t) =$$

$$\frac{2}{L}\sum_{n=0}^{\infty} e^{-(t/\tau)-QB_n^2 t}\cos(B_n x)\left[QB_n(-1)^n\int_0^t e^{(QB_n^2+(1/\tau))t}P(t)dt + \int_0^L f(x)\cos(B_n x)dx\right]$$

where $B_n = (2n + 1)(\pi/L)$

This solution can now be compared with the numerical solution. The comparison is first done with initial condition f(x)=0 and with constant $P(t)=V_c$. The result is shown in figure:6.6.3.1.1. Using

$$P(t)=0.050*[1.0 - 0.5\cos(2*\pi*f*t)] \quad \text{volts}$$

the result is shown in figure:6.6.3.1.2, with τ=5.32 millisec. and D = 1 micron.

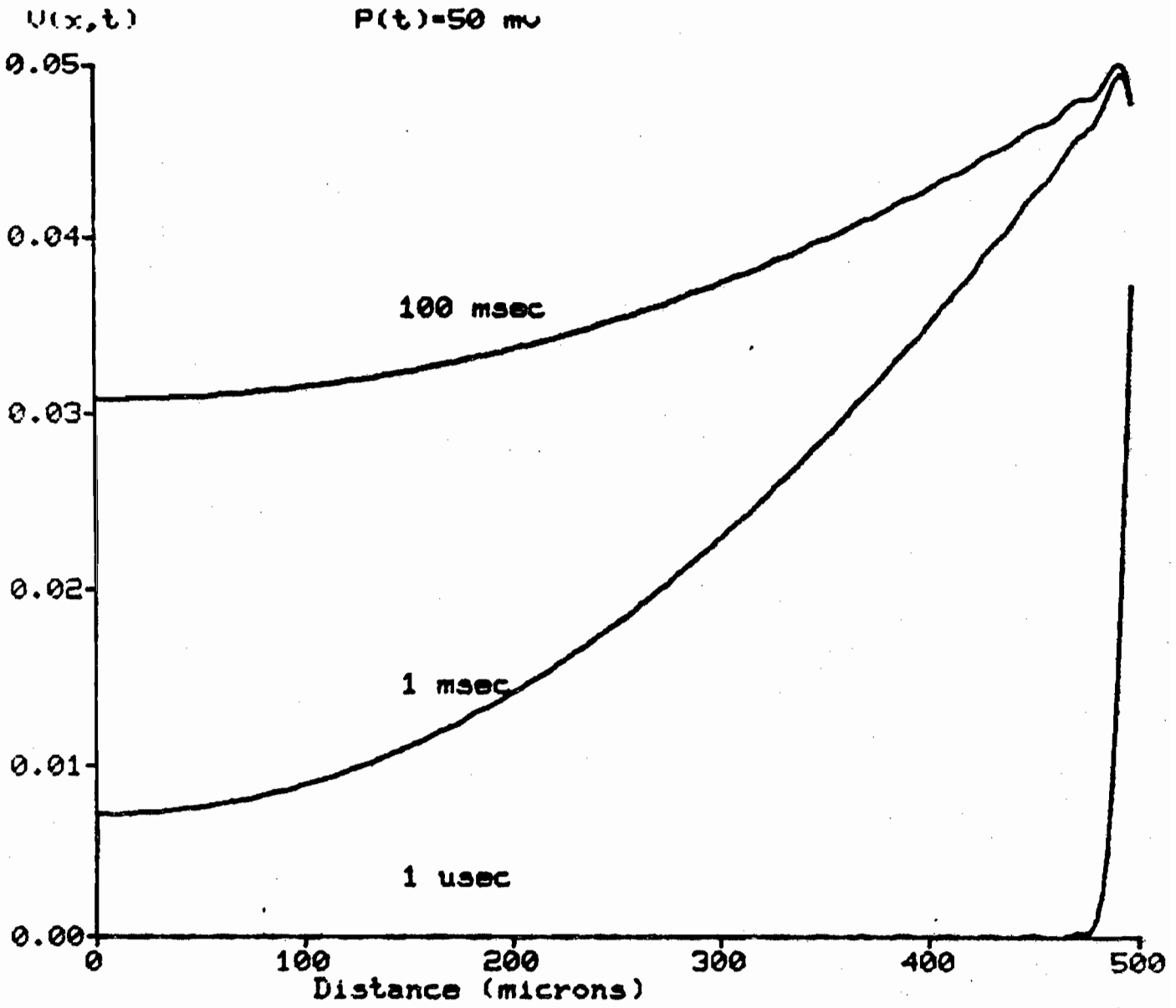

Figure:6.6.3.1.1 The series solution for the voltage varying end. The voltage at the end is held constant at V_c = 50 millivolts. Note the increase in voltage as time increases. The solutions were done using 750 terms in the sums.

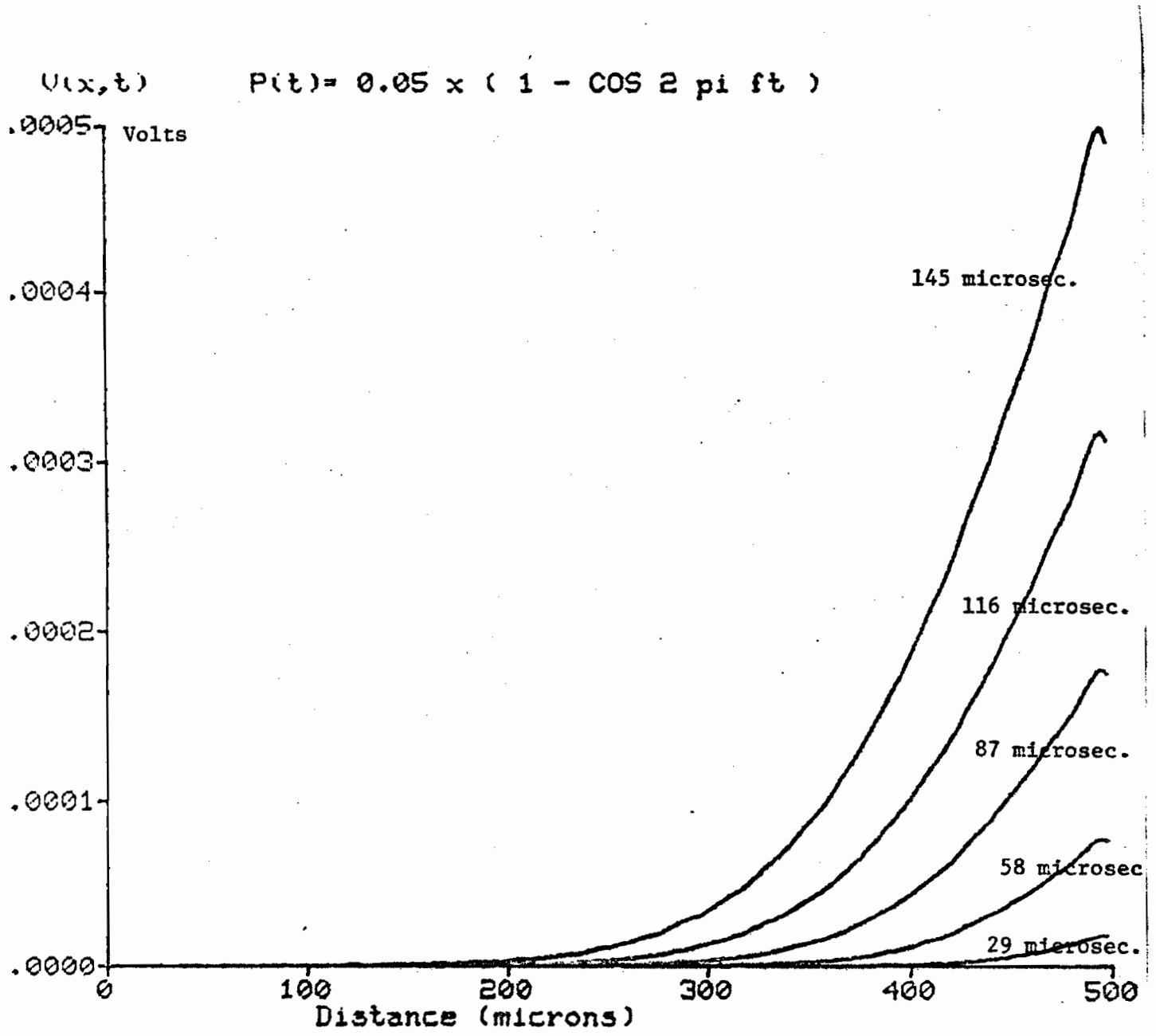

Figure:6.6.3.1.2a Series solution for voltage varying end. Time t<150 microsec.

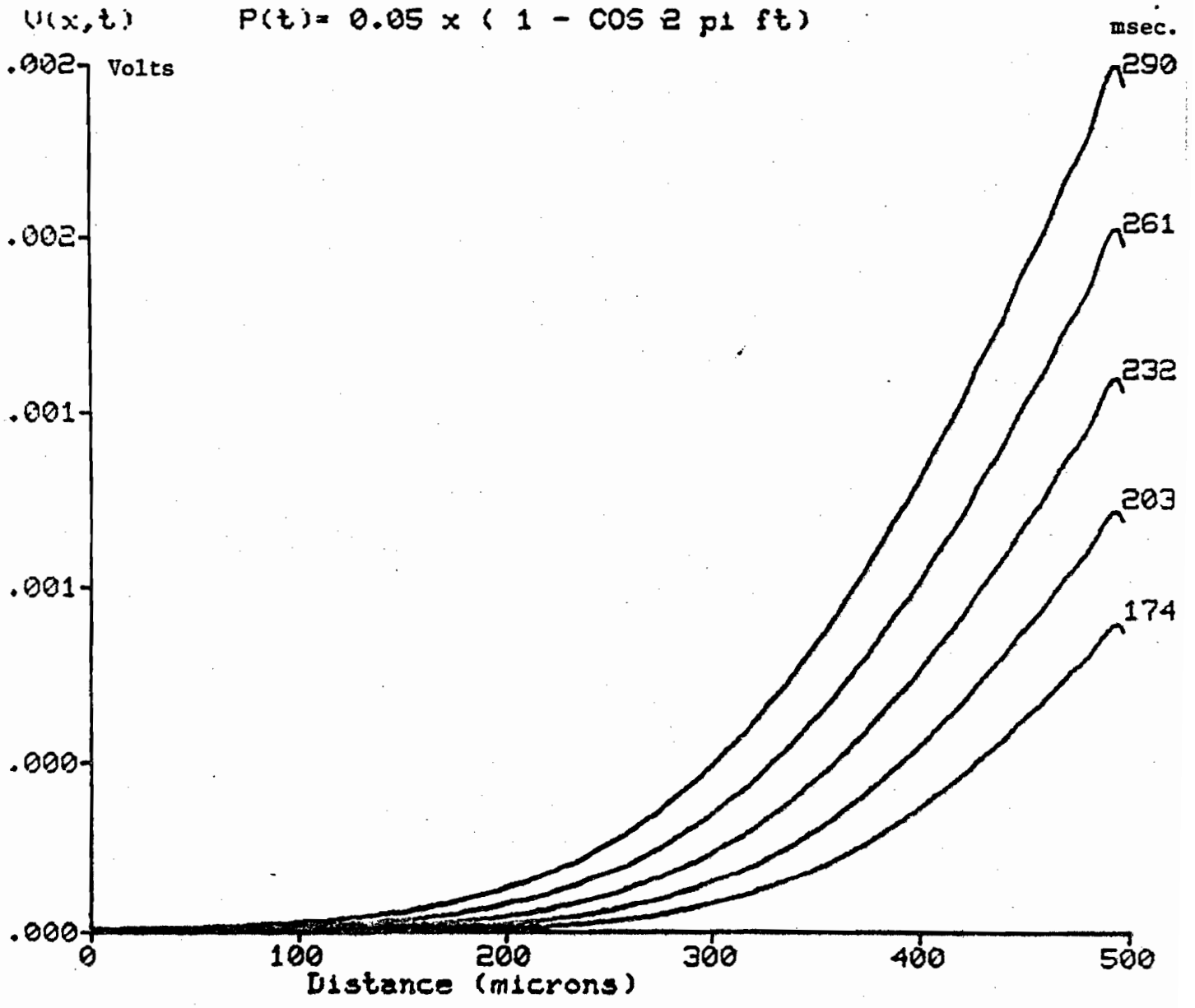

Figure:6.6.3.1.2b Series solution for voltage varying end. Time t>150 microsec.

6.6.3.2 POSSIBLE MODIFICATIONS

What are the possible modifications to the problem that will allow an analytical solution which is physiologically correct at the synapse and provides a good test of the numerical method of solution? Let the response voltage at y=1, u(1,t) be a constant u_0. The possible modifications of the transformed boundary condition at y=1

$$D_y u = -k*L*g(t)*[\, u(1,t) + K*\exp(t/\tau) \,]$$

which lead to a solution are as follows.

case 1: $D_y u = -k*L*g(t)*(u_0 + K)$

case 2: $D_y u = -k*L*g(t)*(u_0 + K*\exp(t/\tau))$

$= -k*L*g(t)*u_0 + k*L*K*g(t)*\exp(t/\tau)$

case 3: $D_y u = -k*L*g_0*(u(1,t) + K)$

case 4: $D_y u = -k*L*g_0*(u(1,t) + K*\exp(t/\tau))$

case 5: $D_y u = -k*L*g_0*K$

Cases 1 and 2 do not allow for changes in the transformed potential, u, thus also for V(x,t). As a result, the description of V(x,t) will be poor.

Cases 3 and 4 allow for changes in potential, but require constant conductance $g(t)=g_0$. This corresponds to a step change in conductance at t=0.

Cases 1,2,3,5 are solvable based on the methods in Carslaw & Jaeger (1959) and Myer (1971); however, case 3 is

the closest to the correct boundary condition.

Case 3 allows the variable to be normalized as

$$U = (u + K)/(u_i + K)$$

where u_i is the initial value of u. The effect is to "remove" the K term in the boundary condition. Case 4 does not permit this since the term is K*exp(-t/T). As a result, case 4 is a nonhomogeneous boundary condition. Homogeneity requires for a constant c, that c*u be a solution when u is a solution. A nonremovable nonhomogeneous boundary condition disqualifies the use of separation of variables to obtain the corresponding homogeneous solution, eigenconditions, and eigenfunctions. Thus the best choice to use for comparison of the numerical solution is case 3. A solution to case 3 is derived below.

It is noted that with case 3, if the boundary condition for the non-synapse end were changed to $\lim_{x\to\infty} V(x,t)=0$, then a solution is obtainable containing the complement error function

$$\mathrm{erfc}(x) = (\pi)^{-0.5} \int_{s=x}^{\infty} e^{-s^2}\, ds$$

However, this boundary condition is not the one used in the simulation; therefore, a solution with it is not used for comparison.

6.6.3.3 CASE 3

6.6.3.3.1 DERIVATION

Using the case 3 boundary condition, the problem is

$$a^2 D_{yy} u = D_t u \qquad \text{where } a^2 = \pi^2/(L^2 * T)$$

$$D_y u = -K*L*g*(u(1,t) + K) \qquad \text{at } y=1$$

$$D_y u = 0 \qquad \text{at } y=0$$

$$u(0,0) = u_i$$

where $g = g_o$.

Normalize by letting

$$U(y,t) = \frac{u(y,t) + K}{u_i + K}, \text{ thus}$$

$$a^2 D_{yy} U = D_t U$$

$$D_y U = -K*L*g*U(1,t) \qquad \text{at } y=1$$

$$D_y U = 0 \qquad \text{at } y=0$$

$$U(y,t) = 1 \qquad \text{for } t=0$$

Since the PDE and boundary conditions are all homogeneous, it qualifies for separation of variables. So let $U(y,t)=X(y)\Theta(t)$ and substitute into the PDE, with some rearrangement, giving

$$a^2((D_{yy} X)/X) = (D_t \Theta)/\Theta$$

For this equality to hold, both sides must be equal to the same constant, say $-c^2$. This gives

$$D_{yy} X + (c/a)^2 = 0$$

which has a solution of the form

$$X(y) = A*\sin(q/a)y + B*\cos(q/a)y$$

The boundary condition at y=0 gives A=0, and the boundary condition at y=1 gives

$$(q/a)\tan(q/a) = k*L*g$$

Thus the eigenvalues are the roots of

$$P_n \tan P_n = k*L*g = H, \quad \text{where } P_n = q_n/a$$

and the eigenfunctions are

$$X_n(y) = \cos(P_n y)$$

Assume a solution of the form

$$U(y,t) = \sum_{n=0}^{\infty} A_n(t)\cos(P_n y)$$

Notice that the time solution, $\Theta(t)$, will come from the the ensemble of the $A_n(t)$, n=0,1,2,.... Multiply both sides by $X_n(y)$, integrate with respect to y on the interval [0,1], and use the orthogonality of the X_n functions to yield

$$\int_0^1 U(y,t)\cos(P_n y)dy = A_n(t) \int_0^1 [\cos(P_n y)]^2 dy = A_n(t)*B_n \qquad \text{(eqn *)}$$

where $B_n = \frac{1}{2} + \frac{\sin(2*P_n)}{4*P_n}$

Differentiate both sides with respect to t and substitute using the PDE to yield, integrating twice by parts,

$$B_n D_t A_n(T) = a^2 \int_0^1 D_{yy} \cos(P_n y)dy$$

$$= a^2\left[U(1,t)\{-k*L*g*\cos(P_n) + P_n \sin(P_n)\} - (P_n)^2 B_n A_n(t)\right]$$

Using the eigencondition gives with rearrangement

$$B_n [\, D_t A_n(t) + a^2 (P_n)^2 A_n(t)] = 0$$

Use the integrating factor $\exp[a^2 (P_n)^2 t]$ to obtain

$$B_n A_n(t) \exp[a^2 (P_n)^2 t] = \text{constant}$$

Using equation (*) with t=0 and U(y,0)=1, the coefficients are

$$A_n(t) = \frac{[\sin(P_n)]e^{-a^2 P_n^2 t}}{B_n * P_n}$$

$$= \frac{2*H*e^{-a^2 (P_n)^2 t}}{P_n (H + \sin^2 P_n)}$$

where $P_n \sin(P_n) = K*L*G*\cos(P_n) = H*\cos(P_n)$. Thus

$$U(y,t) = \sum_{n=1}^{oo} \frac{2*k*L*g*e^{-a^2 P_n t} \sin(P_n)}{P_n (2*k*L*g + \sin^2 P_n)} * \cos(P_n y)$$

and solving for small u

$$u(y,t) = K + (u_i + K) \sum_{n=1}^{oo} \frac{2*k*L*g*e^{-a^2 P_n t} \sin(P_n)}{P_n (2*k*L*g + \sin^2 P_n)} * \cos(P_n y)$$

giving the equation for V(x,t) with $g=g_0$

$$V(y,t) = -K*e^{-t/\tau} + (V_i + K)*e^{-t/\tau} \sum_{n=1}^{oo} \frac{2*k*L*g_0*e^{-a^2 P_n t} \sin(P_n)}{P_n (2*k*L*g_0 + \sin^2 P_n)} * \cos(P_n x/L)$$

where $V_i = V(x,0)$.

6.6.3.3.2 RESULT

Note that the differences in the equation for case 3 and the true synaptic boundary condition are constant boundary conductance g and a modified k*exp(t/τ) term. The solution found is for 0<t<τ such that exp(t/τ) is close to one. The solution for 0<t<<τ and V_i=V(x,0)=0 is

$$V(y,t)= -K*e^{-t/\tau} + (V_i+K)*e^{-t/\tau} \sum_{n=1}^{\infty} \frac{2*K*L*g_0 * e^{-a^2 P_n t} \sin(P_n)}{P_n*(2*k*L*g_0 + \sin^2 P_n)} * \cos(P_n x/L)$$

Recall that $a^2 = m^2/L^2\tau$ and that P_n is given by the eigencondition

$$P_n \tan(P_n) = k*L*g = H$$

For a cochlear inner dendrite r=0.5 micron, L=30 micron, AR=$60*10^4$ ohm*micron, H=0.229. The simple dendrite of diameter 1 micron and length 500 microns has H=3.8. These are medium range values for the Biot number (Myers, 1971, sec.7.2). A small value of H is interpreted as a small internal thermal resistance in comparison to the external resistance. If it is small enough (<.1), the internal resistance can be neglected (as in a lumped-system analysis). A large value of H (>10) means that the size of the external resistance is small in comparison to the

internal resistance. In this case, the internal resistance cannot be neglected, and the internal temperature distribution must be considered. In the dendrite case, both the synapse conduction and internal resistance are important which necessitates a distributed spatial analysis. It mathematically says that synaptic conductance changes and spatial response determine the dendrite potential responses. Further effort in this direction is useless since synaptic conductances change rapidly in time.

6.7 NUMERICAL RESULTS

6.7.1 COMPARTMENT TYPES

A dendrite is specified to the simulation program by a list of compartment types and a list of compartment numbers with connections. The types are given in table:6.7.1. It could be said that types 2,4,5 are the same, but they exist to make book keeping easier.

type	number	description	diam microns	length microns
alpha	(1)	synapse from hair cell	0.2	2.5
beta	(2)	elbow from 1st vertical	0.2	2.5
epsilon	(5)	2 ended comp on vertical (V)	0.2	2.5
delta	(4)	2 ended comp on horizontal (H)	0.5	5.0
gamma	(3)	3 ended comp at juncture of H and V	0.5	5.0
zeta	(6)	long horizontal dendrite	1.0	50.0
eta	(7)	APGS constricture unmyelinated	0.5	2.0
theta	(8)	APGS constricture myelinated	0.5	2.0
iota	(9)	axon myelinated	2.0	50.0

Table 6.7.1: Compartment types.

6.7.2 SIMPLE DENDRITE

The simple dendrite used for comparison of the numerical method with the partial analytical result is chosen as a straight dendrite of length L=50 microns which is shorter than the space constant ($\tilde{\tau}$) when using the membrane resistivity range. The dendrite is divided into twenty compartments, each having length 5 microns and diameter 1 micron. The input specification file is shown in figure:6.7.2.1. The numerical result is shown in figure:6.7.2.2. The synaptic conductance maximum was taken as 10^{-8} mho.

6.7.3 INNER DENDRITE

The mammalian cochlear inner dendrite is 30 microns long, with diameter 1 micron. The dendrite is simulated using 10 compartments each having a length of 3 microns. The input specification file is shown in figure:6.7.3.1. The result over dendrite length for a synaptic input "window function" is shown in figure:6.7.3.2.

The target of interest is how voltage V(L,t) at the action potential generating site (APGS) is influenced by the synaptic conductance g(t).

When the voltage, we, of the fluid surrounding a dendrite is increased it affects the synapses in the form

$$D_x V \Big|_{x=a} = -k*g(t)*[\, V(a,t) + Vr - we - E_{Na} \,]$$

for a synapse at location x=a. Thus, when We is increased, the synaptic input current is larger and thus increases the response. When we is increased by 20 millivolt, the response is shown in figure:6.7.3.3. This corresponds to an increase in the potential of the fluid surrounding the dendrite in the synaptic region. (In the cochlea, this fluid is sometimes called Cortilymph.) As can be seen from the simulations, there is little change due to this increase of extracellular potential.

SIMPLE.DEN

IT	GDM	CM	DIAM	LEN	
01	0.2E-10	1.3E-14	1.0	10.0	SYNAPSE COMPMNT, 1 ENDED
02	0.2E-10	1.3E-14	1.0	10.0	DUMMY TYPE
03	0.2E-10	1.3E-14	1.0	10.0	DUMMY TYPE
04	0.2E-10	1.3E-14	1.0	5.0	HORZ COMPMNT, 2 ENDED
05	0.2E-10	1.3E-14	1.0	5.0	DUMMY TYPE
06	0.2E-10	1.3E-14	1.0	50.0	DUMMY TYPE
07	0.2E-10	1.3E-14	0.5	2.0	AP GEN SITE, 2 ENDED
08	0.2E-13	13.E-14	0.5	2.0	AP GEN SITE, 2 ENDED
09	0.2E-13	13.E-14	2.0	50.0	AXON, 2 ENDED
10	0.2E-13	13.E-14	2.0	50.0	AXON, 2 ENDED, DxxV(x,t)=0
000	0.0	0.0	0.0	0.0	END OF COMPMNT TYPES

IC	IT	IC1	IC2	IC3	IS	
1	1	2	0	0	1	SYNAPSE 1
2	4	3	1	0	0	
3	4	4	2	0	0	
4	4	5	3	0	0	
5	4	6	4	0	0	
6	4	7	5	0	0	
7	4	8	6	0	0	
8	4	9	7	0	0	
9	4	10	8	0	0	
10	4	11	9	0	0	
11	7	12	10	0	0	AP GENERATING SITE
12	8	13	11	0	0	AP GENERATING SITE
13	9	14	12	0	0	
14	9	15	13	0	0	
15	9	16	14	0	0	
16	9	17	15	0	0	
17	9	18	16	0	0	
18	9	19	17	0	0	
19	10	18	0	0	0	LAST COMPMNT

Figure:6.7.2.1 Input specification file for a simple dendrite. The compartment types are specified first. Type is IT, GDM is conductance (mho per square micron), CM is capacitance (Farads per square micron), DIAM is compartment diameter (microns), and LEN is compartment length (microns). The second section is a table specifying connections and type. Compartment number is IC, type is IT, the compartments connecting to the IC-compartment are IC1, IC2, IC3 where a "0" entry denotes not connected. The column under IS is the identification number of the synapse on the IC-th compartment.

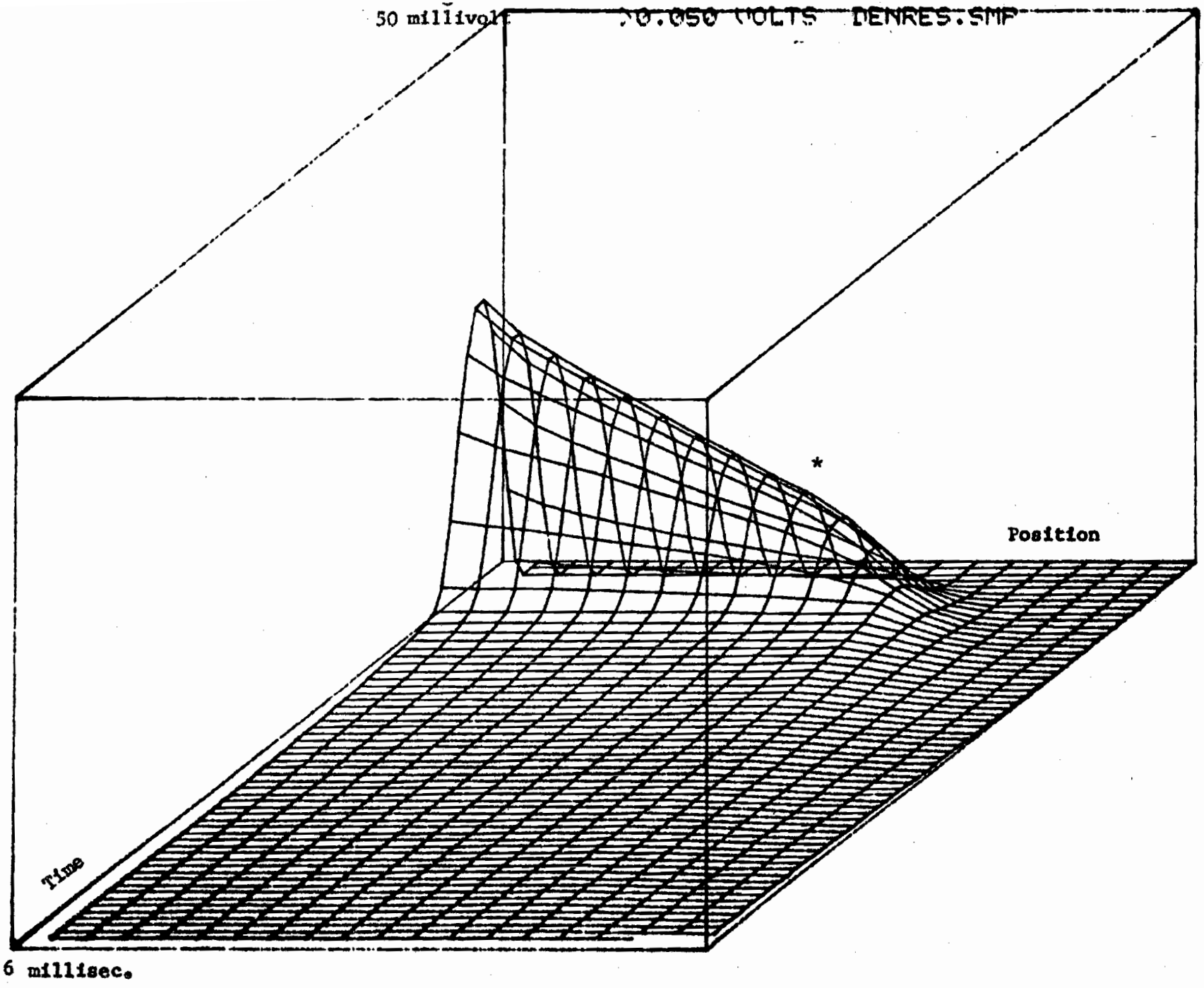
50 millivolt
Position
Time
6 millisec.

Figure:6.7.2.2 Numerical result for a simple dendrite with the synapse activated using a smooth window function with rise time 0.5 msec., duration 0.5 msec., and fall time 0.5 msec. The onset time is 0.2 msec. The synaptic conductance maximum is 10^{-8} mho. The vertical axis is voltage, the horizontal axis is position on the dendrite with the synapse at the origin and axon at the right hand end. The action potential generating site is marked by an "S". The diagonal axis is time ranging from 0.0 to 0.6 msec. The dendrite compartments are 5.0 micro meters long and the axon compartments are 50.0 micrometers long, thus the sharp potential decay on the proximal part of the fiber.

INNER.DEN

IT	GDM	CM	DIAM	LEN	
01	0.2E-10	1.3E-14	1.0	3.0	SYNAPSE COMPMNT, 1 ENDED
02	0.2E-10	1.3E-14	1.0	3.0	DUMMY TYPE
03	0.2E-10	1.3E-14	1.0	3.0	DUMMY TYPE
04	0.2E-10	1.3E-14	1.0	3.0	HORIZ COMPMNT, 2 ENDED
05	0.2E-10	1.3E-14	1.0	3.0	DUMMY TYPE
06	0.2E-10	1.3E-14	1.0	50.0	DUMMY TYPE
07	0.2E-10	1.3E-14	0.5	2.0	AP GEN SITE, 2 ENDED
08	0.2E-13	13.E-14	0.5	2.0	AP GEN SITE, 2 ENDED
09	0.2E-13	13.E-14	2.0	50.0	AXON, 2 ENDED
10	0.2E-13	13.E-14	2.0	50.0	AXON, 2 ENDED, DxxV(x,t)=0
000	0.0	0.0	0.0	0.0	END OF COMPMNT TYPES

IC	IT	IC1	IC2	IC3	IS	
1	1	2	0	0	1	SYNAPSE 1
2	4	3	1	0	0	
3	4	4	2	0	0	
4	4	5	3	0	0	
5	4	6	4	0	0	
6	4	7	5	0	0	
7	4	8	6	0	0	
8	4	9	7	0	0	
9	4	10	8	0	0	
10	4	11	9	0	0	
11	7	12	10	0	0	AP GEN SITE
12	8	13	11	0	0	AP GEN SITE
13	9	14	12	0	0	
14	9	15	13	0	0	
15	9	16	14	0	0	
16	9	17	15	0	0	
17	9	18	16	0	0	
18	9	19	17	0	0	
19	10	18	0	0	0	LAST COMPMNT

Figure:6.7.3.1 Input specification for an inner dendrite.

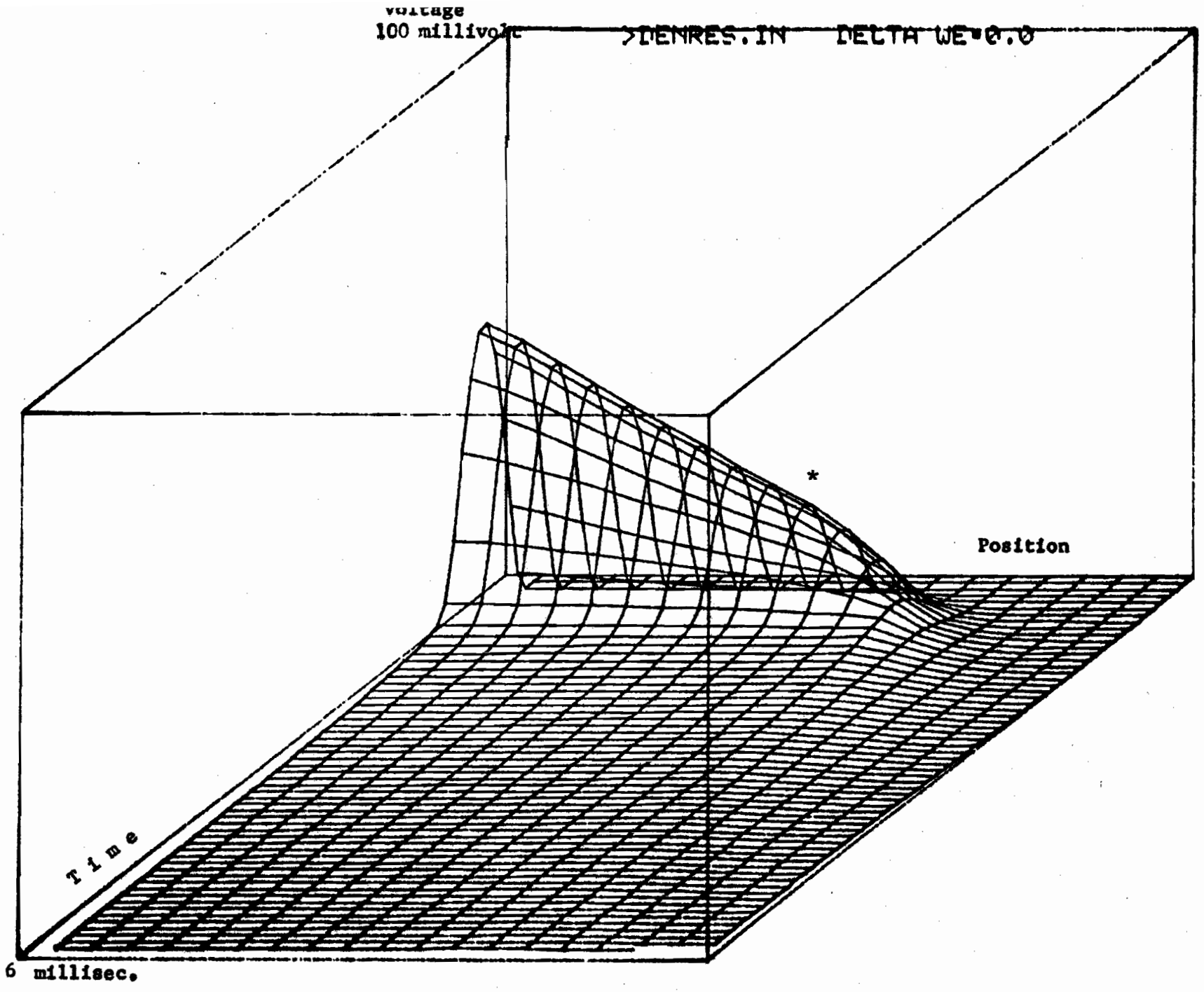
Voltage
100 millivolt
>DENRES.IN DELTA WE=0.0
*
Position
Time
6 millisec.

Figure:6.7.3.2 Numerical result for an inner dendrite for the synapse activated using a smooth window function with rise time 0.5 msec., duration 0.5 msec., and fall time 0.5 msec., with duration 0.5 msec. Onset time is at 0.2 msec. Length of the dendrite is 30 micrometers. Postsynaptic conductance maximum was taken as $2*10^{-8}$ mho.

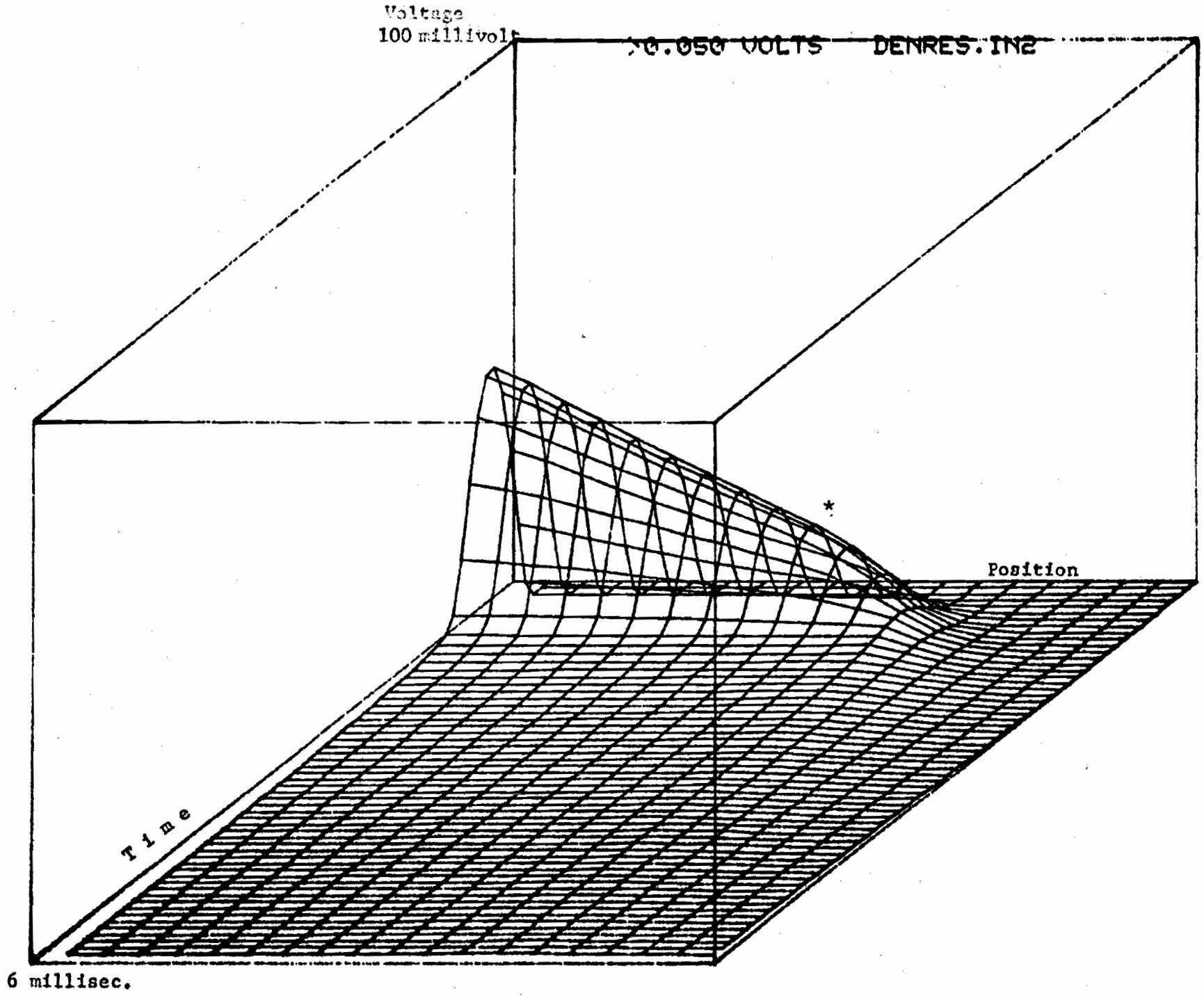

Fig. 6.7.33. p.6-99

Figure:6.7.3.3 Numerical response of an inner dendrite identical to conditions in figure:6.7.3.2 except external voltage, we, is increased by 20 mV.

6.7.4 OUTER DENDRITE

6.7.4.1 RECAPITULATION OF THE PROBLEM

An outer dendrite is arranged such that it receives input from ten outer hair cells over 200 microns in the apical direction along the basilar membrane. Then it continues for 650 microns in the apical direction without synapses, crosses the tunnel of Corti for 80 microns, then enters the habenula perforata with the local neighboring inner dendrites. Spoendlin (1979) found that an outer dendrite after entering the habenula perforata, joins its soma, then continues as an unmyelinated fiber that tapers off without continuing as an afferent fiber in the cochlear nerve. What is the functional response of these fibers from outer hair cells?

The basilar membrane has a frequency response with the highest frequency at the basilar end and the lowest frequency at the apical end (Bekesy,1947). Schuknecht & Neff (1952), Schuknecht (1953), and Schuknecht & Sutton (1953), in cat, using restricted surgical lesions with conditioned response measurements of audiograms, followed by histological localization of the lesions, produced a functional relationship between frequency and position on the basilar membrane. The functional relationship used henceforth for maximal response frequency, MRF, is

$$f = MRF(x) = (52.0*10^{3})*(0.00357)^{(x/L)}$$

where x is the distance from the basal end of the cochlea in millimeters and L=23.0 is basilar membrane length in mm and is shown in figure:6.7.4.1.1. The function is from Kiang, Moxon & Levine (1970, p245) and is based on Schuknecht's curve B (Schuknecht, 1953a). To how much of a frequency change along the basilar membrane does 200 microns in the apical direction correspond? Using the MRF function, the delta frequency, df(x) at location x is given by

$$df(x) = MRF(x) - MRF(x+0.2)$$

A plot of df(x) versus x is given in figure:6.7.4.1.2. It is referenced to the end of the section of dendrite innervated by hair cells which is nearest to the action potential generating site, to have a basis for comparison with the inner dendrite with only one hair cell synapse. As a matter of interest, for the dorsal cochlear nucleus which the cochlear nerve afferent neurons innervate, consider the arrangement of inner and outer dendrites. If the fibers of the inner and outer dendrites, which enter the same habenula perforata hole, were to innervate the same region of the cochlear nucleus, then there would be a response frequency difference for these two fibers. This difference corresponds to a 650 micron shift along the cochlear partition for the non-innervated section of outer dendrite.

This difference is thus

$$df(x) = MRF(x) - MRF(x - 0.650)$$

and is plotted in figure:6.7.4.1.3.

To analyze the outer dendrite, consider the signal processing diagram of figure:6.7.4.1.4. The basilar membrane transmits the displacement signal to ten hair cells in parallel which innervate the outer dendrite. Number the hair cells and the synapses from the high frequency end to low frequency end of the basilar membrane. Consider an input sound signal swept in frequency from $MRF(X_H)$ to $MRF(X_L)$ where X_H is the coordinate of the high frequency end and X_L is the coordinate of the low frequency end. When a tone sweep from $F_H = MRF(X_H)$ to $F_L = MRF(X_L)$ is presented to the tympanum, what happens at the synapses on the dendrite? At a given location x on the cochlear partition, the basilar membrane is oscillating with magnitude

$$DBM(x,f) = \left| H(x,f) * M(f) * P \right|$$

where f is the input frequency and H is the transfer function for BM displacement with respect to stapes, M is the middle ear transfer function of stapes with respect to sound pressure level at the ear drum and P is sound pressure level at the ear drum. The receptor potential of an outer hair cell $G_O(x,t)$ is proportional to displacement of basilar

membrane at location x with sine wave input frequency f, DBM(x,f) (Dallos,1972). The transmitter release is a saturating Hill function or sigmoid curve per the discussion on synapses, hence it obeys a sigmoid response function. Thus synaptic conductance for an outer dendrite obeys approximately a function of the form

$$GS(t) = G_m * 0.5 * (1 - \cos(2*pi*f*(t-t_d))$$

where G_m is maximum synaptic conductance for the maximum of DBM(x,f). $G_o < G_{sm}$ and t_d is the time delay between the tone signal at the ear drum and the signal at the synapse. Now for a time sweep from F_H to F_L, the signal at the i-th synapse is

$$GS_i = GS(t - TD_i)$$

where the time delay TD_i is the solution to the equation

$$MRF(X_I) = F_L + ((F_H - F_L)/T_s) * TD_i, \quad X_L \leq X_i \leq X_H$$

where X_i is the location of the i-th hair cell for an outer dendrite. The solution to this equation gives the time that the frequency $MRF(X_i)$ causes input to synapse at location X_i. The solution can be approximated by

$$TD_i = (T_s/10) * i; \qquad i=1,2,\ldots,10$$

as the function MRF(x) is close to linear on the interval along the cochlear partition corresponding to the interval transversed by an outer dendrite.

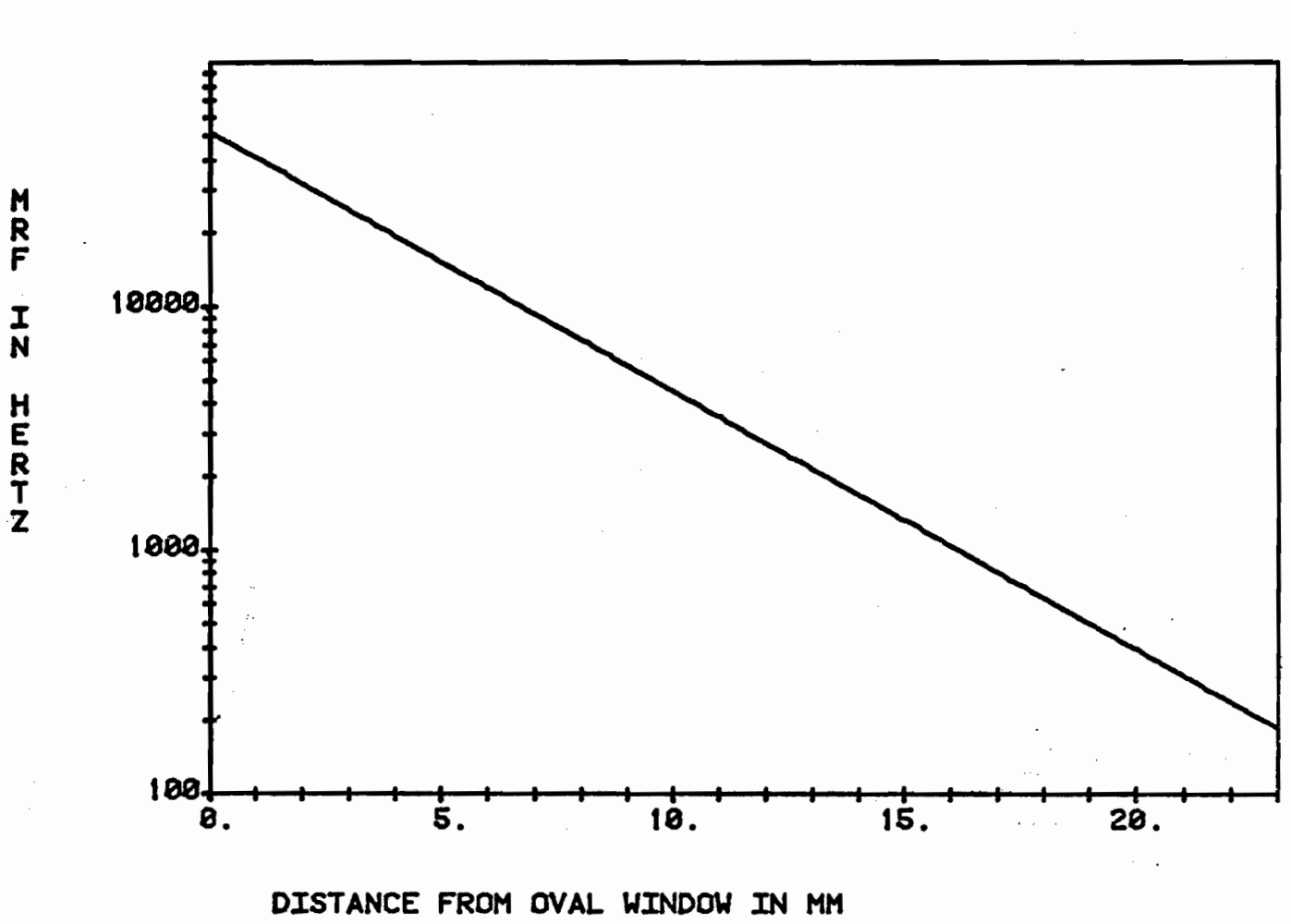

Figure:6.7.4.1.1 Maximum response frequency versus distance along the cochlear partition from the oval window.

DF(X,DX) VERSUS X DF(0.,.200)=2486.7 DF(23.,.200)= 8.9

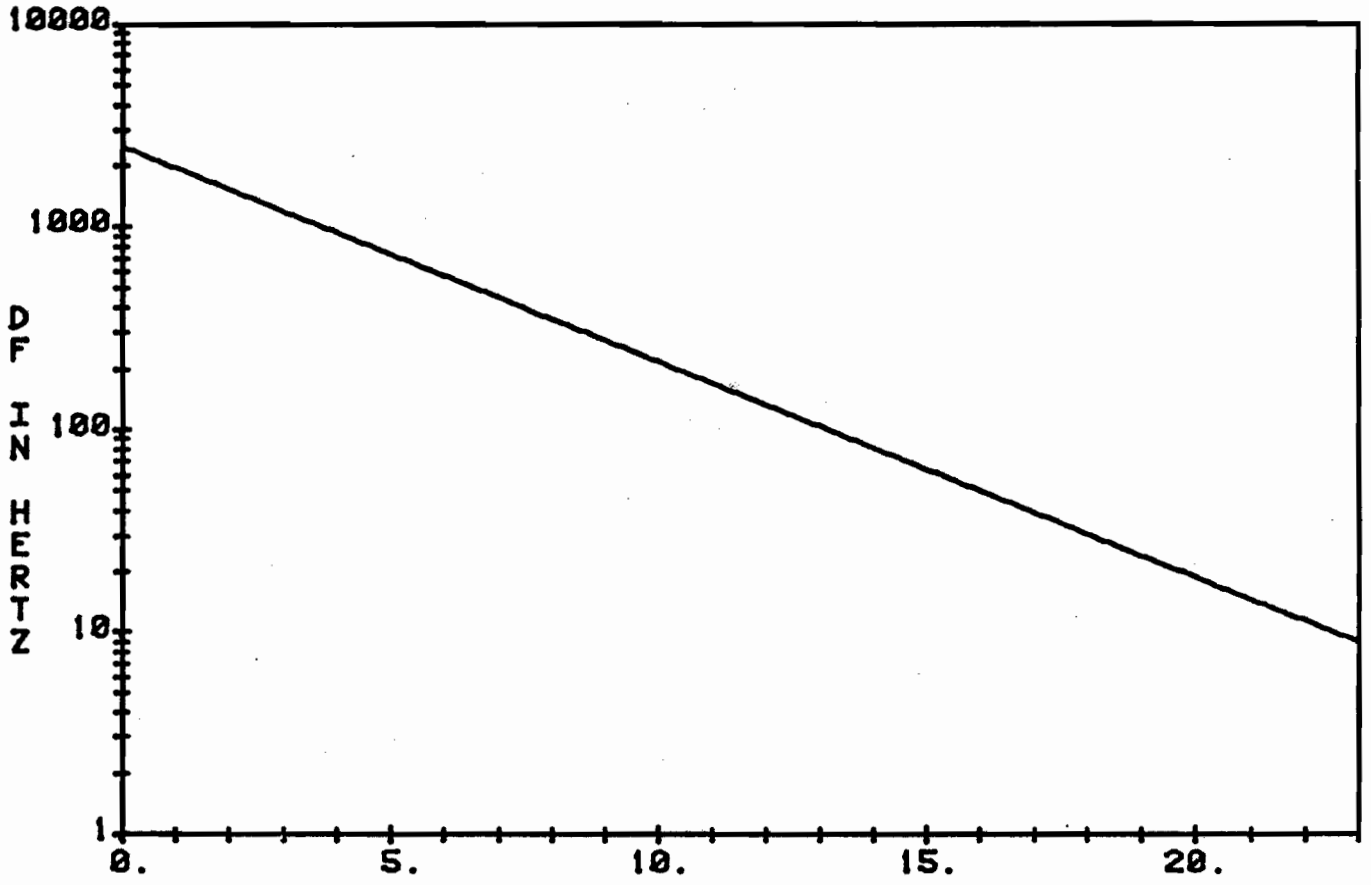

Figure:6.7.4.1.2 Change of maximum response frequency in an interval of 200 micrometers versus distance along the cochlear partition from base.

DFS(X,DX) VERSUS X
DFS(X,DX) = ABS(MRF(X+DX) - MRF(X))
DFS(0.,.650)= 7655.5 DFS(23.,.650)= 27.3

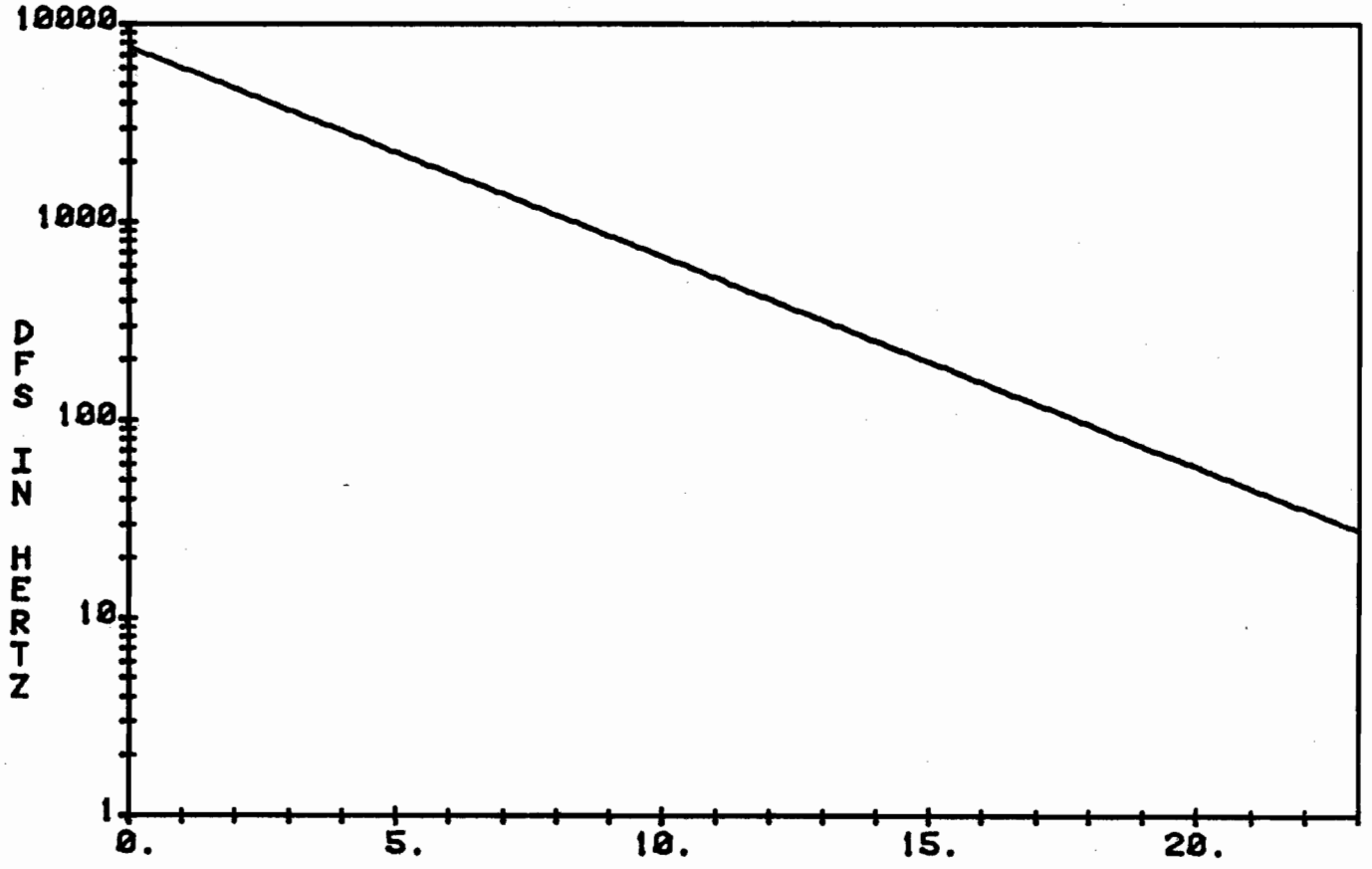

Figure:6.7.4.1.3 Response frequency difference for an inner dendrite and an outer dendrite which enter the same hole of the habenula preforata.

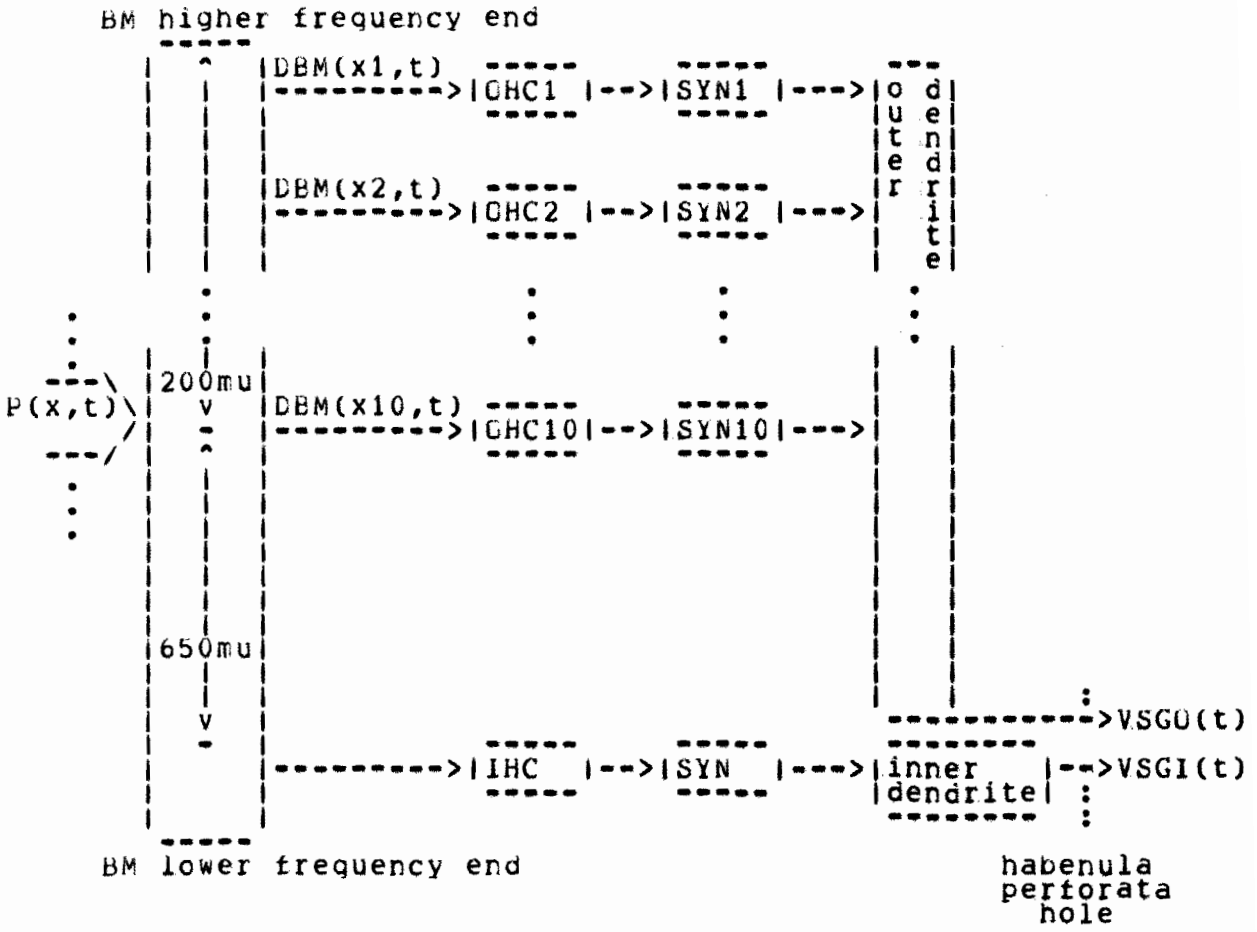

Figure:6.7.4.1.4 Signal processing blocks leading to the dendrites. The basilar membrane, BM, presents the signal to the outer haircells, OHC, and inner hair cells, IHC, which transmit via synapses, SYN, to the inner and outer dendrites which drive the voltage at the spike generating sites, VSG. See text for further discussion.

6.7.4.2 SPECIFICATION

A general outer dendrite is used in the simulation experiments. It has the dimensions previously stated. The specification of the dendrite is given in table:6.7.4.2.1 which is the file read in by the ARKDEN program. Each branch from hair cell synapse to main branch has four compartments of length 2.5 microns and diameter 0.2 microns. The segments between each hair cell branch have four compartments of length 5 microns and diameter 0.5 microns. The long apically going segment is divided into 16 compartments of length 50 microns and diameter 1 micron.

The AP generating site is taken as two compartments, based on the discussion in section 2.3 of this chapter. The first compartment is of length 10 microns, diameter 0.3 microns, $Rm=1.6*10^{5}$ cm^{2} and $Cm=2.5*10^{-9}$ F/cm^{2}. The second compartment is of length 0.7 microns and diameter 0.3 microns with Rm=4000 ohm*cm and $Cm=1.0*10^{-6}$ F/cm^{2}. The axon then begins with 10 compartments each of length 10 microns and diameter 2 microns, with $Rm=1.6*10^{2}$ $ohm*cm^{2}$ and $Cm=2.5*10^{-9}$ F/cm^{2}. The action potentials per second that would be recorded from further along the axon as generated by the AP generating site are directly affected by the events at the site. Also, it is assumed that a good approximation of AP generating site voltage is given by the

post-stimulus time histogram of action potentials. Thus, to avoid complications, the output of the dendrite is taken to be the response voltage at the AP generating site. It corresponds to a narcotized neuron which responds passively to inputs, but elicits no APs.

OUTER.DEN

IT	GDM	CM	DIAM	LEN	
01	0.2E-10	1.3E-14	0.2	2.5	SYNAPSE COMPMNT, 1 ENDED
02	0.2E-10	1.3E-14	0.2	2.5	ELBOW, 2 ENDED
03	0.2E-10	1.3E-14	0.2	2.5	T JUNCTION, 3 ENDED
04	0.2E-10	1.3E-14	0.5	5.0	HORZ COMPMNT, 2 ENDED
05	0.2E-10	1.3E-14	0.5	5.0	VERT COMPMNT, 2 ENDED
06	0.2E-10	1.3E-14	1.0	50.0	LONG COMPMNT, 2 ENDED
07	0.2E-10	1.3E-14	0.5	2.0	AP GEN SITE, 2 ENDED
08	0.2E-13	13.E-14	0.5	2.0	AP GEN SITE, 2 ENDED
09	0.2E-13	13.E-14	2.0	50.0	AXON, 2 ENDED
10	0.2E-13	13.E-14	2.0	50.0	AXON, 2 ENDED, DxxV(x,t)=0
000	0.0	0.0	0.0	0.0	END OF COMPMNT TYPES

IC	IT	IC1	IC2	IC3	IS	
1	1	2	0	0	1	SYNAPSE 1
2	5	3	1	0	0	
3	5	4	2	0	0	
4	5	5	3	0	0	
5	2	6	4	0	0	ELBOW
6	4	7	5	0	0	
7	4	8	6	0	0	
8	4	13	7	0	0	COMP BEFORE T
9	1	10	0	0	2	SYNAPSE 2
10	5	11	9	0	0	
11	5	12	10	0	0	
12	5	13	11	0	0	
13	3	14	12	08	0	T JUNCTION
14	4	15	13	0	0	
15	4	16	14	0	0	
16	4	21	15	0	0	COMP BEFORE T
17	1	18	0	0	3	SYNAPSE 3
18	5	19	17	0	0	
19	5	20	18	0	0	
20	5	21	19	0	0	
21	3	22	20	16	0	T JUNCTION
22	4	23	21	0	0	
23	4	24	22	0	0	
24	4	29	23	0	0	COMP BEFORE T
25	1	26	0	0	4	SYNAPSE 4
26	5	27	25	0	0	
27	5	28	24	0	0	
28	5	29	23	0	0	
29	3	30	28	24	0	T JUNCTION
30	4	31	29	0	0	
31	4	32	30	0	0	
32	4	37	31	0	0	COMP BEFORE T
33	1	34	0	0	5	SYNAPSE 5
34	5	35	33	0	0	
35	5	36	34	0	0	
36	5	37	35	0	0	
37	3	38	36	32	0	T JUNCTION
38	4	39	37	0	0	
39	4	40	38	0	0	
40	4	45	39	0	0	COMP BEFORE T
41	1	42	0	0	6	SYNAPSE 6
42	5	43	41	0	0	
43	5	43	42	0	0	
44	5	45	43	0	0	
45	3	46	44	40	0	T JUNCTION
46	4	47	45	0	0	
47	4	48	46	0	0	
48	4	53	47	0	0	COMP BEFORE T
49	1	50	0	0	7	SYNAPSE 7
50	5	51	49	0	0	
51	5	52	50	0	0	
52	5	53	51	0	0	
53	3	54	52	48	0	T JUNCTION
54	4	55	53	0	0	
55	4	56	54	0	0	
56	4	61	55	0	0	COMP BEFORE T

57	1	58	0	0	8	SYNAPSE 8
58	5	59	57	0	0	
59	5	60	58	0	0	
60	5	61	59	0	0	
61	3	62	60	56	0	T JUNCTION
62	4	63	61	0	0	
63	4	64	62	0	0	
64	4	69	63	0	0	COMP BEFORE T
65	1	66	0	0	9	SYNAPSE 9
66	5	67	65	0	0	
67	5	68	66	0	0	
68	5	69	67	0	0	
69	3	70	68	64	0	T JUNCTION
70	4	71	69	0	0	
71	4	72	70	0	0	
72	4	77	71	0	0	COMP BEFORE T
73	1	74	0	0	10	SYNAPSE 10
74	5	75	73	0	0	
75	5	76	74	0	0	
76	5	77	75	0	0	
77	3	78	76	72	0	T JUNCTION
78	4	79	77	0	0	
79	4	80	78	0	0	
80	4	81	79	0	0	LAST OF BRANCHES
81	6	82	80	0	0	START OF LONG DENDRITE
82	6	83	81	0	0	
83	6	84	82	0	0	
84	6	85	83	0	0	
85	6	86	84	0	0	
86	6	87	85	0	0	
87	6	88	86	0	0	
88	6	89	87	0	0	
89	6	90	88	0	0	CON'T LONG DENDRITE
90	6	91	89	0	0	
91	6	92	90	0	0	
92	6	93	91	0	0	
93	6	94	92	0	0	
94	6	95	93	0	0	
95	6	96	94	0	0	
96	6	97	95	0	0	
97	7	98	96	0	0	AP GEN SITE
98	8	99	97	0	0	AP GEN SITE
99	9	100	98	0	0	
100	9	101	99	0	0	
101	9	102	100	0	0	
102	9	103	101	0	0	
103	9	104	102	0	0	
104	9	105	103	0	0	
105	10	104	0	0	0	LAST COMPMNT

Figure:6.7.4.2.1 Specification file for a general outer dendrite.

6.7.4.3 FREQUENCY BAND INPUT

A first test of the outer dendrite is provided by uniformly exciting all of the ten synapses. This corresponds to a band of frequencies presented to the ear; each of the frequencies has the same amplitude. Thus each synapse receives the input

$$GS(t) = G_{sm} * CS(t)$$

where $G_{sm} = 2.0*10^{-8}$ mho and CS(t) is the continuous window and in the simulation program has the following form, with G_{sm}=SYNSCL,

GS(t) = SYNSCL*WINDOW(T,TON,TOF,TRISE)

as discussed in section 6.5.2.2.4. The response is shown in figures:6.7.4.3-1,2,3,4. The value of synaptic conductance is plotted in the upper right hand corner for synapses 1 to 10, with the maximum value being G_{sm}. The plot at the bottom is the long branch with response voltage versus distance from the first branch from the first hair cell (low frequency side of dendrite). The response of the branches from the hair cells are shown as verticals. It is response voltage V(x,t) versus distance from synapse and the plot is rotated counter clockwise 90 degrees. This arrangement with the vertical plot of the branches and horizontal plot of the long segment depicts the layout. The graph was made as

follows. A conductance plot $GS_i(t)$ is shown for each point in time as a sequence of dots. Each dot represents a point in time. For each point in time, the distribution of voltage versus location is shown as one curve in the graph of that dendrite segment. Thus, the set of synaptic conductance values in time produces a family of voltage versus location curves. The layout of the plot is summarized in figure:6.7.4.3.0.

The response of the dendrite can be understood by first considering the response on the long segment receiving input from the hair cell branches. Note how the left end, with no runoff pathway for current, builds up in voltage compared to the right end with the runoff pathway into the long segment to the habenula perforata. Note the peaking in the center of the region receiving inputs from the hair cell branches with ripples due to the discrete spatial input of the branches. The branches from the hair cells respond to two influences: (1)that from the synaptic input current due to the increased conductance $GS_i(t)$ and (2) the voltage gradient between the horizontal segment and the hair cell branch. Thus magnitude of the hair cell branch response increases just before the horizontal segment response does. The voltage in the 200 micron segment builds up because the only runoff pathway is the long segment. Notice that for

the first increase of synaptic conductances above zero, the 200 micron segment responds to the inputs in a uniform way (marked with a *). After the synaptic conductances are on longer, the center portion of the 200 micron segment increases at a faster rate than the surrounding portions. This could be called a lateral inhibition effect; but it is due to the geometry of the dendrite, which is not an active inhibitory process. As time progresses, the response of the center portion becomes greater and the peak falls off to each side with greater fall off on the side connected to the long dendrite segment.

When the conductance shuts off, the response voltage in the dendrite falls off more uniformly than it increased. Figure:6.7.4.3.2 shows the complete response of the dendrite in time for a continuous window input. The spatial response to the distal synapses excited before the proximal synapses is shown in figure:6.7.4.3.1 (-a is early, -b is late response). Figure:6.7.4.3.1-c shows the ensemble of synaptic conductance changes for an "auditory frequency downsweep". Figure:6.7.4.3.2 shows the response to all ten synapses activated at the same time. This corresponds to an "auditory frequency band" input.

A projected three dimensional plot is used in figure:6.7.4.3.3 to depict the reponse to all ten synapses

activated in synchrony. To facilitate the interpretation of this plot, a gray level plot is shown for this same response in figure:6.7.4.3.4. Response potential is shown as gray level versus spatial postion and time. The important feature of the response to the changing conductance is the evenness in tne spatial coordinate. This is due to the longitudinal conductance in the dendrite core, or equivalently in the partial differential equation, due to the second derivative of response voltage with respect to distance. The decay has the time constant of the partial differential equation.

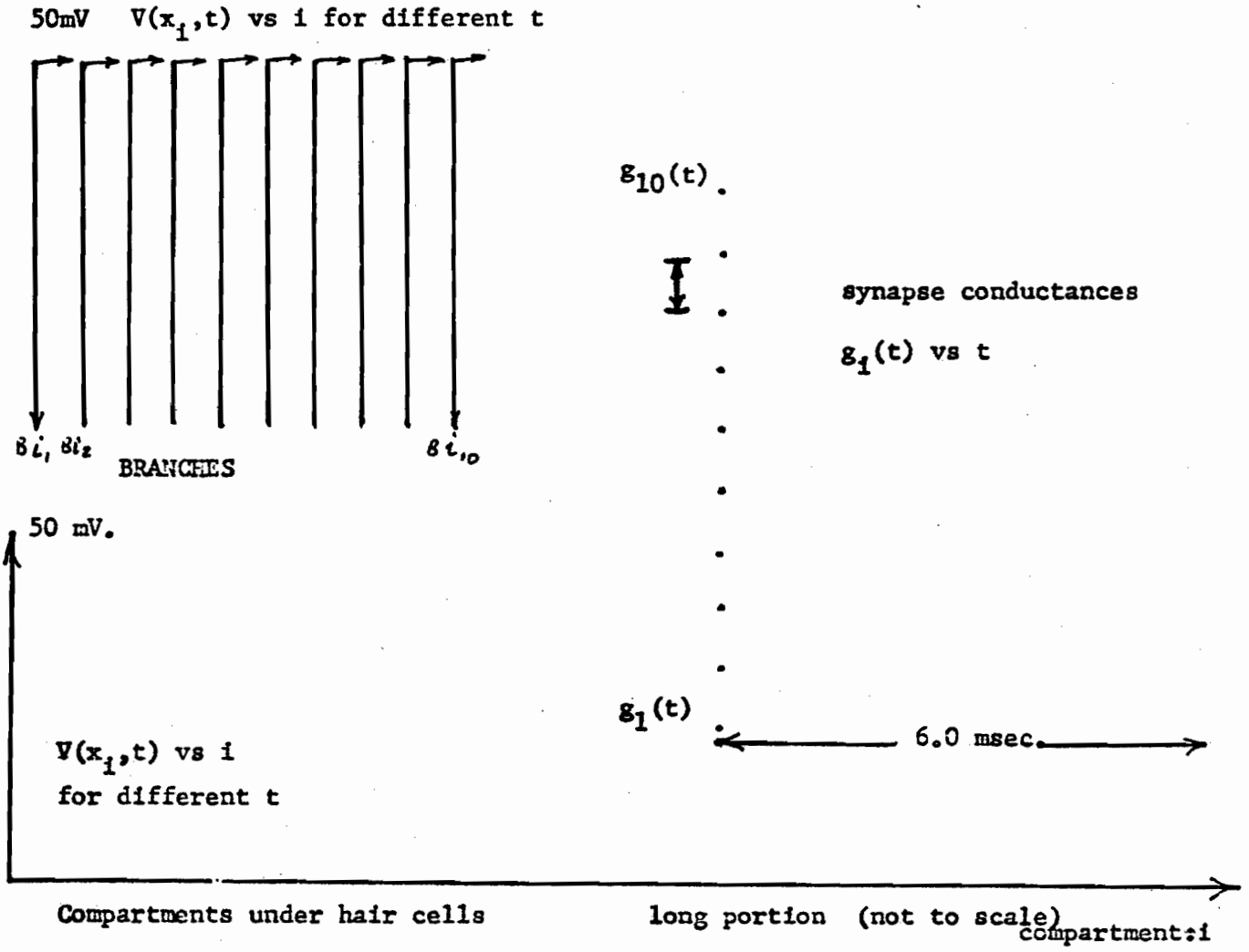

Figure:6.7.4.3.0 Summary of outer dendrite response plots. The upper left graphs are voltage versus distance on each branch for successive time steps. The rightmost graphs are synaptic conductance versus time (one dot per time step) for the 10 synapses. The bottom graph is voltage versus position on the long portion of the denrite, for successive time steps.

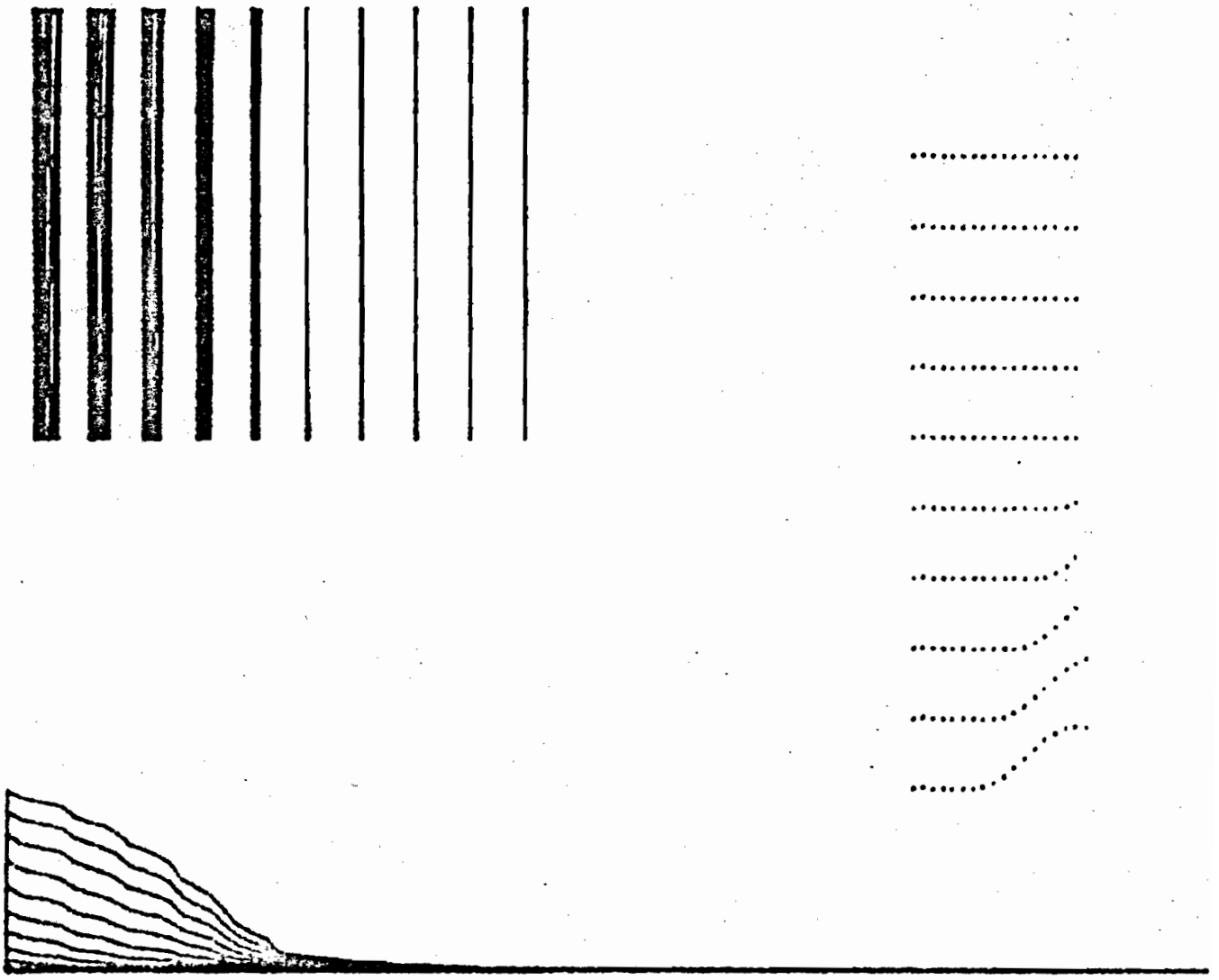

Figure:6.7.4.3.1-a The response of an outer dendrite to excitation of the distal synapses first, followed by excitation of the more proximal synapses.

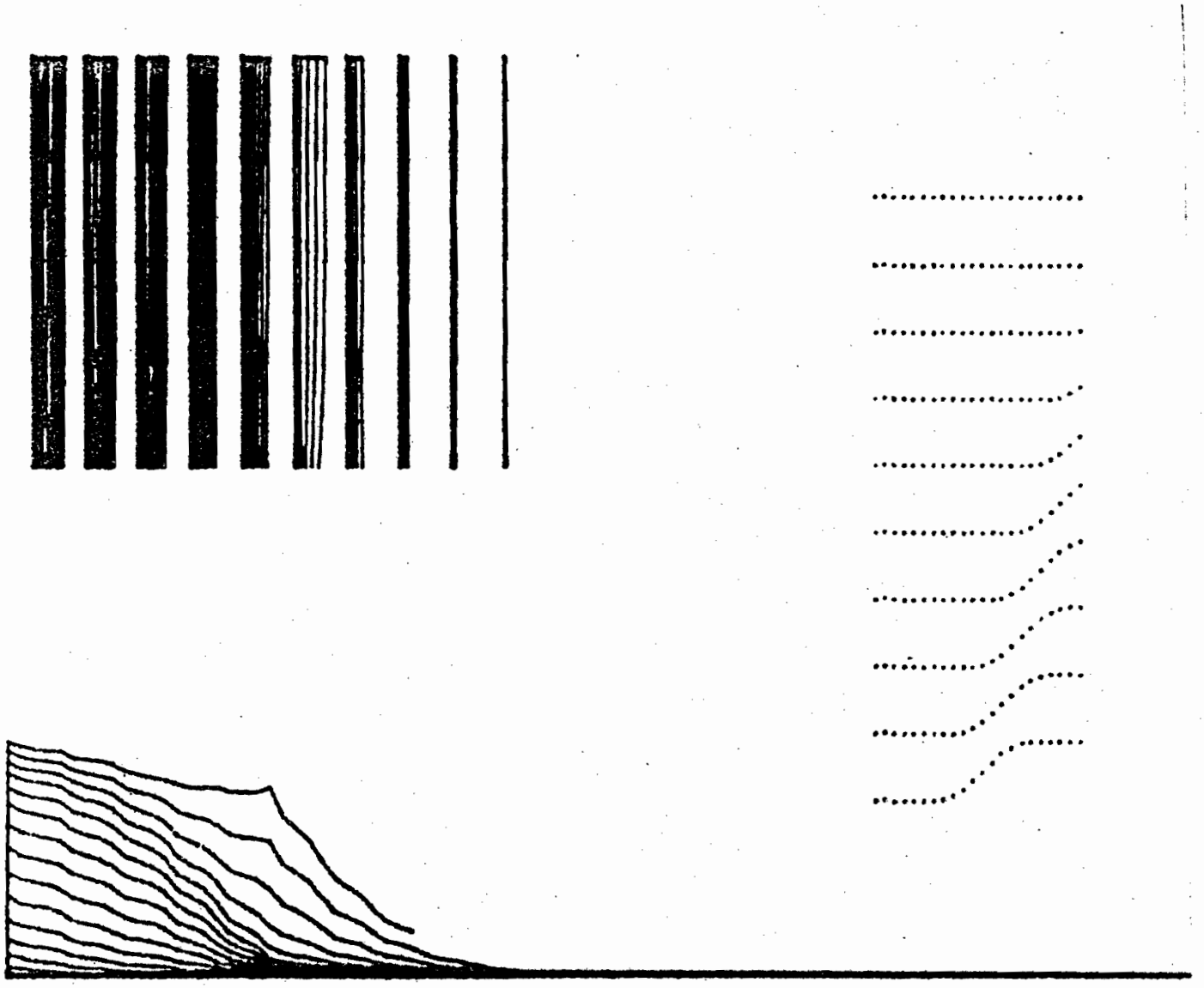

Figure:6./.4.3.1-b Same as for (a) but for later time.

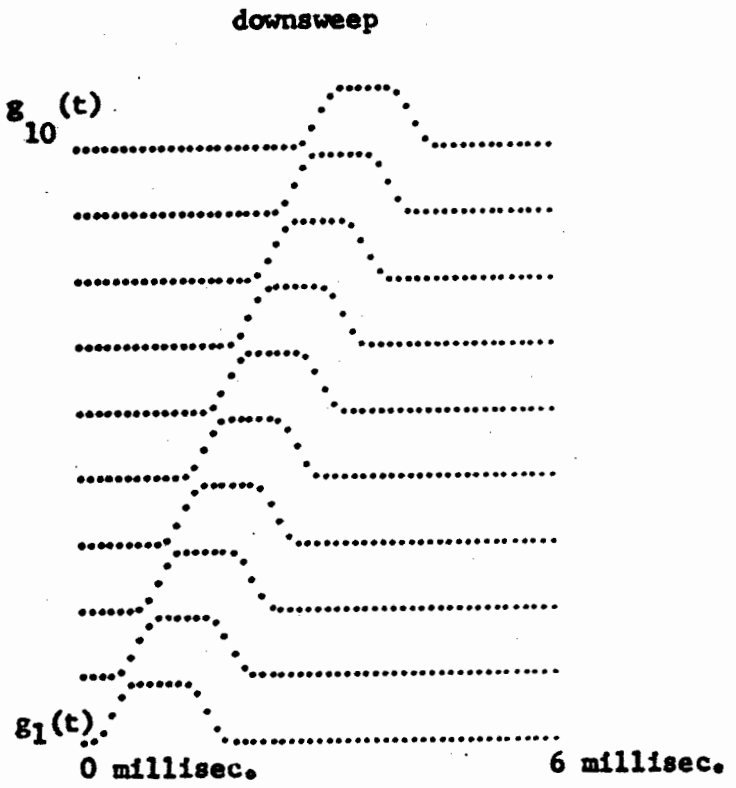

Figure:6.7.4.3.1-c This is the type of synaptic conduction signals used as excitation. Each synaptic conductance $g_i(t)$ is a smooth pulse. The signal $g_1(t)$ is the conductance at the most distal synapse and $g_{10}(t)$ is conductance at the most proximal synapse. Depicted is a down sweep of "auditory input frequency".

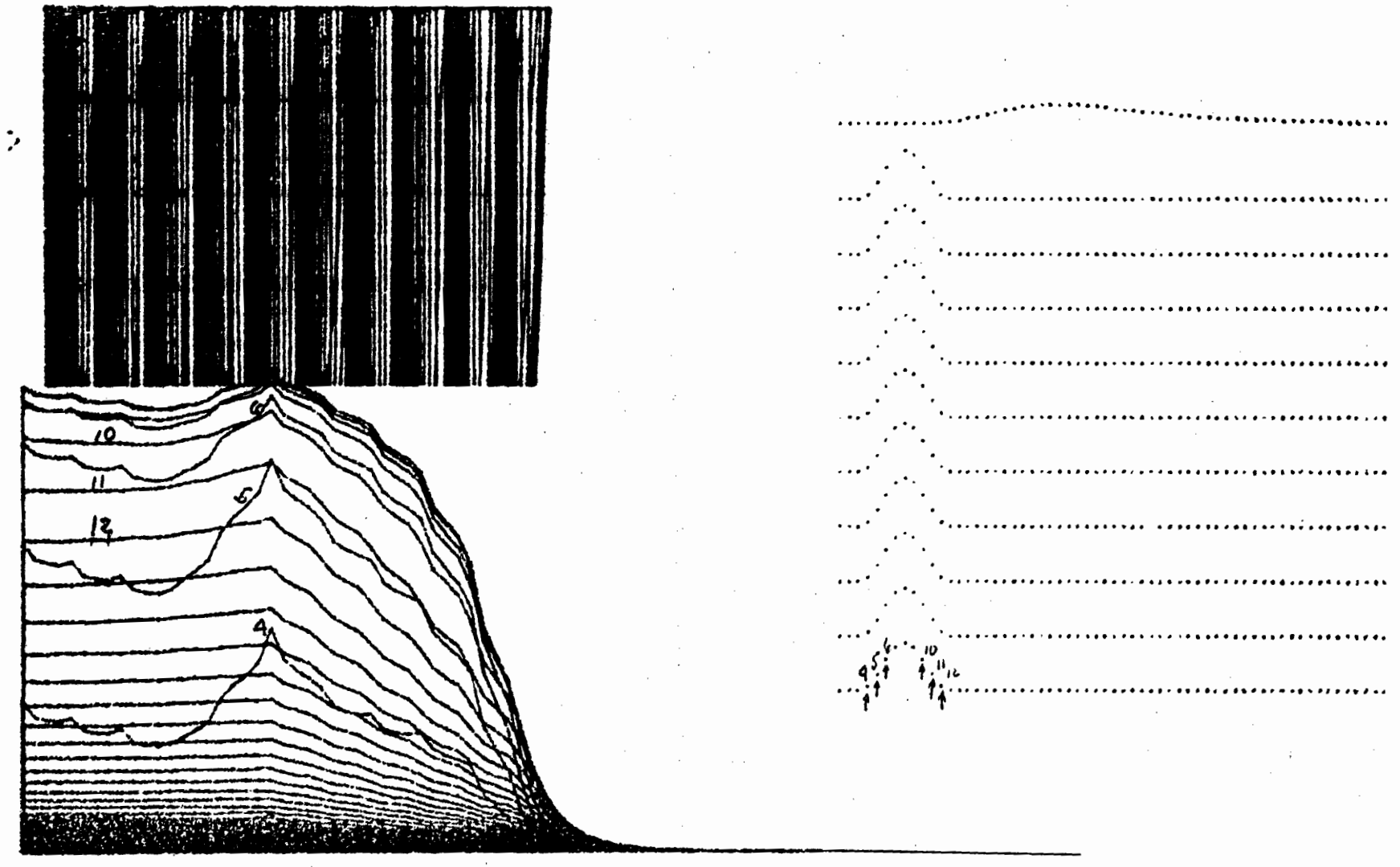

Fig 6.7.4.3.2 p 6-120

Figure:6.7.4.3.2 The response to all synapses active at the same time (frequency band input). The responses to the increasing synaptic conductances are numbered by 4,5,6. The responses to the decreasing part are indicated by 10,11,12.

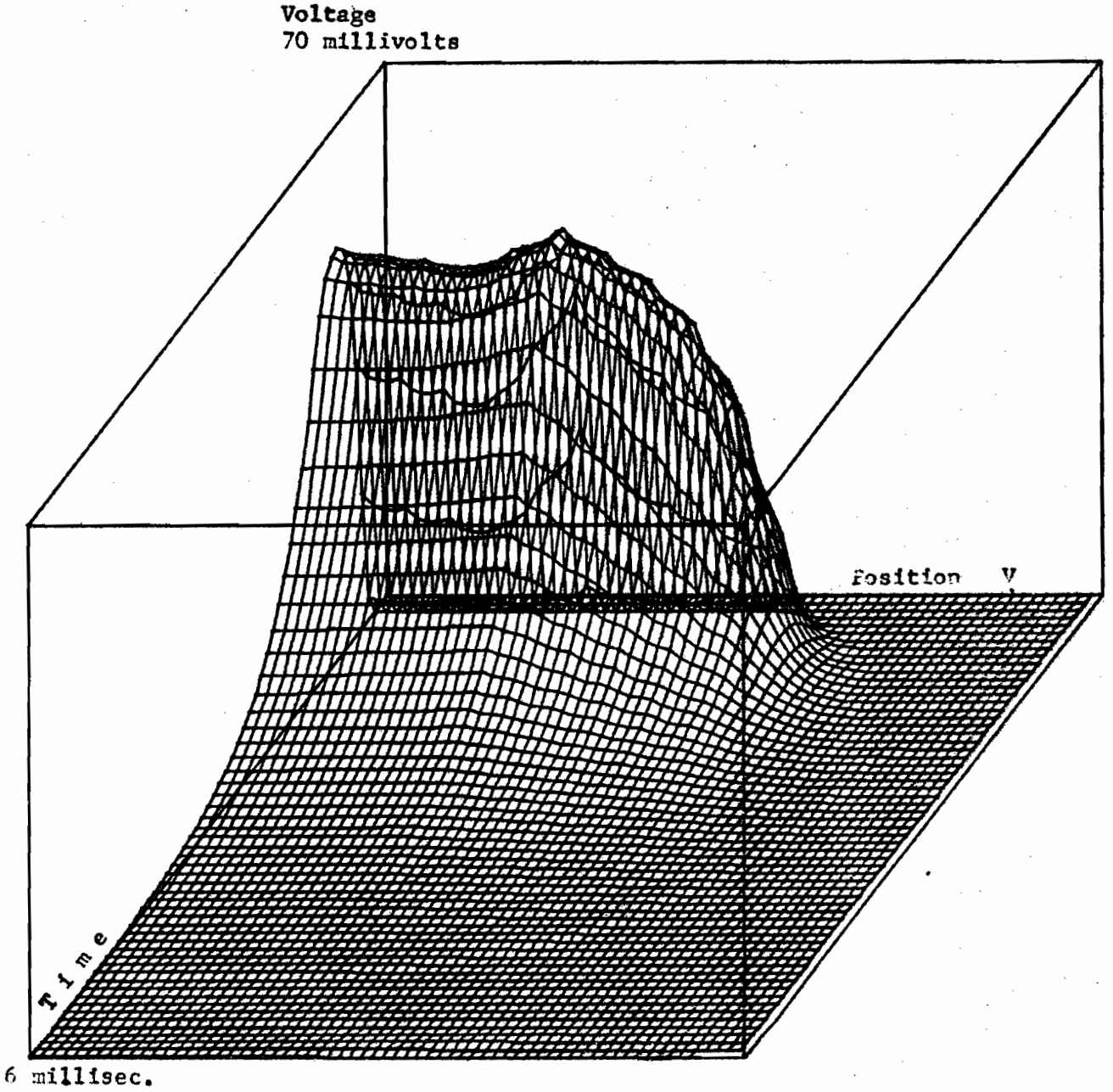

Figure:6.7.4.3.3 The response to all ten synapses activated at the same time, shown as a three dimensional plot. The response voltage is the vertical axis, position is the horizontal axis ("V" denotes the AP generating site), and time is along the diagonal axis (increasing time is downward to the left).

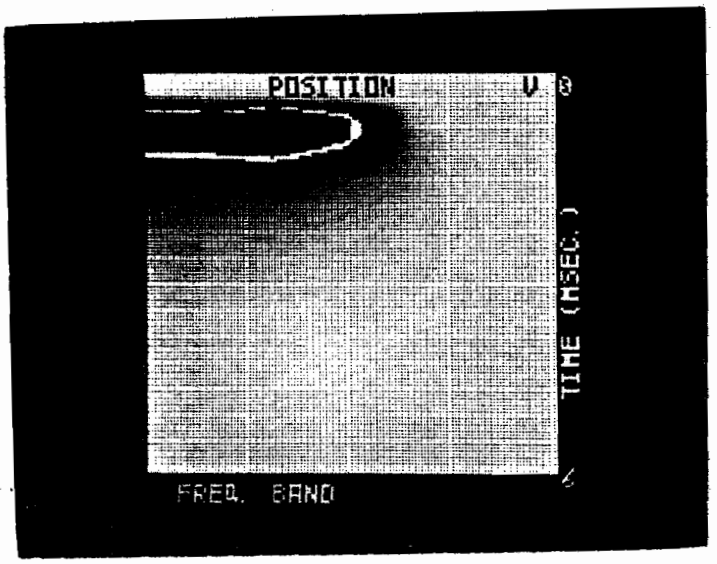

Figure:**6.7.4.3.4** The response to all ten synapses activated at the same time, shown as a gray value plot. The response voltage is plotted as a gray value. A voltage value of 0.0 millivolts is gray value 0 (white), and 63.0 millivolts is gray value 63 (black). The black region indicates an increase in response potential. The white region in the black region indicates the response voltagae interval of 40

to 45 millivolts. The AP generating site is indicated by "V".

6.7.4.4 FREQUENCY SWEEPS

What happens when the synapses on one end of the dendrite are activated before the synapses on the other end? This corresponds to a tone sweep delivered to the ear drum.

6.7.4.4.1 UPSWEEPS

Figures:6.7.4.4.1-a,b,c show the response for synaptic excitation arriving first at the low frequency end (right hand end -- apical end), then progressing along to the high frequency end (basal). There is an increase in response voltage at the low frequency end of the 200 micron segment which is earlier and larger than the response at the other end. Also note that the long segment follows more closely than the high frequency end. This is due to more drain off pathways to the high frequency side and a larger space constant of the long segment. The space constant is proportional to the square root of the fiber radius and the long segment has diameter 2.5 times larger that the 200 micron segment. These plots were done for R_m=1000 ohm*cm.

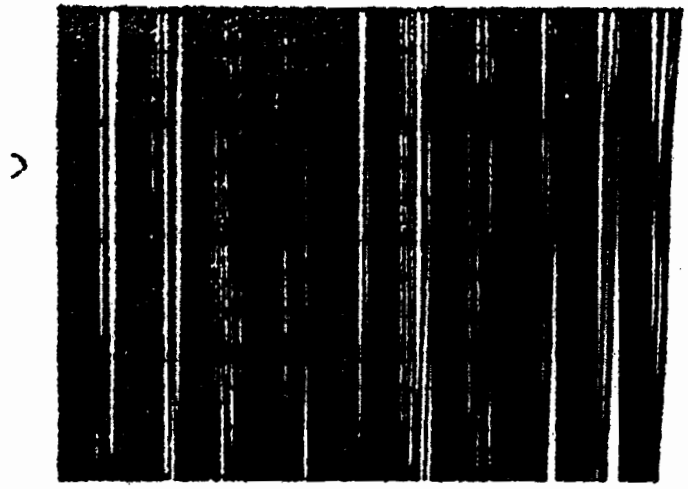

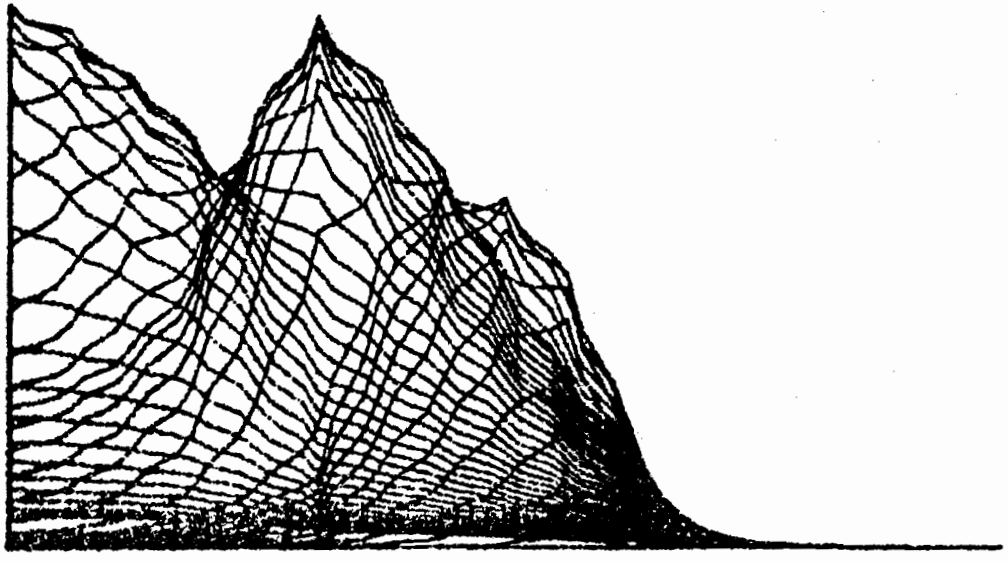

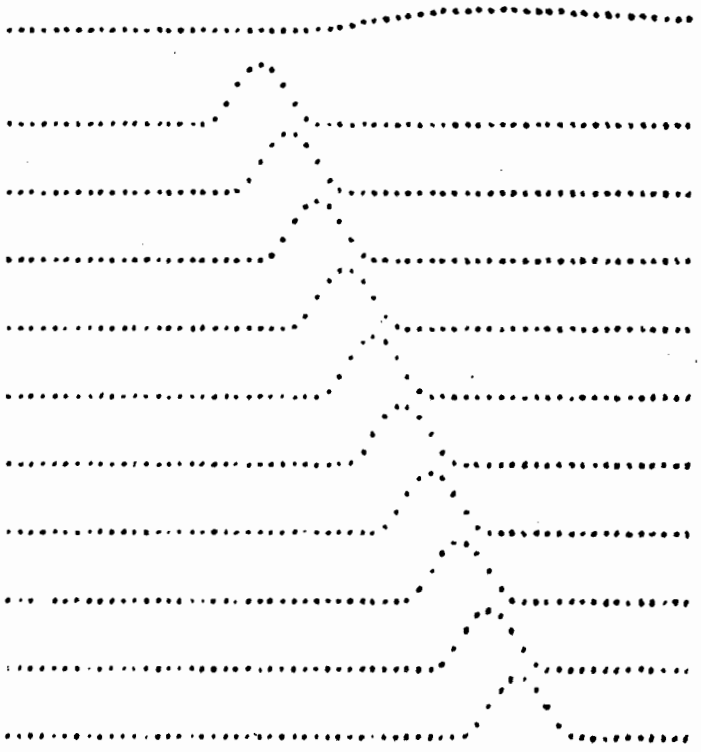

Fig 6.7.4.4.1-a

Figure:6.7.4.4.1-a Dendrite response for synaptic excitation arriving first at the low frequency end (left hand end). This is an upsweep of frequency. See text. Same scale as for band input.

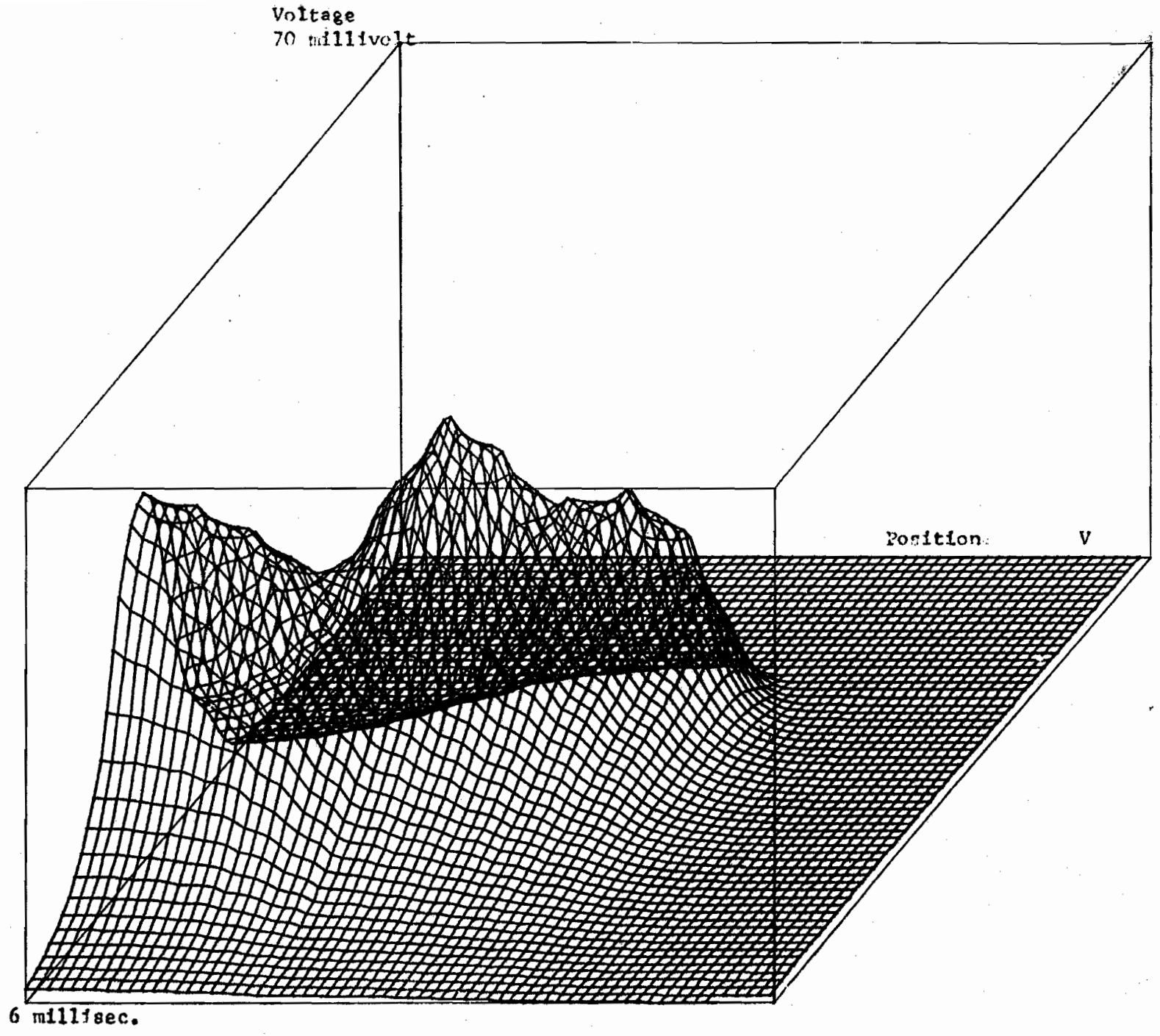

Fig 6.7.4.4.1-b p. 6-126

Figure:6.7.4.4.1-b The response to ten synapses activated in the sequence as would be caused by upsweep in frequency of an auditory signal. It is shown as a three dimensional plot. The response voltage is the vertical axis, position is the horizontal axis ("V" denotes the AP generating site), and time is along the diagonal axis (increasing time is downward to the left). Same scale as for band input.

Figure:6.7.4.4.1-c The response to all ten synapses activated in the sequence as would be caused by an upsweep in auditory input frequency. The response potential is plotted as a gray value. A voltage value of 0.0 millivolts is gray value 0 (White), and 63.0 millivolts is gray value 63 (black). The black region indicates an increase in response potential. The white region in the black region indicates the response voltage interval of 40 to 45 millivolts. The AP generating site is indicated by "V".

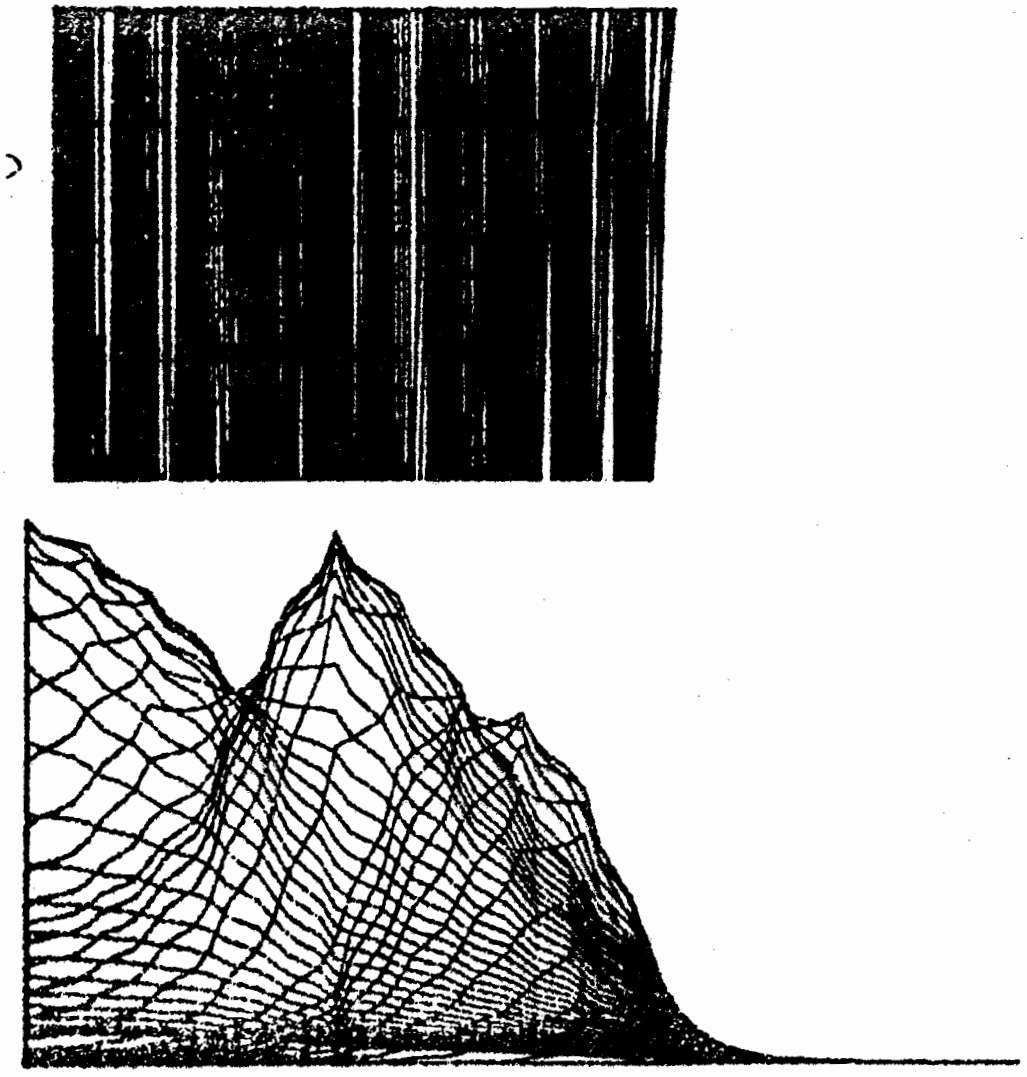

FIG. 6.7.4.4.2-a

Figure:6.7.4.4.2-a Dendrite response for synaptic excitation arriving first at the low frequency end (right hand end). This is a downsweep of frequency. See text.

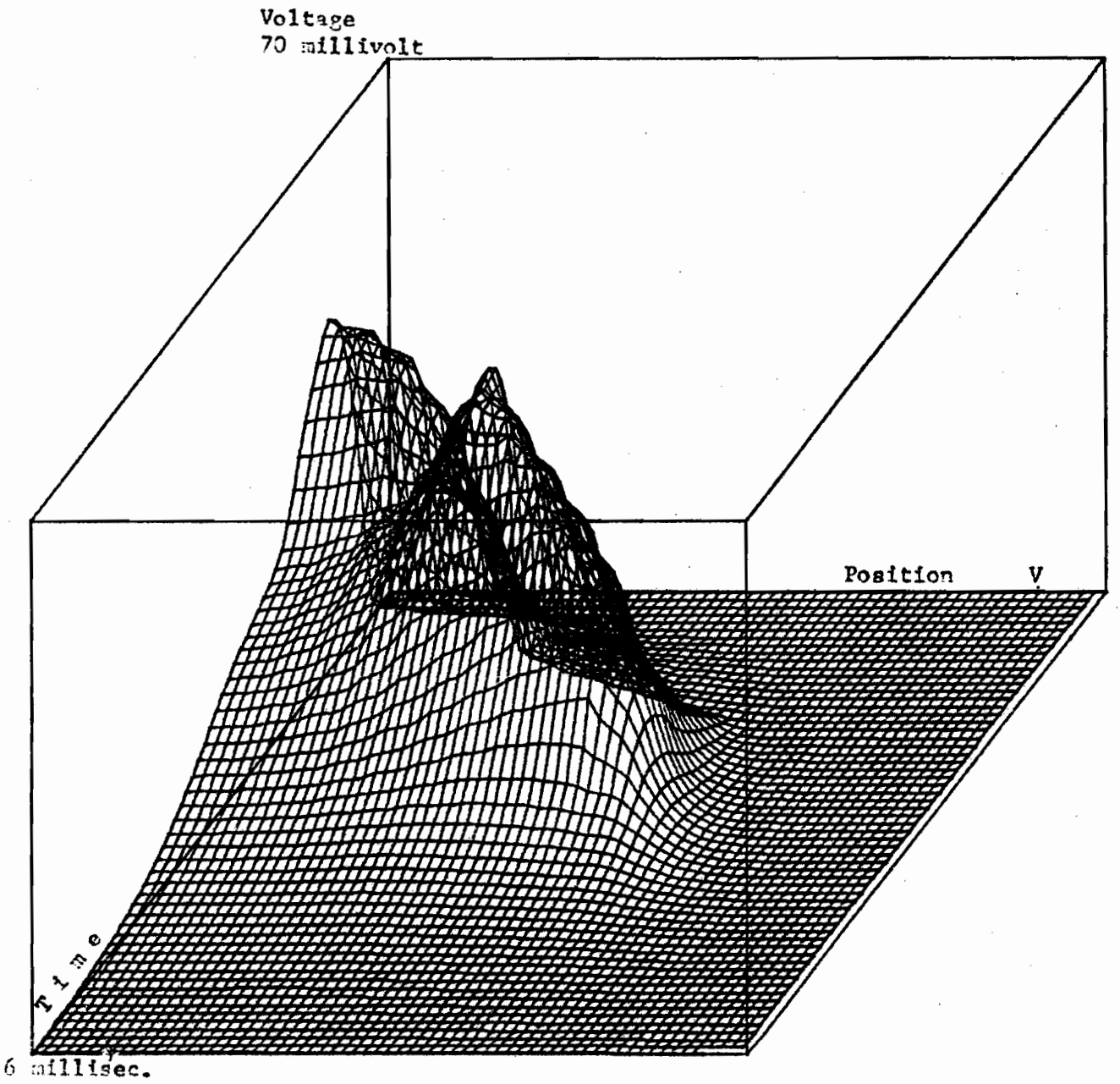

Figure:6.7.4.4.2-b The response to ten synapses activated in the sequence as would be caused by a downsweep in frequency of an auditory signal. It is shown as a three dimensional plot. The response voltage is the vertical axis, position is the horizontal axis ("V" denotes the AP generating site), and time is along the diagonal axis (increasing time is downward to the left).

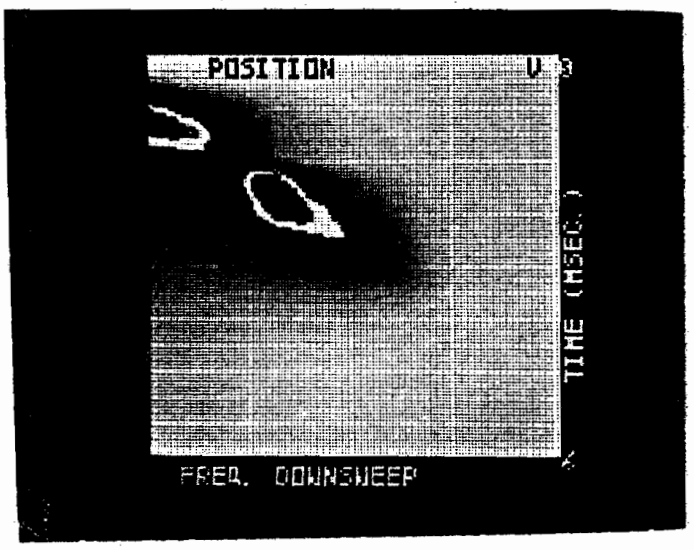

Figure:6.7.4.4.2-c The response to all ten synapses activated in the sequence as would be caused by a downsweep in auditory input frequency. The response potential is plotted as a gray value. A voltage value of 0.0 millivolts is gray value 0 (white), and 63.0 millivolts is gray value 63 (black). The black region indicates an increase in response potential. The white region in the black region indicates the response voltage interval of 40 to 45 millivolts. The AP generating site is indicated by "V".

6.7.4.4.2 DOWNSWEEPS

Figures:6.7.4.4.2-a,b,c show the response of the outer dendrite for synaptic excitation arriving first at the high frequency end (left hand--basal end), then progressing to the other end (low frequency end).

6.7.4.5 OUTER DENDRITE CONCLUSIONS

For an outer dendrite it was seen that the type of inputs that affect the largest response at the AP generating site, in decreasing order of affectiveness are: 1)a frequency band (all synapses active), 2)frequency downsweep (base to apex synapses sequentially activated) and 3)frequency upsweep (apex to base synapses sequentally activated). A frequency band is not as common as frequency sweeps. Thus the outer dendrites are predicted to be frequency downsweep feature detectors.

Having noted that the optimal stimulus is a down sweep in auditory frequency, one may ask what happens at the action potential generating site. Reconsider the figures showing the response for the outer dendrites. The voltage at the spike generating site is in fact too low to generate an action potential, for any AP threshold in the literature. The reason for its small amplitude is that the dendrite fibers are small (diameter 1 micron) and long (650 microns)

in the region from outer hair cells to the habenula. This agrees with the space constant (section 6.3.7) of 408 microns.

Thus it is predicted by these simulations that afferent fibers from outer hair cells do not generate action potentials. It is suggested that the absence of AP's results in a lack of trophic influence necessary for the axons to grow up the cochlear nerve.

6.8 DENDRITE CONCLUSION

It was found that it is possible to simulate dendrites which have irregular unsymmetric geometries. The synapses need not have a prescribed timing pattern of excitation dependent on the geometry of the dendrite tree for simulation. It was seen that the synapses constitute a non-linear boundary condition that makes it impossible for even a simple straight unbranched dendrite to yield an analytic solution, even in series form.

A method of simulating any geometric branching pattern was developed which allows dendrite parameters that change with respect to position in the dendrite tree. The simulation uses a new direct integration technique, the Wynn-Lau-Houwen FORTRAN subroutine ARK. The technique uses an adaptive Runge-Kutta method which is stabilized for a

large number of equations, as arise in the simulation of partial differential equations. The technique also allows for greatly different size compartments and different values of membrane resistivity and capacitance. These differences of parameters are expressed in the system of differential equations as greatly different magnitudes of the elements in the system Jacobian matrix.

It was found that a dendritic tree has two kinds of nonlinearities, the first being the synapse and a second, the effect which the dendrite tree shape has on the action potential shape. These nonlinearities are unconditional nonlinearities, in that a dendrite is nonlinear even for small time or a particular frequency range.

It was found that the inner dendrites reflect what is happening in the one innervating hair cell because the space constant of an inner dendrite is much longer that the length of the dendrite from synapse to AP generating site and the inner dendrite is unbranched. It was found that an outer dendrite responds optimally to synaptic excitation which is uniformly presented, compared to a sweep of synaptic excitation along the synapse. This uniform excitation of synapses provides the maximal synaptic input current in synchrony, an instance of both spatial and temporal summation. The frequency band input does not occur commonly

in nature. A more common naturally occuring auditory signal is a tone sweep which is very common as a dominant component of animal distress cries and human whine vocalizations. It was found that downsweeps in frequency causes maximal excitation of the outer dendrites as compared to upsweeps. The downsweep in frequency causes a sweep of synaptic excitation from the distal to proximal end of a cochlear outer dendrite. The voltage response to a downsweep is larger than an upsweep because the response to the high initial frequencies is conducted to the low frequency end (proximal end) so that when the response to low frequencies arrives, there is temporal summation to produce a larger result than if the event times were reversed. This result agrees with the behavioral and psychophysical evidence that the frequency downsweeps are dominant features of mammalian distress vocalizations (Winter et al, 1966; Worden & Galambos, 1972).

For the outer dendrite, it was found that the voltage at the AP generating site is too small to generate action potentials. This is interesting in that the space constant, 408 microns, is in the range where it is hard to say unequivocally that at a distance 650 microns from the synaptic input, that the response voltage is too small to trigger action potentials.

REFERENCES: CHAPTER 6

Ades,H.W. & Engstrom,H. (1972) Inner ear studies. Acta Otolaryngol. Suppl. 301.

Armstrong,C.M. (1975) Ionic pores and gates in nerve membranes. Nineteenth Bowditch lecture. Physiologist 18(2):93-98.

Bekesy,G. von (1949) The vibration of the cochlear partition in anatomical preparation and in models of the inner ear. J.Acous.Soc.Amer.21:233-245.

Bekesy,G. von (1960) Experiments in Hearing. McGraw-Hill, New York. 745P.

Barrett,J.N. & Crill,W.E. (1974) Specific membrane properties of cat motoneurones. J. Physiol. (London) 239(2):301-324.

Billone,M.C. (1972) Mechanical stimulation cochlear hair cells. Thesis. Northwester Univ. Evanston, Ill.

Cajal,R. (1909) Histololgie du systeme nerveux de l'homme et des vertebres. Norbert Malonie, Paris, 2 vols.

Carnahan,B., Luther,H. & Wilkes,J. (1969) Applied Numerical Methods. John Wiley & Sons, Inc., N.Y. 604P.

Carslaw,H.S. and Jaeger,J.C.(1959) Conduction of Heat in Solids, 2nd Ed. Oxford University Press, London. 510P.

Cole,K.S. & Baker,R.F. (1941a) Transverse impedance of the squid giant axon during current flow. J.Gen. Physiol. 24:535.

Cole,K.S. & Baker,R.F. (1941b) Longitudinal impedance of the squid giant axon. J.Gen. Physiol. 24:771.

Cole,K.S. & Hodgkin, A. L. (1939) Membrane and protoplasm resistance in the squid giant axon. J. Gen. Physiol. 22:671.

Curtis,D.R., Duggan,A.W., Felix,D., Johnston,G.A.R., Tebecis,A.K., & Watkins,J.C. (1972) Excitation of mammalian central neurons by acidic amino acids. Brain Res. 41:283.

Dallos,P.M., Billone,M.C., Durrant,J.D., Wang,C.y., and Raynor,S. (1972) Cochlear inner and outer hair cells: Functional differences. Science 177:356-358.

Dallos,P.M.(1973) Cochlear potentials and cochlear mechanics. In: Basic Mechanisms in Hearing. Moller,A. (ed.) Academic Press, N.Y., pp335-372.

D'Angelo,H.(1970) Linear Time-Varying Systems. Allyn and Bacon, Boston. 346P.

DEC (1977) RSX-11M Task Builder Reference Manual, Order No. AA-2588D-IC Digital Equipment Corporation, Manyard, Mass.

Duifhuis,H. (1976) Cochlear nonlinearity and second filter: Possible mechanism and implications. J.Acoust.Soc.Am. 59(2):408-423.

Dunn,R.A. (1975) A comparison of Golgi impregnated innervation patterns and fine structural synaptic morphology in the cochlea of the cat. Ph.D. Thesis. Harvard Univ. Cambridge,Mass. 165P.

Eccles,J.C. (1964) The Physiology of Synapses. Springer-Verlag, Berlin.

Elliot,I.B.(1972) FLAP, a simplified simulation system for time share users. Simulation. July 1972:19-32.

Engstrom,H., Ades,H.W. & Anderson,A. (1966) Structural Pattern of the Organ of Corti. Almquist & Wiksell, Stockholm. 172P.

Evans,E.F. & Wilson,J.P. (1973) The frequency selectivity of the cochlea. In: Basic Mechanisms in Hearing, A.R. Moller (ed.) Academic Press, N.Y. pp519-554.

Fatt,P. & Katz,B. (1951) An analysis of the end-plate potential recorded with an intracellular electrode. J. Physiol. 115:320-370.

Fatt,P. (1954) Biophysics of junctional transmission. Physiol. Rev. 34:674-710.

Frankenhauser,B., Hodgkin,A.L., & Huxley,A.F. (1963) A quantitative description of potassium currents in myelinated nerve fibers of Xenopus laevis. J. Physiol. 129:424.

Gacek,R.R. (1967) Afferent auditory neural system. In: Sensorineural Hearing Processes and disorders. Graham,A.B. (ed.) Little, Brown & Co.,Boston. pp49-59.

Gacek,R.R. & Rasmussen,G.L.(1961) Fibre analysis of the statoacoustic nerve of guinea pig, cat, and monkey. Anat. Rec. 139:455-463.

Geer,C.W.(1971a) The automatic integration of ordinary differential equations. Comm. A.C.M. 14(March,1971):176-179.

Geer,C.W.(1971b) DIFSUB for solution of ordinary differential equations. Comm. A.C.M. 14(March,1971):185-190.

Hearon,J.Z.(1963) Theorems on Linear Systems. Ann. N.Y. Acad. Sci. 108(1):36-39.

Hodgkin,A.L. & Rushton,W.A.H. (1946) The electrical constants of a crustacean nerve fiber. Proc. Roy. Soc. Ser. B. (Lond.) 133:444-479.

Hodgkin,A.L. & Katz,B. (1949) The effect of sodium on the electrical activity of the giant axon of the squid. J.Physiol. 108:37.

Hodgkin,A.L. & Huxley,A.F. (1952) A quantitative description of membrane current and its application to conduction and excitation in nerve. J. Physiol. 117:500-544.

Houwen,P.J.van der (1971a) Stabilized Runge-Kutta methods with limited storage requirements. Report TW 124/71, Mathematisch Centrum, Amsterdam.

Houwen,P.J.van der (1971b) A survey of stabilized Runge-Kutta methods. MC-25 Informatica Symp., Mathematich Centrum. Amsterdam.

Hull,T.E., Enright,W.H. Fellen,B.M., & Sedgwick,A.E. (1972) Comparing numerical methods for ordinary differential equations. SIAM J. Numer. Anal. 9(4):603-637.

IMSL (1975) IMSL Library Reference Manual International Mathematical and Statistical Libraries,Inc. 7500 Bellair Blvd. Houston, Texas. 3vols.

Inselberg,A. (1978) Cochlear dynamics: The evolution of a mathematical model. SIAM Rev. 20(2):301-351.

Johnstone,B.M. and Boyle,A.J.T.(1967) Basilar membrane vibration examined with the Mossbauer technique. Science 158:389-390.

Johnstone,B.M., Taylor,K.J., and Boyle,A.J.T. (1970) Mechanics of guinea pig cochlea. J.Acous.Soc.Amer. 47:504-509.

Katz,B.(1966) Nerve, Muscle, and Synapse. McGraw Hill Book Co. N.Y.

Katz,B.(1967) A study of synaptic transmission in the absence of nerve impulses. J. Physiol. 192:407-436.

Katz,B.(1969) The release of neural transmitter substances. Thomas, Springfield, Ill.

Kiang,N.Y.S, Sachs, M.B. & Peake,W.T. (1967) Shapes of tuning curves for single auditory-nerve fibers. J. Acoust. Soc. Amer. 42(6):1341-1342.

Lawson,J.D.(1966) An order five Runge-Kutta process with extended region of stability. SIAM J. Numer. Anal. 3:593.

Liniger,W. and Willoughby,R.A.(1970) Efficient integration methods for stiff systems of ordinary differential equations. SIAM J. Numer. Anal. 7:47.

Lorente de No,R. (1935) The function of the central acoustic nuclei examined by means of the acoustic reflexes. Laryngoscope 45(8):573-595.

Lorente de No,R. (1937) The sensory endings in the cochlea. Laryngoscope 47:373-377.

Manley,G. (1977) Personal communication.

Myers,G.E.(1971) Analytical Methods in Conduction Heat Transfer. McGraw Hill Book Co., N.Y. 508P.

Parlette,B. (1978) Progress in Numerical Analysis. SIAM Rev. 20(30):443-456.

Perkins,R.E. & Morest,D.K. (1975) Innervation pattern in the cochlea of the cat and rat: Study of surface preparations with rapic Golgi techniques and differential interference constrast microscopy. J.Comp.Neurol. 163:129-158.

Rall,W. (1959) Branching dendritic tress and motorneuron membrane resistivity. Exp.Neurol. 1:491-527.

Rall,W. (1960) Membrane potential transient and membrane time constants of motor neurnons. Exp.Neurol. 2:503-532.

Rall,W. (1962a) Theory of physiological properties of dendrites. Ann.N.Y.Acad.Sci. 96:1071-1092.

Rall,W. (1962b) Electrophysiology of a dendritic neuron model. Biophys.J. 2:145-167.

Rall,W. (1964) Theoretical significance of dendritic trees for neuronal input-output relations. In: Neural Theory and Modeling. R.F.Reiss (ed.) Stanford Univ. Press. Stanford. pp73-97.

Rall,W. (1970) Cable properties of dendrites and effects of synaptic location. In: Excitory Synaptic Mechanisms. P.Anderserson & J.K.S.Jansen (eds.) Universitetsforlaget. Oslo. pp173-187.

Rhode,W.S. (1971) Observations of the vibration of the basilar membrane in squirrel monkeys using the Mossbauer technique. J.Acous.Soc.Amer. 49:1218-1231.

Russell,I.J. & Sellick,P.M. (1977) Tuning properties of cochlear hair cells. Nature 267:858-860.

Shampine,L.F. and Gordon,M.K. (1975) Computer Solution of Ordinary Differential Equations--The Initial Value Problem. Freeman Co., San Francisco. 318P.

Sohmer,H.S., Peake,W.T. & Weiss,T.F. (1971) Intracochlear potential recorded with micropipets. I. Correlations with micropipet location. J. Acoust. Soc. Am. 50:572-586.

Smith,G.D.(1969) Numerical Solution of Partial Differential Equations. Oxford Mathematical Handbooks, Oxford University Press, Toronto. 179P.

Spoendlin,H.H. & Gacek,R.R. (1963) Electronmicroscopic study of the efferent and afferent innervation of the organ of Corti in the cat. Ann. Otol. Rhin. Laryng. 72(3):660-687.

Spoendlin,H.H. (1962) Ultrastructural features of the organ of Corti in normal and Acoustically stimulated animals. Ann. Otol. 71:657-677.

Spoendlin,H.H. (1966) The organization of the cochlear receptor. Adv. Oto-Rhinolaryng. (Fortschitte der Hals-Nasen-Ohrenheilkunde) Vol. 13 227P.

Spoendlin,H.H. (1969) Innervation patterns in the organ of Corti of the cat. Acta Otolaryngol. 67:239-254.

Spoendlin,H.H. (1970) Structural basis of peripheral frequency analysis. In: Frequency Analysis and Periodicity Detection in Hearing. Plomp,R, Smoorenburg,G.F., & Soesterberg,J. (ed.) Sijthoff, Leiden. pp1-40.

Spoendlin,H.H. (1971a) Degeneration behavior of the cochlear nerve. Arch. klin. exp. Ohr., Nas. u. Kellk. Heilk. 200:275-291.

Spoendlin,H.H. (1971b) Primary structural changes in the organ of Corti after acoustic overstimulation. Acta Otolaryngol. (Stockh.) 71:166-186.

Spoendlin,H.H. (1972) Innervation densities of the cochlea. Acta Otolaryngol. 73:235-248.

Spoendlin,H.H. (1973) The innervation of the cochlear receptor. In: Basic Mechanisms in Hearing, Moller,A. (ed.) Academic Press. N.Y. pp185-234.

Spoendlin,H.H. (1974) Neuroanatomy of the cochlea. In: Facts and Models in Hearing. Zwicker,e. & Terhardt,E. (eds.) Springer-Verlag. N.Y. pp18-36.

Spoendlin,H.H. (1979) Neural connections of the outer haircell system. Acta Otolaryngol. 87:381-387.

Stampfli,R. (1954) Saltatory conduction in nerve. Physiol. Rev. 34:101.

Weinstock,R. (1952) Calculus of Variations. McGraw-Hill Book Co. New York.

Wiley,C.R. (1960) Advanced Engineering Mathematics, 2nd Ed. McGraw-Hill Book Co., New York. 696P.

Wilson,J.P. (1974) Basilar membrane vibration data and their relation to theories of frequency analysis. In: Facts and Models in Hearing, E.Zwicker & E.Terhardt (eds.) Springer-Verlag, N.Y. pp56-74.

Woodward,J.K., Bianchi,C.P. & Erulkar,S.D. (1969) Electrolyte distribution in rabbit superior cervical ganglion. J. Neurochem. 16:289-299.

Worden,F.G. & Galambos,R. (1972) Auditory Processing of Biologically Significant Sounds. Neurosci. Res. Prog. Bull. 10 (Feb. 1972)

Winter,P., Ploog,D. & Latta,J. (1966) Vocal repertoire of the squirrel monkey (Saimiri sciureus), its analysis and significance. Exp. Brain Res. 1:359-384.

Wynn,P. and Lau,H.T. (1978) Notes for the operation of ARK. Computer Science Dept., McGill University, Montreal.

Zadeh,L.A. and Desoer,C.A. (1963) Linear System Theory. McGraw Hill Book Co., N.Y. 628P.

Zienkiewicz,O.C. (1967) The Finite Element Method in Structural and Continuum Mechanics. The McGraw-Hill Publishing Co. Ltd. London.

Chapter 7: CONCLUSION

7.1 Introduction

7.2 Model Development

7.3 Results

7.4 Future Directions

7.4.1 Theoretical Work

7.4.2 Experimental Work

7.5 Contributions to Knowledge

CHAPTER 7
CONCLUSION

7.1 INTRODUCTION

The overall aim of the project was to analyze the signal processing mechanisms in the cochlea. This is important because: (1)It integrates a large amount of experimental data and verifies that the data fit together. (2)Cochlear prosthesis implant technology requires that this be achieved for identification of the proper electrical signals to present to the Corti's organ. (3)It can be used to distinguish the role of the two types of afferent dendrites emanating from the organ of Corti. (4)The source of nonlinearities influencing the neural tuning curve differences from the basilar membrane tuning can be identified by such a complete ear model.

To analyze the mechanisms, it was necessary to evaluate existent individual models of the middle ear, basilar membrane, and Corti's organ. It required development of quantitative models for hair cells, synapses and dendrites. Models for a hair cell and synapse are non-linear, but are relatively straight forward. The model for an outer

dendrite has a non-linear boundary condition, irregular geometry, and parameters which render it unsuitable for a dendrite equivalent cylinder analysis or standard numerical simulation methods.

7.2 MODEL DEVELOPEMENT

To make the model testable, it was decided to construct the model for one mammal, the cat, for which most of the experimental and anatomical literature is available. The Guinan and Peake (1967) model of their data, was chosen for the middle ear after checking their constants. Kim's (1972) model was used for the basilar membrane (BM), using normalized displacement in a system of nonlinear differential equations based on the Mossbauer measurements of Rhode (1971) and Rhode and Robles (1974). The proper displacement was obtained using Wilson's (1974) analysis of displacements for different species of mammals, which found that the ratio of BM displacement to stapes displacement versus frequency is very close for all mammals measured. The only available analysis of hair cilia response driven by BM displacement is that of Billone (1973) and Billone and Raynor (1973) based on an analysis of the microanatomy of Corti's organ.

A hair cell (HC) model was developed based on the

geometry of the hair cell and its electrical environment. It assumed the hair cell membrane to have the properties of passive neural membrane. The resultant equation expressing receptor voltage of the hair cell (RVHC) versus conductance change (GHC) at the top of the cell is highly nonlinear. On examination of constant values to determine their operating range, the equation became linear. Thus a system transfer function was obtained. It was found that the gain of the hair cell is proportional to the voltage across the receptor surface. Also, a transfer function and differential equation was obtained for the receptor potential when the cell is driven by voltage changes in scala tympani.

The afferent synapse was found to be nonlinear in each subcomponent. Katz (1967) plotted the relation between frequency of miniature end plate potentials (mepps) and depolarization of an axon presynaptic terminal for the rat diaphragm neuromuscular junction, based on an experiment in which the extracellular concentration of potassium was changed, causing changes in presynaptic transmembrane voltage. Thus, a prediction of transmitter quanta released as a function of presynaptic depolarization is available. Based on the dimensions of the afferent synapse intercellular space, the concentrations of transmitter were used as the input variable for a Michaleson-Morley binding

association of transmitter molecules with receptor site molecules on the postsynaptic membrane.

The dendrites are based on the geometry of the two afferent types, per Spoendlin (1972,74). Type I is a straight unbranched fiber from hair cell to axon. Type II dendrites have short branches which receive synaptic input from outer hair cells for 200 micrometers along the BM, proceeding in the apical direction. (It looks like a lady's long handle comb, pointing to the apex of the cochlea.) The formulation of the dendrite model determines the practicality of computer simulation. There are two types of formulations of the equations for simulation: (1)a compartment formulation which is equivalent to a finite difference scheme with unequal mesh intervals and (2) the finite element method. The finite element formulation was developed to obtain static solutions of structural problems such as bridges and ear drums with irregular geometries. First a compartmental formulation was utilized but found to have numerical instabilites. Next a formulation in finite element form for a dynamic simulation solution was constructed. Although it worked reasonably well with extremely small time steps, it took far too much storage space for variables and needed to manipulate large matrices (100X100 elements), which caused even a simple dendrite to

take a long time (over six hours on a quiet PDP 11-70 with cache memory). Its major advantage is that it allowed specification of irregular branching easily as input to the program. Upon analysis of the compartment formulation, it was found that in discretizing the space variable with non-uniform intervals, a system of ordinary differential equations result with time constants differing by several orders of magnitude. This severely limiting computation problem was solved by a stiff differential equation method of Houwen (1971b) which was written for large numbers of equations.

7.3 RESULTS

The hair cell gain (RVHC/GHC) was found to be proportional to a change of scalae media voltage. Frequency response curves were calculated for the hair cell. Using the model, it was possible to derive an equation relating receptor conductance change to whole cell resistance change in response to auditory stimuli. It was found that the hair cell operates in a linear range at low sound input amplitudes and in a nonlinear range for larger input amplitudes. It was also found that changing the voltage of the endolymph surrounding the hair cells, as would be altered by an implanted array of electrodes in scala

tympani, changes the receptor voltage.

The synapse was found to be a saturating non-linearity, which could be the source of the neural tuning being sharper than the basilar membrane tuning curve.

The simulation results for the outer dendrites showed that the response potential at the AP generating site is far less than the absolute threshold required to trigger an AP. The input auditory signal can be ranked as to effectiveness of response in the dendrite. In decreasing response effectiveness: a frequency band in the corresponding frequency interval along the BM, down sweeps in frequency in the afferent direction of the dendrite, up sweeps in frequency, single tones. This correlates with the psychophysical finding that animal distress cries are predominantly down sweeps in frequency. It was observed that these downsweeps are over a frequency interval corresponding to the interval on the BM in the outer dendrites which receive their synaptic input from outer hair cells.

Thus it was shown to be possible to construct a computational model for the peripheral auditory system as an input organ to the brain. The only missing signal processing block was shown to be that for hair cell receptor conductance as a function of forces on its cilia. Neither

the experimental data nor theory for conductance change as a function of membrane distortion is available. The method of simulating irregular branching dendrites is a general method which can be applied to other systems such as the retina or any central nervous system nucleus.

7.4 FUTURE DIRECTIONS

After doing a research project, there are always directions to be taken in new research. Particularly, in a project of this type, a certain perspective is attained. Thus I now will make some remarks about possible new research in the peripheral auditory system.

7.4.1 THEORETICAL WORK

More work should be done on dendrites of increasingly complex geometries. Especially good candidates are the dendrite systems of the cochlear nucleus.

Investigate the nature of motion of the cilia on the shape deformation of the cuticular plate of the hair cells.

The functional relationship for ionic conductance as a function of receptor membrane deformation should also be investigated.

These last two are especially important since the hair cell receptor conductance as a function of forces on the cilia is the "cochlear missing link".

It could be possible to calculate the hair cell conductance as a function of BM displacement of cilia forces by mathematically "driving" an inner dendrite, the synapse, and the hair cell backwards. The middle ear and BM equation would be used in the normal forward direction. Using a known experimentally measured rate function of AP's per second as a function of input sound amplitude, one would proceed to calculate the hair cell conductance and BM displacement, thence calculate forces on the cilia. Thus, the desired relationship could be obtained. The major problems possibly could be solved as follows: (1)To go from AP's per second to AP generating voltage. One could use the AP rate value as a reasonable first approximation (multiplied by a constant) to a voltage value. (2)Evaluation of the postsynaptic conductance to produce the proper AP generating site voltage. This could be found by trial and error or a parameter identification technique. (3)Using an average constant removal rate for transmitter in the synaptic cleft rather than a rate proportional to concentration which makes the overall synapse equation an invertable function. (4)The hair cell, being a linear

system, can of course be directly inverted by using receptor voltage as input and conductance as output. The result is then directly obtainable by examing conductance as a function of BM displacment and cilia forces.

When this conductance investigation is accomplished, then it could be possible to put all the cochlear blocks together for an overall input-output simulation. It then would be appropriate to calculate a neural tuning curve for comparison with the basilar membrane tuning curve.

The methods employed in predicting the response of the dendrites are particulary well suited to analyze stretch receptors found in muscle spindles. In fact, I feel that many of the problems encountered are due to the use of lumped parameter models for quantizing a process distributed in a branching geometry such as a stretch receptor.

A natural extension of the hair cell, synapse and dendrite analysis cum simulation is to include the efferent innervation from the brain stem. This would be an interesting study because it could offer further understanding of the role that the two types of cochlear hair cells and dendrites play.

Another excellent place to apply the compartment model of dendrites with unequally sized branches is on the giant fiber synapse of Loligo. This large synapse has an

irregular dendritic tree receiving synapses from a large presynaptic fiber and the dendritic fibers go into another large fiber (Young, 1973). Even this system is much more complex than the simple cochlear outer dendrites with 181 collateral dendrite fibers and at least 100 final twigs per collateral. Observe that this is in the order of 18,100 normal synapses acting in parallel. It would interesting to use the method to predict the experimental results obtained from this structure (e.g., Miledi, 1967).

I would like to see this kind of analysis done for the retina. Such an analysis is now possible for other processing blocks in the brain, now that there are the following: (1)A general model for synapses (requiring only the dissociation constant and removal rate for the transmitter, and the number of receptor sites). (2)A general analysis method for dendrites requiring only the geometry. (3)A stiff differential equation integration routine with limited storage requirements.

7.4.2 EXPERIMENTAL WORK

The research notebook of scientific investigation is totally dominated by experimental results. Without experimental results, theoretical work is almost impossible.

Theoretical investigations integrate and codify existant experimental results. Optimally, they make predictions as to what may be found in the next steps of experimentation. So I suggest a list of what experiments could be done in auditory research.

Measurement of hair cell gain for changes in extracellular potential. This would verify or refute the predictions of the hair cell analysis of chapter 4. Further, the prediction of hair cell receptor potential as a function of voltage in scala tympani needs to be verified.

Further work on identification of the transmitter at the afferent synapse of the hair cells shoud be done.

Using the dendrite partial differential equation with proper synaptic conductances and correct anatomy of cochlear outer dendrites, it was predicted that the most response affective auditory stimuli in decreasing order of response are (1)frequency band, (2)downsweeps in frequency and (3)upsweep in frequency. To verify this prediction the following experiment could be done. Record from a cochlear spiral ganglion soma. Measure its characteristic frequency f_{CF}. From the maximum resonse frequency curve, compute X_{CF}, the corresponding position on the basilar membrane for f_{CF}. The length of an outer dendrite segment receiving hair cell innervation is 200 microns, DX. Let

$$f_1 = MRF(X_{CF} - DX)$$

$$f_2 = MRF(X_{CF})$$

Now a frequency sweep from f_1 to f_2 is a downsweep and f_2 to f_1 is an upsweep. The ensemble of frequencies $\{f_k; k=0,1,2,\ldots,N\}$ where

$$f_k = X_{CF} - DX + (DX/N)*k$$

is a frequency band input for the dendrite, if it where an outer dendrite. The frequency sweep time interval, Dt, should be in the order of one millisecond to two hundred milliseconds, based on normal speech frequency downsweeps (Fletcher,1953). Since 5% of the cochlear afferent fibers are from outer hair cells, I make the following predictions. Of the somas for which f_{CF} is measured, responses measured in response to frequency sweeps from f_1 to f_2 and f_2 to f_1, and frequency band input, the axons should have two populations. One population (5% of total) should have post stimulus responses with largest amplitude for frequency band input, frequency downsweeps, and frequency upsweeps, in descending order of response magnitude. The other population (95% of total) should have significantly smaller

response differences.

The fact that the outer dendrites do not have response potentials that are large enough to trigger action potentials, as demonstrated by the simulations, and Spoendlin's (1979) finding that the outer afferent fibers do not continue up the nerve, causes me to speculate that action potentials are necessary for axon growth. It is well known that muscles atrophy when dennervated. An important clinical treatment in the regrowth of sectioned nerve that has been surgically rejoined, may be to electrically stimulate the distal portion of a damaged nerve to promote its regrowth.

7.5 CONTRIBUTIONS TO KNOWLEDGE

The contributions to knowledge are summarized as follows.

A large amount of existing but unrelated experimental information and analysis was integrated in a coherent theory of signal processing mechanisms in the cochlea.

It was shown that available mechanical experimental results and models are sufficient to provide an overall dynamic computational model.

A quantitative model for a cochlear hair cell was developed and used to show that the hair cell input-output

equation is linear for low amplitue sound input and nonlinear for higher input amplitudes. In the linear range it acts as a low pass filter with gain proportional to voltage across the receptor surface. When the hair cell is driven by extracellular changes as would occur for a scala tympani implanted prosthesis, the system is again linear.

The overall input-output functions for a synapse were quantified with the input as presynaptic depolariztion and output as postsynaptic membrane conductance. It is suggested that the synaptic nonlinearities are a possible cause of the difference between the basilar membrane and neural tuning curves.

A method of analysis and simulation was developed for dendrites with any geometry and proper synapses. The method allows unsymmetric irregular branching and nonuniform branch diameters.

It was observed that using synaptic conductance as input causes a time varying nonlinear boundary condition for the dendrite partial differential equation. The solution of such a system is unsolvable by analytical methods. Furthermore, when the dendrite equation is discretized in a manner that preserves geometry, the resulting system of equations has rate constants that differ by orders of magnitude. The system was shown to solvable by a stiff

differential equation method.

It was demonstrated that known membrane properties can be applied in new geometrical configurations to obtain useful results.

It was shown that a practical method of numerically solving a system of differential equations with time varying coefficients as input and nonlinearities is to put the equations in state variable form and use a stabilized integration subprogram such as ARK.

The mathematics cum simulation of the cochlear outer dendrites showed that those dendrites respond better to downsweeps than upsweeps of sound frequency at the same amplitude.

The simulation work showed that for normal postsynaptic conductance values, which are large enough for inner cochlear afferent fibers to generate action potentials, the outer afferent fibers do not generate action potentials. The outer dendrite response potentials do not become large enough to exceed action potential absolute threshold.

REFERENCES: CHAPTER 7

Billone,M.C. (1973) Mechanical stimulation of cochlear hair cells. Ph.D. Thesis, Northwestern Univ. Evanston, Ill.

Billone,M.C. and Raynor,S. (1973) Transmission of radial shear forces to cochlear hair cells. J.Acous.Soc.Am. 54:1143-1156.

Fletcher,H. (1953) Speech and Hearing in Communication. Van Nostrand,Inc. N.Y. 461P.

Guinan,J. and Peake,W.T (1967) Middle ear characteristics of anesthetized cats. J.Acous.Soc.Am. 41(5):1237-1261.

Houwen,P.J. van der (1971a) A survey of stabilized Runge-Kutta methods. MC-25 Informatica Symp., Mathematisch Centrum. Amsterdam.

Houwen,P.J. van der (1971b) Stabilized Runge-Kutta methods with limited storage requirements. Report TW 124/71, Mathematisch Centrum, Amsterdam.

Katz,B. (1967) A study of synaptic transmission in the absence of nerve impulses. J.Physiol. 192:407-436.

Kim,D.O. (1972) A nonlinear model for basilar membrane motion and related phenomena of single cochlear nerve fibers. Ph.D. Thesis, Washington University, St. Louis, Missouri.

Miledi,R. (1967) Spontaneous synaptic potentials and quantal release of transmitter in the stellate ganglion of the squid. J. Physiol. 192:379-406.

Rhode,W.S. (1971) Observations of the vibration of the basilar membrane in squirrel monkeys using the Mossbauer technique. J.Acous.Soc.49:1218-1231.

Rhode,W.S. and Robles,L. (1974) Evidence from Mossbauer experiments for nonlinear vibrations in the cochlea. J.Acous.Soc.Am. 55:588-596.

Spoendlin,H. (1973) Innervations densities of the cochlea. Acta Otolaryng. 73:235-248.

Spoendlin,H. (1974) Neuroanatomy of the cochlea. In: Facts and Models in Hearing, E. Zwicker and E. Terhardt, Eds. Springer-Verlag pp18-36.

Spoendlin,H. (1979) Neural connections of the outer haircell system. Acta Otolaryngol. 87:381-387.

Wilson,J.P. (1974) Basilar membrane data and their relation to theories of frequency analysis. In: Facts and Models in Hearing, E.Zwicker and E.Terhardt, Eds. Springer-Verlag, Berlin. pp55-63.

Young, J.Z. (1973) The giant fiber synapse of Loligo. Brain Res. 57:457-460.

CHAPTER 8
ACKNOWLEDGEMENTS

First of all, I respectfully thank Dr. John Outerbridge, the Director of Biomedical Engineering Unit at McGill University, for providing the freedom of opportunity for me to do a large scale model, the managerial foresight to keep blocks from the progress of this project, and his comments during the project and the writing.

I thank Dr. Ronald Poulsen, the director of the MacDonald-Stewart Biomedical Image Processing Laboratory at McGill University, for teaching me much about computers and letting me work in his image processing laboratory. He also provided comments on the thesis at a critical stage in the writing. Dr. Poulsen, Dr. Les Oliver, Dr. Richard Brannan and Ms Claude Louis of that laboratory made a valuable contribution in convincing me not to give up before the solution using the methods for integrating stiff differential equations was found. Without that technique the problem was unsolvable. The gray level plots in the dendrite chapter were done using the real time 64 gray level

display for 144x144 pixels developed by Dr. Poulsen.

Dr. P. J. van der Houwen, whom I never met, except through his papers, initially developed the algorthm for integrating a system of stiff differential equations. Dr. Peter wynn made available his personal FORTRAN version of the numerical integration subroutine, coded for limited storage requirements. Mr. Hang Tong Lau translated the orginal ALGOL program into FORTRAN and freely answered questions as to its implementation in the dendrite system of equations. This application of sophisticated applied mathematics solved a very difficult problem in numerical simulation. Furthermore, it made possible a solution of a real world complex biological problem.

Dr. Robert Funnell made helpful comments on an early version of the models. Dr. Charles Laszlo and Dr. Funnell made a filing cabinet of auditory reprints available to me, for which I am ever in debt.

Mr. Alex Brown, who was my student in two courses, FORTRAN and Automata theory at Concordia University, became my teacher in patiently answering many questions on RSX 11-M and the PDP 11-70 after he became a systems programmer at McGill's Biomedical Engineering Unit.

Mr. Gary Bernstein runs a wonderfully tight ship in managing the computing facility for the McGill Medical

Faculty in Biomedical Engineering. The smoothly running, 24 hour a day, facility made this project possible.

Mr. Carmelo Granja, the systems engineer, kept the PDP 11-70 running smoothly and patiently fixed the system software when the large simulations on dendrites used the system in a new way.

Mr. Serge Lafontaine and Dr. Robert Funnell made a variety of improvements to DEC's word processing program. The mathematical notation would have been impossible to keep free of typographical errors without it.

Dr. George Mandl of Aviation Medical Research Unit at McGill taught me the value of scientific integrity and the basics of neurophysiology.

There is something ironic about the fact that the RP04 computer disk read-write head is in the exact position where I had inserted microelectrodes in exposed cat cochlear nerve. The dendrite simulations are an alternative path to answer the question of whether the cochlear outer dendrites respond better to downsweeps than upsweeps in frequency of sound signals presented to the ear.

Ms Mary Lou Smith caretully proof read the entire thesis. A prodigious task, for which I am grateful. She also provided perspective encouragement, and much soul time. For that, I am ever in debt.

The MacDonald-Stewart Foundation provided the major equipment grant to start the McGill University Biomedical Computing Facility. Dr. John Outerbridge organized the facility and by actively using it for his own projects, ensured that the facility is efficient and practical to use.

Dr. Nelson Kiang, Dr. Thomas Weisz, and Dr. John Guinan actively critized my initial thoughts about the models. They provided a means of testing my understanding of the peripheral auditory system.

It was fun to find a namesake, James Winslow, who remained in Europe to work on the cochlea, while the New England Winslows were settling the Massachusetts Bay Colony in the early 1700's.

Dr. Domina Eberle Spencer showed me the usefulness of mathematics in my undergraduate courses at the University of Connecticut. From those experiences I learned to not be bounded by what is not yet done in science.